Thermo-Responsive Small and Polymeric Amphiphiles for Drug Delivery

A Thesis

Submitted in Partial Fulfillment of the Requirements
Of the Degree of
Doctor of Philosophy

By

Smita Kashyap

Reg. No. 20093037

Department of Chemistry
INDIAN INSTITUTE OF SCIENCE EDUCATION AND RESEARCH, PUNE
Pune 411008, Maharashtra, India

July 2015

Dedicated to

My Parents

For their endless love, support and encouragement…

भारतीय विज्ञान शिक्षा एवं अनुसंधान संस्थान पुणे
INDIAN INSTITUTE OF SCIENCE EDUCATION AND RESEARCH PUNE
(An Autonomous Institution of Ministry of Human Resource Development, Govt. of India)
Dr. Homi Bhabha Road, Pune - 411 008.

Dr. M. Jayakannan
Associate Professor
Department of Chemistry

CERTIFICATE

Certified that the work incorporated in the thesis entitled "***Thermo-Responsive Small and Polymeric Amphiphiles for Drug Delivery***" Submitted by **Ms. Smita Kashyap** was carried out by the candidate under my supervision. The work presented here or any part of it has not been included in any other thesis submitted previously for the award of any degree or diploma from any other University or institution.

Dr. M. Jayakannan

(Thesis supervisor)

Date: 29 July 2015

DECLARATION

I declare that this written submission represents my ideas in my own words and where others' ideas have been included; I have adequately cited and referenced the original sources. I also declare that I have adhered to all principles of scientific honesty and integrity and have not misrepresented or fabricated or falsified any idea/data/fact/source in my submission. I understand that violation of the above will be cause for disciplinary action by the institute and can also evoke penal action from the sources which have thus not been properly cited or from whom proper permission has not been taken when needed.

Date: 29/07/2015

(Smita Kashyap)

Pune (MH), India

Roll. No. 20093037

ACKNOWLEDGEMENTS

I thank, Dr. M. Jayakannan, my research supervisor, for his excellent guidance, constant encouragement, invaluable suggestions, and supporting this work with ideas and criticism. His determination, energy and dedication for research motivated me to do science when I joined IISER. I will be always grateful to him for teaching, guiding and counseling me for all these years of my PhD at IISER, Pune.

I am extremely thankful to Prof. K.N. Ganesh, Director, IISER-Pune for providing all the facilities for carrying out this research work.

I would like to thank my research advisory committee (RAC) members; Dr. S. G. Srivatsan and Dr. Manohar V. Badiger from NCL for their interactive discussions and valuable suggestions.

Special thanks to Dr. Asha, S. K. for her constant support and intellectual scientific discussions.

I would like to thank all the faculty members in the department of chemistry for extending their research facilities, interactive scientific discussions and teaching me various courses.

I specially thanks my present and former lab mates for their support and cooperation especially, Jinish, Bala, Mahima, Ananthraj, Pramod, Bapu, Narshima, Bhagyashree, Moumita,Sonashree, Nilesh, Nitesh, Shraddha, Hemlata, Mehak, Khoshboo, Vikas, Uma, Vivek, Rekha, Kaushal, Nagesh, Chinmay, Shekhar, Nisha, Senthil, Saibal, Prajitha, Swapnil, Sarabjot, and Sandeep for their love, care and support which made my life memorable at IISER, Pune.

I would like to thank all instruments' technicians of IISER Pune for their support: Pooja, Deepali (NMR) Swati (MALDI), Neetha (HRMS), Megha (AFM), Anil, Yatish (FE-SEM), Archana (XRD). I thank National Chemical Laboratory (NCL) Pune for HR TEM and SLS facilities.

I wish to express my sincere thanks to all my friends at IISER-Pune, especially, Padma, Ramya (room mate), Himani, Neha, Madhuri, Dharmaraja, Mani, Mano, Ravi, Shankar for friendly chats during tea sessions.

I also thank all the staff members in administration, finance, accounts, stores, library, especially, Ms. Naina, Mr. Mayuresh, Mr. Mahesh and Mr. Nitin for their immediate help whenever needed.

I am deeply indebted to my family for their whole hearted support and encouragement at every step of my life, especially, my father for believing in me as well as for his constant support and motivation. I would like to use this opportunity to thank my mother for everything that I have achieved in life, without her none of this would have been possible.

I would like to specially acknowledge with tremendous and deep thanks to my life partner, **Manoj**. I have been able to complete this long dissertation journey because of his love, patience, and support. Special thanks to Manoj's parents and brothers (Ram, Sanoj and SachinAnd last but not least, I thank my brother (Alok) and my younger sister (Sakshi) for their everlasting support and encouragement.

Financial support from Council of Scientific and Industrial Research (CSIR) is greatly acknowledged.

.

Smita

SYNOPSIS

Polymer based nanocarriers are emerging as important biomaterials for delivering anticancer drugs or genes to cancer tissues. Polymeric drug carriers such as micelles, vesicles and nanoparticles have been fabricated till date to achieve site-specific drug delivery. These nanocarriers have advantage of undergoing passive selective accumulation in tumor tissues through EPR effect. The advent of stimuli-responsive drug carriers has amplified the targeting ability and specificity of the nanocarriers. In a view of designing stimuli-sensitive polymeric vehicles, the unusual physiochemical environments of the cancer tissues such as high temperature (40-43°C), acidic pH (6.1 to 6.8), over-expression of enzymesand hypoxic conditions have been used as a trigger for releasing drug at cancer site. Among all these stimuli-based materials, thermo-sensitive polymers provide unique opportunity for delivering chemotherapeutic agents to tumor tissues without affecting the micro-environment of tissues. Unfortunately, thermos-responsive polymeric materials are much less explored compared to other stimuli-based materials; hence, new smart amphiphilic designs (both small and polymeric) are required to accomplish better treatment for cancer therapy.

This thesis work is focused on the design and development of an efficient nanocarrier for targeting tumor or cancer cells using temperature as a stimulus for releasing the loaded cargoes. Small amphiphilic molecules based thermo-responsive scaffolds were synthesized in order to understand the role of hydrophobic and hydrophilic segments on the thermal-behavior of their drug-release mechanism. These amphiphiles were designed with hydrophobic unit from renewable recourse 3-pendadecyl phenol which is one of the main constituent of cashew nut shell liquid. The self-assembled nanostructure formed from the amphiphile was further employed for loading fluorescent dyes and various anti-cancer drugs.

This thesis has been divided into five major chapters:

1. Introduction Chapter: The first chapter provides a complete literature survey on polymer based drug delivery and importance of stimuli-responsive nanocarrier in the field of drug delivery.
2. Thermo-responsive and shape transformable amphiphiles: A renewable resource based amphiphilic molecules having shape transforming ability upon exposure to temperature variation was developed.The drug loading capabilities and thermally-induced drug release kinetics from these unique core-shell nanoparticles was investigated in detail.
3. Thermal and enzyme dual responsive polymeric scaffold:New series of amphiphilic copolymers composed of hydrophobic acrylate unit and ethylene glycols were synthesized. These nanoparticles were loaded with anticancer drug doxorubicin and their cytotoxicity was studied in breast cancer (MCF 7) and cervical cancer (HeLa) cell lines.
4. The Hofmeister effect: An amphiphilic molecule with "*super-LCST characteristics"* was developed in order to study the influence of biologically relevant anions on the thermo-responsive properties of nanocarriers.
5. Multivesicular amphiphilic scaffolds: New amphiphiles were designed to produce small unilamellar vesicles (SUVs) and multi-vesicular bodies (MVBs). The drug loading and delivering capabilities of both SUVs and MVBs were investigated under physiological conditions (pH=7.4, PBS) and in presence of esterase enzyme.

The ***chapter-1*** provides a brief introduction to drug delivery with emphasis on advantages of polymeric materials as drug vehicles for treatment of cancer.A detailed literature survey on different types of small amphiphile based drug delivery systems which are commonly used as nanocarrier, their properties and limitations have been discussed.This chapter also provides a complete literature survey on importance of stimuli-responsive polymeric nano-vehicles and highlighting their application in the field of biotechnology and drug delivery. Thermo-responsive

nanocarriers have been discussed as an important approach for efficiently delivering the chemotherapeutic agents in tumor microenvironment.

The ***second chapter*** describes the drug loading and delivering capabilities of temperature induced shape-transformable carrier's at cancer tissue temperature. Amphiphilic molecule based on renewable resource hydrophobic 3-pendadecylphenol connected to hydrophilic oligoethylene glycol via hydrogen bonded amide linkage were tailor made through multi-step organic synthesis. The thermo-responsive behaviour and self-assembly of the amphiphiles were analysed. The three dimensional core-shell nanoparticles underwent temperature induced shape transformation in to one-dimensional rod-like structures. The temperature driven *in-situ* transformation of the amphiphilic scaffold from three dimensional core-shell at temperature below LCST to rod-like structures at higher temperature in water (or PBS at pH= 7.4). The thermo-responsive core-shell nanoparticles were employed for encapsulating anticancer drugs such as doxorubicin (DOX) and camptothecin (CPT). The release profile of the DOX under *in-vitro* conditions revealed that the DOX can be selectively release at cancer tissue temperature (40-43°C) as compared to normal body temperature (37 °C). The cytotoxicity studies of the nascent scaffold and drug loaded was carried out on cervical cancer (HeLa) cell lines using MTT assay method.

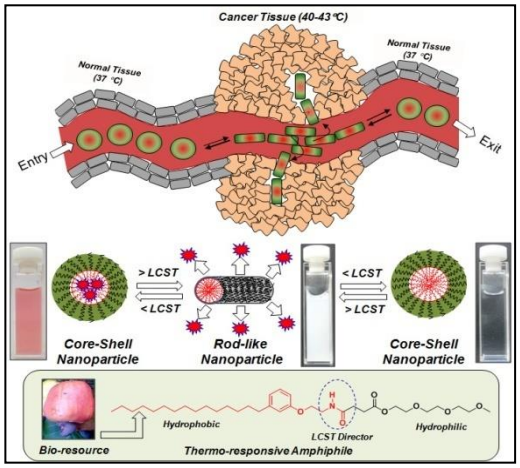

The ***third chapter*** describes the role of dual responsive polymer nano-scaffolds for administrating anticancer drugs both at extracellular level in tumor tissues and intracellular compartments of cancer cells for improving drug efficacy. For this purpose, a new class of thermo and enzyme dual responsive polymeric amphiphiles was tailor-made through copolymerization of hydrophobic acrylate monomer from 3-pentadecylphenol (PDP, a renewable resource) and oligoethylene

glycol acrylate (as hydrophilic monomer). The copolymers synthesized varied in the composition of hydrophilic and hydrophobic segment in their structure. The thermo-responsive behaviour of the various amphiphilic copolymers was investigated. The copolymers with 6 % hydrophobic unit in their backbone showed LCST close to cancer tissue temperature. These copolymers self-assembled to produce spherical core-shell nanoparticles in water at temperature below LCST. The dual responsive polymer scaffold was found to be capable of loading both hydrophobic dye (Nile red) and drug (DOX). The release profile of DOX at normal body temperature (below LCST, ≤ 37 ◦C) revealed that DOX was preserved in the core-shell assemblies, while at temperature closer to cancer tissue (above LCST, ~ 43◦C), the polymeric scaffold underwent burst release to deliver 90 % of loaded drugs within 2 h. On the other hand, under conditions similar to in intra-cellular compartment (pH = 7.4, 37 ◦C, esterase enzyme); the amphiphilic copolymer ruptured slowly leading to controlled release of drug (> 95 %) for 12 h. Thus, both burst release of cargoes at the tumor microenvironment and control delivery at intracellular compartments were accomplished. Cytotoxicity assay of the nascent and DOX loaded polymer were carried out in breast cancer (MCF-7 cells) and cervical cancer (HeLa cells). Among the two cell lines, the DOX loaded polymers showed enhanced killing in breast cancer cells. Confocal microscopic images confirmed that DOX loaded core-shell nanoparticles were taken up by MCF-7 cells, showing a distinctly perinuclear localization in cell.

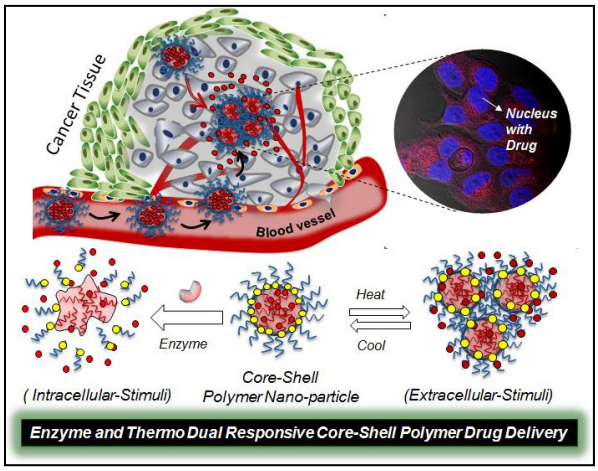

The ***fourth chapter*** deals with the design and development of super LCST thermo-responsive amphiphilic nanoparticle assembly for detection of adenosine triphosphate (ATP) through Hofmeister effect. A new diblock molecular based on hydrophilic polyethylene glycol and PDP as hydrophobic unit was designed to study

the role of biologically relevant anions on the thermo-responsive behavior of the nanocarriers. The amphiphile self-assembled as 150 nm micellar nanoparticle and showed super lower critical solution temperature (LCST) above 90 °C. The effect of anions on the phase-transition temperature (LCST) of the amphiphile was in consistent with the "Hofmeister series" with higher selectivity for the recognition of ATP over its adenosine precursors such as ADP, AMP and inorganic phosphate (Pi). The preferential binding for ATP is attributed to the encapsulation in the hydrophobic pocket and modification of hydration shell at the periphery of the amphiphilic nanoparticles.The binding constants for the amphiphilic nanoparticle binding to ATP were determined by isothermal calorimetric measurements. The cytotoxicity of the super LCST amphiphile carried out on cervical cancer (HeLa) cells revealed that the amphiphile was non-toxic in cells.

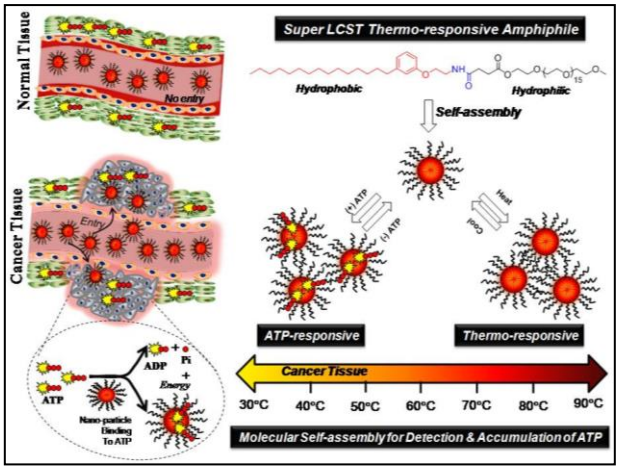

In the ***fifth chapter***fluorophore encapsulation pathways and drug loading abilities in synthetic macromolecular amphiphiles sorting into mutivesicular bodies (MVB)s was reported. For this purpose, renewable resource based amphiphiles having hydrophobic units and flexible hydrophilic polyethylene glycols (PEG) were custom designed. To prove the existence of the strong inter-molecular interactions and the formation of uni-lamellar layer-like self-assemblies single crystal structure was resolved. Small uni-lamellar vesicles (SUV)s or MVBs were produced from these

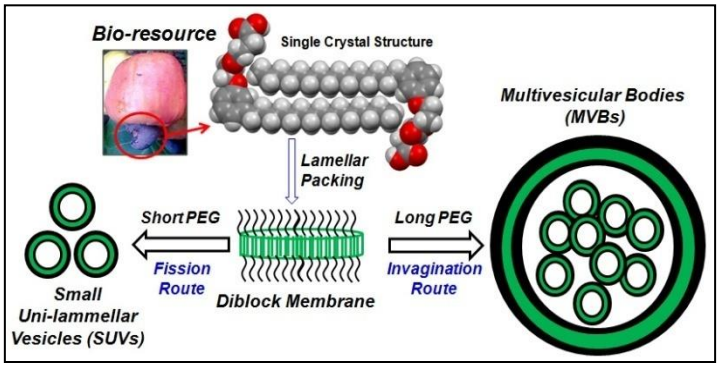

amphiphilic AB amphiphiles through selective vesicular fission either by outward budding or inward invagination, respectively. The mechanistic aspects of the MVB andformations was studied by encapsulating environment sensitive fluorescent probe, pyrene. An un-usual non-linear trend was observed in the pyrene dynamic excimer formation with respect to the sorting of diblock membrane into MVBs. Doxorubicin, the anti-cancer drug was employed for studying the encapsulation capabilities of both MVBs and SUVs. The drug release profile of DOX loaded MVBs and SUVs under physiological conditions (pH = 7.4, PBS) revealed that DOX was stable in MVBs while SUVs released more than 90 % of the drug. MVBs showed two step DOX release profileswith respect to outer and inner vesicles cleavage in the presenceof esterase enzyme.

The last chapter summarizes the overall outcome of thesis work and future directions

TABLE OF CONTENTS

Chapter 5: Amphiphilic Amphiphiles Sorting into Multivesicular *191-238*Bodies and their Encapsulation Capabilities

Chapter 1

Introduction

1.1. Introduction to Drug delivery

Eradication of cancer entirelyhas become one of the most challenging tasks and several anti-cancer drugs have been formulated till date for the treatment of cancer.[1]Conventionally, these therapeutic agents are administered directly into blood stream and the typical profile of drug concentration in plasma as a function of time after oral or intravenous administration is shown in figure 1.1.[2] From the plot it is evident that drug concentration in the blood rises at the time of drug intake, followed by peak and then subsequently declining in the drug profile.[3]Each drug has a plasma level above which it is toxic and below which it is ineffective. Thus, the plasma drug concentration in a patient at a particular time to be in the therapeutic window or at therapeutic dose level requires multiple administrations.[4] Majority of therapeutic agents employed for curing cancer are low molecular weight compounds.As a result,these drug molecules undergo rapid renal clearance. Furthermore, the absorption of thedrug molecules after systemic administrationis mainly driven by diffusion mechanism. Thus, the drug molecules get evenly distributed throughout the entire body thereby, lacking tumour selectivity and causing damage to healthy tissues.[5]

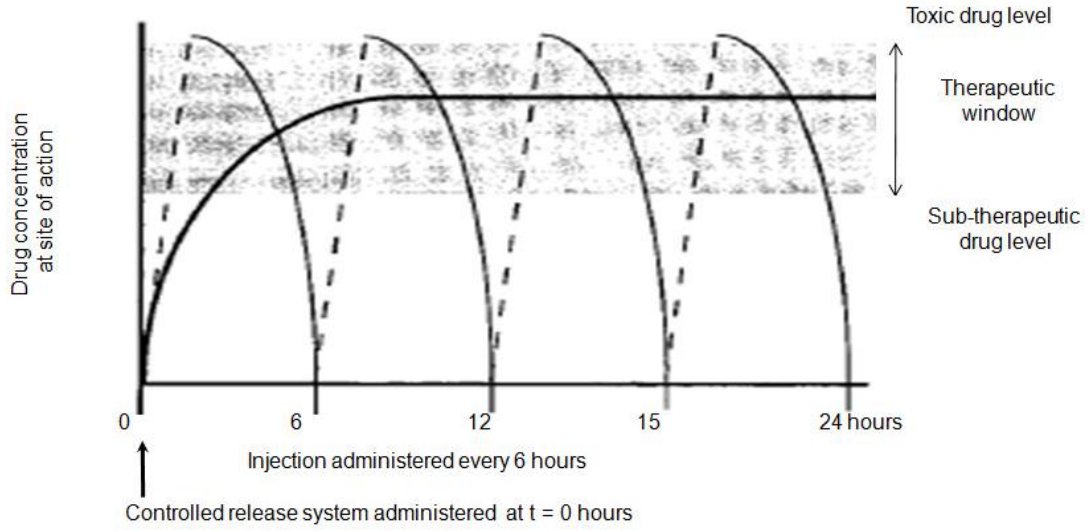

Figure 1.1.*Comparison of conventional and controlled drug delivery system (adopted from Uhrich et al. Chem. Rev.* ***1999****, 99, 3181-3198).*

In order to circumvent the shortcomings of conventional drug therapy, the concept of drug delivery was introduced in 1906 by Paul Ehrlich who coined the term "magic bullets".[6] Since then an explosion has been witnessed in design and development of new methods of delivering drug at the target site. Several drug carriers were developed, aiming (a) controlled drug release, and (b) site-specific drug delivery.In controlled release system drug is generally delivered at a pre-determined rate for an explicit time period (see figure 1.1).[7]The rate of drug release from these systems depends on the design but is completely independent of the surrounding environmental conditions. On the other hand, the site specific drug delivery is generally achieved by incorporating targeting ligands. It amplifies the drug efficacy by increasing the local drug concentration at the desired site of therapeutic need.[8] Thus, the drug concentration is retained in the therapeutic window in case of controlled delivery system for longer time (see figure 1.1). Therefore, sustained release of drug is achieved in controlled release system over oscillating drug plasma level in conventional delivery. Several other advantages has also being provided by these controlled drug release system over the conventional drug therapies such as (a) enhanced bioavailability of drug, (b) preventing premature degradation of therapeutic agents, (c) avoiding rapid renal clearance, (d) reducing the dose level, (e) minimized side effects (local/systemic) and (f) improved patient compliance etc.[9]

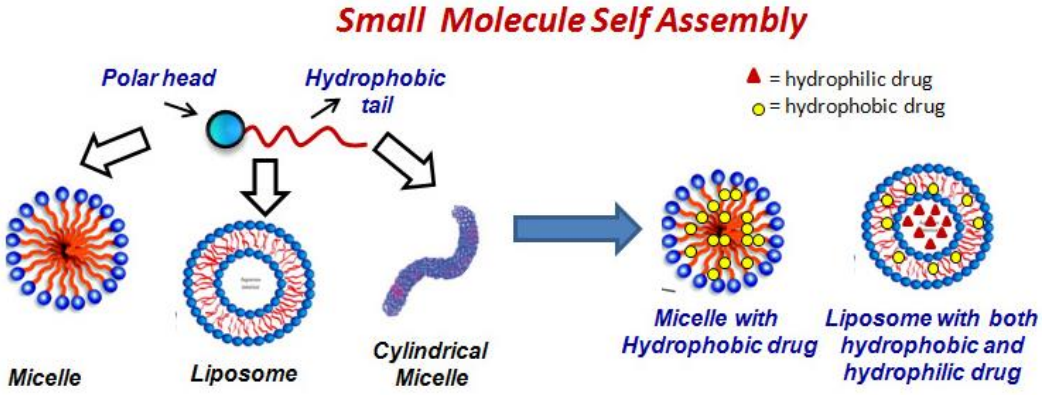

Figure 1.2.*Various amphiphilic small molecule based nano-carriers for drug delivery.*

Various small molecule amphiphilesand surface-active agents (surfactants) have been employed owing to their biocompatibility and biodegradability to overcome the above limitations. These amphiphilic small moleculesself assemble to form broad range of nano-carriers. These self-assembled nano-sized carriers basically include nano-particulate drug delivery systems.[10]Nano-particulate drug delivery system consists ofliposomes, micelles, nanoparticles etc (see figure 1.2). In these nano-carriers, the drug molecules are physically entrapped via non-covalent interaction which further confers stealth character to the drug molecule.[10] This minimizes the binding of plasma proteins to the drug molecules followed by reduced uptake by reticulo-endothelial system (RES) or macrophages. In other words, the opsonisation of drug and clearance by mononuclear phagocytic system is eliminated, thereby increasing the blood circulation time or half-life of the drug molecule.[12] Bothhydrophobic and hydrophilic therapeutic agents can be encapsulated in these carriers. For instance, small molecule based micelle can sequester hydrophobic drugs in their inner hydrophobic pocket; while presence of outer hydrophobic layer and inner aqueous interior in liposomes facilitates the encapsulation of both hydrophilic and hydrophobic drug molecules.

1.2. Enhanced Permeability and Retention Effect

The accumulation of these nano-carriers at tumor site is achieved through passive and active targeting. Passive targeting is usually accomplished due to presence of defective, leaky architecture of the tumour blood vessels.[13,14] The large fenestrations formed by the disorganized endothelial cells on the inner lining of tumour blood vessels leads to enhanced vascular permeability, thereby assisting in better penetration of the nano-carriers in tumour tissue (see figure 1.3). This in turn increases the local drug concentration 10-50 fold times higher in tumour tissues as compared to normal tissue.[15] Likewise, the dysfunctional lymphatic drainage of tumour tissues retains these drug carriers for longer time thereby allowing them to release drug in tumour vicinity. This phenomenon of higher accumulation and retention of drug carrier in tumour tissue was termed as “enhanced permeability and

retention (EPR) effect".[16] This EPR driven efficient strategy for anticancer drug design having high selectivity towards tumour tissues was discovered by Maeda and Matsumura in 1986.[17] On the contrary, the EPR effect is not applicable for low molecular weight drugs or conventional chemotherapeutic agent (see figure 1.3). Though, the concept of EPR was first demonstrated in literature for polymers, it is also widely accepted for liposomal delivery.[18]

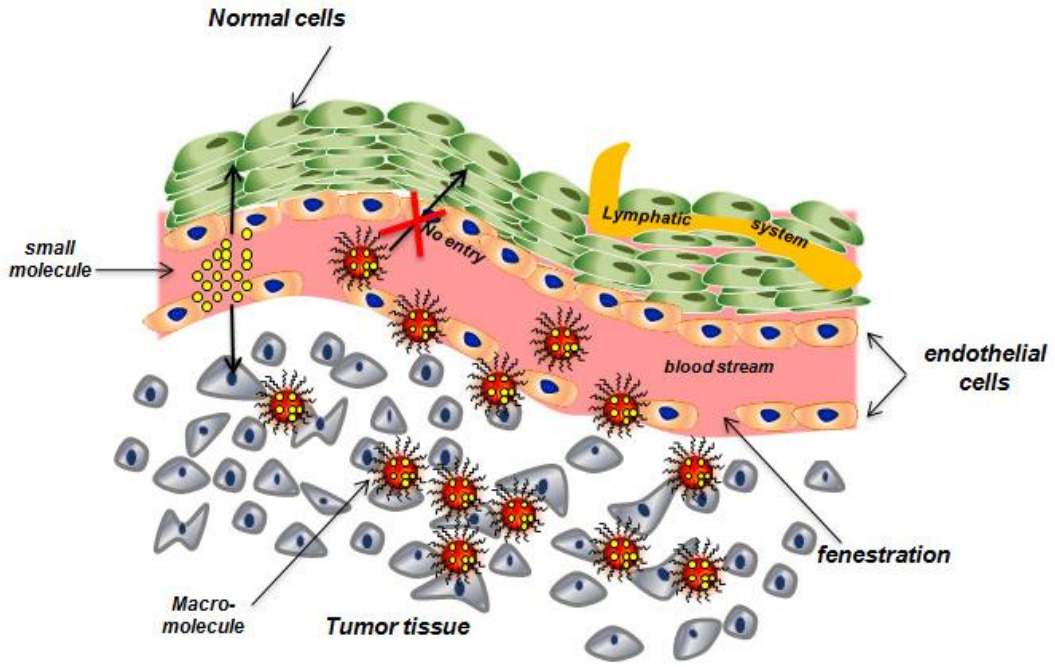

Figure 1.3.*The enhanced permeability and retention effect of nano-carriers as compared to conventional therapeutic agents.*

Although this passive targeting approach was capable to annihilate the use of conventional drugs for cancer treatment, it suffered from several limitations such as (a) penetration and accumulation of drug carriers in tumor non-specifically, (b) release of drug molecules before reaching the target site, and (c) low level of drug concentration in tumour tissues.[19]In other words, only fraction of drug molecule is delivered at the diseased site resulting in low therapeutic efficacy and undesirable systemic side effects[20,21] (see figure 1.4a and 1.4b).In order to overcome the intrinsic limitation of passive targeting with respect to its specificity, surface of drug carriers were modified with various molecules capable of binding to receptors that are over

expressed on cancer cells.[22,23] This approach of conjugating ligands having affinity for cancer specific receptors for delivering drug at desired site was termed as 'active targeting' or 'ligand-mediated targeting'.[24] Ligands generally used for conjugation are antibodies, aptamers, proteins, peptides, nucleic acids and sugar molecules.[25] This ligand- receptor interaction leads to preferential accumulation of the drug carriers in tumour tissue followed by cellular internalization and release of the therapeutic agent in intracellular compartment[26,27] (seefigure 1.4c). Thus, active targeting increases the intracellular drug concentration and minimizes the toxicity to non-cancerous cells adjacent to tumour tissues.[25] In other words, actively targeted nanosystems in combination with EPR effect are promising strategy for further augmenting efficacy of nanomedicines for cancer treatment.

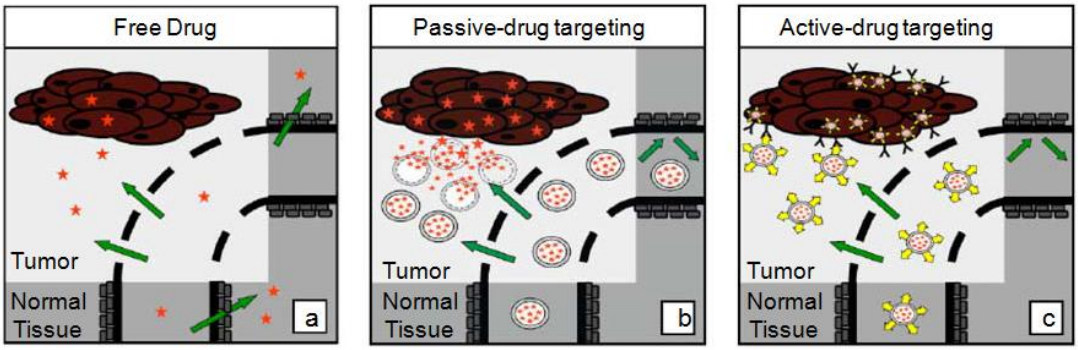

Figure 1.4.*Comparison of three different drug targeting strategies (a) free drug, (b) passive targeting and (c) active targeting (adopted from Lammers et al. Br. J. Cancer,* ***2008****, 99, 392-397).*

The conjugation of these ligands on to the drug carrier surface imparts hydrophobicity to these targeted nanosystems. The hydrophobicity of these nano-carriers further influences their *in vivo* fate. In other words, these hydrophobic targeted nano-systems aggravate reticulo-endothelial systems (RES) or macrophages and are massively cleared by mononuclear phagocyte system. Thus, half-life or blood circulation time of these carriers drops down. Therefore, to achieve prolonged blood circulation time of these actively targeted nanosystems for retaining higher local drug concentration along with increased cellular uptake;these ligand conjugated systems are coated with hydrophilic polymers or surfactants.[28]

Polyethylene glycol (PEG) is one of the most widely used polymers for this application.[29]In general, PEG forms a protective layer surrounding the nano-carrier thereby shielding its interaction with the plasma proteins. As a consequence, the binding of blood components with the nano-systems is sterically hindered [30,31]and accumulation of the nano-particulate systems in the RES cells is reduced.[32,33,34] Thus, the opsonisation of the drug carriers gets decelerated. This phenomenon of increasing the *in vivo* longevity of the nano-carriers by alleviating macrophage-mediated renal clearance is termed as "steric stabilization" and the polymers used for this application are known as "steric protectors".[35]Even at very low polymer concentration, the polymer coating remains impermeable to several solutes which in turn impart low toxicity. In addition to function as polymer coating, PEG also enhances solubility as well as does not alter the biological properties of the encapsulated chemotherapeutic agent. Apart from PEG, polyethylene oxide, polyoxamer, polyoxamine and polysorbate 80 (Tween80) are few other examples of polymers which are employed as steric protectors.[35,36]

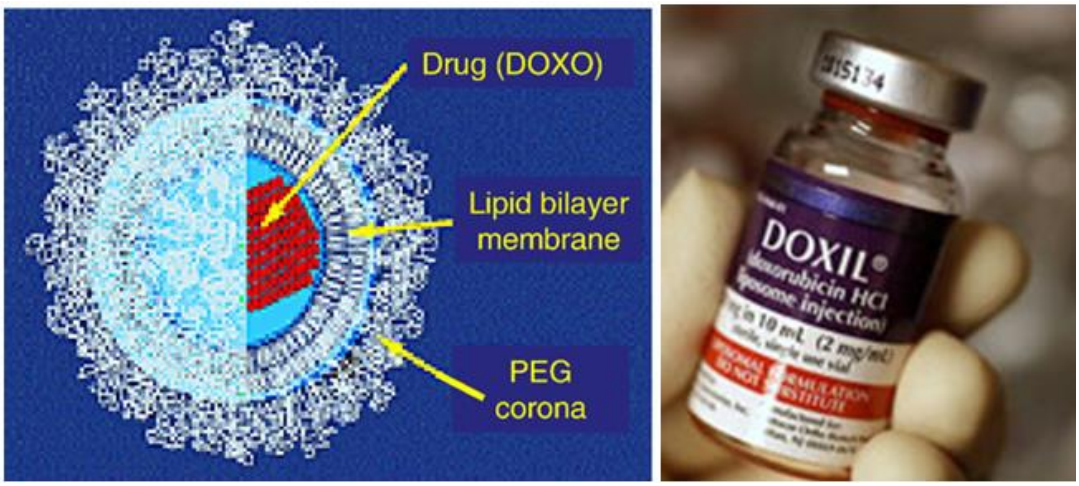

Figure 1.5. A PEGylated liposome containing the anti-cancer drug Doxorubincin was developed in the early 1990s at Liposome Technology, Inc. by Martin Woodle and Frank Martin. It is called "DOXIL" and was approved for clinical use in 1995. *(adopted from Hoffman et al. J. Controlled Release,* ***2008****, 132, 153-163).*

Several PEGylated therapeutics have reached up to clinical trials whereas few of the PEGylated lipid based carriers have been approved by FDA for cancer

treatment. Doxil (liposome encapsulated doxorubicin) was the first PEG-liposome based nano-medicine developed by Martin Woodle and Frank Martin to be approved by FDA in 1995 for treatment of AIDS-related Kaposi's sarcoma as well as ovarian cancer (see figure 1.5).[37,38,39]By encapsulation of DOX in PEGylated liposome, therapeutic index of doxorubicin was enhanced. The enhancement was attributed to the reduction in the cardiotoxicity upon encapsulationas compared to free DOX. Subsequently Doxil also improved pharmacokinetics and biodistribution of the drug thereby facilitating higher intratumoral accumulation and blood circulation half-life of DOX. Apart from Doxil, a number of other targeted nanosystems have also been approved by FDA for clinical trials such as MM-302, MCC-465, MBP-426, and SGT53.[40]

Despite theclinical validation of a number of liposome based products, there are several challenges associated with the liposome technology. The major reason which impedes the effective clinical translation of these carriers includes; (a) lower stability of liposomes, (b) lack of controlled release of the chemotherapeutic agent, (c) propensity of liposomal phospholipids to undergo oxidation, (d) faster disintegration of nano-carrier leading to burst release of encapsulated drug*in vivo,* (e) poor drug loading capacity, (f) poor compatibility with broad range of pharmaceutically active agents such as proteins and nucleic acids and (g) fast capture and clearance by RES or macrophages.[9,20,32,41,42,43] These limitations associated with the lipid-based carriers led to the incarnation of polymer based therapeutics. Therefore, with the aim of achieving higher stability *invivo,* polymer based nano-carriers were fabricated.[9]

1.3. Polymeric drug carriers

With the commencement of use of polymers for devising nano-carriers tremendous progress has been made in the field of drug delivery.Apart from being biodegradable and biocompatible,[44] polymers provide wide range of opportunities to modulate the properties of drug delivery systems with respect to achieve either spatial or temporal control of drug delivery.Spatial control typically includes

implantation of the drug carrier at the desired site.[45] Whereas, in case of temporal control the drug delivery system or the drug carriers release the loaded cargoes over an extended duration of time with a pre-determined rate during treatment.[46] Thesustained release of drug molecules from temporal controlled devices is achieved by either (a) delayed dissolution or (b) by controlling the diffusion rate of the drug molecule or (c) by controlling the flow of drug solutions.[2] The various mode of drug release in case of temporal control is shown in figure 1.6.

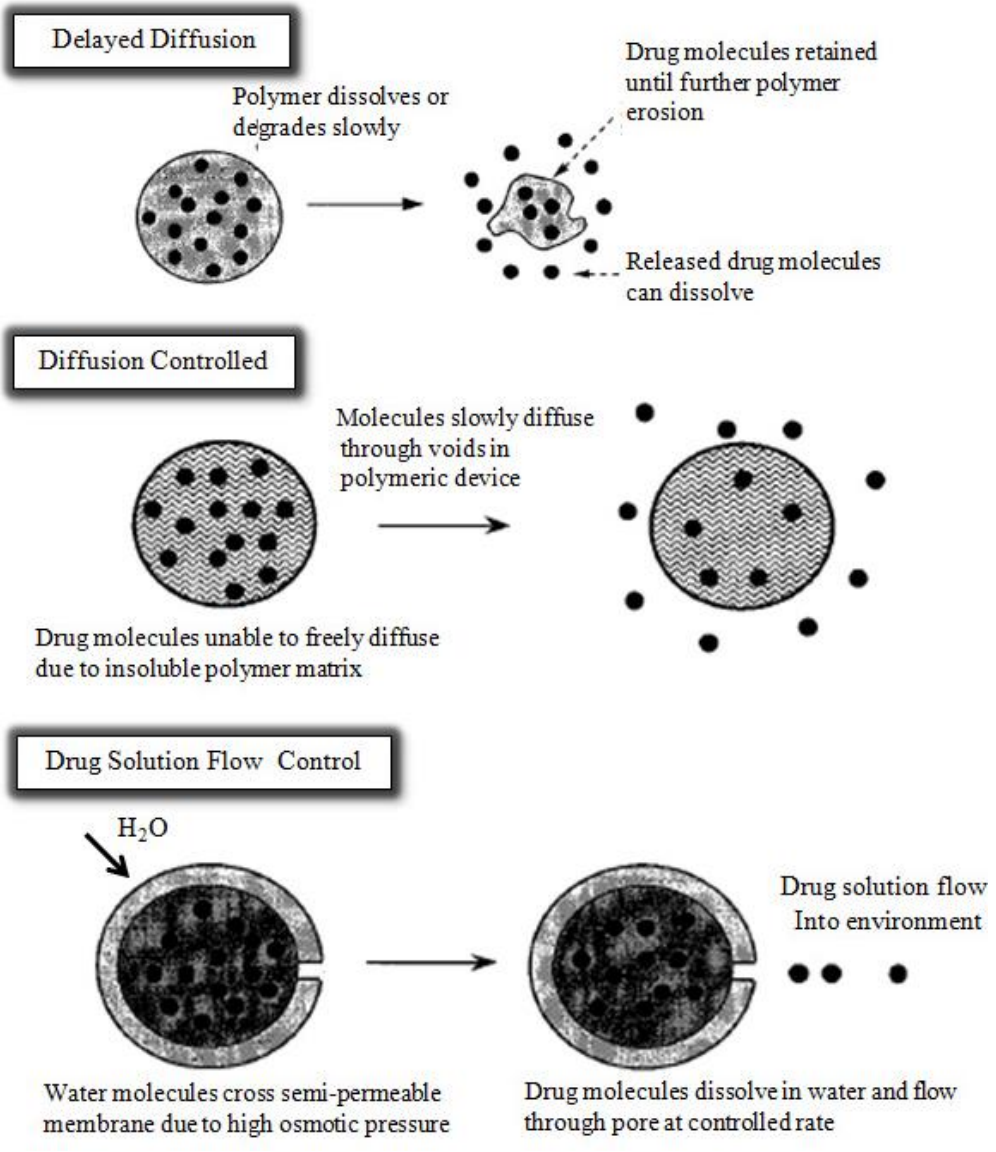

Figure 1.6.*Examples of mechanisms of temporal controlled release (adopted from Uhrich et al. Chem. Rev.**1999**, 99, 3181-3198).*

In case of delayed dissolution the exposure rate of drug molecules to the surrounding aqueous environment is generally decelerated. This is achieved by coating the drug delivery system by a polymer which dissolves at slower rate as compared to the drug molecule. On the other hand, in diffusion controlled systems cross-linked polymeric hydrogel or polymeric matrix is employed which act as a diffusion barrier for the embedded drug molecules.[2] Likewise, the devices which control the flow of drug solution consist of chambers made up of semi-permeable polymers with drug solution inside. The drug molecules leach out from these chambers through the pores present in the polymer which in turn lowers the rate of drug release. In other words, in all the three modes of drug release from the temporal controlled devices, the polymer acts as a barrier thereby restricting the drug molecules from being exposed to aqueous environment. Thus, the temporal controlled devices use polymers in order to protect the drug molecules from the surrounding aqueous environment for a pre-determined period of time.[2]

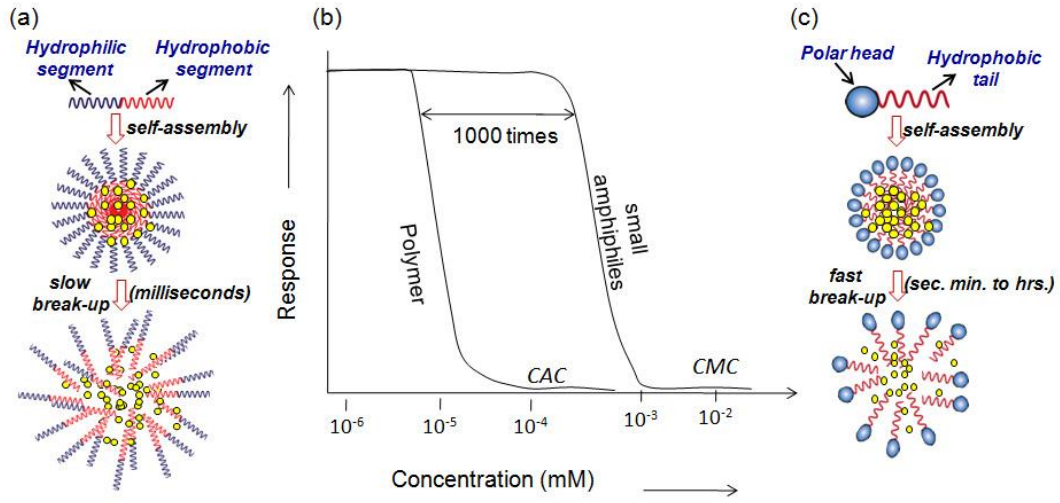

Figure1.7.*(a) Drug release rate of polymeric amphiphile based drug carriers (b)Comparison of CAC and CMC of polymeric and small amphiphile based drug carriers, respectively. (c)Drug release rate of low molecular weight amphiphile based drug carriers.*

Similar to temporal controlled devices which basically includes polymer matrix or cross-linked hydrogel for protection of drug molecules, spatial control

typically includes polymer-drug conjugates and colloidal carriers for controlled release of drug molecules. The colloidal carriers include polymeric cylindrical micelles, polymeric micelles and polymersomes.These polymeric carriers undergo preferential accumulation in tumor tissues through EPR effect taking the advantage of leaky and defective architecture of blood vessels.[47]

One of the major advantages of these polymeric drug carriers over small amphiphile based nano-carriers is the higher *in-vivo* stability of these macromolecular drug carriers.The minimum concentration of polymeric amphiphile required for the formation of self-assembled nano structures is 1000 times lower as compared to small amphiphiles. In other words, the large CMC (critical micellar concentration) values of small amphiphile based nano-carriers leads to their poor thermodynamic and kinetic instability as compared to polymer based nano-carriers[48,49,50](see figure 1.7).As a result, the polymeric drug carriersdisassemble at a slower rate as compared to surfactant based nano-carriers. Thus, the macromolecular drug carriers need hours to disintegrate in to individual components whereas low molecular weight based carriers fall apart within few seconds (see figure 1.7). As a consequence, the loaded cargoes releases out from the polymeric carriers in a progressive manner. On the other hand, fast disintegration of small molecule based carriers leads to burst release of the loaded cargoes (see figure 1.7). Thus, polymeric micelles are more stable as compared to small amphiphile based nano-carriers.[51,52]

In order to achieve temporal and spatial controls, variety of other polymeric drug delivery systems such as implantation devices, tablets, microspheres, films etc have also been fabricated.[53]The polymers employed for design and fabrication of above mentioned drug delivery systems are typically classified into two categories: synthetic and natural polymers. Both synthetic and natural polymers have gained tremendous importance in the field of drug delivery. Synthetic polymers include polyester, polyanhydrides and polyamides. Polyester consists of poly (lactic acid), poly(glycolic acid), poly(hydroxy butyrate), poly(ε-caprolcatone)etc. While, poly(sebacic acid), poly(adipic acid) and poly(terpthalic acid) are examples of

poly(anhydrides).[54] Likewise, polyaminoacids and poly(imino carbonates) comes under polyamides. On the other hand, natural polymers consist of polysaccharides and protein based polymers which generally comprises of collagen, albumin, gelatin, agaraose, alginate, dextran, chitosan and hyaluronic acid etc.[54]

1.4. Polymer Architecture for Drug Delivery

The efficacy of the polymeric self-assembled structures formed either by synthetic or natural polymers depend on the polymer architectures. Polymer architecture plays a crucial role in determining the physicochemical properties of the polymer chains which in turn governs the targeting ability and accumulation efficacy of nano-carriers in tumor tissues.At the same time it also influences the drug loading efficiency, drug-release rate, biodistribution as well as interaction of drug molecules with specific tissue or cells *in-vivo*. On the grounds of polymer architecture the polymers employed for formulation of drug carriers are basically classified into three broad categories (a) linear polymers, (b) branched polymers and (c) cross-linked polymers.[55]The various polymer architectures for drug delivery application are shown in figure 1.8.

A linear polymer generally comprises water soluble polymers which can be homopolymer, diblock copolymer, triblock copolymer, random copolymer, or alternating copolymer (see figure 1.8). Typically, drug molecules are conjugated to these polymers leading to the formation of polymer-drug conjugate. In other words, these linear polymers are employed as a drug carrier in form of polymer-drug conjugate.[55]Polymer drug-conjugates comprises of polymer backbone attached to drug moiety through a cleavable linkage.The idea of utilizing polymer-drug conjugates for delivering drugs at the diseased site was commenced by Ringsdorf in 1975.[10,56,57]

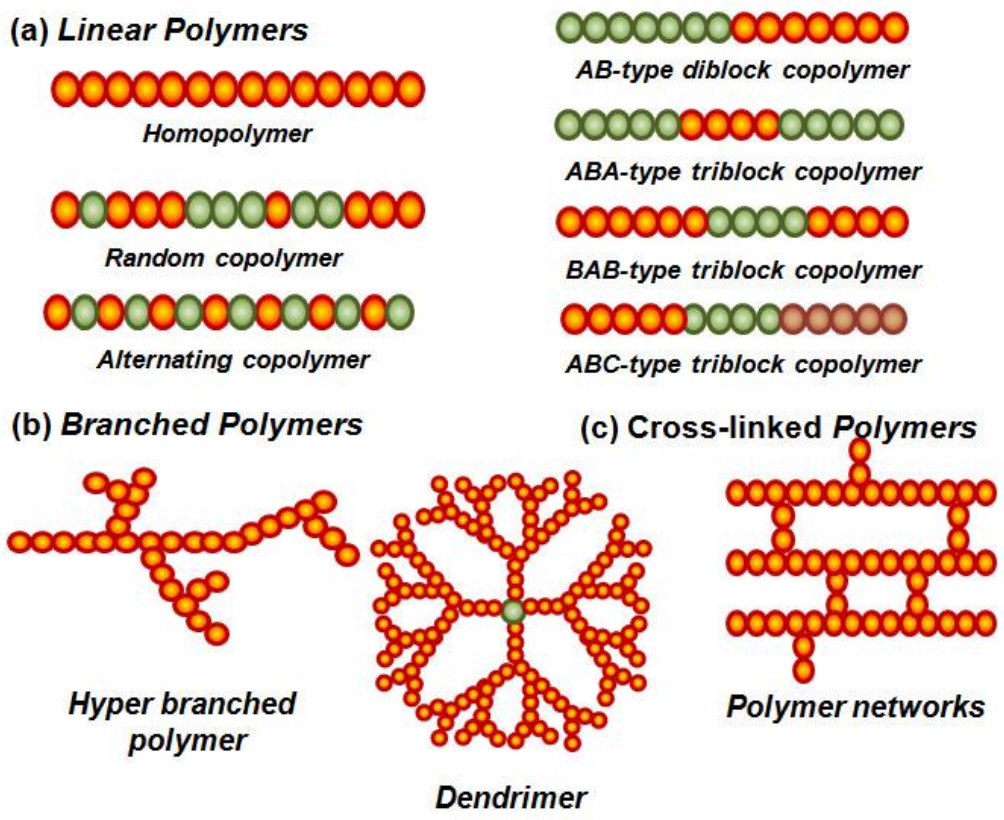

Figure 1.8.*Polymer architectures: (a) linear polymers, (b) branched polymers, and (c) cross-linked polymers (adopted from Qiu et al. Pharm. Res.* ***2006****,23,1-30).*

The Ringsdorf model containing drug molecule attached to a macromolecule through a spacer having cleavable linkage along with solubilising and targeting moiety is shown in figure 1.9a. Numerous polymer-drug conjugates have been developed till date and almost all are derived from the Ringsdorf model. Various examples of linear polymers which are being used for delivering drug at the diseased site via drug conjugation comprises of vinyl polymers, poly γ(amino acids), polysaccharides, proteins and poly (ethylene glycol). Considering vinyl polymers, *N*-(2-hydroxypropyl methacrylamide) (HPMA) is one of the most extensively studied polymer. Several HPMA copolymer based polymer-drug conjugate have even reached clinical trials. PK1, which consists of HPMA as polymer backbone conjugated to anti-cancer drug doxorubicin was the first polymer-drug conjugate to enter phase I clinical trials in 1994[58] (see figure 1.9b).Apart from HPMA based

polymer-drug conjugate, PEG and poly γ (glutamic acid) conjugates have also been clinically evaluated. Several polymer-drug conjugates which are in phase I/ II/ III clinical trials are listed in table 1.1.

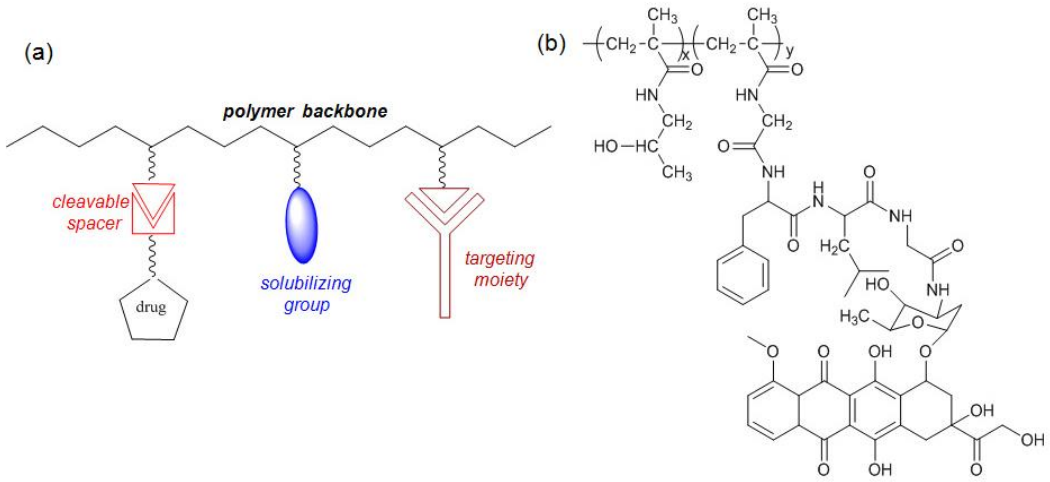

Figure 1.9. *(a)The Ringsdorf model for drug delivery (adopted from Haag et al. Angew. Chem. Int. Ed.* ***2006****, 45, 1198-1215) (b) Chemical structure of PK1 [poly {N (2-hydroxypropyl methacrylamide)}], the first clinically tested polymer-drug conjugate (adopted from Haag et al. Angew. Chem. Int. Ed.* ***2006****, 45, 1198-1215).*

Block copolymers are classified as AB type diblock copolymer, ABA or BAB type triblock copolymers, where A and B represent two different blocks[59] (see figure 1.8). These block copolymers have tendency to further self-assemble into various kinds of nanostructures such as polymeric micelle, polymeric cylindrical micelle (filomicelles) or polymersomes.[60] One of the most commonly used polymers for the fabrication of these colloidal particles is amphiphilic block copolymers which consist of both hydrophilic and hydrophobic segments.[61] The formation of either polymeric micelle or filomicelles or polymerosomes upon self-assembly of amphiphilic block copolymers is governed by the ratio of the hydrophilic and hydrophobic segment in the copolymer structure. Discher *et al.* has put forward an empirical rule for determining the type of self-assembled structure formed, from the ratio of hydrophilic and hydrophobic segment. According to this unifying rule, amphiphilic block copolymers having hydrophilic segment i: e $f_{\text{hydrophilic}} \approx 35$ %forms polymersome. On the other hand, $f_{\text{hydrophilic}} < 50$ %leads to formation of filomicelles

while block copolymer with $f_{hydrophilic} > 45$ %self-assemble in to polymeric micelles.[62,63] These nanostructure based drug delivery system came into picture in late 1980s and early 1990s when Kazunori Kataoka, Teruo Okano and Masayuki Yokoyama reported the first PEGylated polymeric micelle formed from PEG-P-asp {poly (ethylene oxide)-b-poly(α,β –aspartic acid)}diblock copolymer.[64,65,66] On the other hand, at the same time Alexander Kabanov also reported PEO-PPO-PEO tri-block based drug loaded PEGylated polymeric micelle which was termed as "Pluronics P-85"[67] (see figure 1.10).

Table 1.1. Drug-polymer conjugates in clinical trials*(adopted from Haag et al. Angew. Chem. Int. Ed. **2006**, 45, 1198-1215).*

Compound	Drug	Polymer	Cancer	Status
PK1	Doxorubicin	HPMA copolymer	Breast and lung cancer	Phase II
PK2	Galactosaminated doxorubicin	HPMA copolymer	Hepatocellular Carcinoma	Phase I discontinued
PNU-166945	Taxol	HPMA copolymer	Solid tumors	Phase I completed
AP5346	Diammineplatinum (II)	HPMA copolymer	Ovarian and colorectal cancer	Phase I completed
Prothecan	Camptothecin	PEG conjugate	Lung, ovarian, breast and esophageal cancer	Phase II

Since the ground breaking invention of PEGylated polymeric micelle by Katoka, Okano and Yokoyama, various polymerization techniques such as radical, anionic, cationic, photo or group transfer polymerization have been exploited for synthesizing variety of amphiphilic block copolymers. This in turn has led to development of a number of polymeric micelle for delivering variety of hydrophobic drugs such as anticancer, antibacterial, antiviral, anti-inflammatory etc. At present,

three major types of polymeric micelles are known (a) conventional micelles, (b) drug-conjugated micelles and (c) polyion complex micelles.[55] For construction of hydrophobic segment of the conventional micelles poly (amino acids), poly (ε-caprolactone) (PCL), polylactide (PDLLA), poly (lactide-co-glycolide) (PLGA) are the most extensively studied hydrophobic polymers.[68] On the other hand, PEG, poly(*N*-vinyl pyrrolidone) (PVP), poly(*N*-isopropyl acrylamide) (PNIPAM), PPHPMA are utilized as shell forming blocks.[68] Among all the hydrophilic polymers, the hydrophilicity, low immunogenicity, non-toxicity and flexibility of the PEG polymer have led to its massive application as hydrophilic block. For instance, PEG-*b*-PCL, PEG-*b*-PLGA, and PEG-*b*-PDLLA were synthesized for loading and delivering of paclitaxel, the anti-cancer drug[69] (see figure 1.11). Typically, these conventional micelles physically entrap the drug molecules which are then further released by diffusion mechanism. However, the dynamic nature of the polymeric micelles leads to instabilities under certain conditions such as high temperature, low concentration etc. Thus significant interest has been increased in the stabilisation of polymeric micelles by either cross-linking the outer hydrophilic shell or the inner hydrophobic core.[70] Typically, these polymeric micelles are stabilised by incorporating either polymerizable or photo/UV crosslinkable groups.[71-73] Incorporation of difunctional cross-linking reagents or external stimuli is alternative cross-linking strategy. [74]

In case of drug-conjugated micelle, unlike the conventional micelle, the drug molecules are loaded in to the hydrophobic core of the micelle by using electrostatic interaction or ligand exchange mechanism. For constructing such hydrophobic core of the micelle through various polymer-drug interactions, cationic polymers such as PEG-*b*-poly(L-lysine)(PLL), PEG-*b*-poly(dimethylaminoethyl methacrylate) (DMAEMA), PEG-*b*-poly(aspartic acid) (PEG-*b*-PAsp)[75,76] and PEG-*b*-polyγ (glutamic acid) (PEG-*b*-PGlu)[77,78] are mostly utilized. Metal-complex based anti-cancer drugs such as cisplatin (*cis*-diamminedichoroplatinum(II)) and DACHPt (dichloro(1,2-diamino-cyclohexane)platinum(II)) are incorporated into the hydrophobic core of these micelles through ligand exchange, which generally occurs

between carboxyl group of the poly (amino acid) blocks and the chlorine or oxygen present in the platinum complex[79](see figure 1.11).

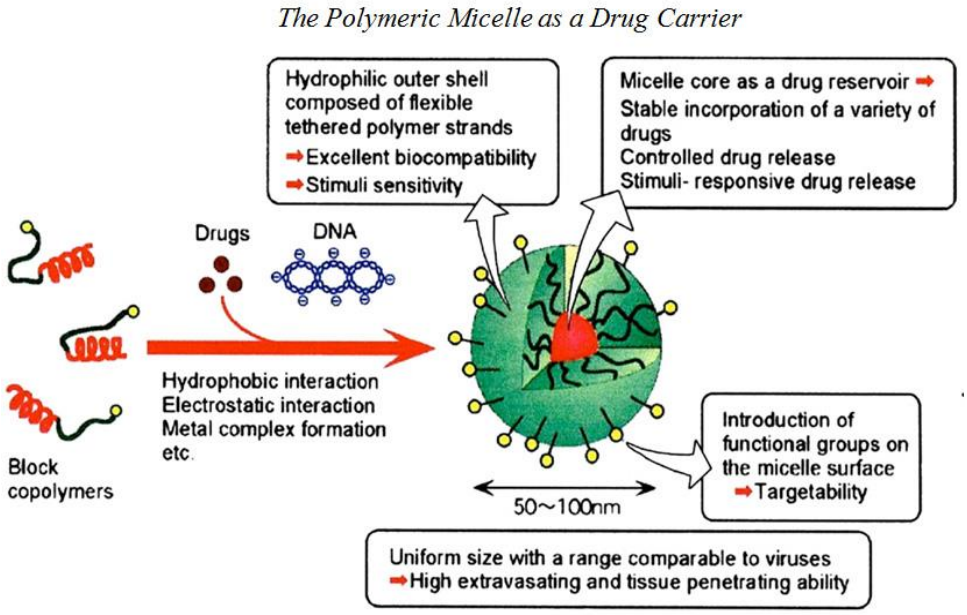

Figure 1.10. *The PEGylated polymeric micelle developed by Kazuroni Kataoka, Teruo Okano and Masayuki Yokoyama in the late 1980s and early 1990s (adopted from Hoffman et al. J. Control. Rel.**2008**, 132, 153-163).*

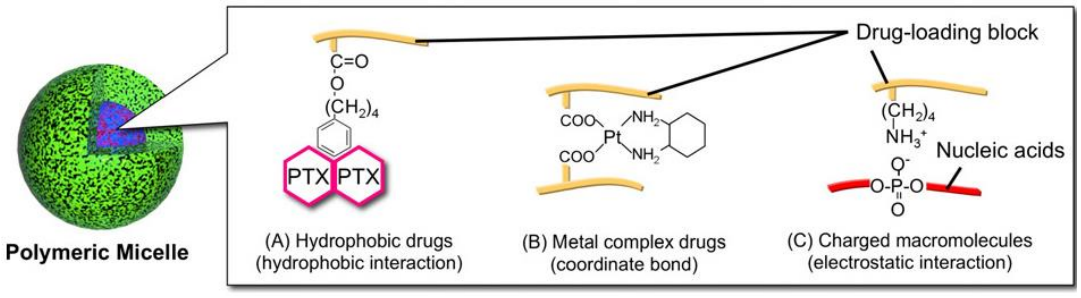

Figure 1.11. *Examples of drug encapsulation in polymeric micelle (adopted from Miyata et al. J. React. Function.Polym.**2011**, 71, 227-234).*

Apart from hydrophobic or metal-complex based drugs, polymeric micelles are also being employed for delivering proteins, plasmid DNA and even short interfering RNA (siRNA).[80]Polyion complex (PIC) micelles are typically employed for encapsulation of these nucleic acids or proteins. The hydrophobic cores of these

PIC micelles are generally formed of cationic polymers.[81] Polyethyleimine (PEI) and Poly (L-Lysine) PLys, are widely used cationic polymers for the formation of positively charged hydrophobic core of the PIC micelles.[80] The sequestration of the nucleic acids in the hydrophobic core of the PIC micelle occurs through electrostatic interactions between negatively charged phosphate groups of the nucleic acid and the positively charged hydrophobic core of the micelle (see figure 1.11). The first PIC micelle formed from (PEG-*b*-PAsp) and (PEG-*b*-PLL) block copolymers were reported by Kataoka and Harada.[82]

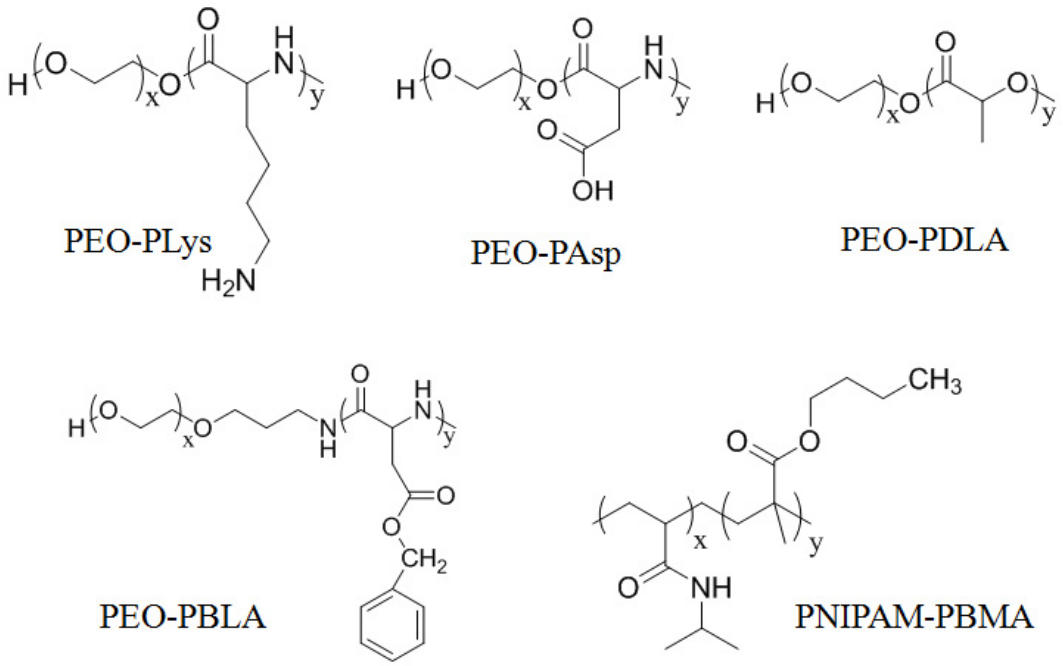

Figure 1.12. *Examples of various amphiphilic polymers forming micelle and capable of loading chemotherapeutic agents.*

In addition to above mentioned block copolymers, several other amphiphilic block copolymers have also been exploited for loading variety of hydrophobic drugs or nucleic acids or proteins.[83] Various amphiphilic block copolymer based polymeric micelle used for loading different chemotherapeutic agents are listed in figure 1.12. From the figure 1.12, it is evident that from past few decades a range of amphiphilic block copolymers have been synthesised and the micelles formed from these block copolymers are being used for encapsulation of various hydrophobic drug

molecules, plasmid DNA, metal complex based drugs as well as various inhibitors. Among the various drug loaded polymeric micelle developed, a few promising candidates currently are in different phases of clinical trials.[84]The lists of polymeric micelle loaded with different drugs which are being clinically evaluated are given in table 1.2.

Table 1.2. Drug loaded polymeric micelles in clinical trials*(adopted from Matsumura et al. Adv. Drug Del. Rev. **2008**, 60, 899-914).*

Compound	Drug	Block Copolymer	Cancer	Status
SP1049C	Doxorubicin	PEG-PPO	Adenocarcinoma of oesophagus	Phase III
NK105	Paclitaxel	PEG-Polyaspartate	Colon and pancreaticcancer	Phase II
Genexol-PM	Paclitaxel	PEG-Polylactide	Metastatic breastcancer	Phase II
NK012	SN-38	PEG-Polyglutamate	Colon cancer	Phase II
NC-6004	Cisplatin	PEG-Polyglutamate	Lung and gastrointestinal cancer	Phase II

Although polymeric micelles have reached clinical trials, there are few intrinsic limitations associated with them. For instance, polymeric micelle can encapsulate only hydrophobic drug. At the same time, these polymeric micelles cannot facilitate dual drug loading. Polymersomes, having thick hydrophobic membrane and aqueous interior lumen also formed from amphiphilic block copolymers[85] can overcome these limitations. In other words, the hydrophobic membrane and hydrophilic core of the polymersomes assists in loading both hydrophobic and hydrophilic drug molecules independently as well as simultaneously. Ahmed *et al.* has reported encapsulation of hydrophilic drug

doxorubicin as well as hydrophobic drug paclitaxel in the inner hydrophilic lumen and outer hydrophilic shell of the PLA-copolymer based polymersome. This cocktail of paclitaxel and doxorubicin has shown better tumor regression as compared to drug alone.[86] Thus, the dual drug loading in polymerosome seems to be a promising strategy for targeting tumor tissues. However, many of these drug loaded polymeric vesicles or polymersomes are still at *in vivo* stage, only few of them have entered the clinical trials.

Polymers possessing branching points or more than two end groups are termed as "branched polymers". In general, these branched polymers basically includes: hyperbranched polymers, star-shaped polymers, star-shaped block copolymer, dendrimers and graft polymers[55,87] (see figure 1.13).These advanced polymeric architectures were capable of loading and delivering various anti-cancer, antiviral chemotherapeutic agents. However, at present the self-assembled structures formed by the above mentioned branched polymers investigated are either at *in vitro* or at *in vivo* stage.

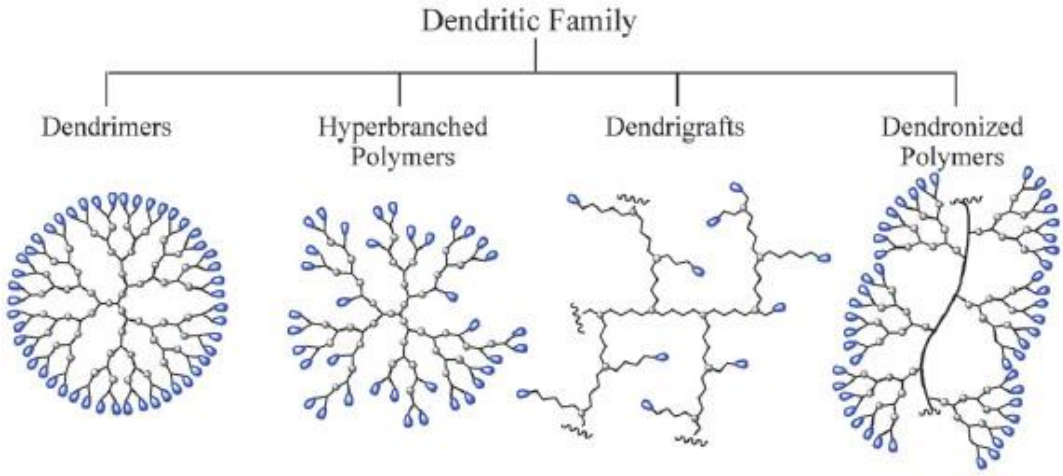

Figure 1.13. *Schematic representation of sub-classes of dendritic family (adopted from Carlmark et al. Chem. Soc. Rev.***2009**, 38, 352-362).

In order to translate these polymeric materials based drug carrier in to clinical level requires tuning of architecture of polymeric nano-carriers or polymers for increasing their efficiency regarding the release of their payload exclusively at the site of action.[55]Among the various nanostructures based on amphiphilic copolymers,

polymeric micelles and polymerosome proved to be potent polymeric carriers and large number of these drug loaded polymeric carriers are being clinically evaluated. However, these nanocarriers belong to first generation where the drug molecules are released gradually over a period of time, but release of the drug molecules from these polymeric carriers generally follows Fickian diffusion which is non-specific to cells, tissues or organs.[68]Also, the function of these controlled release systems gets hampered due to metabolic changes occurring in the living system. This led to the incarnation of stimuli responsive polymeric drug carriers also known as 'smart' or 'intelligent' drug delivery systems.

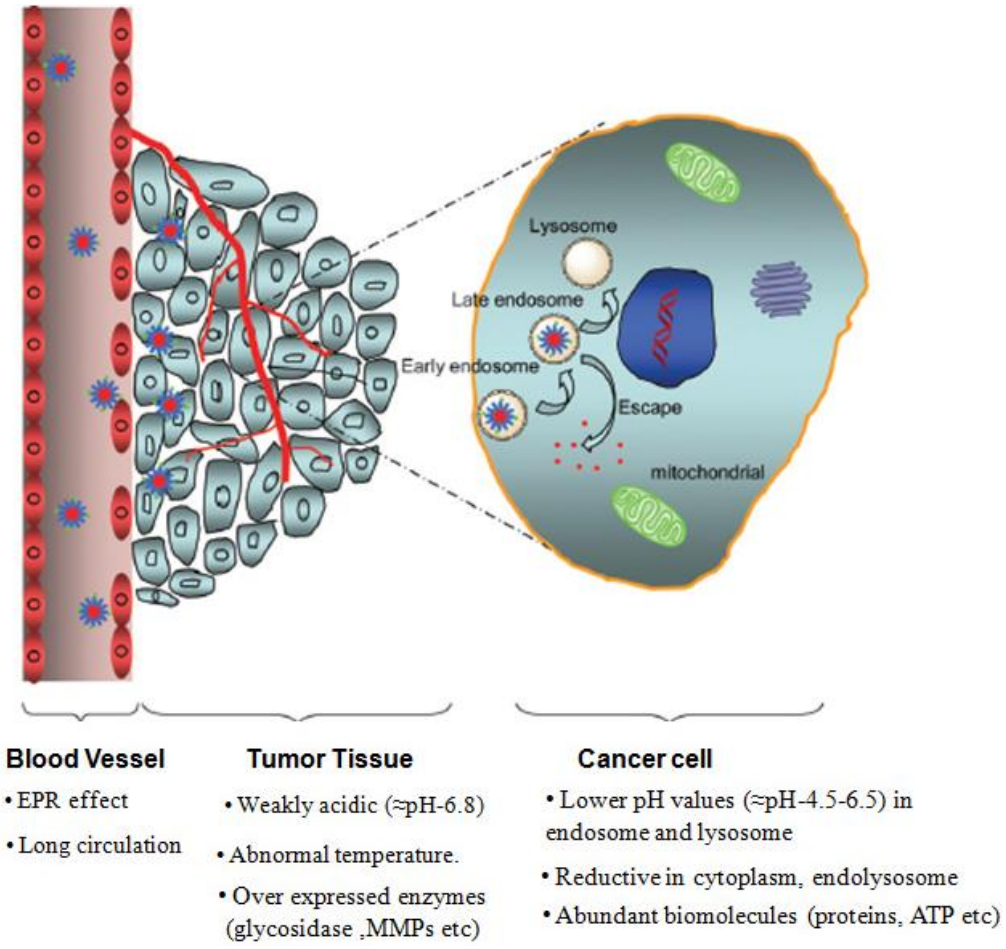

Figure 1.14. *Schematic diagram depicting the stimuli-responsive behavior of block copolymer nanoassemblies in response to a range of stimuli associated with tumor tissues and intracellular microenvironment (adopted from Ge et al. Chem. Soc. Rev.* ***2013****, 42, 7289-7325).*

1.5. Stimuli -responsive Drug Carriers

The macromolecular drug carriers capable of releasing encapsulated drugs or therapeutic agents in response to the changes in their surrounding microenvironment or in other words, the nanocarriers exhibiting environment-responsive behavior are termed as "stimuli-responsive" or "smart" drug carriers.[88-90] The introduction of these second generation nanocarriers into the field of drug delivery has accelerated the site-specific triggered drug release in synchronization with the surrounding environment i.e. the tumor-microenvironment upon being administered. In order to amplify the drug efficacy, these stimuli-responsive nano-sized vehicles are fabricated by utilizing the unusual physicochemical environment associated with tumor tissue (extracellular level) and cancer cell (intracellular level). Extracellularly, tumor tissues possess low pH (6.1 to 6.8),[91] abnormal temperature gradients,[92] over expression of enzymes,[93] reductive environment[94]and hypoxia condition as compared to normal tissues.[95] Likewise, cancer cells are allied with more acidic environment in endosomes and lysosomes (pH = 4.0-6.5), elevated levels of cysteine or glutathione in cytoplasm and endolysosomes, higher concentration of H_2O_2 in mitochondria as well as increased level of other biomolecules like proteins and ATP etcas compared to normal cells[92] (see figure 1.13).These unusual microenvironments of tumor tissues act as a trigger for releasing the drug molecules at the desired site. Therefore, the block copolymers are engineered with stimuli-responsive modules associated with tumor tissue and cell which in turn boosts the targeting efficiency of the nanovehicles and therapeutic efficacy of the drug by elevating the drug concentration both in tumor tissues and in intracellular compartments.

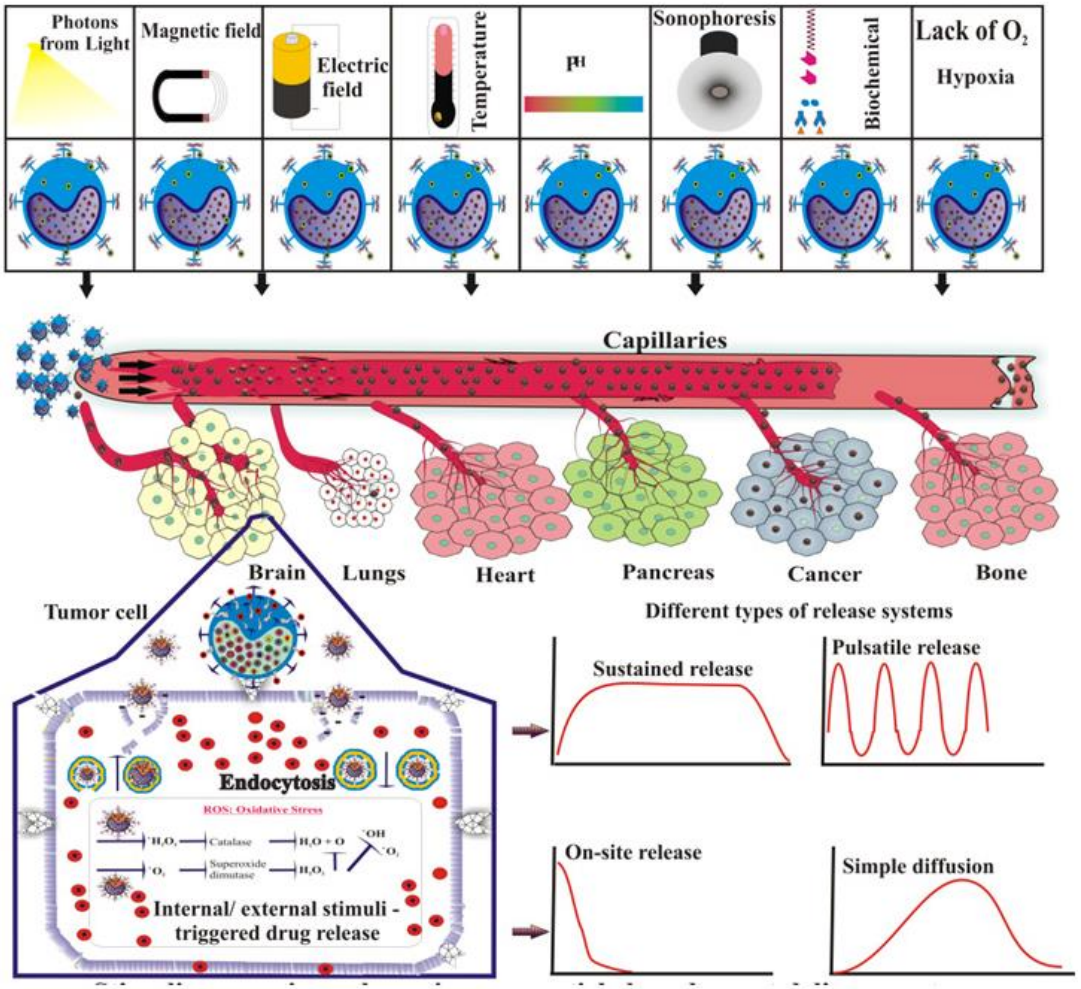

Figure 1.15. S*timuli-responsive polymer nanoassemblies in response to a range of internal and external triggers (adopted from chapter 8 of book with title "Application of Nanotechnology in drug delivery" written by Beenet et al.).*

Apart from the stimuli associated with tumor microenvironment, release of drug molecules at the diseased site from the block copolymer self-assembled nanostructures can also be achieved in response to external local environmental stimulus such as ultrasound, magnetic field, electric field etc.[3,96,97,98]The various triggers used for releasing the therapeutic agents from this smart drug delivery system in controlled manner to a specific site or organ are categorized under various classes such as physical, chemical, electrical, biochemical, or environmental (see

figure 1.13).Responses to these stimuli are expressed in several forms: such as changes in the size, shape, surface characteristics, solubility, sol-gel transformation and degree of intermolecular association[99,100,101] (see figure 1.13). The physical or chemical changes exhibited by these stimuli responsive polymers in response to diverse type of external or internal stimuli are typically reversible in nature. These unique features of these smart polymers have made them one of the most attractive candidates for targeted drug delivery.

Among several stimuli used for drug delivery application, (a) pH,(b) temperature and (c) enzyme have been exploited extensively for fabrication of trigger-responsive drug carriers.Variety of amphiphilic block, random block and graft copolymers sensitive to temperature and pH have been synthesized till date. Also, combination of more than one stimuli in one single system for efficiently delivering dug in tumor microenvironment has become more popular.

1.5.1 pH-responsive Drug Delivery System

A plethora of pH-responsive polymeric carriers have been fabricated with aim of achieving on-site delivery of therapeutic agents in response to acidic nature of tumor microenvironment. The low pH of tumor microenvironment is consequence of irregular angiogenesis which in turn leads to deficiency of nutrition and oxygen in rapid and fast dividing cancer cells. As a result; tumor cells adopt glycolysis pathway for gaining energy and nutritionresulting in accumulation of lactic acid and other acidic metabolites in tumor interstitium.[91,102] This causes slight variation in pH of tumor tissues (6.5-7.2) as compared to normal tissues(7.4).[103] Apart from extracellular tumor microenvironment, there exists a large variation in the pH of intracellular compartment of tumor tissues also. For instance pH of early endosome comes in the range of 6-6.5; of late endosome varies from pH 5-6 and of lysosome is from pH 4.5-5.[96]This gradient of pH which exists from early endosome to late endosome to lysosome has also been exploited for release of loaded cargoes from nanocarriers in intracellular compartments upon being endocytosed.

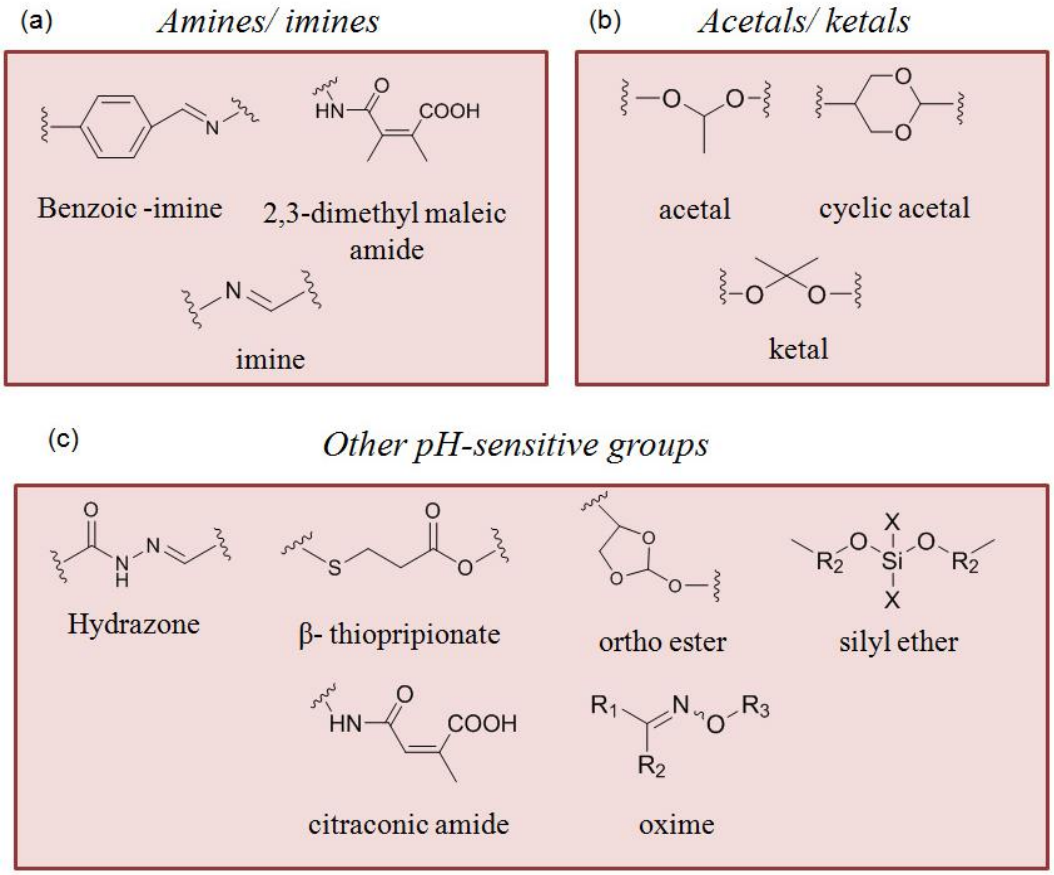

Figure 1.16.*Tumoral and intracellular pH responsive polymers containing pH reactive chemical bonds (a) amines/ imines, (b) acetals/ ketals and (c) other pH sensitive bonds (adopted from Ge et al. Chem. Soc. Rev.* ***2013****, 42, 7289-7325).*

In order to trigger release of therapeutic agents in tumor tissues in response to acidic tumor microenvironment, pH responsive polymeric carriers were routinely designed using two strategies:[104] (a) insertion of acid-labile chemical linkages such as imine, acetal, hydrazone etc in the polymer backbone or while conjugating drug molecule with the polymer, that gets ruptured or cleaved in the acidic environment, thereby delivering the drug,[105] and (b) design of polymers with ionisable groups i :e utilization of cationic or anionic polymers which undergoes conformational and/or solubility changes in response to environmental pH variation, thereby releasing and increasing local drug concentrations.[106] The various acid-sensitive bonds used for design of pH responsive polymeric drug carriers[89,92]are shown in figure 1.16. These

pH-responsive bonds are either cleavable in tumoral extracellular acidic condition or in intracellular compartments such as endosome or lysosome.[92]These linkages (see figure 1.16) are either incorporated in the polymer backbone, thereby forming polymeric backbone responsive scaffolds or they are used for conjugation of drugs to the polymer backbone. Generally, chemotherapeutic agents are conjugated to the functional group of polymers using these acid-sensitive linkages which upon alteration in pH of the surrounding environment getscleaved and the drug molecules get released at the desired sit.[107,108]

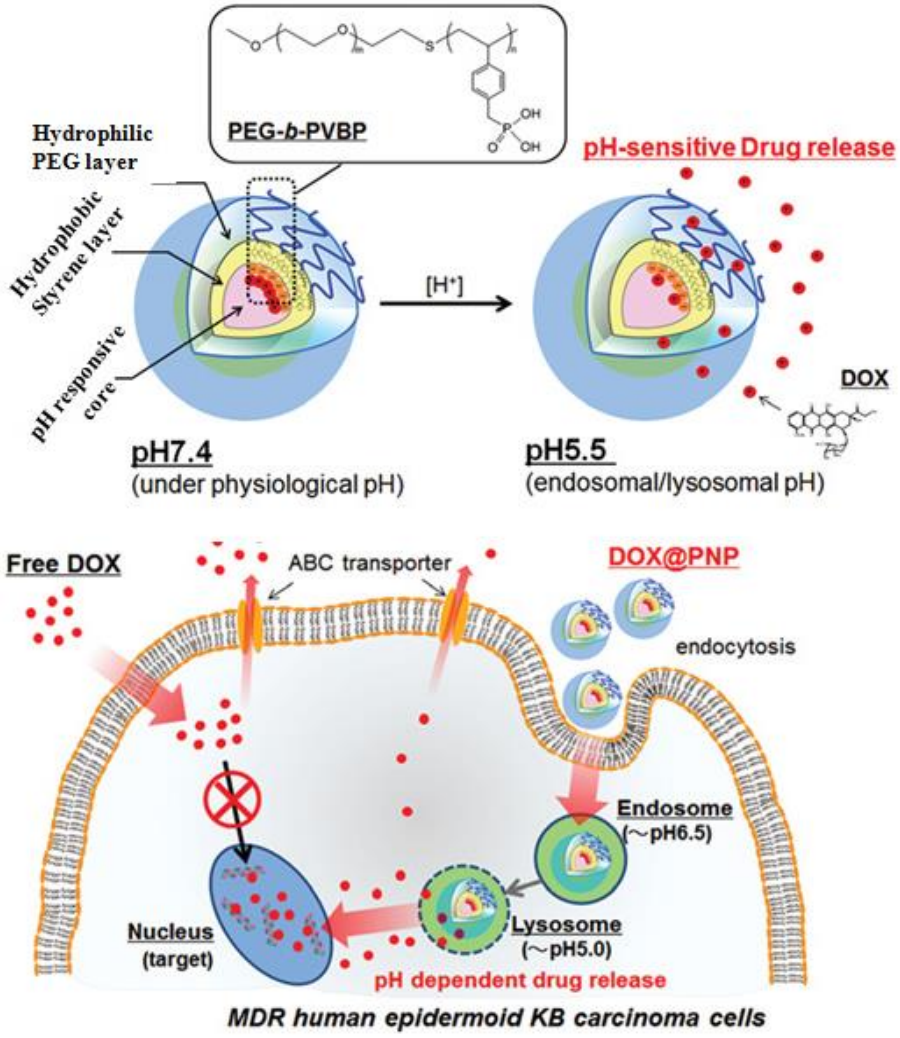

Figure 1.17. *Schematicillustration of pH-responsive polymer nanoassemblies inintracellular compartments (adopted from Kamimura et al. Biomater. Sci.* ***2013****, 1, 361-367).*

On the other hand, the most commonly used pH- tunable moieties for fabrication of pH-responsive particles are carboxyl groups and tertiary amine group. These groups undergo protonation-deprotonation phenomena thereby altering the hydrophobicity/hydrophobicity of the polymers.[109,110,111] Kamimura *et al.* has recently reported a poly(ethylene glycol)-b-poly(4-vinylbenzylphosphonate) block copolymer where phosphonate group acts as an ionisable moiety, which undergoes protonation under acidic pH conditions similar to late endosome/lysosome (see figure 1.17).As a result, the anti-cancer drug (DOX) encapsulated in the inner core is released out in the cytosolic compartment.[112]

1.5.2. Enzyme-responsive Drug Delivery System

Incorporation of biochemical stimuli or enzyme-responsive unit in macromolecules has become a developing arena in the field of stimuli responsive nanomaterials.[113]Since enzymes play a crucial role in various biological pathways, several diseases are associated with the dysregulation of enzymatic activity and its expression. In other words, numerous diseased states lead to over expression of enzymes.[114] Also, enzymes are highly efficient and selective towards specific substrates.[115] Thus, the nanocarrier responsive to enzyme will undergo site-specific enzymatic cleavage in order to release its payload such as chemotherapeutic agents, protein, gene etc.[116] Therefore, enzyme has become one of the most promising triggering motifs. Numerous enzymes are over expressed in case of tumors. For instance, carboxylesterase, matrix metalloproteases (MMP-2 and MMP-9), plasmin, cathepsin D, cathepsin B, β-glucuronidase etc are few enzymes that are found to be over expressed in cancer cells.[89,117] The unit susceptible to these enzymes are employed for either linking the drug and the macromolecule or they are incorporated in the polymer backbone. In view of fabrication of enzyme-responsive polymeric scaffold, Graaff *et al.* has recently synthesised pOEGMA-*b*-peptide-*b*-pNIPAM triblock copolymer, which is thermo-responsive in nature as well as susceptible to matrix metalloproteases (MMP-2 and MMP-9).[118] Since the peptide is flanked in between the hydrophobic pNIPAM block and hydrophilic pOEGMA, the cleavage of

protease-specific peptide linkage in presence of MMP leads to shedding of pOEGMA corona. Thus, the nanocarrier undergoes disassembly in presence of enzyme. Similarly from our group, Pramod *et al.* has developed a polysaccharide (dextran) based polymeric vesicle, responsive to pH and enzyme (see figure 1.18). Both pH sensitive imine linkage and esterase enzyme responsive units were employed for connecting the hydrophobic segment to the hydrophilic dextran backbone. The polymeric vesicle successfully encapsulated the anti-cancer drug, DOX in its inner core. Further, the *in vitro* studies carried out in presence of esterase enzyme and pH (similar to tumor microenvironment) revealed that the physically encapsulated anti-cancer drug DOX from the polymeric vesicle leaches out 100%, thereby proving the vesicle to be promising candidate for drug delivery applications.[119]

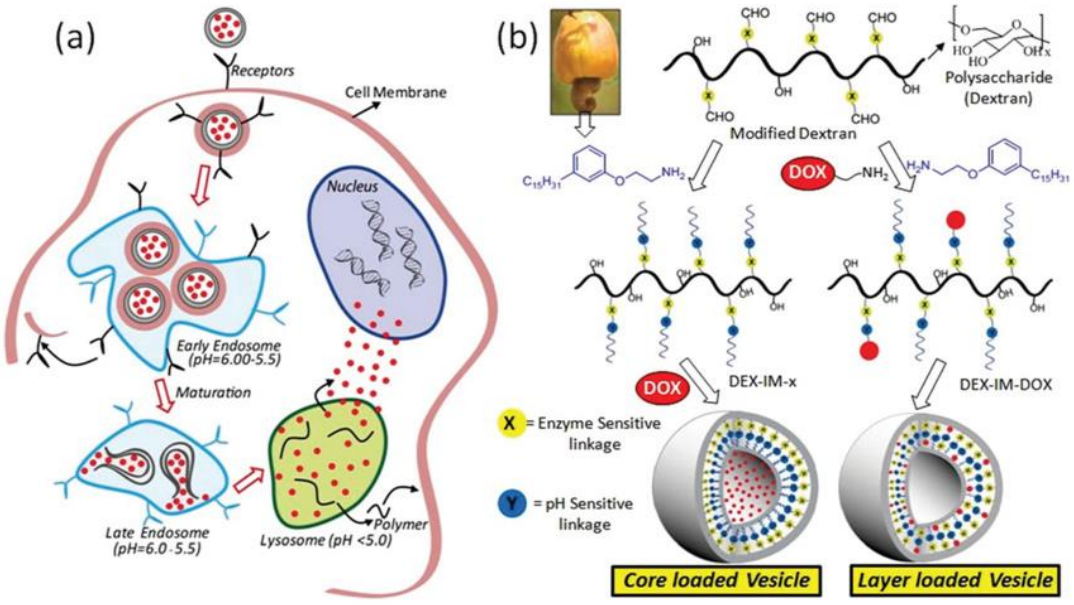

Figure 1.18. *Schematic representation of polymer–drug nanovesicle cellular uptake and their degradation in endocytic compartments. (b) Structural engineering of pH and enzyme dual responsive polysaccharide vesicles. (adopted from Pramod et al. Nanoscale* ***2015****, 7, 6636-6652).*

1.5.3. Thermo- responsive polymer drug delivery

For using temperature as a stimulus for facilitating temperature-triggered drug release several thermo-responsive polymers have been designed. These polymers undergo structural changes in response to temperature, which in turn leads to difference in their solubility in aqueous medium, thereby resulting in release of loaded cargoes. The temperature at which this phenomenon occurs is known as cloud point (Tcp) and the lowest cloud point is known as lower critical solution temperature (LCST).[120] Typically, this phase-separation phenomena occur as it is energetically more favorable. With increase in temperature the polymer undergoes phase separation which in turn leads the surrounding water less ordered. Thus, entropy of the system increases. In other words, due to higher entropy of the system at higher temperature the phase separation of the polymer is more favored. Thus, LCST is an entropically driven effect.

Because of this unique property, these thermo responsive polymers have attracted significant interest in the field of drug delivery in recent years. These structural changes in thermo-responsive polymers are either induced by external or internal heat source. In case of hyperthermia, such structural changes in thermo-responsive polymers are induced by three major external heat sources i.e. microwave radiation, infrared radiation and radio frequency.[121] Whereas, the intrinsic higher temperature of tumor tissues act as an internal heat source for generating such conformational or structural changes in the thermo-responsive polymers. From the past few years PNIPAM has been extensively studied thermo responsive polymers and it undergoes phase separation at ~32 ^{o}C. In other words, the LCST of PNIPAM polymer is ~32 ^{o}C[122] (see figure 1.19).

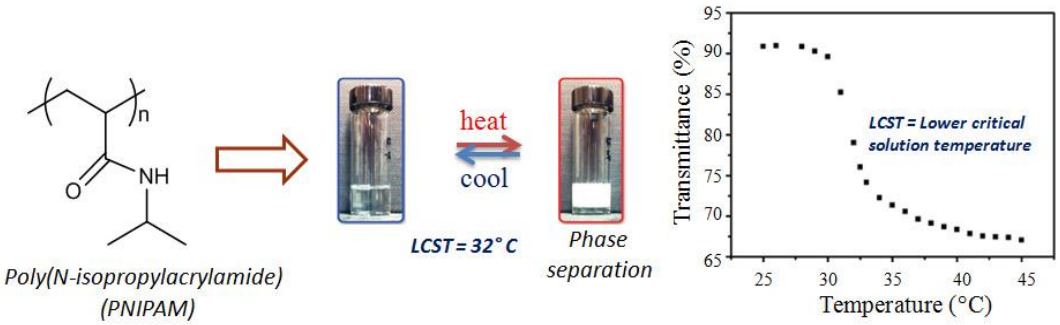

Figure 1.19.*Temperature induced phase-separation phenomena exhibited by PNIPAm polymer (adopted from Jin et al.Soft Matter**2012**, 8, 11809-11816.)*

Typically, these thermo-responsive polymers are completely soluble at temperature below LCST. The clear solution obtained at lower temperature is due to the fact that polymer chains are solvated by water molecules through weak hydrogen-bonding interaction. With the increase in temperature above LCST, the hydrogen-bond between polymer chains and water molecules becomes weak. Consequently, the water molecules are expelled from the vicinity of the polymers which in turn leads to partial dehydration of the polymer chains followed by precipitation or aggregation. Thus, the polymer which was hydrophilic in nature at lower temperature becomes hydrophobic at higher temperature. Therefore, the clear solution turns in to a turbid solution thereby initiating the phase-separation of polymer chains from the solvent at higher temperature.[123,124,125] The mechanism of phase-separation thermo-responsive polymers is shown in figure 1.20.

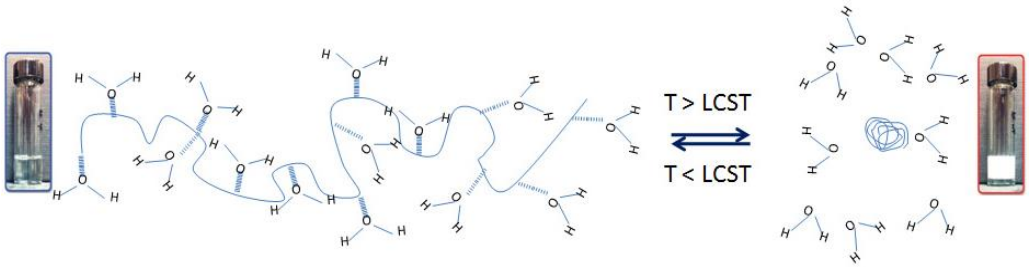

Figure 1.20. *Diagram illustrating the phase-separation mechanism of PNIPAM polymer in water (adopted from Pennadam et al.J of Nanobiotechnology, **2004**, 2, 1-8).*

With the aim of achieving such temporal control drug delivery, several attempts were made for synthesizing thermo-responsive polymeric nano-carriers, where drug release can be controlled by changing the temperature of the surrounding microenvironment. To design and develop such thermo-responsive nano-carriers PNIPAM has been extensively used as building blocks. Since LCST of PNIPAM falls around 32^{o}C, it has been copolymerised with other comonomers such as acrylic acid, methyl methacrylate, 2-hydroxy ethyl methacrylate, D, L-lactide etc in order to tune its LCST close to cancer tissue temperature (40-43^{o}C) (see figure 1.21). The copolymerisation resulted in construction of various PNIPAM based diblock, triblock or random copolymers. Among various copolymers reported, PNIPAAm-b-PMMA[126] diblock copolymer, PMMA-*b*-PNIPAM-*b*-PMMA triblock,[127]PNIPAM-*b*-PBMA,[128] PAA-*b*-PNIPAM,[129] PNIPAM- PSt copolymer,[130] PNIPAAm-*b*-PVim[131] and Biotin-PEG-*b*-P(NIPAAm-co-HMAAm)[132] are some of the important examples for modified PNIPAM to obtain the LCST close to or higher than body or cancer tissue temperature (40-43 ^{o}C) . However, LCST of most of the copolymers is close to 25 ^{o}C except Biotin-PEG-*b*-P(NIPAAm-co-HMAAm) and PNIPAAm-*b*-PVim whose LCST was found to be 40 ^{o}C. These polymer based micelles were further utilised to encapsulate anticancer drugs like doxorubicin (DOX), anti-inflammatory drug and so on. Therefore, several synthetic strategies have been employed till date to tune the thermal response of PNIPAM.

The use of PNIPAM polymers for fabrication of thermo-responsive nanocarriers is limited due to its ability to undergo hydrogen bonding with the proteins.[133,134]This problem was overcome by replacing PNIPAM with other class of thermo-sensitive polymers such as poly(alkyl oxide), oligo(ethylene glycol) based graft copolymers, polypeptides[135]etc. The examples of thermo-responsive polymers belonging to these polymer families are shown in figure 1.21.Thus, at present these polymers are being used as a building block for fabrication of thermo-sensitive nanocarriers for efficient drug release in tumor tissues or in intracellular compartments in response to temperature.

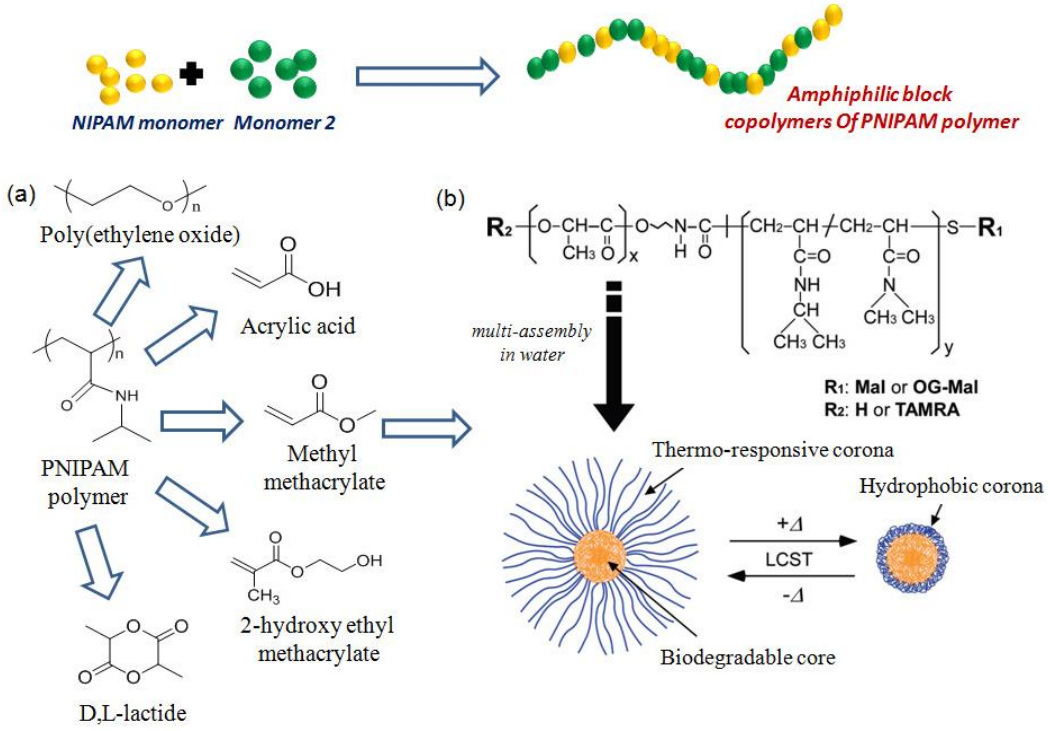

Figure 1.21.*(a)Various comonomers used for copolymerization with PNIPAM polymer in order to tune its LCST.(b)Chemical structure of P(IPAAmDMAAm)-b-PLA and temperature induced property change of polymeric micelle having outer thermo-responsive corona(adopted from Akimoto et al. Mol. Pharm.**2010**,7, 926-935.*

The LCST of all the above mentioned polymers are either lower than the body temperature or very far from the cancer tissue temperature for example LCST of poly(ethylene oxide) falls in the range of 100 to 175 °C, while of poly(propylene oxide) is -5 °C . Likewise, polymers belonging to poly (alkyl vinyl methyl ether) family undergo phase-separation in the temperature range varying from 24 to 49 °C.[130] Also, these polymers are either hydrophilic or hydrophobic in nature. As a consequence, these polymers cannot be directly employed for the fabrication of thermo-responsive nanocarriers. Efforts are being made to tune the LCST of these polymers close to cancer tissue temperature by introducing either a hydrophobic or

hydrophilic segment via copolymerization technique, resulting in various amphiphilic copolymers.

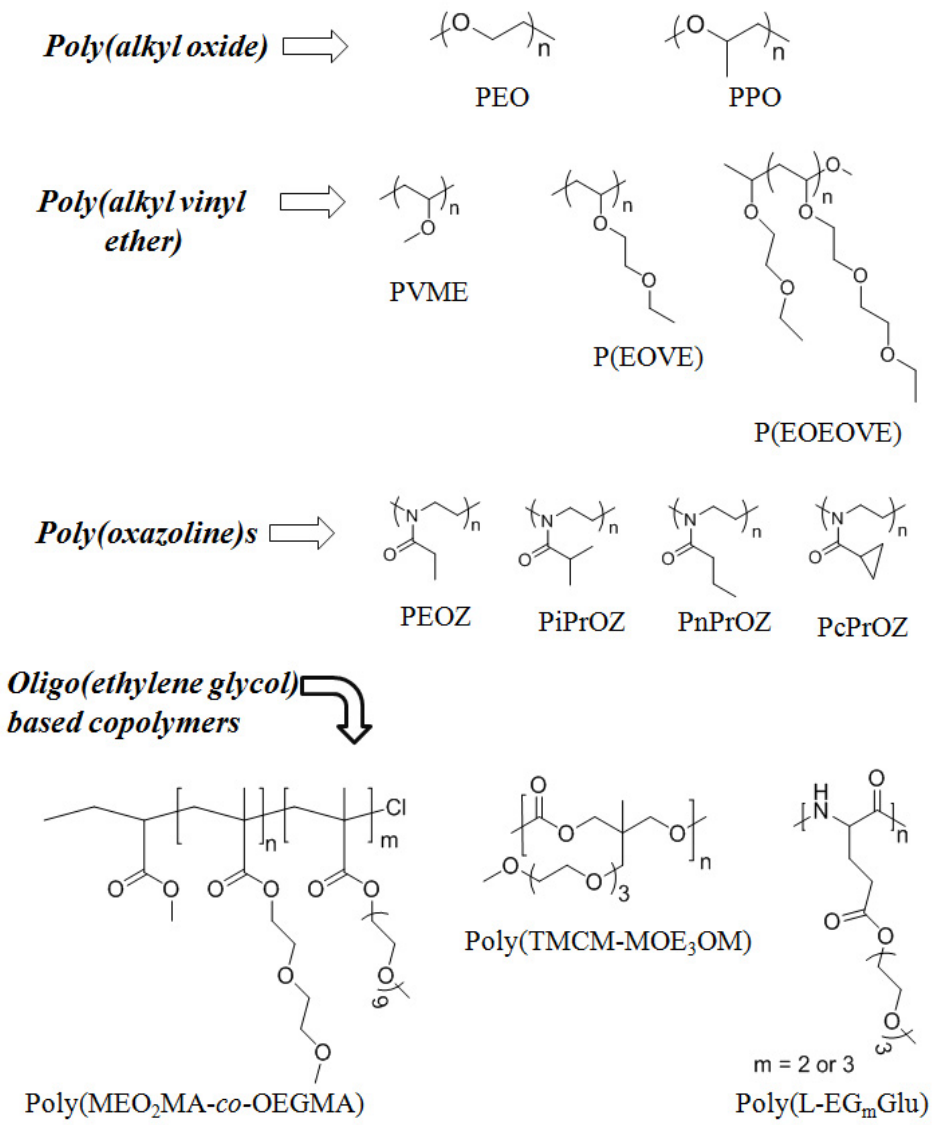

Figure 1.22.*Structure of the most commonly described thermo-sensitive polymers belonging to poly (alkyl oxide), poly (alkyl vinyl ether), poly (oxazoline)s and oligo(ethylene glycol) based copolymers families (adopted from Hocine et al. Soft Matter, **2013**, 9, 5839-5861).*

1.6. Thermo-responsive nanocarriers

The various thermo-responsiveamphiphilic copolymers synthesised lead to the formation of a range of self-assembled structures such as (a) polymeric micelle, (b) vesicles, and (c) hydrogels.

1.6. (a) Core-shell Polymers

Most of these amphiphilic copolymers self-assemble to form core-shell micellar nanoparticles in aqueous medium. The efficacy of these core-shell micellar nanoparticles to hold the drug under physiological condition and release it upon reaching the target site in response to small variation in temperature depends on the position of the thermo-sensitive unit. In other words, the thermal properties of the nanocarriers formed from the above mentioned polymers are influenced by whether these thermo-sensitive units make the core or the shell of the core-shell micellar nanoparticles. Thus, on the basis of the position of the thermo-responsive unit the micellar nanoparticles are categorized as: micelle having (i) thermo-sensitive shelland (ii) thermo-sensitive core.[130]

(i) Micelles with Thermo-sensitive Shell

Fabrication of core-shell micelle or micellar nanoparticles with thermo-responsive outer shell assists in modulating the size as well as morphology of the micelles. Numerous examples are present in literature where PEG and PNIPAM have been utilized for forming outer thermo-responsive shell of the micelle.For instance, Pispas *et al*synthesised thermo-responsive poly (ethylene oxide)-*b*-poly (butadiene) block copolymer based micelle, where poly (ethylene oxide) forms the outer shell and poly (butadiene) the inner hydrophobic core. Upon heating at temperature above the LCST of poly (ethylene oxide) these micelles underwent reduction in the size due to collapse of the outer thermo-responsive shell.[136]Similar, reduction in size due to collapse of the hydrophilic corona was also observed in case of vesicles reported by Peng and co-workers. The vesicles were formed from poly (*N*-isopropylacrylamide)-*b*-poly (2-cinnamoylethyl methacrylate) (PNIPAM-*b*-

PCEMA), where PNIPAM formed the outer shell and inner hydrophilic core of the vesicle with PCEMA as the hydrophobic layer. At temperatures above LCST of PNIPAM, the collapse of hydrophilic corona resulted in decrease in the hydrodynamic size of the vesicle followed by slow release of loaded cargoes.[137] Thus, size of the thermo-responsive nanocarriers can be regulated with thermo-responsive unit as hydrophilic segment in the copolymer structure. Similarly, the thermo-responsive unit as outer hydrophilic corona aids in transition of micelles to hollow vesicles, which in turn alters the sequestration properties of the nanostructures.

Moughton *et al.* has recently synthesised P*t*BuA-*b*-PNIPAM block copolymer with a charged end group using RAFT polymerisation technique, where PNIPAM is flanked between hydrophobic poly (*tert*-butylacrylate) and hydrophilic charged quaternary amine polar head group (see figure 1.23). Under ambient condition the block copolymer self-assembles in to micelles, which further transforms into vesicles upon heating at temperature greater that LCST of PNIPAM polymer.[138] Grubbs and co-workers noticed similar temperature induced switching of morphology from micelles to vesicles by heating poly(ethylene glycol)-*b*-poly(*N*-isopropylacrylamide)-b-poly(isoprene)(PEO-*b*-PNIPA-*b*-PI) micelles above the LCST temperature of PNIPAM polymer.[139]

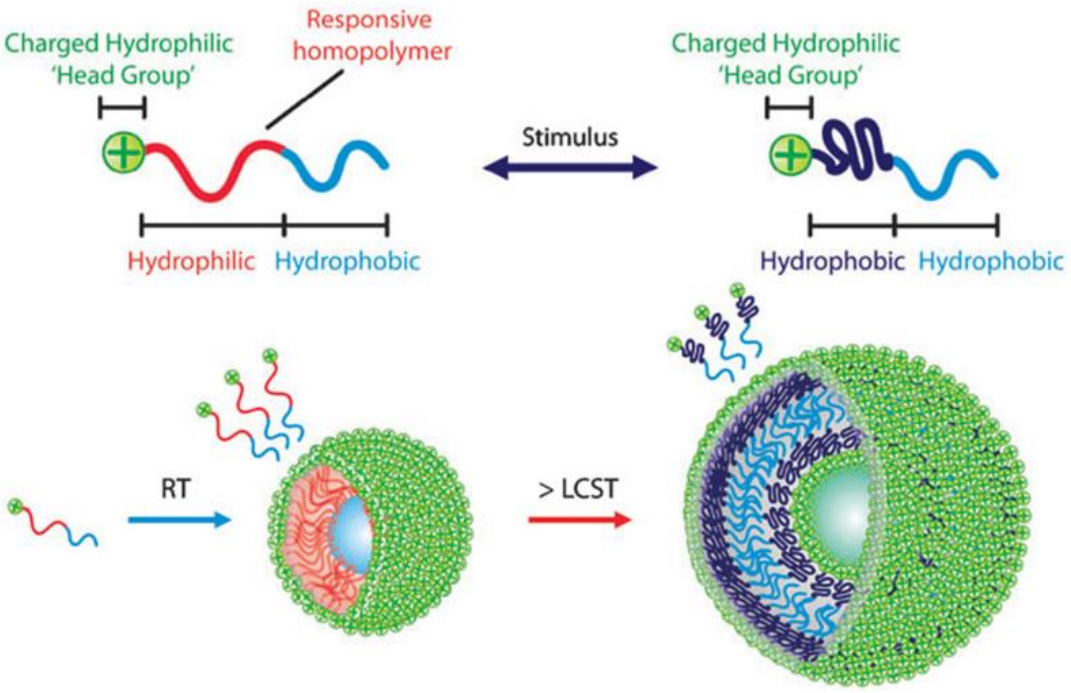

Figure 1.23. *Thermally induced transition from micelle to vesicle (adopted from Moughton et al. Chem. Comm.* ***2003****, 46, 1091-1093).*

Apart from assisting in modulating the sequestration properties and size of the nanocarriers, the outer thermo-responsive shell of the micelles endow with additional advantage of enhanced cellular uptake by the cancer cells when incubated at elevated temperature. The higher uptake of thermo-responsive nanocarriers in the collapsed state was demonstrated by Alexander and co-workers.[140] They prepared poly(lactide-co-glycolide)-block-poly[poly(ethylene glycol) monomethyl ether methacrylate-co-poly(propylene glycol) methacrylate] (PLGA-b-(PEGMEMA-co-PPGMA)) particles comprising inner poly(lactide-co-glycolide) hydrophobic core and outer PEG-based thermo-responsive shell. The polymer particle sequestered paclitaxel in its hydrophobic core and exhibited enhanced cytotoxicity as well as higher cellular uptake in human breast adenocarcinoma MCF7 cells at 40 ^{o}C (>LCST) as compared to when cells were heated at 37 ^{o}C (see figure 1.24a). Similarly, gold nanoparticle functionalised with thermo-responsive PNIPAM based copolymer prepared by the same group showed 80 times higher uptake in MCF7

cells when incubated at 40 ^{o}C than when incubated at 37 ^{o}C[141] (see figure 1.24b). However, the drug release profile from these nanocarriers also depends on the hydrophobicity of the inner core.

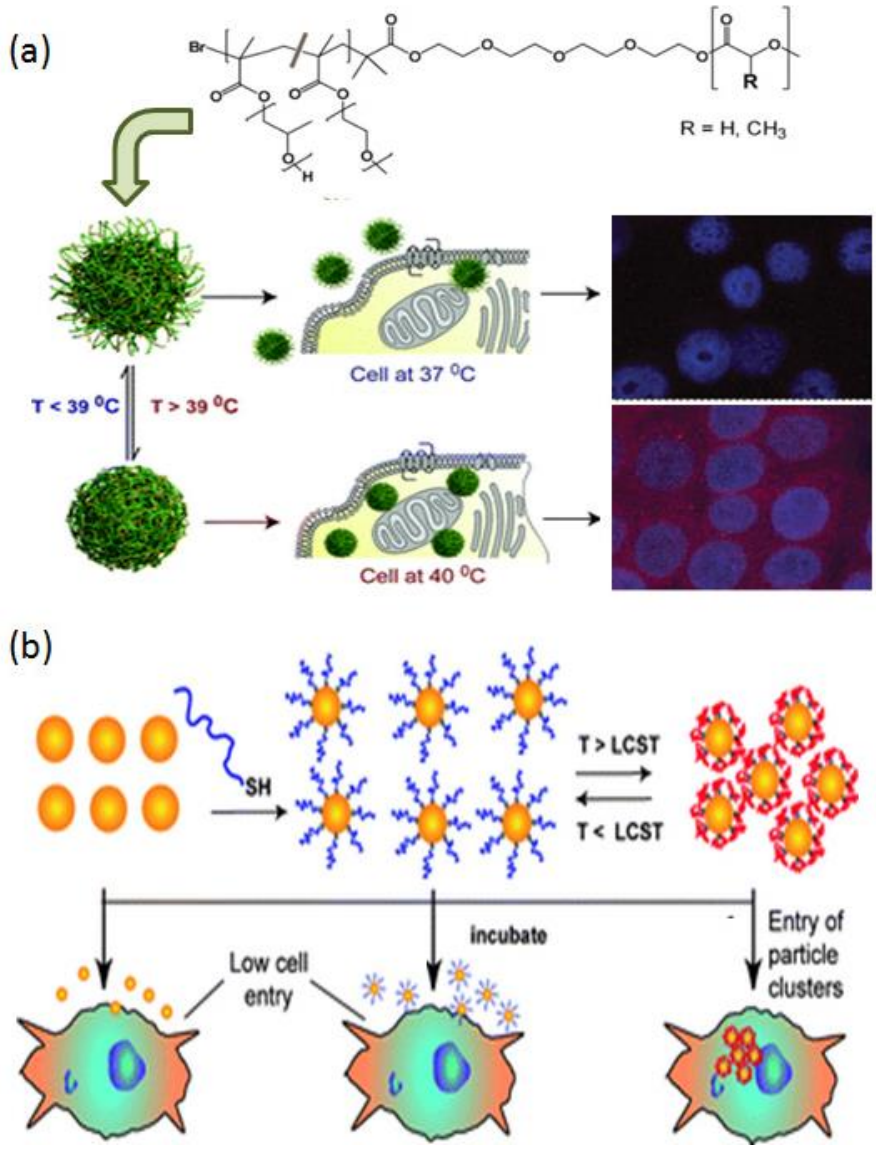

Figure 1.24. *(a)Schematic diagram showing enhanced uptake of thermo responsive nanoparticles due to change in surface corona at higher temperature (above LCST) (adopted from Abulaateefeh et al. Biomater Sci.* ***2013****, 1, 434-442).(b)Enhanced uptake of gold-nanoparticles coated with thermo-responsive polymer at temperature above its LCST (adopted from Salmaso et al. J. Mater. Chem.* ***2009****,* ***19****, 1608-1615).*

With thermo-responsive unit as an outer hydrophilic block, the hydrophobicity of the inner core plays a significant role in achieving the fine control over the drug release profiles at higher temperature (above LCST). For instance, Chung *et al.*[142] prepared three different copolymers such as PNIPAM-*b*-C_{18}, PNIPAM-*b*-PSt, and PNIPAM-*b*-PBMA {where, C_{18}- corresponds to stearoyl unit, PSt stands for polystyrene and PBMA stands for poly (n-butyl methacrylate)}. These copolymers self-assembled to form core-shell micelle under ambient condition, where C_{18}, PSt and PBMA forms the inner core and PNIPAM forms the outer shell of the micelles. These three block copolymers with different core-forming segments exhibited reversible intermicellar aggregation upon heating and cooling above and below LCST as well as successfully encapsulated the anti-cancer drug, doxorubicin. However, the drug release profiles of all the three thermo-responsive polymeric micelles differed. The polymeric micelle with C_{18} chain as the inner hydrophobic core forming segment was not able to hold the drug even at physiological condition. Whereas drug molecule could not diffuse from the inner core of the PNIPAM-*b*-PSt based micelle although it underwent aggregation upon heating. In contrast, the micelle formed from PNIPAM-*b*-PBMA copolymer preserved the drug under physiological condition and exhibited accelerated drug release upon heating. Thus, the hydrophobicity of the inner core of the micelles affects the thermo-responsive release profiles of encapsulated anticancer drugs.

(ii) Micelles with Thermo-sensitive Core

The colloids with thermo-responsive core were reported by Lou and co-workers.[143] They used poly(*N*-isopropylacrylamide-*co*-N,N dimethylacrylamide)as a thermo-responsive core, and poly(aspartic acid) as a shell. The core-shell micellar stucture formed from the poly(aspartic acid)-g-poly(*N*-isopropylacrylamide-*co*-N,N dimethylacrylamide) exhibited temperature dependent phase separation. Reduction in size of the micelle due to shrinkage of PNIPAM core followed by aggregation at temperature above LCST confirmed the thermosensitive behaviour of the micelle.

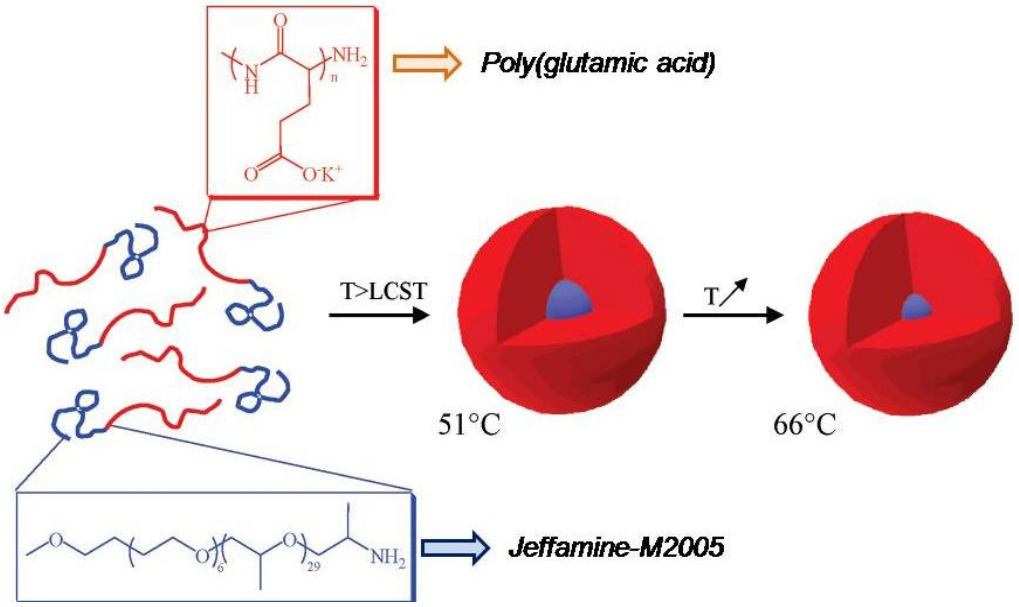

Figure 1.25. *Schematic representation of formation of micelles with temperature. The core of the micelle shrinks upon going from temperature 51 °C to 66 °C (adopted from Agut et al. Langmuir* ***2007****, 23, 11526-11533).*

In addition to acryl amide based polymers, Pluronics® are another class of polymers that undergo phase-separation in response to temperature. For instance, Jeffamine® M 2005 a polyetheramine which consists of 6 units of ethylene oxide and 29 units of propylene oxide displays a LCST of ~ 30 °C. This thermo-responsive behaviour of Jeffamine was further exploited by Lecommandoux and co-workers[144] for fabrication of thermo-responsive micelles (see figure 1.25). They ring opened γ-benzyl-L-glutamate N-carboxyanhydride with amine-terminated Jeffamine, resulting in the formation of double hydrophilic block copolymer. Since Jeffamine segment becomes hydrophobic in nature above LCST, core-shell micelles were formed with thermo-responsive Jeffamine segments as the core and poly(glutamic acid) unit as the shell. With increase in temperature upto 66 ^{o}C, the size of the hydrophobic core of the micelle reduced due to dehydration of the core. Similar, dehydration of the hydrophobic core was also observed by Cai *et al.* in case of PLGA-b-PPO-b-PLGA triblock based colloid upon heating.[145]The core of the micelle formed of thermo-

responsive poly(propylene oxide) shrinks due to the partial removal of water molecules from the core at temperature above its LCST. Although polymeric micelles both with thermo-responsive core and thermo-responsive shell have proven to be efficient enough for delivering loaded cargoes at the desired site in response to small variation in temperature of tumor tissues as compared to normal tissues. One of the major limitations of this polymeric micelle is their capability of shielding only hydrophobic drug from the surrounding environment. Therefore, more efficient nanocarriers such as polymersomes were fabricated in order to overcome this limitation of polymeric micelle.

1.6. (b) Thermo-responsive Vesicles

Along with polymeric micelle, polymeric vesicle which is also termed as "polymersome" are one of the most common self-assembled nanostructures formed from amphiphilic block copolymers.These polymeric vesicles have advantage over polymeric micelle of encapsulating hydrophilic molecules in their interior in addition to integration of hydrophobic molecules in the hydrophobic layer.As compared to conventional liposomes that are composed of low molecular weight surfactants or phospholipids, polymersomes based on high molecular weight block copolymers possess higher physical and mechanical stability.[146,147]The thickness of the hydrophobic membrane typically determines the mechanical stability and permeability of the vesicles, which in turn is dependent on the molecular weight of the hydrophobic segment. Therefore, the thickness of the hydrophobic membrane of the vesicle can be tuned by varying the molecular weight of the hydrophobic segment of the copolymer. This in turn helps in regulating the mechanical stability of the vesicle. The higher is the molecular weight of the hydrophobic segment, the stronger and tougher is the membrane of the polymersomes.[148] This robustness of the hydrophobic membrane of the vesicle is beneficial for the encapsulation of chemotherapeutic agents, genes, proteins etc.

The efficacy of these polymersomes is further increased by incorporating stimuli-responsive unit in the copolymer structure. In order to fabricate polymersomes sensitive to temperature, either hydrophobic or hydrophilic segment of the amphiphilic block copolymer forming vesicle is thermo-responsive in nature. In general, temperature plays a dual role of inducing formation of polymeric vesicle at higher temperature as well as triggering release of loaded cargoes from the hydrophobic /hydrophilic cavity of the polymersome. Several thermo-responsive polymersomes are reported in literature.

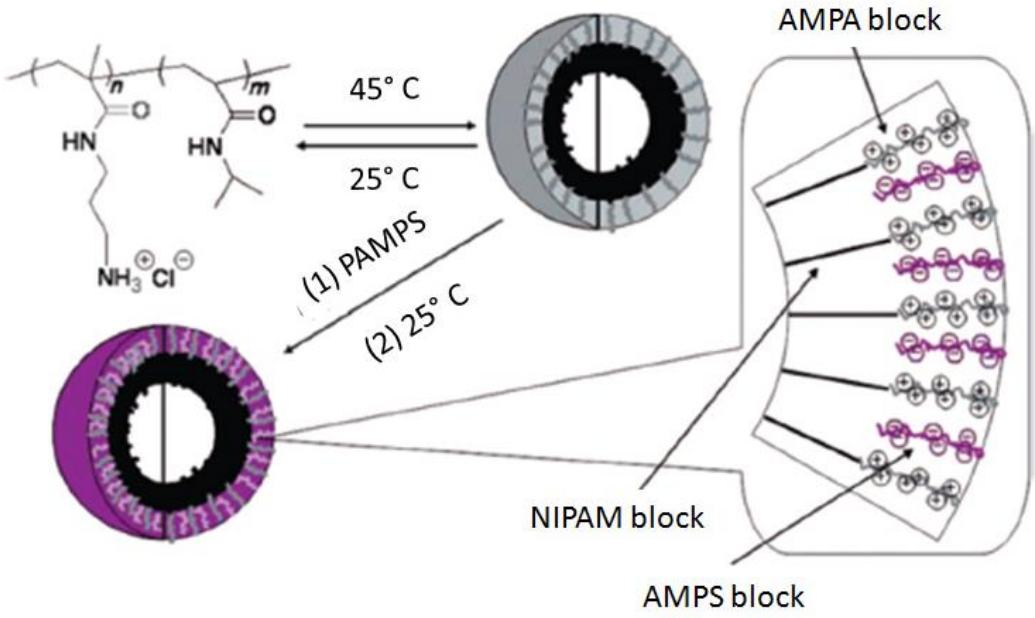

Figure 1.26. *Thermally induced formation of vesicles from PAMPA-PNIPAM diblock copolymers and its subsequent cross-linking by PAMPS (adopted from McCormick and co-workers Angew. Chem. Int. Ed.* ***2006****, 45, 5792-5795).*

Temperature induced formation of polymeric vesicle was reported by McCormick and co-workers[149] (see figure 1.26). They prepared poly(*N*-(3-aminopropyl) methacrylamide hydrochloride)-*block*-(*N*-isopropylacrylamide)(PAMPA-*b*-PNIPAM) diblock copolymer. At room temperature the block copolymer existed in the form of unimers, while it self-assembles into vesicular structure at temperature above LCST of PNIPAM polymer chains. This transition from unimers to vesicle formation upon heating was

completely reversible in nature. The authors further locked the polymeric vesicle by cross-linking the PAMPA block through polyelectrolyte complex formation. They used oppositely charged polyelectrolyte such as (sodium 2-acrylamido-2-methylpropanesulfonate) (PAMPS) for the complex formation (see figure 1.26).

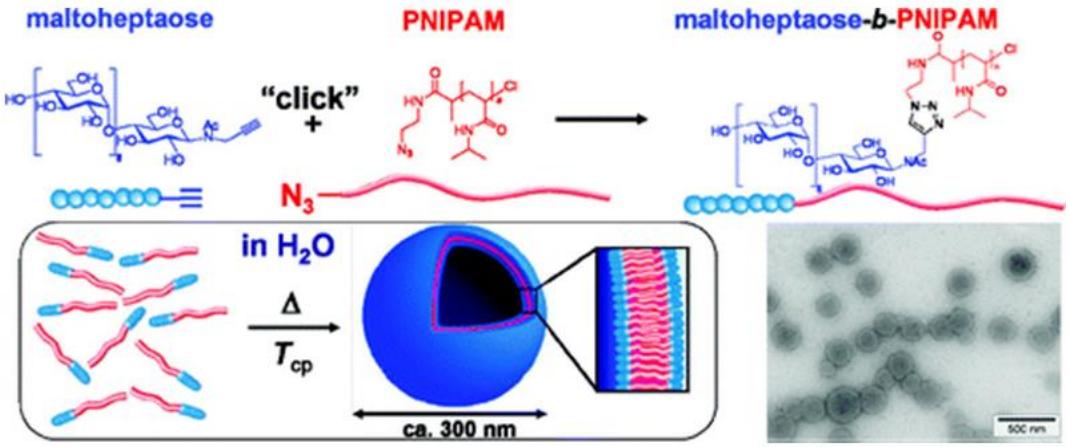

Figure 1.27.*Formation of vesicles from maltoheptaose-b-PNIPAM diblock copolymers at higher temperature (adopted from Ostuka et al. Langmuir,* ***2010****, 26, 2325-2332).*

Formation of polymeric vesicles at temperature above LCST of thermo-responsive block was also reported by Ostuka *et al.* (see figure 1.27). They coupled PNIPAM polymer to oligosaccharide backbone; specifically matoheptaose through click chemeistry, resulting in the formation specifically maltoheptaose-*block*-poly (N-isopropylacrylamide) hybrid block copolymer.[150] This hybrid block copolymer was completely hydrophilic at room temperature, while the PNIPAM segment became hydrophobic at temperature above its LCST thereby leading to the formation of well-defined vesicular structure.

1.6. (c) Thermo-responsive Hydrogels

Hydrogels are three-dimensional networks of hydrophilic polymers capable of imbibing large amount of water or biological fluids. The network structure of hydrogels is typically formed by either physical or chemical cross-linking of polymer

chains. Based on type of cross-linking present, gels are classified as either physical gels or chemical gels. Physical gels also termed as "reversible gels"mainly involvesecondary forces such as hydrogen-bond, hydrophobic interaction, Vander Waals interaction or macromolecular entanglements. On the other hand, chemical gels are composed of cross-linked structure formed via covalent bond formation.[151] Several hydrogels exhibit a unique property of undergoing abrupt changes in volume in response to small changes in environmental parameters such as pH, temperature, light, electric or magnetic field.[152] The gels demonstrating these extraordinary capabilities of sensing stimulus and inducing changes in volume are termed as "smart gels" or stimuli-responsive gels". These stimuli-responsive gels have gained wide interest in the field of drug delivery. Of all, thermo-responsive hydrogels are one of the most commonly studied systems.

Macromolecules of various topologies can be employed for fabrication of thermo-sensitive hydrogel such as linear polymers, graft copolymers, and branched copolymers etc. Generally, polymers exhibiting LCST phenomena are copolymerised with other comonomers for incorporation of thermal-responsive unit in hydrogels. These thermo-responsive hydrogels either display swelling-shrinking phenomenaor undergo sol-gel transition in response to small variation in temperature. In case of hydrogels exhibiting swelling-shrinking transition, hydrogels remains in swollen state at room temperature (below LCST) while when temperature is increased above LCST the hydrogel shrinks. So if hydrogels shows this shrinking behaviorat temperature close to tumor tissue temperature, it can successfully load chemotherapeutic agents at lower temperature i.e. in the swollen state and can deliver the loaded cargoes at tumor site by undergoing contraction(see figure 128).[151,153]

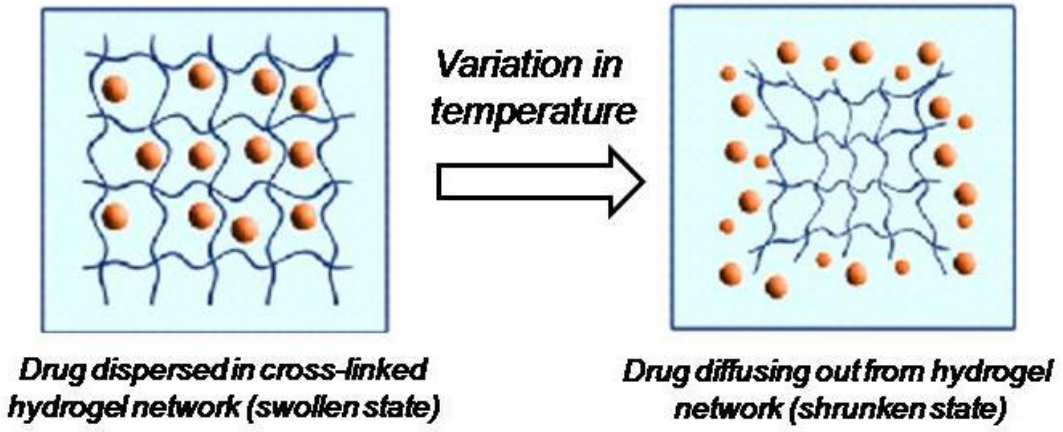

Figure 1.28. *Drug loading and release from the hydrogel in respective swollen (below LCST) and contracted state (above LCST) of the hydrogel (adopted from Vashist et al. Orient. J. Chem.**2013**, 29, 861-870).*

The hydrogels in absence of covalent cross-linking undergo sol-gel transitions. These hydrogels remains in the sol state at lower temperature and goes to gel state upon heating (above LCST).[151] Thus, the chemotherapeutic agents or proteins etc to be delivered at the target site are administered intravenously by dispersing them in the sol at lower temperature, which then undergoes gel formation after reaching the target site. Therefore, the gel formed at diseased site act as a drug depot and undergoes slow degradation leading to slow release of the loaded cargoes. Recently, this sol-gel concept for delivering drug at the tumor site is being demonstrated by Ding and co-workers.[154] They prepared a thermogel composed of poly(D,L-lactide-co-glycolide)-b-poly(ethylene glycol)-b-poly(D,L-lactide-co-glycolide)(PLGA-PEG-PLGA) triblock copolymer which exists in sol state at room temperature and undergoes gelation at body temperature. Irinotecan, the water soluble analogue of anti-tumor drug camptothecin was dispersed in the sol at lower temperature and was injected in to nude mice having human colon tumor. Upon reaching the tumor site the drug containing sol spontaneously undergoes gel formation thereby forming an *in-situ* drug release matrix. From the matrix, drug

releases continuously for 2 weeks. Thus, the mice treated with IRN-loaded thermogel displays a significant regression in the tumor.

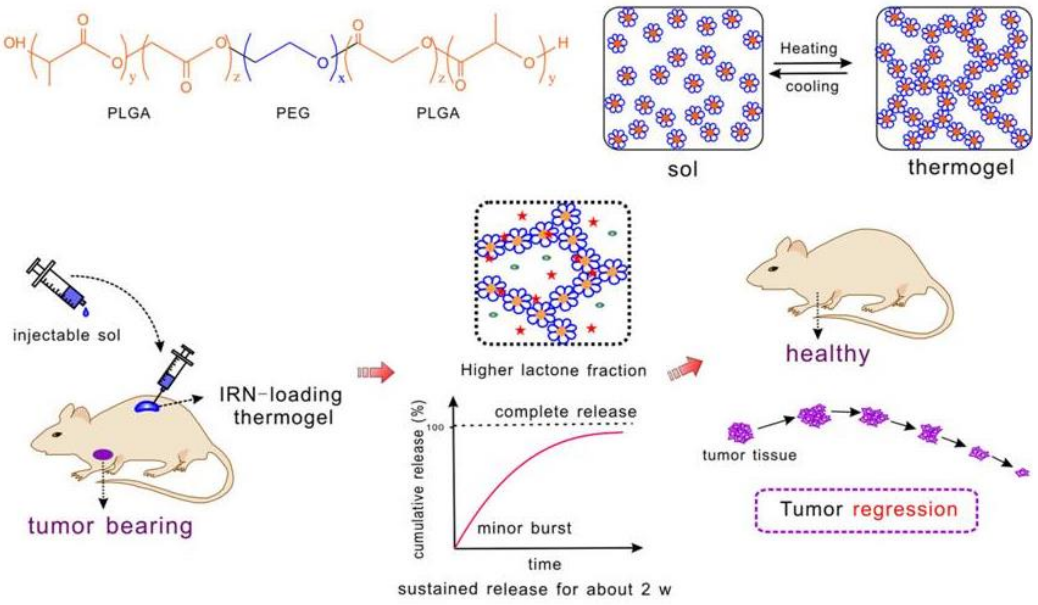

Figure 1.29. *(a)Chemical structure of PLGA-b-PEG-b-PLGA triblock copolymer undergoing temperature induced sol-gel transition in water. (b) Schematic diagram depicting the action of IRN-loaded thermogel upon injecting in the nude-mice bearing human colon cancer cells and subsequent release profile of irinotecan leading to regression of tumor (adopted from Ci et al. Sci. Rep.**2014**, 4, 5473).*

Although a number of thermo-responsive scaffolds are made till date in order to treat tumor and reduce the side effects of chemotherapeutic agents, the thermal-response associated with most of the nanocarriers fabricated are far from the cancer tissue temperature (see table 1.3). Also, of all the thermo-responsive scaffolds synthesised for treatment of cancer only one thermosensitive liposome "Thermodox" has reached up to clinical trials.

Table 1.3: Overview of particle size, temperature and drug encapsulation efficiency of various PNIPAAm- based micelles *(adopted from H. Wet et al, Prog. Polym. Sci. **2009**, 34, 893-910).*

Copolymer	***Micelle Size, Temperature***	***Drug, EE***
P(NIPAAm-co-DMAAm-co-UA)	160-200nm, 20° C	Doxorubicin, 2.7%
PNIPAAm-b-PSt	24nm, 25° C	Doxorubicin, 5%
PNIPAAm-b-PBMA	338nm, 20° C	Doxorubicin, 9.6%
P(NIPAAm-co-DMAAm)-b-PLA	69.2nm	Doxorubicin
PNIPAAm-b-PMMA	190nm, 25° C	Prednisone acetate, 11.5%
P(NIPAAm-co-MPMA)-b-PMMA	80nm, 25° C	Prednisone acetate, 32%
PUA-b- PNIPAAm	160nm, 25° C	Prednisone acetate, 25%
Biotin-P(NIPAAm-co-HMAAm)-b-PMMA	278nm, 25° C	Methotrexate, 25%

Therefore, there is an urgent need of an efficient thermo-responsive nanocarrier, which upon being administered intravenously does not undergoes any disintegration. In other words, the nanocarrier should be efficient enough to retain the loaded cargo under physiological condition (pH =7.4, 37°C). Upon reaching the target site, it should accumulate in the tumor tissues through enhanced permeability and retention (EPR) effect. Once accumulated, the nanocarriers should be capable of sensing the small variation in temperature i.e. from normal cells (37 °C) to tumor tissue (40-43 °C) thereby releasing the loaded cargoes at the target site, keeping the pharmacokinetic properties of the drug intact.

1.7. Aim of the thesis

From the previous discussion, it is understood that stimuli responsive nanocarriers leads to targeted drug delivery with high selectivity and efficacy. The nanocarriers responsive to local environment of tumor tissues (acidic pH, elevated temperature, over expression of enzymes) exclusively are of great importance.Fabrication of drug carriers sensitive to temperature is crucial, since the thermo-responsive nanocarrier should be able to sense the small temperature difference between normal tissues (37° C) and tumor tissues (40-43°C). It has been established that both temperature sensitivity as well as drug-loading capacity of the nanocarrier is governed by the hydrophobic-hydrophilic balance of the amphiphile. However, the present approach is associated with few limitations, such as (a) dependence of cloud point temperature (Tcp) on amphiphile concentration as well as salt concentration of surrounding environment and (b) rise in body temperature due to intensive activity may also pose risks.Thus, design and development of thermo-responsive nanocarriers with appropriate hydrophobic/hydrophilic components with respect to its temperature sensitivity and drug loading efficiency is a major challenge.

This thesis work is focussed on the development of an efficient thermo-responsive nanocarrier for targeting tumor or cancer cells. In order to study the effect of hydrophobic and hydrophilic components of the amphiphilic scaffold on its thermal-response as well as the mode of drug release in response to variation in temperature thermo-responsive nanocarriers based on small amphiphilic molecules were synthesized. For this purpose, the hydrophobic part was chosen from renewable resource based pentadecyl phenol (PDP), a main bi-product of cashew nut shell liquid (CNSL). The outcome of the work carried out in the present thesis using PDP is schematically represented in figure 1.30. Various hydrophobic anti-cancer drugs and fluorescent dyes were loaded in the self-assembled structure formed by the thermo-responsive scaffold. The temperature-driven transformation in morphology, drug-release kinetics and the cytotoxicity of the nascent and loaded scaffold was

studied. Upon understanding the drug-release mechanism and the role of hydrophobic/hydrophilic balance using small amphiphilic scaffolds, amphiphilic polymers with thermo-responsive unit were prepared. Similar to small molecules, the drug-loading capacity, drug-release mechanism and cytotoxicity of the thermo-responsive polymeric carrier was investigated in detail.

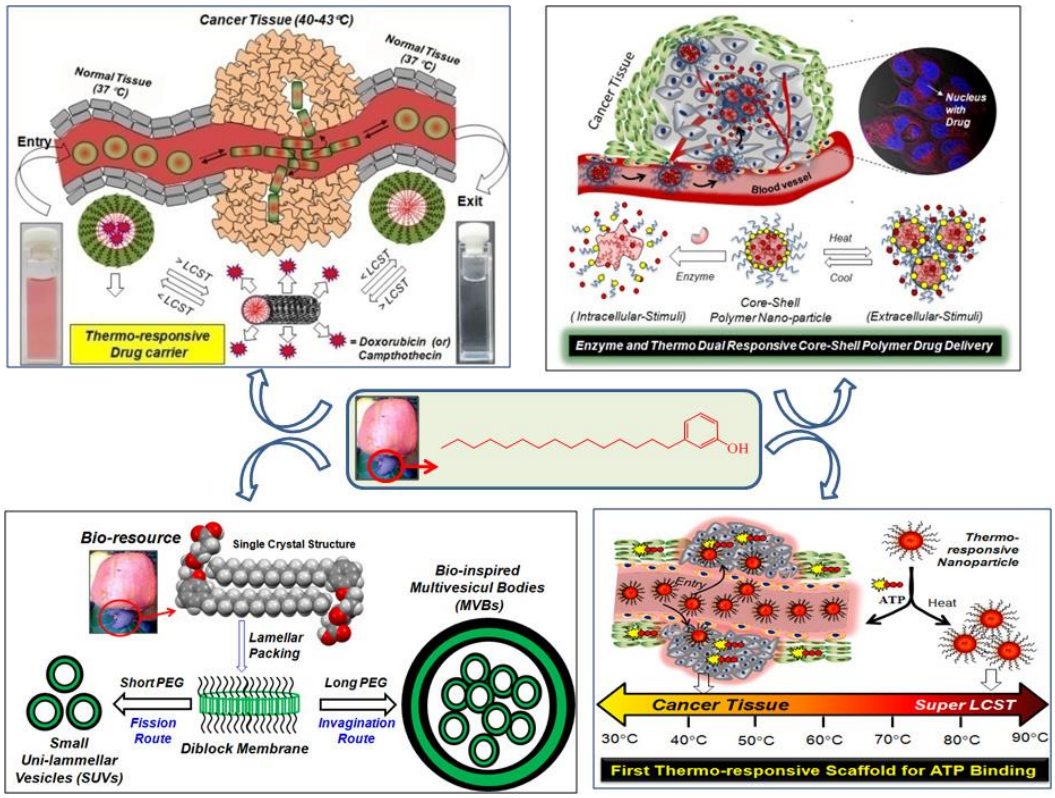

Figure 1.30. *Schematic representation of work carried out in four chapter using 3-pentadecyl phenol as hydrophobic unit for development of thermo-responsive nanocarriers.*

In the second chapter, temperature induced *in-situ* shape change from core-shell to rod-like structure at temperature close to cancer tissue was studied. The shape change was investigated in detail using microscopy techniques. Also, the effect of loaded drug on the shape-transformation and thermal-response of the amphiphilic scaffold was investigated. The third chapter deals with influence of anions present in the biological system on the temperature sensitivity of the amphiphilic molecule. In the fourth chapter, series of acrylate based amphiphilic

polymers with hydrophobic PDP and ethylene glycol units as a pendant group was synthesised and the role of various composition of hydrophobic and hydrophilic segment on the temperature-sensitivity and drug/dye loading ability of the polymers was investigated. The fifth chapter describes the synthesis of various small molecules having ester-linkage in the backbone. Finally, the overall conclusion of the thesis has been summarized.

1.8. References

1. Rothenberg, M. L.; Carbone, D.P.; Johnson, D. H. *Nat. Rev. Cancer* **2003**, 3, 303-309.
2. Uhrich, K. E.; Cannizzaro, S. M.; Langer, R.; Shakesheff, K. M. *Chem. Rev.***1999**, 99, 3181-3198.
3. Kost, J.; Langer, R. S. *Adv. Drug Deliv. Rev.* **2012**, 64, 327-341.
4. Kim, S.; Kim, J.-H.; Jeon, O.; Kwon, I. C.; Park, K. *Eur. J. Pharm. Biopharm.* **2009**, 71, 420-430.
5. Cho, K.; Wang, X.; Nie, S.; Chen, Z.; Shin, D. M. *Clin. Cancer Res.* **2008**, 14, 1310-1316.
6. Duncan, R. *Nat. Rev. Drug Discov.***2003**, 2, 347-360.
7. Sun, T.; Zhang, Y. S.; Pang, P.; Hyun, D. C.; Yang, M.; Xia, Y. *Angew. Chem. Int. Ed.***2014**, 53, 12320-12364.
8. Maruyama, K.; Ishida, O.; Takizawa, T.; Moribe, K.*Adv. Drug Deliv. Rev.***1999**, 40, 89-102.
9. Peer, D.; Karp, J. M.; Hong, S.; Farokhzad, O. C.; Margalit, R.; Langer, R. *Nat.Nanotechnol.***2007**, 2, 751-760.
10. Haag, R.; Kratz, F. *Angew. Chem. Int. Ed.***2006**, 45, 1198-1215.
11. Singh, R.; Lillard Jr, J. W. *Exp. Mol. Pathol.* **2009**, 86, 215-223.
12. Adair, J. H.; Parette, M. P.; Altınoglu, E. I.; Kester, M. *ACS Nano* **2010**, 4, 4967-4970.
13. Fang, J.; Nakamura, H.; Maeda, H. *Adv. Drug Deliv. Rev.* **2011**, 63, 136-151.
14. Hobbs, S. K.; Monsky, W. L.; Yuan, F.; Roberts, W. G.; Griffith, L.; Torchilin, V. P.; Jain, R. K. *Proc. Natl. Acad. Sci.* **1998**, 95, 4607-4612.
15. Gu,F. X.; Karnik, R.; Wang, A. Z.; Alexis, F.; Levy-Nissenbaum, E.; Hong, S.; Langer, R. S. *Nano Today***2007**, 2, 14-21.
16. Maeda, H. *Bioconjugate Chem.* **2010**, 21, 797-802.
17. Matsumura, Y.; Maeda, H. *Cancer Res.***1986**, 46, 6387-6392.
18. Maruyama, K. *Adv. Drug Delive. Rev.***2011**, 63, 161-169.

19. Bertrand, N.; Wu, J.; Xu, X.; Kamaly, N.; Farokhzad, O. C. *Adv. Drug Deliv. Rev.***2014**, 66, 2-25.
20. Brigger, I. Dubernet, C.; Couvreur, P. *Adv. Drug Deliv. Rev.***2002**, 54, 631-651.
21. Ferrari, M. J. *Nat. Rev. Cancer***2005**, 5, 161-171.
22. Sykes, E. A.; Chen, J.; Zheng, G.; Chan, W. C. W. *ACS Nano***2014**, 8, 5696-5706.
23. Marcucci, F.; Lefoulon, F. *Drug Discov. Today***2004**, 9, 219-228.
24. Moghimi, M. S.; Hunter, A. C.; Murray, J. C. *Pharmocol. Rev.***2001**, 53, 283-318.
25. Choi, K. Y.; Chung, H.; Min, K. H.; Yoon, H. Y.; Kim, K.; Park, J. H.; Kwon, I. C.; Jeong, S. Y.*Biomaterials***2010**, 31, 106-114.
26. Torchilin, V. P. *Nat. Rev.Drug Discov.***2005**, 4, 145-160.
27. Byrne, J. D.; Betancourt, T.;Brannon-Peppas, L.*Adv. Drug Deliv. Rev.***2008**, 60, 1615-1626.
28. Papahadjopoulos, D.; Allen, T. M.; Gabizon, A.; Mayhew, E.; Matthay, K.; Huang, S. K.; Lee, K.-D.; Woodle, M. C.; Lasic, D. D.; Redemann, C.; Martin, F. J. *Proc. Natl. Acad. Sci.* **1991**, 88, 11460-11464.
29. Knop, K.; Hoogenboom, R.; Fischer, D.; Schubert, U. S. *Angew. Chem. Int. Ed.***2010**, 49, 6288-6308.
30. Allen, T. M. *Adv. Drug Deliv. Rev.***1994**, 13, 285-309.
31. Woodle, M. C. *Chem. Phys. Lipids***1993**, 64, 249-262.
32. Kamaly, N.; Xiao, Z.; Valencia, P.M.; Radavic-Moreno, A. F.; Farokhzad, O. C. *Chem. Soc. Rev.***2012**, 41, 2971-3010.
33. Klibanovl, A. L.; Maruyamal, K.; Torchilin, V. P.; Huang, L. *FEBS Lett.* **1990**, 268, 235-237.
34. Senior, J. H. *Crit. Rev.Ther. Drug Carr. Syst.* **1987**, 3, 123-193.
35. Torchilin, V. P. *Adv. Drug Deliv. Rev.***2006**, 58, 1532-1555.
36. Torchilin, V. P.; Trubetskoy, T. S. *Adv. Drug Deliv. Rev.***1995**, 16, 141-155.
37. Hoffman, A. S.*J. Control. Release* **2008,** 132, 153-163.

38. Farokhzad, O. C., Langer, R. *Adv. Drug Deliv. Rev.***2006**, 58, 1456-1459.
39. Mitragotri, S.; Burke, P. A.; Langer, R. *Nat. Rev.Drug Discov.***2014**, 13, 655-672.
40. Davis, M. E.; Chen, Z., Shin, D. M. *Nat. Rev.Drug Discov.***2008**, 7, 771-782.
41. Kreuter, J.; Higuchi, T. *J. Pharm. Sci.***1979**, 68, 451-454.
42. Shi, J.; Xiao, Z.; Kamaly, N.; Farokhzad, O. C. *Acc. Chem. Res.***2011**, 44, 1123-1134.
43. Davis, M. E. *Mol. Pharmaceutics***2009**, 6, 659-668.
44. Twaites, B.; Alarcon, C. D. L. H.; Alexander, C. *J. Mater. Chem.***2005**, 15, 441-445.
45. Walter, K. A.; Tamargo, R.; Olivi, A.; Burger, P. C.; Brem, H. *Neurosurgery***1995**, 37, 1129-1145.
46. Rosler, A.; Vandermeulen, G. W. M.; Klok, H-A. *Adv. Drug Deliv. Rev.***2001**, 53, 95-108.
47. Torchilin. V.*Adv. Drug Deliv. Rev.* **2011**, 63, 131-135.
48. Ahmad, Z.; Shah, A.; Siddiq, M.; Kraatz, H.-B. *RSC Adv.* **2014**, 4, 17028-17038.
49. Kataoka, K.; Harada, A.; Nagasaki, Y. *Adv. Drug Deliv. Rev.***2001**, 47, 113-131.
50. Chiapetta, D. A.; Sosnik, A. *Eur. J. Pharm. Biopharm.* **2007**, 66, 303-317.
51. Kataoka, K.; Kwon, G. S.; Yokoyama, M.; Okano, T.; Sakurai, Y. *J. Control. Release* **1993**,24, 119-132.
52. Soussan, E.; Cassel, S.; Blanzat, M.; Rico-Lattes, I. *Angew. Chem. Int. Ed.***2009**, 48, 274-288.
53. Kearney, C. J.; Mooney, D. J. *Nat. Mat.* **2013**, 12, 1004-1017.
54. Pillai, O.; Panchagnula, R. *Curr. Opinion Chem. Biol.***2001**, 5, 447-451.
55. Qiu, L. Y.; Bae, Y. H. *Pharm. Res.***2006**, 23, 1-30.
56. Gros, L.; Ringsdorf, H.; Schupp, H. *Angew. Chem.***1981**, 93, 311-331; *Angew. Chem. Int. Ed. Engl.***1981**, 20, 305-325.
57. Ringsdorf, H. *J. Polym. Sci. Symp.* **1975**, 51, 135-153.

58. Vasey, P. A.; Kaye, S. B.; Morrison, R.; Twelves, C.; Wilson, P.; Duncan, R.; Thomson, A. H.; Murray, L.S.; Hilditch, T. E.; Murray, T.; Burtles, S.; Fraier, D.; Frigerio, E.;Cassidy, J. *Clin. Cancer Res.* **1995**, 5, 83-94
59. Kumar, N.; Ravikumar, M. N. V.; Domb, A. J. *Adv. Drug Deliv. Rev.***2001**, 53, 23-44.
60. Letchford, K.; Burt, H. *Adv. Drug Deliv. Rev.***2007**, 65, 259-269.
61. Smart, T.; Lomas, H.; Massignanni, M.; Flores-Merino, M. V.; Perez, L. R.; Battaglia, G. *Nano Today***2008**, 3, 38-46.
62. Discher, D. E.; Eisenberg, A. *Science***2002**, 297, 967-973.
63. Mai, Y.; Eisenberg, A. *Chem. Soc. Rev.***2012**, 41, 5969-5985.
64. Yokoyama, M. Miyauchi, M.; Yamada, N. Okano, T.; Sakurai, Y.; Kataoka, K.; Inoue, S. *J. Control. Release* **1990**,11, 269-278.
65. Kwon, G.; Suwa, S.; Yokoyama, M.; Okano, T.; Sakurai, Y.; Kataoka, K. *J. Control. Release* **1994**,29, 17-23.
66. Nishiyama, N.; Kataoka, K. *Pharmacol.Ther.* **2006**,112, 630-648.
67. Kabanov, A. V.; ChekhoninV. P.; Alakhov, V.; Batrakov, E. V.; Lebedev, A. S.; Melik-Nubarov, N. S.; Arzhakov, S. A.; Levashov, A. V.; Morozov, G. V.; Severin, E. S. *FEBS Lett.* **1989**, 258, 343-345.
68. Miyata, K.; Christie, R. J.; Kataoka, K. *React. Func. Polym.* **2011**, 71, 227-234.
69. Liggins, R. T.; Burt, H. M. *Adv. Drug Deliv. Rev.***2002**, 54, 191-202.
70. Rosler, A.; Vandermeulen, G. W. M.; Klok, H. A. *Adv. Drug Delivery Rev.* **2001**, 53, 95-108.
71. Prochaska, K.; Baloch, M. K.; Tuzar, Z. *Makromol. Chem*. **1979**, 180, 2521-2523.
72. Guo, A.; Liu, G. J.; Tao, J. *Macromolecules* **1996**, 29, 2487-2493.
73. Iijima, M.; Nagasaki, Y.; Okada, T.; Kato, M.; Kataoka, K. *Macromolecules* **1999**, 32, 1140-1146.
74. Zhang, L.; Katapodi, K.; Davies, T. P.; Barner-Kowollik, C.; Stenzel, M. H. *J. Polym. Sci., Part A: Polym. Chem.* **2006**, 44, 2177-2194.

75. Yokoyama, M.; Okano, T.; Sakurai, Y.; Suwa, S.; Kataoka, K. *J. Control. Release* **1996**,39, 351-356.
76. Nishiyama, N.; Yokoyama, M.; Aoyagi, T.; Okano, T.; Sakurai, Y.; Kataoka, K. *Langmuir***1999**,15, 377-383.
77. Nishiyama, N.; Okazaki, S.; Cabral, H.; Miyamoto, M.; Kato, Y.; Sugiyama, Y.; Nishio, K.; Matsumura, Y.; Kataoka, K. *Cancer Res.***2003**,63, 8977-8983.
78. Uchino, H.; Matsumura, Y.; Negishi, T.; Koizumi, F.; Hayashi, T.; Honda, T.; Nishiyama, N.; Kataoka, K.; Naito, S.; Kakizoe, T. *Brit. J. Cancer* **2005**,93, 678-687.
79. Haxton, K. J.; Burt, H. M. *J. Pharm. Sci.***2009**,98, 2299-2316.
80. Kakizawa, Y.; Kataoka, K. *Adv. Drug Deliv. Rev.***2002**, 54, 203-222.
81. Kabanov, A. V.; Kabanov, V. A. *Bioconjugate Chem.***1995**, 6, 7-20.
82. Harada, A.; Kataoka, K. *J. Macromol. Sci.,Pure Appl. Chem.***1997**, A34, 2119-2133.
83. Jones, M.-C.; Leroux, J.-C. *Eur. J. Pharm. Biopharm.* **1999**, 48, 101-111.
84. Matsumura, Y. *Adv. Drug Deliv. Rev.***2008**, 60, 899-914.
85. Discher, B. M.; Won, Y.-Y.; Ege, D. S.; Lee, J. C.-M.; bates, F. S.; Discher, D. E.; Hammer, D. A. *Science***1999**, 284, 1143-1146.
86. Ahmed, F.; Discher, D. E. *J. Control. Release* **2004**,96, 37-53.
87. Carlmark, A.; Hawker, C.; Hult, A.; Malkoch, M. *Chem. Soc. Rev.***2009**, 38, 352-362.
88. Galaev, I.; Mattiasson, B. *Trends Biotechnol.***1999**, 17, 335-340.
89. Fleige, E.; Quadir, M. A.; Haag, R. *Adv. Drug Delivery. Rev.* **2012**, 64, 866-884.
90. Ganesh, V. A.; Baji, A.; Ramakrishna, S. *RSC Adv.***2014**,4, 53352-53364.
91. Kim, J.; Dang, C. V. *Cancer Res.***2006**,66, 8927-8930.
92. Ge, Z.; Liu, S. *Chem. Soc. Rev.***2013**,42, 7289-7325.
93. Matrix, E.; Declerck, Y. A.; Mercurio, A. M.; Stack, M. S.; Chapman, H. A.; Zutter, M. M.; Muschel, R. J.; Raz, A.; Matrisian, L. M.; Sloane, B. F.; Noel,

A.; Hendrix, M. J.; Coussens, L.; Padarathsingh, M. *Am. J. Pathol.***2004**,164, 1131-1139.

94. Kuppusamy, P.; Li, H.; Ilangovan, G.; Cardounel, A. J.; Zweier, J. L.; Yamada, K.; Krishna, M. C.; Mitchell, J. B. *Cancer Res.***2002**,62, 307-312.
95. Szatrowski, T. P.; Nathan, C. F. *Cancer Res.***1991**,51, 794-799.
96. Kaur, S.; Prasad, C.; Balakrishnan, B.; Banerjee, R.*Biomater. Sci.* **2015**, 3, 955-987.
97. Mura, S.; Nicolas, J.; Couvreur, P. *Nat. Mater.***2013**, 12, 991-1003.
98. Blum, A. P.; Kammeyer, J. K.; Rush, A. M.; Callmann, C. E.; Hahn, M. E.; Gianneschi, N. C. *J. Am. Chem. Soc.***2015**, 137, 2140-2154.
99. Stuart, M. A. C.; Huck, W. T. S.; Genzer, J.; Muller, M.; Ober, C.; Stamm, M.; Sukhorukov, G. B.; Szleifer, I.; Tsukruk, V. V.; Urban, M.; Winnik, F.; Zauscher, S.; Luzinov, I.; Minko, S. *Nat. Mater.***2010**, 9, 101-113.

100 Cayre, O. J.; Chagneux, N.; Biggs, S. *Soft Matter***2011**, 7, 2211-2234.

101 Kumar, A.; Srivastava, A.; Galaev, I. Y.; Mattaison, B. *Prog. Polym. Sci.***2007**, 32, 1205-1237.

102 Warburg, O. *Science***1956**, 123, 309-314.

103. Estrella, V.; Chen, T.; Lloyd, M.; Wojtkowiak, J.; Cornnell, H. H.; Ibrahim-Hashim, A.; Bailey, K.; Balagurunathan, Y.; Rothberg, J. M.; Sloane, B. F.; Johnson, J.; Gatenby R. A.; Gillies, R. J. *Cancer Res.***2013**, 73, 1524–1535.

104. Liu, J.; Huang, Y.;Kumar, A.; Tan, A.; Jin, S.;Mozhi, A.; Liang, X.-J.*Biotechnol. Adv.* **2014**, 32, 693-710.

105.Chen, W.; Zhong, P.; Meng, F.; Cheng, R.; Deng, C.; Feijen, J.; Zhong, Z.*J. Control. Release* **2013**,169, 171-179.

106. Felber, A. E.; Dufresne, M.-H.; Leroux, J.-C. *Adv. Drug Deliv. Rev.* **2012**, 64, 866-884.

107.Lee, C. C.; Gillies, E. R.; Fox, M. E.; Guillaudeu, S. J.; Frechet, J. M. J.; Dy, E. E.; Szoka, F. C. *Proc. Natl. Acad. Sci.* **2006**, 103, 16649-16654.

108.Calderon, M.; Welker, P.; Licha, K.; Graeser, R.; Kratz, F. Haag, R. *J. Control. Release***2010**,148, e24-e25.

109.Ambade, A. V.; Savariar, E. N.; Thayumanavan, S. *Mol. Pharm.* **2005**,2, 264-272.

110.Alarcon, C. D. I. H.; Pennadam, S.; Alexander, C. *Chem. Soc. Rev.* **2005**,34, 276-285.

111.Schmaljohann, D. *Adv. Drug Deliv. Rev.* **2006**,58, 1655-1670.

112. Kamimura, M.; Furukawa, T.; Akiyamac, S.-I.; Nagasaki, Y. *Biomater. Sci.* **2013**, 1, 361-367.

113.Zhuang, J.; Gordon, M. R.; Ventura, J.; Li, L.; Thayumanavan, S. *Chem. Soc. Rev.* **2013**,42, 7421-7435.

114.Ding, Y.; kang, Y.; Zhang, X. *Chem. Comm.* **2015**,51, 996-100.

115.Hu, J.; Zhang, G.; Liu, S. *Chem. Soc. Rev.* **2012**,41, 5933-5949.

116.Hu, Q.; Katti, P. S.; Gu, Z. *Nanoscale* **2014**,6, 12273-12286.

117.Kratz, F.; Muller, I. A.; Ryppa, C.; Warnecke, A.*ChemMedChem***2008**,3, 20-53.

118.Graaf, A. J. D.; Mastrobattista, E.; Vermonden, T.; Sinkovits, R. S.; Olson, N. H.; Baker, T. S.; Gianneschi, N. C. *Macromolecules* **2012**,45, 842-851.

119.Pramod, P. S.; Shah, R.; Jayakannan, M. Nanoscale 2015, 7, 6636-6652.

120.Chilkoti, A.; Dreher, M. W.; Meyer, D. E.; Raucher, D. *Adv. Drug Deliv. Rev.* **2002**, 54, 613-630.

121.Issels, R. D. *Eur. J. Cancer*. **2008**, 44, 2546-2554.

122.Wei, H.; Cheng, S.-X.; Zhang, X.-Z.; Zhuo, R.-X. *Prog. Polym. Sci.* 2009, 34, 893-910.

123.Fujishige, S.; Kubota, K.; Ando, I. *J. Phys. Chem*. **1989**, 93, 3311–3313.

124.Ruel-Gariépy, E.; Leroux, J.-C. *Eur. J. Pharm. Biopharm*. **2004**, 58, 409–426.

125. Phillips, D. J.; Gibson, M. I. *Polym. Chem.*2015, 6, 1033-1043.

126.Wei, H.; Zhang, X. Z.; Zhou, Y.; Cheng, S. X.; Zhuo, R. X. *Biomaterials* **2006**, 27, 2028–34.

127.Chang, C; Wei, H.; Quan, C. Y.; Li, Y. Y.; Liu, J.; Wang, Z. C.; et al. *J. Polym. Sci. Part A: Polym. Chem.* **2008**, 46, 3048-3057.

128.Chung, J.-E.; Yokoyama, M.; Yamato, M.; Aoyagi, T.; Sakurai, Y.; Okano, T. *J Control. Release***1999**,62, 115-127.

129.Li, G.Y.; Song, S.; Guo, L.; Ma, S.M.; *J. Polym. Sci. Part A: Polym. Chem.* **2008**,46, 5028-5035.

130.Cammas, S.; Suzuki, K.; Sone, C.; Sakurai, Y.; Kataoka, K.; Okano, T. *J Control. Release***1997**,48, 157-164.

131.Ge, Z.; Xie, D.; Chen, D.; Jiang, X.; Zhang, Y.; Liu, H.; Liu, S. *Macromolecules***2007**, 40, 3538-3546.

132.Cheng, C.; Wei, H.; Shi, B.-X.; Cheng, H.; Li, C.; Gu, Z.-W.;Cheng, S.-X.; Zhang, X.-Z.; Zhuo, R.-X. *Biomaterials***2008**, 29, 497-505.

133.Cui, Q.; Wu, F.; Wang, E. *J. Phys. Chem. B* **2011**, 115, 5913-5922.

134.Bianco-Peled, H.; Gryc, S. *Langmuir* **2004**, 20, 169-174.

135.Hocine, S.; Li, M.-H. *Soft Matter* **2013**, 9, 5839-5861.

136.Pispas, S.; Hadjichristidis, N. *Langmuir***2003**, 48-54.

137.Chen, X.;Ding, X.;Zheng, Z.;Peng, Y. *New J. Chem.* **2006**,30, 577-582.

138.Moughton, A. O.; Patterson, J. P.;O'Reilly, R. K. *Chem. Comm.* **2003**, 46, 1091-1093.

139.Sundararaman, A.; Stephan, T.; Grubbs, R. B. *J. Am. Chem. Soc.* **2008**, 130, 12264–12265.

140.Abulateefeh, S. R.;Spain, S. G.; Thurecht, K. J.;Aylott, J. W.;Chan, W. C.;Garnetta, M. C.;Alexander, C.*Biomater Sci.***2013**, 1, 434-442.

141.Salmaso, S.; Caliceti, P.; Amendola, V.; Meneghetti, M.; Magnusson, J. P.; Pasparakis, G.;Alexander, C.*J. Mater. Chem.***2009**, 19, 1608-1615.

142.Chung, J. E.;Yokoyama, M.;Okano, T. *J. Control. Release***2000**, 65, 93-103.

143.Yeha, J.-C.; Yang, H.-H.; Hsua, Y.-T.;Sua, C.-M.;Leeb, T.-H.;Loua,S.-L.*Colloids and Surfaces A: Physicochem. Eng. Aspects***2013**, 421, 1– 8.

144.Agut, W.;Brulet, A.; Taton D.;Lecommandoux, S. *Langmuir***2007**, 23, 11526-11533.

145.Cai, C.;Zhang, L.;Lin, J.; Wang, L. *J. Phys. Chem. B***2008**, 112, 12666-12673.

146.Li, M.-H.;Keller, P.*Soft Matter***2009**, 5, 927-937.

147. Kim, K. T.;Meeuwissen, S. A.;Nolte, R. J. M.; Hest, J. C. M. V.*Nanoscale* **2010**, 2, 844-858.

148. Meng, F.; Zhong, Z.; Feijen, J. *Biomacromolecules***2009**, 10, 197-209.

149. Li, Y.;Lokitz, B. S.;McCormick, C. L. *Angew. Chem. Int. Ed.***2006**, 45, 5792-5795.

150.Otsuka, I.; Fuchise, K.; Halila, S.; Fort, S.; Aissou, K.; Pignot-Paintrand, I.; Chen, Y.; Narumi, A.; Kakuchi, T.; Borsali, R.*Langmuir***2010**, 26, 2325-2332.

151.Qiu, Y.;Park, K.*Adv. Drug Deliv. Rev*.**2012**,64, 49-60.

152.Vashist, A.; Vashist, A.; Gupta, Y. K.;Ahmad S.*J. Mater. Chem. B***2014**, 2, 147-166.

153.Vashist, A.; Ahmad S. *Orient. J. Chem*. **2013**, 29, 861-870.

154.Ci, T.; Chen, L.;Yu, L.; Ding, J.*Sci. Rep*.**2014**, 4, 5473.

Chapter 2

Shape Transformable and Thermo-responsive Amphiphiles and their Drug Delivering Capabilities

Chapter 2

Shape Transformable and Thermo-responsive Amphiphiles and their Drug Delivering Capabilities

In-situ temperature induced shape-transformable carrier's efficiency for loading and delivering anticancer drugs has been studied. Thermo-responsive amphiphilic scaffolds consisting of hydrophilic oligoethylene glycol and hydrophobic renewable resource 3-pendadecylphenol tied via hydrogen bonded amide linkage were tailor made through multi-step organic synthesis. The thermo-responsive behavior and self-assembly of the amphiphiles were analysed. The transformation of the amphiphilic scaffold from three dimensional spherical core-shell at temperature below LCST to rod-like structures at higher temperature in water (or PBS at pH= 7.4) was confirmed by light scattering studies, electron microscopy, atomic force microscopy, variable temperature NMR and single crystal structure studies. The thermo-responsive scaffolds were employed for encapsulating anticancer drugs such as doxorubicin (DOX) and camptothecin (CPT) while retaining the shape transformation ability of the scaffold. The release profile of the DOX under in-vitro conditions revealed that the DOX can be selectively release at cancer tissue temperature (40-43 ℃) as compared to normal body temperature (37 ℃). The mode of DOX release from the DOX loaded scaffold was found to follow non-Fickian diffusion process at cancer tissue temperature. Therefore, the uniqueness of the present approach lies in the development of thermo-responsive scaffolds capable of undergoing temperature driven in-situ shape transformation followed by release of chemotherapeutic agents under the cancer tissue temperature.

2.1. Introduction

Stimuli responsive polymers are gaining increased scientific interest because of their emerging application in the field of pharmaceutics and nanotechnology.[1] Responsive polymeric materials also termed as "smart materials" or "intelligent materials" have been extensively investigated for development of various kinds of drug carriers, protein/gene delivery vectors, optical and electronic devices, tissue engineering scaffolds etc. These smart or responsive polymeric materials undergo changes in size, shape, surface characteristics, solubility, sol-gel transformation and degree of intermolecular association.[2] These changes are generally triggered in response to external stimuli; such as temperature, pH, enzyme, magnetic field, electric field, ultrasound etc (see figure 2.1). The physical or chemical changes exhibited by these stimuli responsive polymers in response to diverse type of external stimuli are typically reversible in nature. These unique features of these smart polymers have made them one of the most attractive candidates for targeted drug delivery.[3,4]

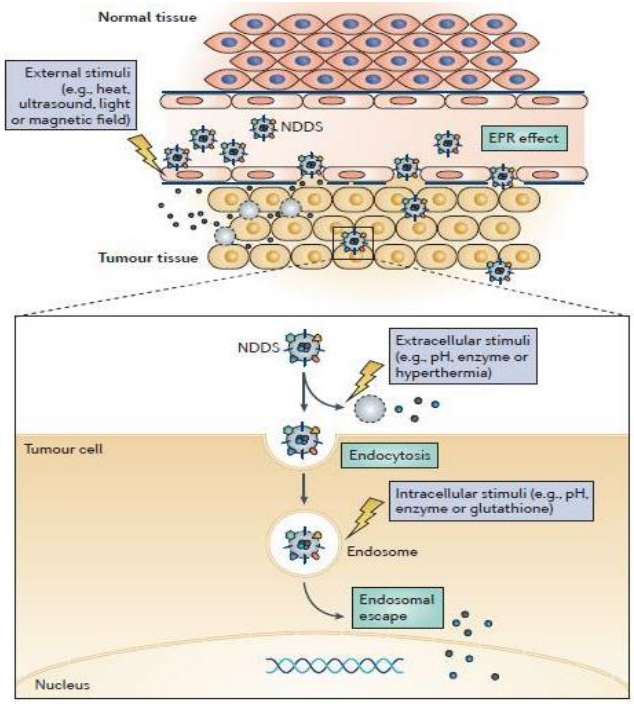

Figure 2.1. *General scheme of various stimuli-responsive drug delivery strategies(adopted from Torchilin et al. Nat. Rev. Drug Discov.* ***2014****, 13, 813-827).*

The abnormal cell growth and imperfect lymphatic drainage of the cancer tissues accumulates larger size nano-assemblies (or aggregates of >100 nm size) through enhanced permeability and retention (EPR) effect.[5-7] Recently researchers have identified that apart from size and stimuli; the shape of the nano-carriers played crucial role in cellular internalization, biodistribution, phagocytosis and so on.[8-12] The inspiration for the fabrication of nano-carriers of various shapes comes from the nature itself.[13] The human own blood cells are of various shapes such as erythrocytes are of discoidal shape; platelets have disc-like shape etc (see figure 2.2).[14] The non-spherical geometries of these cells help them to escape from phagocytosis. On the other hand, various pathogens invading into human body also found to have diverse shapes such as *Salmonella, Shigella* and *Bacillus anthracis* are rod-shaped, and *Campylobacter jejuni* is spiral shaped (see figure 2.2). The entry of these pathogens in to non-phagocytic mammalian cells is assisted by their non-spherical geometry. [15,13]

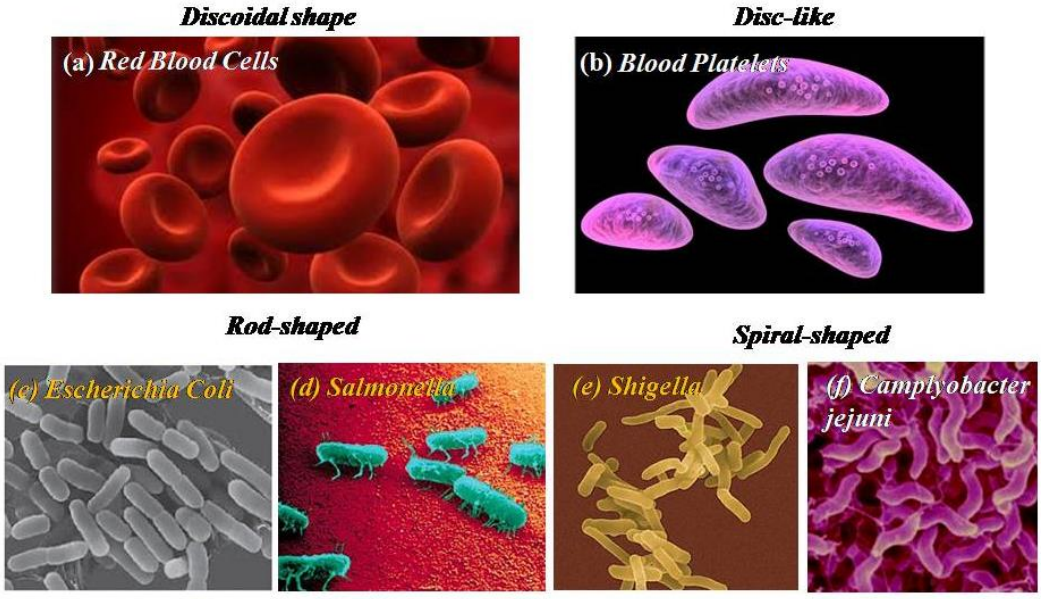

Figure 2.2. *Various examples of non-spherical particles and pathogens such as (a) Discoidal shape-RBCs , (b) Disc-like blood platelets, Rod-shaped (c) Escherichia coli (d) Salmonella and Spiral-shaped (e) Shigella (f) Camplyobacter jejuni (adopted from Mitragotri et al. J. Nat. Mat.* ***2009****, 8, 15-23).*

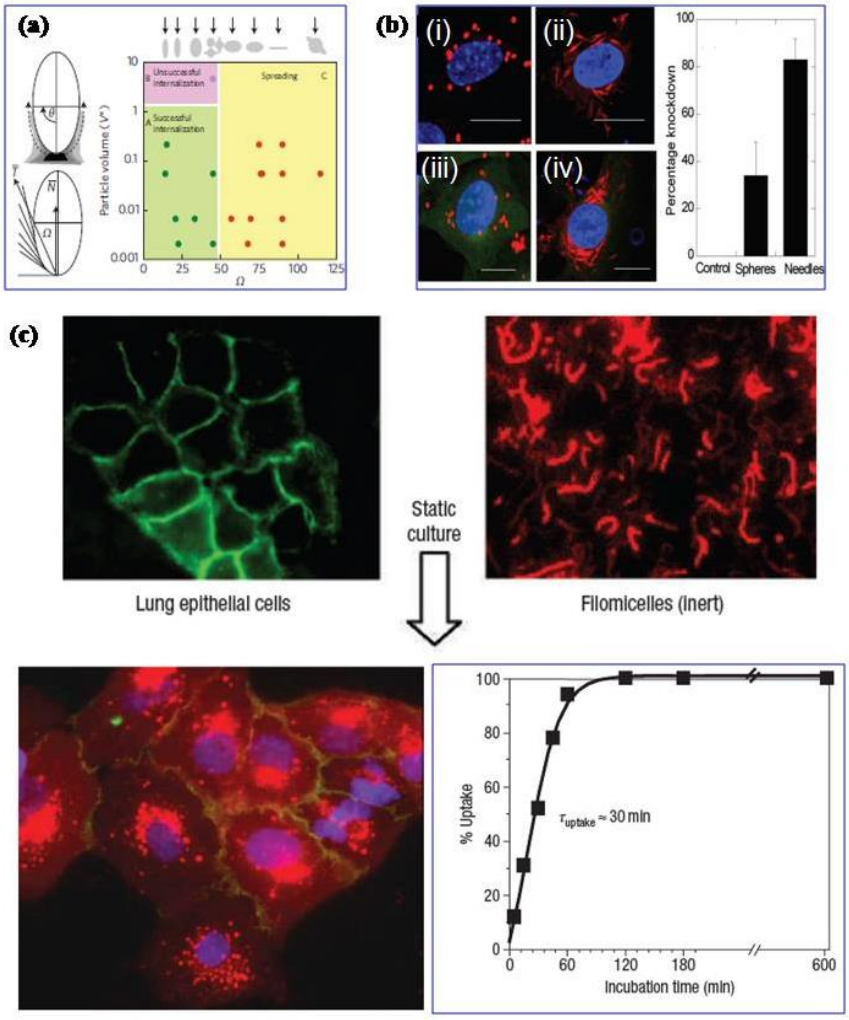

Figure 2.3. *(a) Phagocytosis of particles depends on shape (adopted from Champion et al. PNAS* ***2006****, 103, 4930-4934). (b) Confocal micrographs showing internalization of siRNA(red) into endothelial cells after co-delivery with spheres (1 μ m) and corresponding needles, respectively. The reduction in green color in (iv) indicates knockdown of GFP when needles are used. Scale bar: 10 μ m. Needle shaped particles induce significantly higher knockdown compared to spheres (adopted from Kolhar et al. Small* ***2011****, 7, 2094-2100). (c)Internalization of filomicelles in vitro by human lung derived epithelial cells (adopted from Geng et al. Nat. Nanotechnol.* ***2007****, 2, 249-255).*

It was also reported that non-spherical objects like rod-like particles[16] filomicelles[17] and elliptical disk[18] with pointed ends were readily internalized by cells compared to spherical objects like micelles and vesicles (see figure 2.3). For

instance, Gratton *et al.* have established that non-spherical particles are readily internalized by Hela cells, particularly the rod-like particles.[19] Discher and co-workers found that filomicelles have longer blood circulation life and can efficiently deliver drug as compared to spherical particles.[17] Moreover, Champion and Mitragotri investigated the importance of shape on phagocytosis and found that elliptical disk encountering macrophage cells through their pointed end was internalized in few minute while attachment via flat region leads to no internalization even after exposure for 12hours.[18] Recently, Szoka and Frechet[20,21] proposed membrane model for the entry of various polymer architectures and concluded that rod-shape carriers have better ability to penetrate the cell membrane (see figure 2.4).

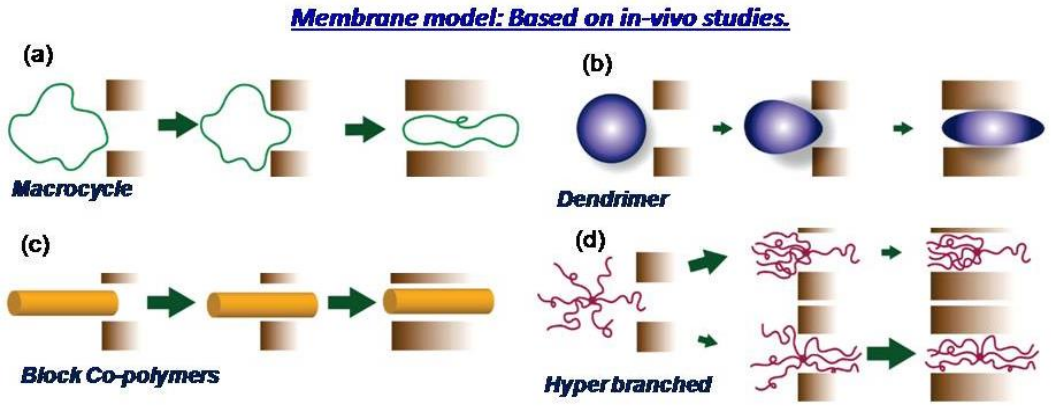

Figure 2.4. *Effect of penetration of polymeric carriers of various shapes inside cell (a) a macrocycle, (b) dendrimer, (c) block copolymers and (d) hyper-branched(adopted from Frechet and co-workers Acc. Chem. Res.* ***2009****, 42, 1141-1151.*

Several new methods such as soft lithography,[23-24] micro-fluidics,[25-28] mechanical stretching,[29,30] self-assembly[31,32] etc have been developed for fabrication of particles of diverse shapes. Among all the methods developed, molecular self-organization is one of the most powerful techniques for the fabrication of nanostructures of various shapes. It mainly occurs via non-covalent interactions such as hydrogen bond, electrostatic interactions, van der Waals interactions, hydrophobic interactions etc.[33] Hydrophobic interactions play a crucial role in the thermo-responsiveness of polymers that undergo structural changes in response to

temperature. For instance, the structural changes occurring in thermo-responsive polymers in response to temperature generally takes place via hydrophobic interactions. A distinct characteristic feature of these polymers is the presence of lower critical solution temperature (LCST); the temperature above which these polymers undergo phase-separation.[34] These thermo-responsive polymers generally undergo conformational changes in response to variation in temperature which result in terms of difference in their solubility in aqueous medium. This unique property of these thermo responsive polymers can be conveyed directly to the nano-carriers fabricated from this polymers.[35] Therefore, thermo-responsive polymers are ideally expected to retain the loaded cargoes (drugs) at the body temperature (37 °C) and expected to rupture to deliver their load at cancer tissue temperature (40-43°C).[36,37] From the past few years, poly (*N*-isopropyl acrylamide) i.e. PNIPAM has been extensively used as building blocks for developing several thermo-responsive polymers with the LCST at ~32 ^{o}C.

Several synthetic strategies have been employed till date to tune the thermal response of PNIPAM close to cancer tissue temperature (40-43 ^{o}C) so that it could be employed as drug delivery vehicle. PNIPAAm-b-PMMA diblock block copolymer,[38] PMMA-*b*-PNIPAM-*b*-PMMA triblock,[39] PNIPAM-Poly(lactic acid) copolymer,[40] PNIPAM-co-acrylamide-*b*-Poly(caprolactone) random block copolymer,[41] PNIPAM- octadecyl acrylate copolymer[42] are some of the important examples for modified PNIPAM to obtain the LCST close to or higher than body or cancer tissue temperature (43 ^{o}C) temperatures. These polymer based micelles were further utilized to encapsulate anticancer drugs like doxorubicin (DOX), anti-inflammatory drug and so on. Zhuang and co-workersreported another classes of PLG-g-PMEO$_i$MA polypeptide with tuneable LCST in the range of 19 to 40 ^{o}C for delivering DOX at low temperature and pH.[43] Nevertheless, one of the major drawbacks of this polymer is its hydrogen bonding ability with proteins which limits its application in the field of biotechnology.[44,45] This problem was overcome by replacing PNIPAM with poly (ethylene glycol). However, LCST of PEG was found to be higher than 100^{o}C. Hereafter, the most challenging task was to tune its phase-

transition temperature.[46]Numerous examples are present in literature where covalent synthesis methods have been exploited to synthesize various PEG based thermo-responsive polymers having LCST close to body temperature.[47,89]Apart from covalent synthesis and polymerization technique, non-covalent interaction based supramolecular self-assembly method can also be utilized to achieve thermal-sensitivity.[49,50]However, very limited reports are available in literature.Hence, fabrications of new thermo-responsive assemblies are being awaited.

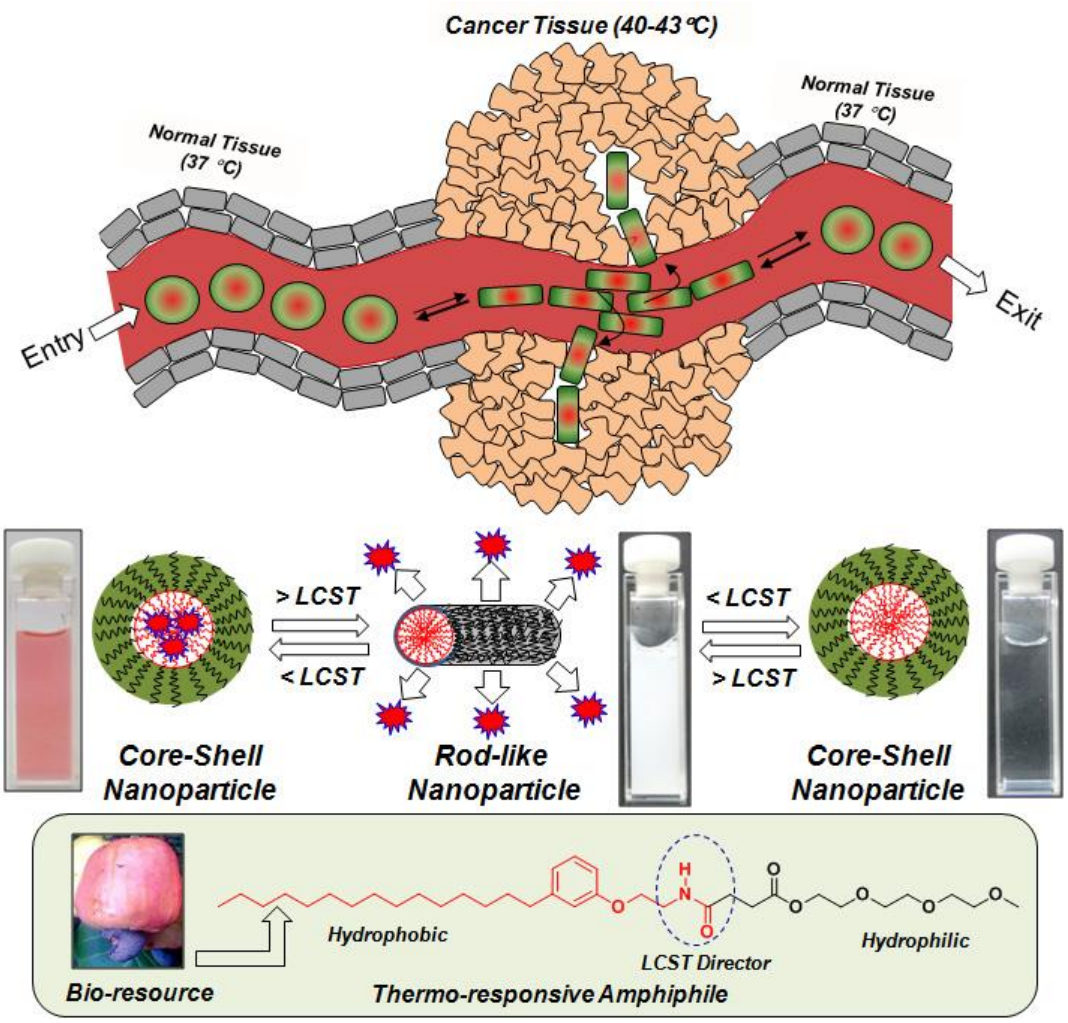

Figure 2.5. *Schematic representation of shape transformable and thermo-responsive nano-scaffolds at cancer tissue.*

The retention of the spherical shape of the nano-carriers is very important since they possess uniform flow behavior in all three dimensions required for long

circulation time, for example in blood plasma during intravenous delivery.[51]This would allow the drug carriers to have both enhanced transportation and membrane penetration in a single system for maximizing the treatment efficacy. Hence, hypothetically the ideal polymeric or small molecular carriers should retain their three dimensional spherical shape under the normal tissue conditions and should be capable of undergoing in-situ shape transformation into one dimensional structures at the cancer tissue environment (high temperature or low pH). This concept is schematically shown in figure 2.5

In this chapter shape tunable thermo-responsive amphiphilic drug carriers were developed and proof-of-concept with respect to their loading and delivering capabilities was demonstrated. New amide functionalized amphiphiles have been synthesized based on 3-pentadecylphenol, renewable resource hydrophobic unit along with oligoethylene glycols as hydrophilic unit. The amphiphile self-organized as spherical core shell nanoparticle at ambient conditions and underwent morphological transformation into rod-like structures at higher temperatures (above LCST). Single crystal structure, variable temperature NMR studies, light scattering techniques, electron and atomic force microscopy provided evidence for the reversible morphological transformation. Anticancer drugs such as doxorubicin and camptothecin were successfully encapsulated in these thermo-responsive scaffolds. In vitro release kinetic studies revealed that the scaffolds were stable at 37 °C in PBS buffer and they selectively undergo phase transformation at higher temperatures > 42°C in PBS buffer to release > 90 % of the loaded cargoes. Thus, the present investigation opens new area of shape transformable thermo-responsive nano-carriers for loading and delivering anticancer drugs.

2.2. Experimental Methods

2.2.1. Materials: 3-Pentadecylphenol, 2-ethanolamine, succinic anhydride, Boc-anhydride, triethylamine (Et_3N), triethyleneglycol monomethylether, ethylene glycol monomethylether, diethylene glycol monomethyl ether, 1-ethyl-3-(3-dimethylaminopropyl) carbodiimide (EDC), dicyclohexylcarbodiimide, DIAD (diisopropyl azodicarboxylate)diisopropyl ethylamine (DIPEA), 4-dimethylamino pyridine were purchased from Aldrich chemicals. And all other reagents and solvents were purchased locally and purified following the standard procedure. Breast cancer cells (MCF-7) and HeLa cells were maintained in DMEM (phenol red free medium: Gibco) containing 10 % (v/v) fetal bovine serum (FBS) and 1% (v/v) penicillin−streptomycin at 37 °C under a 5% CO2 humidified atmosphere. Cells were trypsinized using 0.05% trypsin (Gibco) and seeded in 96- or 6-well (as per experiment) flat bottomed plastic plates (Costar) for all assays. Tetrazolium salt, 3-(4,5 dimethylthiazol)-2,5-diphenyl tetrazolium bromide (MTT), DMSO, and paraformaldehyde were obtained from Sigma.

2.2.2. General procedures: ^{1}H-NMR and ^{13}C-NMR spectra were recorded using 400-MHz Jeol NMR spectrophotometer in $CDCl_3$ containing small amount of TMS as internal standard. Infra-red spectra were recorded using a Thermo-Scientific Nicolet 6700FT-IR spectrometer in KBr. The mass of all the amphiphiles as well as intermediate compounds was analysed by Applied Biosystems 4800 PLUS MALDI TOF/TOF analyser.

Size Exclusion Chromatography (SEC): The purity of the amphiphile was determined by size exclusion chromatography (SEC) using a Viscotek VE 1122 pump, ViscotekVE 3580 RI detector, and Viscotek VE 3210 UV/Vis detector in tetrahydrofuran (THF) using polystyrene as standards. The optical transmittance measurement was done by a Perkin-Elmer Lambda 45 UV-Visible spectrophotometer.

Dynamic and Static Light Scattering Measurement: DLS of the amphiphile was carried out using a Nano ZS-90 apparatus utilizing 633 nm red laser (at 90° angle) from Malvern instruments.The static light scattering experiment (SLS) was carried out using 3D-DLS spectrometer, from LS Instruments, Switzerland utilizing toluene as a reference. The measurement was performed in autocorrelation mode from 30 to 100° by steps of 5°.

Morphology analysis: FE-SEM images were recorded using Zeiss Ultra Plus scanning electron microscope. For FE-SEM analysis, the samples were prepared by drop casting on silicon wafers and coated with gold. TEM images were recorded

using a Technai-300 instrument by drop casting the sample on Formvar -coated copper grid. Atomic force microscope images were recorded for drop caste samples using JPK instruments attached with Nano wizard-II setup.The reproducibility of the data was checked for at least three independent amphiphile solutions.

Single Crystal X-Ray Analysis: Single crystals were subjected to data collection at 100 K on Bruker APEX duo CCD-X ray diffractometer equipped with graphite monochromator Mo Ka radiation(λ=0.71073 Å). The frames were integrated with Bruker APEX software package. The structures were solved by direct methods and refined using SHELX S v97 programs. The crystallographic parameters for PDP-amine Boc molecule have been summarized in table 2.1.Crystal structures were visualized using Mercury 3.0 software.

Photophysical Characterization: The absorption and emission studies were done by a Perkin-Elmer Lambda 45 UV-Visible spectrophotometer and SPEX Flurolog HORIBA JOBIN VYON fluorescence spectrophotometer with a 450W Xe lamp as the excitation source at room temperature. Fluorescence intensity decays were collected by time correlated single photon counting technique (TCSPC) setup from Horiba Jobin Yvon, using NanoLED-460 for DOX and NanoLED-374 for CPT as sample excitation source.

Optical Transmittance measurement: Optical transmittance of amphiphile and drug loaded nanoparticles was measured using quartz cell (path length: 1cm) with Perkin-Elmer Lambda 45 UV-Visible spectrophotometer which was equipped with temperature-controller. The sample was heated from 30 °C to 80 °C in stepwise manner with an interval of 5 °C. Similarly, cooling cycle was recorded from 80 °C to 30 °C with an interval of 5 °C.

Doxorubicin and CPT encapsulation: The ability of these core-shell nanoparticles to encapsulate hydrophobic molecules in the hydrophobic inner core was determined by using DOX. DOX.HCl (0.5mg) was neutralized with triethylamine prior to the encapsulation. DOX (0.5 mg), PDP- TEG (5.0mg) were taken in DMSO (1.0 mL).To it triethylamine (1.5equivalents to DOX) and water (3.0 mL) was added and stirred at 25°C for 12 h. It was then extensively dialyzed (SPECTRA/POR, MWCO-500-1000) against deionized water (200mL) for 48h. The DOX encapsulated solution was filtered through 0.45 μm filter and the sample was freeze-dried in lyophilizer.

CPT was encapsulated as described. PDP-TEG (10.0mg) and CPT (1.0mg) was dissolved in 2.0 mL of DMSO and stirred for 15 minutes at 25 °C. Water (5.0 mL) added to the above solution drop wise and the mixture was further stirred for 12

h. It was transferred to dialysis bag (SPECTRA/POR, MWCO-500-1000) and dialyzed against deionized water (200mL) for 48h. The CPT encapsulated solution was filtered through 0.45µm filter and the sample was freeze-dried in lyophilizer. Drug loading efficiency (DLE) and drug loading content (DLC) of were calculated using following equations:DLE (%) = {weight of encapsulated CPT/ weight of CPT in feed}x 100%.DLC (%) = {weight of CPT in nanoparticles/weight of CPT loaded nanoparticles} x 100%.

For the above purpose, approximately 1.5mg of drug loaded nanoparticles was dissolved in DMSO (2.0 mL) and their absorbance was measured to determine the DLE and DLC using their molar extinction coefficients {ε_{CPT} = 10,500(in PBS), ε_{CPT} = 11,250 (in DMSO) and ε_{DOX}= 4188 (in PBS), ε_{DOX} = 7035 (in DMF)}.

Table 2.1.Unit cell parameters for PDP-amine-Boc molecule.

Compound	**PDP-amine-Boc**
formula	$C_{27}H_{44}O_5$
recrystnsolv	DCM/MeOH
molwt	447
Colour, habit	Colorless,rectangular
temp(K)	100
system	Triclinic
space group	P-1
a, (Å)	5.39
b, (Å)	10.53
c, (Å)	23.86
α, (deg)	83.74
β, (deg)	88.42
γ, (deg)	86.78
V, Å^3	1346.30
d $_{cacl}$,g cm^{-1}	1.203
µ(mm^{-1})	0.08
GOF	0.708
no. of unique reflections	4663
Reflections collected	6781
θ range	1.34 to 24.04
No. of refined parameters	293
R_1 (on F, I>2σ (I))	0.0554
wR_2 (on F^2, all data)	0.1960

In Vitro **drug release studies:** The release profile of DOX was studied using

dialysis method. Briefly, 3.0 mg of drug loaded sample was dispersed in 3.0 mL of PBS and the content was transferred in to dialysis bag, which was then immersed in 100mL of PBS and was incubated at 37°C. Periodically; 3.0 mL of solution was withdrawn from the system and was replaced with 3.0 mL of fresh PBS solution. The aliquots obtained were then subjected to absorbance measurement and amount of DOX released was calculated. The release profile of DOX was also studied at 25°C and 44°C. Similarly, 3.0 mg of CPT loaded nanoparticles were subjected to in vitro release studies at 25°C, 37°C and 55°C.

Cell Viability Assay (MTT Assay): To test the cytotoxicity of the **PDP-TEG** a cell viability assay was performed in HeLa cell lines using the tetrazolium salt 3-(4,5 dimethylthiazol)-2,5-diphenyl tetrazolium bromide (MTT). HeLa Cell lines (1×10^3) and were seeded per well in a 96- well plate (Corning, U.S.A.) in 100 μL of DMEM with 10% FBS (fetal bovine serum) and allowed to adhere for 16 h. Prior to drug treatment, medium from cells was aspirated and various concentration of was prepared. These were added to 100 μL of DMEM with FBS in which the cells were incubated. Blank controls, DMEM with FBS in the absence of cells, were used in each experiment. All control and treated experiment wells were in triplicate. Cells were incubated for 72 h without a change in medium, and after 72 h medium were aspirated. Freshly prepared stock of MTT in sterile PBS (5 mg/mL) was diluted to50 μg/mL in 100 μL of DMEM with FBS and was added to cells. Cells were then incubated with MTT for 4 h at 37°C. Medium with MTT was then aspirated from wells and the purple formazan crystals formed as a result of reduction of MTT by mitochondrial dehydrogenase enzyme from cells were dissolved in 100μL of 100% DMSO (added per well). The absorbance from formazan crystals was immediately measured using microplate reader at 570 nm (Varioskan Flash) and is representative of the number of viable cells per well Values from the triplicates for each control and treated set were noted and their means used for calculations. The mean of the absorbance values for the blank control samples was subtracted from the average of treated samples. The values thus obtained for the control samples were equated to 100% and relative percentage values was calculated accordingly.

2.2.3. Synthesis

Synthesis of 4-(2-methoxyethoxy)-4-oxobutanoic acid (1a): Ethylene glycol monomethylether (5.00 g, 65.0 mmol) and succinic anhydride (7.89 g, 78.0 mmol) were dissolved in dry dichloromethane (25 mL) under N_2 atmosphere. To this reaction mixture, Et_3N (9.15 mL, 65.0 mmol) was added drop wise (Caution: the mixtures start boil vigorously just after the addition of Et_3N). The reaction mixture was then stirred at 25 °C for 24 h under nitrogen. It was poured into water (60 mL)

and neutralized with 2N concentrated HCl (2.0 mL) .The organic layer was then washed with brine solution, dried over anhydrous sodium sulphate and was concentrated to obtain pale yellow liquid as product. It was purified by passing through silica gel column of 60-120 mesh using 5% methanol in chloroform as eluent. Yield = 8.0 g (69 %).^{1}H NMR ($CDCl_3$, 400 MHz) δ: 4.24 ppm (t, 2H, CO-OC**H$_2$**), 3.60 ppm (t,2H, C**H$_2$**-O), 3.38 ppm (s, 3H, CH_2-OC**H**$_3$), 2.66 ppm (s, 4H, CO-C**H**$_2$-C**H**$_2$). ^{13}C NMR ($CDCl_3$, 100 MHz) δ: 177.05 (**C**OOH), 171.88 (**C**OO-CH_2), 69.93 (COO- **C**H_2), 58.51 (C-O**C**H_3), 28.45 (CO-**C**H_2-**C**H_2). FT-IR (cm^{-1}): 3495, 2926, 2852, 1714, 1453, 1406, 1381, 1351, 1198, 1161, 1125, 1096, 1028, 982, 957, 906, 863, 833, 638. MALDI-TOF-MS: m/z calculated for $C_7H_{12}O_5$:176.07; and Found: 215.03($M^+ + K^+$).

Synthesis of 4-(2-(2-methoxyethoxy) ethoxy)-4-oxobutanoic acid (1b): Diethyleneglycol monomethylether (5.00 g, 42.0 mmol), succinic anhydride (5.00 g, 50.0 mmol) and Et_3N (7.00 mL, 50.0 mmol) were used as given in procedure for compound **1a**. The product was purified by passing through silica gel column of 60-120 mesh using 5% methanol in chloroform as eluent. Yield = 2.50 g (30 %). ^{1}H NMR ($CDCl_3$, 400 MHz) δ: 4.24 ppm (t, 2H, CO-OC**H$_2$**), 3.60 ppm (t,2H, C**H$_2$**-O), 3.38 ppm (s, 3H, CH_2-OC**H**$_3$), 2.66 ppm (s, 4H, CO-C**H**$_2$-C**H**$_2$). ^{13}C NMR ($CDCl_3$, 100 MHz) δ: 177.05 (**C**OOH), 171.88 (**C**OO-CH_2), 69.93 (O**C**H_2-**C**H_2-O), 58.51 (C-O**C**H_3), 28.45 (COOH-**C**H_2-**C**H_2-CO). FT-IR (cm^{-1}): 2923, 1728, 1450, 1351, 1244, 1201, 1162, 1134, 1101, 1028, 934, 839, 625. MALDI-TOF-MS: m/z calculated for $C_7H_{12}O_5$: 220.22, and Found: 259.93($M^+ + K^+$).

Synthesis of 12-oxo-2, 5, 8, 11-tetraoxapentadecan-15-oic acid) (1c): Triethyleneglycol monomethylether (10.00 g, 60.0 mmol), succinic anhydride (7.30 g, 73.0 mmol) and Et_3N (8.5 mL, 60.0 mmol) were used as given in procedure for compound **1a**. The product was purified by passing through silica gel column of 60-120 mesh using 10% methanol in chloroform as eluent. Yield = 10.0g (62 %).^{1}H NMR ($CDCl_3$, 400 MHz) δ: 4.14 ppm (t, 2H, CO-OC**H$_2$**), 3.60 ppm (t,2H, C**H$_2$**-O), 3.56-3.46 ppm (t, 8H, OC**H$_2$**C**H$_2$**O), 3.27 ppm (s, 3H, C**H**$_2$-OCH_3), 2.54 ppm (s, 4H, CO-C**H**$_2$-C**H**$_2$). ^{13}C NMR ($CDCl_3$, 100 MHz) δ: 177.05 (**C**OOH), 171.88 (**C**OO-CH_2), 70.56 (O**C**H_2-**C**H_2-O), 69.93 (COO-**C**H_2), 58.51 (C-O**C**H_3), 28.45 (CO-**C**H_2-**C**H_2). FT-IR (cm^{-1}): 3471, 2881, 2933, 1792, 1453, 1392, 1349, 1244, 1199, 1094, 1026, 941, 846, 751, 666, 622. MALDI-TOF-MS: m/z calculated for $C_7H_{15}NO_3$: 264.12, and Found: 287.04($M^+ + Na^{+)}$

Synthesis of *tert*-butyl (2-hydroxyethyl) carbamate (2): Ethanolamine (10.00 g, 164.0 mmol) was taken in the mixture of 10% Na_2CO_3 (60 mL) and THF (5 mL) and

stirred at 25 °C for 10 minutes. Boc-anhydride (42.0 g, 196.0 mmol) in THF (40 mL) was added drop wise in the reaction mixture. After the addition, the content was stirred at 25°C for 12 h. At the end of the reaction, white color precipitate was observed. THF was removed by rota evaporator and the content was extracted with ethyl acetate (60mL). The organic layer was neutralized with 5% HCl (40mL), dried over anhydrous sodium sulphate and the solvent was removed to obtain colorless liquid as product. It was purified by passing through silica gel column of 60-120 mesh using 10% methanol in chloroform as eluent. Yield = 23.0 g (88 %).^{1}H NMR ($CDCl_3$, 400 MHz) δ: 3.64 ppm (t, 2H, C**H**$_2$-OH), 3.23 ppm (t, 2H, C**H**$_2$-NH), 1.41 ppm (s, 9H, OC-(C**H**$_3$)$_3$, 5.25ppm (s, 1H, CH_2-N**H**). ^{13}C NMR ($CDCl_3$, 100 MHz) δ: 156.84(**C**OO), 79.65(O**C**-CH_3**)** 62.48(**C**H2-OH), 43.09(**C**H_2-NH) 28.33(O**C**-CH_3**).** FT-IR (cm^{-1}): 3352, 2976, 2933, 2881, 1683, 1518, 1453, 1393, 1365, 1274, 1249, 1164, 1064,999,972, 900, 862, 781, 650. MALDI-TOF-MS: m/z calculated for $C_7H_{15}NO_3$: 161.11, and Found: 184.03($M^+ + Na^+$).

Synthesis of *tert*-butyl (2-(3-pentadecylphenoxy) ethyl carbamate (3): Compound **2** (2.64 g, 16.0 mmol), 3-pentadecylphenol (5.00 g, 16.0 mmol), and triphenylphosphine (4.30 g, 16.0 mmol) was dissolved in of dry tetrahydrofuran (20 mL). The reaction mixture was then kept in ice-cooled bath for 10 minute under N_2 purge. Diisopropyl azodicarboxylate (3.65 mL, 18.0 mmol) was added drop wise and the reaction mixture was stirred at 25 °C for 24 h. The mixture was directly loaded in silica gel column of 60-120 mesh and was eluted using 1% ethyl acetate in hexane as eluent. Yield = 4.2g (58 %).^{1}H NMR ($CDCl_3$, 400 MHz) δ: 7.19 ppm (t, 1H, Ar-**H**), 6.80-6.70 ppm (m, 3H, Ar-**H**),5.02 ppm (s, 1H, N**H**), 4.02 ppm (t, 2H, Ar-OC**H**$_2$), 3.54 ppm (t, 2H, C**H**$_2$-N), 2.58 ppm (t, 2H, Ar-C**H**$_2$), 1.46 ppm (s, 9H, OC-C(C**H**$_3$)$_3$, 1.6-0.88 ppm (m, 29H, Aliphatic H). ^{13}C NMR ($CDCl_3$, 100 MHz) δ: 158.62(Ar-C), 155.98 (**C**O-O), 144.85, 129.29, 121.32, 114.75, 111.40 (Ar-C), 79.57 (O**C** $(CH_3)_3$, 67.08 (Ar-OCH_2), 40.26(C**H**$_2$-N), 36.09, 32.00, 29.76, 26.47, 22.77, 14.20. FT-IR (cm^{-1}): 3396, 2916, 2850, 1690, 1590, 1512, 1453, 1362, 1250, 1157, 1060, 959, 866, 778, 690.MALDI-TOF-MS: m/z calculated for $C_{28}H_{49}NO_3$: 447.37, and Found: 470.29 ($M^+ + Na^+$).

Synthesis of 2-(2-(2-methoxyethoxy)ethoxy)ethyl 4-oxo-4-((2-(3-pentadecylphenoxy)ethyl)amino)butanoate(PDP-TEG):):Trifluoroacetic acid (10 mL, 134.2 mmol) was added drop wise in to compound 3 (2.00 g, 4.5 mmol) in dichloromethane (5 mL) After string the reaction mixture for 1 h at 25 °C the solvent was removed by rotavapour. Fresh dichloromethane (5mL) was added to the product and washing was repeated for 3 times to remove TFA. The content was poured in ice-cooled diethyl ether (15 mL). The white solid mass (2.00 g, 5.7 mmol) obtained

was dissolved in dry dichloromethane (15 mL) and purged with nitrogen for 15 minutes. To this reaction mixture, 1c (1.52 g, 5.7 mmol) was added and the content was purged under nitrogen for 15 minutes. EDC (1.32 g, 6.9 mmol) and diisopropylethylamine (2.0 mL, 11.5 mmol) was added to the reaction mixture under nitrogen atmosphere and the reaction was continued for 24 h at 25 °C. The mixture was poured into water (30 mL) and extracted with chloroform (20 mL). The organic layer obtained was neutralized with 2N HCl (2 mL), washed with aqueous 5 % $NaHCO_3$ (50 mL) and brine. After drying over anhydrous sodium sulphate, the solvent was removed to obtain yellow liquid as product. It was further purified by passing through silica gel column of 60-120 mesh using 25% methanol in chloroform as eluent. Yield = 2.5 g (78.0 %).^{1}H NMR ($CDCl_3$, 400 MHz) δ: 7.18 ppm (t, 1H, Ar-**H**), 6.80-6.69 ppm (m, 3H, Ar-**H**),6.26 (CO-N**H**), 4.24 ppm (t, 2H,COO-C**H**$_2$), 4.02 ppm (t, 2H, Ar-OC**H**$_2$), 3.69-3.54 ppm (m, 10H, O-C**H**$_2$-C**H**$_2$),3.56 ppm (t, 2H, C**H**$_2$-N), 2.70 ppm (t, 2H, Ar-C**H**$_2$), 3.38 ppm (s, 3H, CH_2-OC**H**$_3$), 2.57 ppm (t, 2H, NH-CO-C**H**$_2$), 2.51 ppm (t, 2H, C**H**$_2$-COO), 1.6-0.88 ppm (m, 29H, Aliphatic **H**). ^{13}C NMR ($CDCl_3$, 100 MHz) δ: 172.75(NH-CO),171.52(CO-O), 158.42, 144.74, 129.20, 121.27, 114.58, 111.32 (Ar-C), 71.85 (CH_2-OCH_3), 70.48 (O-CH_2-CH_2),68.92, 66.52(Ar-OCH_2), 63.70 (COO-CH_2), 58.96(O-CH_3), 39.05(CH_2-N), 35.97, 31.87, 31.38, 29.64, 29.32, 22.64, 14.08.FT-IR (cm^{-1}): 3309, 2848, 2915, 1741, 1640, 1552, 1454, 1405, 1351, 1293, 1249, 1203, 1166, 1106, 1045, 952, 857, 777, 696. MALDI-TOF-MS: m/z calculated for $C_{34}H_{59}NO_7$: 593.43, and Found: 616.35 ($M^+ + Na^+$).

Synthesis of 2-methoxyethyl 4-oxo-4-((2-(3-pentadecylphenoxy) ethyl) amino) butanoate (PDP-EG): Compound **3** (2.00 g, 4.5 mmol), trifluoroacetic acid (10 mL, 134.2 mmol), **1a** (0.50 g, 2.8 mmol), EDC (0.59 g, 2.2 mmol) and diisopropylethylamine (0.98 mL, 5.7 mmol) were used. The product was purified by passing through silica gel column of 60-120 mesh using 70 % ethyl acetate in pet ether as eluent Yield = 0.6 g (42.0 %). ^{1}H NMR ($CDCl_3$, 400 MHz) δ: 7.19 ppm (t, 1H, Ar-**H**), 6.80-6.69 ppm (m, 3H, Ar-**H**), 6.13 ppm (CO-N**H**),4.24 ppm (t, 2H,COO-C**H**$_2$), 4.02 ppm (t, 2H, Ar-OC**H**$_2$), 3.67 ppm (t, 2H, C**H**$_2$-OCH_3), 3.56 ppm (t, 2H, C**H**$_2$-N), 3.38 ppm (s, 3H, CH_2-OC**H**$_3$), 2.73 ppm (t, 2H, Ar-C**H**$_2$), 2.57 ppm (t, 2H, NH-CO-C**H**$_2$), 2.52 ppm (t, 2H, C**H**$_2$-COO), 1.6-0.88 ppm (m, 29H, Aliphatic H). ^{13}C NMR ($CDCl_3$, 100 MHz) δ: 172.95(NH-**C**O),171.52(**C**O-O), 158.52, 144.89, 129.33, 121.43, 114.71, 111.45 (Ar-C), 70.42(Ar-O**C**H_2), 66.66**(C**H_2-OCH_3),63.79 (COO-**C**H_2), 59.07 (O-**C**H_3), 39.16 (**C**H_2-N), 36.10, 32.00, 31.51, 31.07, 29.64, 29.77, 22.77, 14.21 (Aliphatic C).FT-IR (cm^{-1}): 3318, 2845, 2915, 1731, 1647, 1542, 1449, 1406, 1351, 1256, 1179, 1124, 1042, 982, 925, 761,724, 690. MALDI-TOF-MS: m/z calculated for $C_{30}H_{51}NO_5$: 505.38 and Found: 528.37

($M^+ + Na^+$).

Synthesis of 2-(2-methoxyethoxy) ethyl 4-oxo-4-((2-(3-pentadecylphenoxy) ethyl) amino) butanoate (PDP-DEG): Compound **3** (2.00 g, 4.5 mmol), trifluoroacetic acid (10 mL, 134.2 mmol) was added drop wise, **1b** (1.20 g, 5.5 mmol) DCC (1.35 g, 6.5 mmol) and DMAP (0.07g, 0.6 mmol) were used. The product was purified by passing through silica gel column of 60-120 mesh using 50% ethyl acetate in pet ether as eluent. Yield = 1.2 g (40.0 %).^{1}H NMR ($CDCl_3$, 400 MHz) δ: 7.19 ppm (t, 1H, Ar-**H**), 6.81-6.70 ppm (m, 3H, Ar-**H**), 6.18 ppm (CO-N**H**), 4.24 ppm (t, 2H,COO-C**H**$_2$), 4.03 ppm (t, 2H, Ar-OC**H**$_2$), 3.70-3.63 ppm (m, 6H, OC**H**$_2$C**H**$_2$O), 3.56 ppm (t, 2H, C**H**$_2$-N), 3.39 ppm (s, 3H, CH_2-OC**H**$_3$), 2.70 ppm (t, 2H, Ar-C**H**$_2$), 2.57 ppm (t, 2H, NH-CO-C**H**$_2$), 2.51 ppm (t, 2H, C**H**$_2$-COO), 1.6-0.88 ppm (m, 29H, Aliphatic H). ^{13}C NMR ($CDCl_3$, 100 MHz) δ: 172.88 (NH-**C**O), 171.61 (**C**O-O), 158.54, 144.86, 129.31, 121.40, 114.71, 111.46 (Ar-**C**), 71.93(**C**H_2–OCH_3), 70.50(Ar-O**C**H_2), 69.10, 66.65 **(C**H_2-O**C**H_2),63.81 (COO-**C**H_2), 59.11 (O-**C**H_3), 39.16 (**C**H_2-N), 36.09, 31.99, 31.49, 29.75, 29.67, 22.76, 14.19 (Aliphatic C).FT-IR (cm^{-1}): 3306, 2848, 2913, 1739, 1639, 1551, 1454, 1402, 1348, 1250, 1203, 1134, 1047, 961, 863, 757, 713. MALDI-TOF-MS: m/z calculated for $C_{30}H_{51}NO_5$: 549.40 and Found: 572.32($M^+ + Na^+$).

Synthesis of *tert*-butyl (2-(3-pentadecy-8-en-1-yl) phenoxy) ethyl) carbamate (CAR-amine-Boc): Compound **2**(3g, 18.6mmol)), Cardanol (5.62g, 18.6mmol) and triphenylphosphine (5.34g, 20.4mmol) was dissolved in of dry tetrahydrofuran (40 mL). The reaction mixture was then kept in ice-cooled bath for next 10 min along with N_2 purging. Diisopropyl azodicarboxylate (3.62ml, 17.7mmol) was added drop wise and reaction mixture was stirred at 25 ˚C for 24 h. The mixture was directly loaded in silica gel column of 60-120 and was eluted using 2.5% ethyl acetate in hexane as eluent.Yield = 4.1g (49.0 %).^{1}H NMR ($CDCl_3$, 400 MHz) δ: 7.19 ppm (t, 1H, Ar-**H**), 6.83-6.73 ppm (m, 3H, Ar-**H**),5.38 ppm (d,2H, C**H**=C**H**), 5.02 ppm (s, 1H, N**H**), 4.03 ppm (t, 2H, Ar-OC**H**$_2$), 3.53 ppm (t, 2H, C**H**$_2$-N), 2.58 ppm (t, 2H, Ar-C**H**$_2$), 2.05 ppm (m, C**H**$_2$ CH=CHC**H**$_2$), 1.46 ppm (s, 9H, OC-C(C**H**$_3$)$_3$, 1.6-0.88 ppm (m, 21H, Aliphatic H). ^{13}C NMR ($CDCl_3$, 100 MHz) δ: 158.62(Ar-C), 155.98 (**C**O-O), 144.85, 129.29, 121.32, 114.75, 111.40 (Ar-C), 130.03 (**C**H=**C**H), 79.57 (O**C** $(CH_3)_3$, 67.08 (Ar-OCH_2), 40.26(C**H**$_2$-N), 36.09, 32.00, 29.76, 26.47, 22.77, 14.20. FT-IR (cm^{-1}): 3396, 2916, 2850, 1690, 1590, 1512, 1453, 1362, 1250, 1157, 1060, 959, 866, 778, 690.MALDI-TOF-MS: m/z calculated for $C_{28}H_{47}NO_3$: 445.68 and Found: 468.23($M^+ + Na^+$).

Synthesis of 2-(2-(2-methoxyethoxy)ethoxy)ethyl 4-oxo-4-((2-(3-pentadec-8-en-1-yl)phenoxy)ethyl)amino)butanoate (CAR-TEG):): Trifluoroacetic acid (14.81 mL, 67.4 mmol) was added drop wise in to Car-amine-Boc (2.87 g, 6.45 mmol) in dichloromethane (7 mL). After string the reaction mixture for 1 h at 25 ˚C the solvent was removed by rotavapour. Fresh dichloromethane (5mL) was added to the product and washing was repeated for 3 times to remove TFA. The content was poured in ice-cooled diethyl ether (15 mL). The yellow liquid (0.64 g, 1.85 mmol) was dissolved in dry dichloromethane (15 mL) under N_2atmosphere. To this reaction mixture **1c**(0.443 g, 1.68 mmol) was added and purging was continued for another 15 minutes. Then DCC (0.414 g, 2.06 mmol) and DMAP (0.021 g, 0.168 mmol) were added to the reaction mixture under nitrogen atmosphere and the reaction was continued for 24 h at 25 ˚C. The mixture was poured into water (30 mL) and extracted with chloroform (20 mL). The organic layer obtained was neutralized with 2N HCl (2 mL), washed with aqueous 5% $NaHCO_3$ (50 mL) and brine. After drying over anhydrous sodium sulphate, the solvent was removed to obtain pale yellow liquid as product. It was further purified by passing through silica gel column of 60-120 mesh using 25% methanol in chloroform as eluent. Yield = 0.22 g (23.0%).^{1}H-NMR ($CDCl_3$, 400 MHz) δ: 7.16 ppm (t, 1H, Ar-**H**), 6.78-6.68 ppm (m, 3H, Ar-**H**),6.32 (CO-N**H**), 5.33 ppm (d,2H, C**H**=C**H**), 4.21 ppm (t, 2H,COO-C**H**$_2$), 4.01 ppm (t, 2H, Ar-OC**H**$_2$), 3.67-3.63 ppm (m, 10H, O-C**H**$_2$-C**H**$_2$),3.54 ppm (t, 2H, C**H**$_2$-N), 2.70 ppm (t, 2H, Ar-C**H**$_2$), 3.36 ppm (s, 3H, CH_2-OC**H**$_3$), 2.57 ppm (t, 2H, NH-CO-C**H**$_2$), 2.50 ppm (t, 2H, C**H**$_2$-COO), 2.00 ppm(m, C**H**$_2$ CH=CHC**H**$_2$), 1.6-0.88 ppm (m, 21H, Aliphatic H). ^{13}C NMR ($CDCl_3$, 100 MHz) δ: 172.89(NH-**C**O),171.66(**C**O-O), 158.53,144.84, 129.90, 121.40, 114.70, 111.45 (Ar-C), 130.04(**C**H=**C**H), 71.97 (**C**H_2-OCH_3), 70.61 (O-**C**H_2-**C**H_2),69.06, 66.64(Ar-OCH_2), 63.84 (COO-**C**H_2), 59.10(O-CH_3), 39.17(C**H**$_2$-N), 36.09, 32.00, 31.50, 29.77, 29.07, 22.74, 14.20.FT-IR (cm^{-1}): 3309, 2848, 2915, 1741, 1640, 1552, 1454, 1405, 1351, 1293, 1249, 1203, 1166, 1106, 1045, 952, 857, 777, 696. MALDI-TOF-MS: m/z calculated for $C_{34}H_{59}NO_7$: 591.41 and Found: 614.41($M^+ + Na^+$).

Synthesis of 2-(2-(2-methoxyethoxy)ethoxy)ethyl 4-(dodecylamino)-4-oxobutanoate (DD-TEG):. Dodecyl amine (1.31 g, 8.33 mmol) was dissolved in dry dichloromethane (15 mL) and purged with nitrogen for 15 minutes. To this **1c** (2.0 g, 7.5 mmol) was added and the content was purged under nitrogen for 15 minutes DCC (1.87 g, 9.09 mmol) and diisopropylethylamine (0.09 g, 0.75 mmol) was added to the reaction mixture under nitrogen atmosphere and the reaction was continued for 24 h at 25 ˚C. The mixture was poured into water (30 mL) and extracted with chloroform (20 mL). The organic layer obtained was neutralized with 2N HCl (2 mL), washed with aqueous 5% $NaHCO_3$ (50 mL) and brine. After drying over

anhydrous sodium sulphate, the solvent was removed to obtain yellow liquid as product. It was further purified by passing through silica gel column of 60-120 mesh using 80% ethyl acetate in hexane as eluent. Yield = 1.5 g (46.0%).^{1}H NMR ($CDCl_3$, 400 MHz) δ: 4.20 ppm (t, 2H,COO-C**H**$_2$), 3.93 ppm (t, 2H, COOC**H**$_2$C**H**$_2$), 3.67-3.61 ppm (m, 8H, O-C**H**$_2$-C**H**$_2$),3.53 ppm (t, 2H, C**H**$_2$-N), 3.35 ppm (s, 2H, CH_2-OC**H**$_3$), 2.70 ppm (t, 2H, NH-CO-C**H**$_2$), 2.63 ppm(t, 2H, C**H**$_2$-COO), 1.87-0.72 ppm (m, 23H, Aliphatic H). ^{13}C NMR ($CDCl_3$, 100 MHz) δ: 172.75(NH-**C**O),171.52(**C**O-O), 158.42, 144.74, 129.20, 121.27, 114.58, 111.32 (Ar-C), 71.85 (**C**H_2-OCH_3), 70.48 (O-**C**H_2-**C**H_2), 68.92, 66.52(Ar-OCH_2), 63.70 (COO-**C**H_2), 58.96(O-CH_3), 39.05(C**H**$_2$-N), 35.97, 31.87, 31.38, 29.64, 29.32, 22.64, 14.08. FT-IR (cm^{-1}): 3309, 2848, 2915, 1741, 1640, 1552, 1454, 1405, 1351, 1293, 1249, 1203, 1166, 1106, 1045, 952, 857, 777, 696. MALDI-TOF-MS: m/z calculated for $C_{34}H_{59}NO_7$: 431.32 and Found: 509.23 ($M^+ + K^+$).

2.3. Results and Discussion

2.3.1. Synthesis and Characterization of Amphiphiles

The synthesis of amphiphilic molecules from commercially available ethylene glycols as hydrophilic part and renewable resource 3-pentadecylphenol (PDP) as the hydrophobic part is shown in scheme 2.1. Briefly, succinic anhydride was ring opened with oligoethylene glycol monomethyl ether derivatives $CH_3O(CH_2CH_2)_xOH$, where x=1, 2 and 3 in presence of Et_3N to give acids **1a-1c**. Ethanolamine was reacted with Boc-anhydride to give *tert*-butyl (2-hydroxyethyl) carbamate (**2**). Compound **2** was reacted with PDP under Mitsonoubu coupling reaction in the presence of triphenylphosphine and diisopropyl azodicarboxylate to give *tert*-butyl (2-(3-pentadecy-8-en-1-yl) phenoxy) ethyl) carbamate (**3**). Compound **3** was further hydrolysed by trifluoroacetic acid (TFA) and coupled with **1a-1c** to give the designed amphiphiles. These amphiphiles are named as PDP-X, where x= EG, DEG, and TEG with respect to the number of $(CH_2CH_2)_xO$ units x=1, 2, and 3, respectively. Two more amphiphiles based on cardanol (CAR, have unsaturated double bonds in the C15 alkyl tail) and dodecyl amine (DD) (see structures in scheme 2.1) was also prepared. The details of their synthesis are given earlier in experimental section.

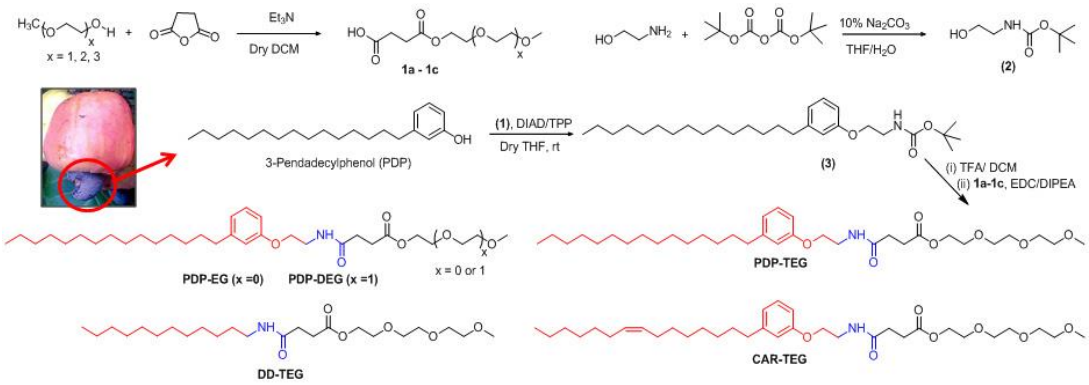

Scheme 2.1. *Synthesis of thermo-responsive amphiphiles.*

The structures of the amphiphiles were characterized by ^{1}H, ^{13}C-NMR, and MALDI-TOF-TOF mass spectrometers. Figure 2.6 shows the ^{1}H-NMR, ^{13}C NMR and MALDI-TOF-TOF spectra of a representative PDP-TEG amphiphile. The Ar-**H**

(type a) in PDP-TEG appears as a triplet at 7.18 ppm and type b, and c as a multiplet at 6.80-6.69 ppm. The broad N**H** peak appears at 6.26 ppm. Two tripletsappear for the COOC**H**$_2$ protons (type e) and Ar-OC**H**$_2$ protons (type f) at 4.24 ppm and 4.02 ppm, respectively. A multiplet appears for the all the ethylene glycol protons (type g, h) at 3.69-3.54 ppm. A triplet corresponding toC**H**$_2$-N at 3.56 ppm gets merged with oligotheylene peaks. Singlet appears for the O-CH_3 proton (type j) at 3.38 ppm. A triplet appears for the NH-CO-C**H**$_2$- protons (type k) at 2.57 ppm. Triplet appears for the Ar-CH_2 protons at 2.51 ppm. All alkyl protons appear at 1.55-0.82 ppm. All the other amphiphiles were similarly characterised and the detailed analysis has been given earlier in the experimental section.

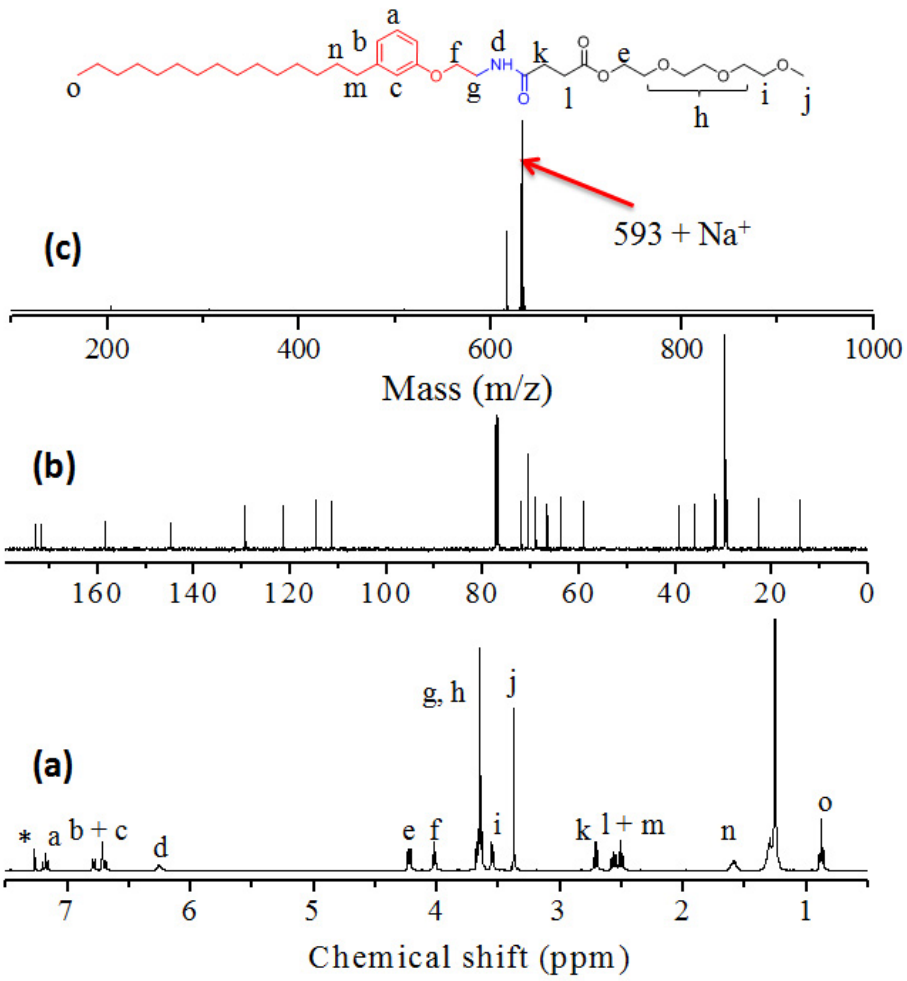

Figure.2.6. *(a) ^{1}H-NMR spectrum (b) ^{13}C-NMR spectrum (c) MALDI-TOF-TOF spectrum of PDP-TEG.*

All other amphiphiles such as PDP-EG, PDP-DEG, DD-TEG and CAR-TEG were characterised by by ^{1}H, ^{13}C-NMR, and MALDI-TOF-TOF mass spectrometers. The ^{1}H spectra of all amphiphiles are shown in figure 2.7. The purity of the amphiphiles was determined by size exclusion chromatography.

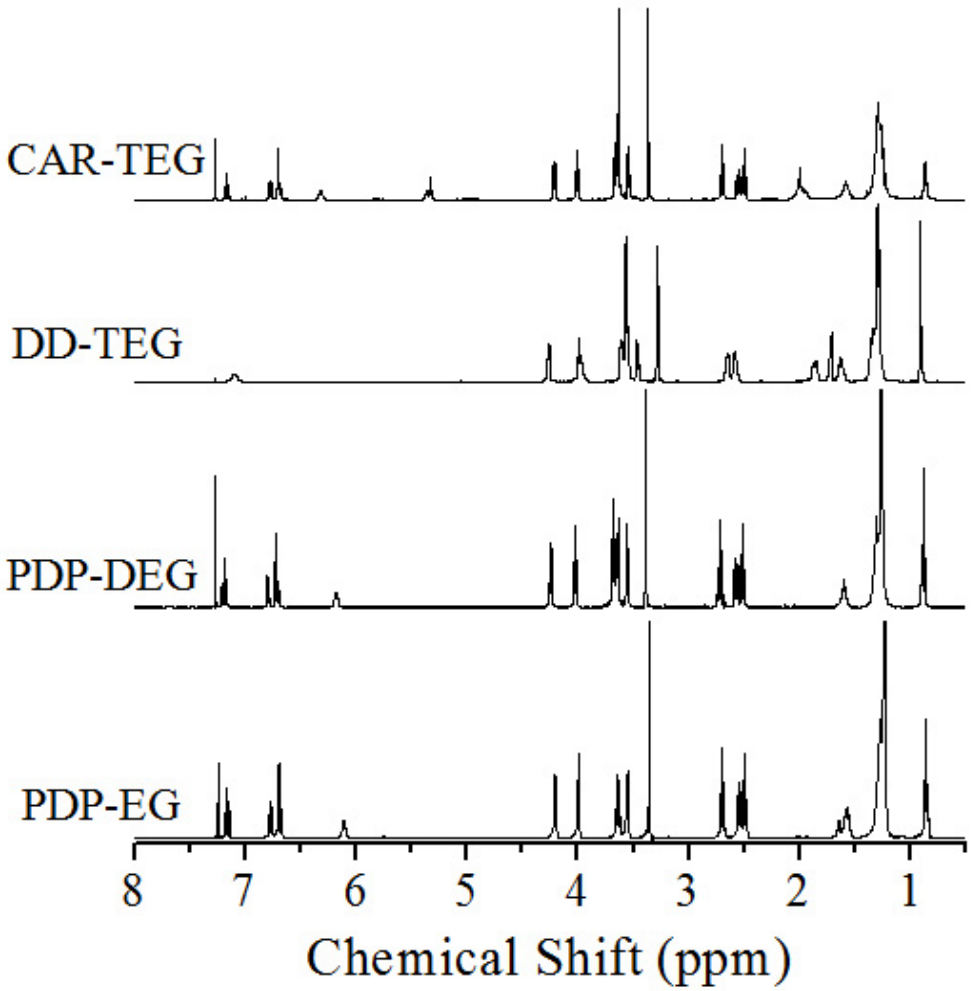

Figure.2.7. *^{1}H-NMR spectrumof all PDP-EG, PDP-DEG, DD-TEG and CAR-TEG*

The solubility of the amphiphiles in water was found to be dictated by the number of the ethylene oxy units rather than the hydrophobic units (PDP, CAR or DD). For example, the amphiphiles with very short $(CH_2CH_2O)_x$ units: PDP-EG and PDP-DEG were found to be completely insoluble in water (thus, these two short amphiphiles were not included for further studies). On the other hand, all other three

amphiphiles PDP-TEG, CAR-TEG, DD-TEG were found to be dispersible in water or PBS buffer (pH = 7.4) at 25 °C.

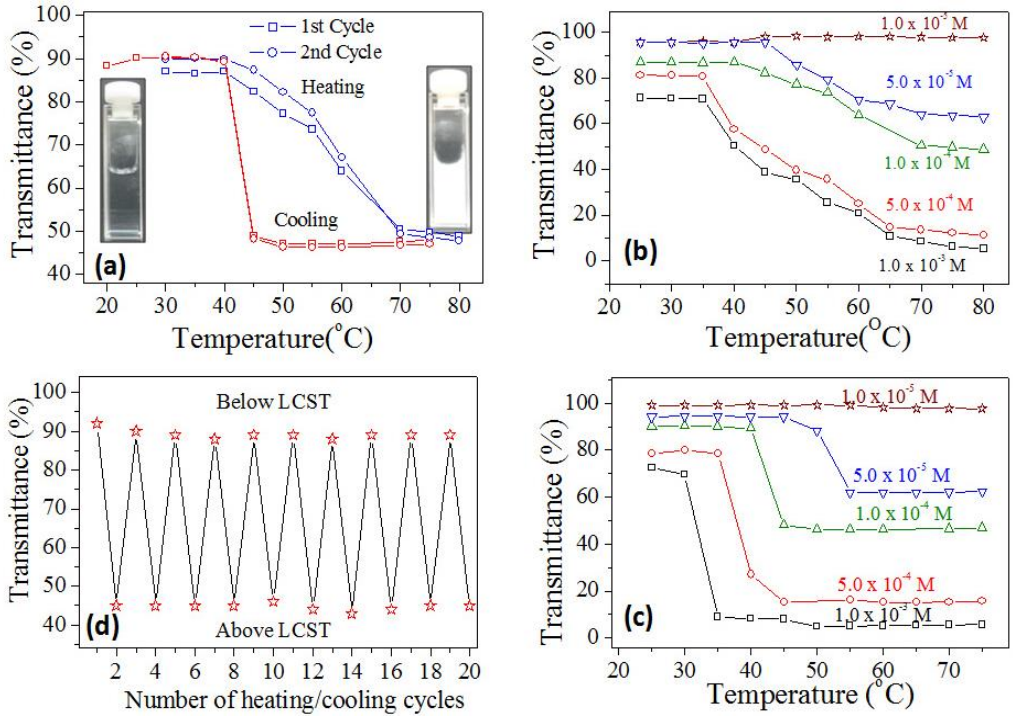

Figure.2.8. *(a) Temperature dependent optical transmittance of PDP-TEG (10^{-4}M) in water in consecutive heating and cooling cycles. Optical transmittance of PDP-TEG in the (b) heating cycle and (c) cooling cycle for concentration varying from 10^{-3}M to 10^{-5} M. (d) Reversible phase transition phenomena in ten consecutive heating and cooling cycles.*

2.3.2. Thermo-responsive Behavior of PDP-TEG

To study the thermo-responsive behaviours of the amphiphiles, they were subjected for optical transmittance measurement as a function of temperature using absorption spectroscopy. The plot of optical transmittance of PDP-TEG is shown in figure 2.8a. The plot consisted data from two consecutive heating and cooling cycles from 30 °C to 80 °C. The plots revealed that the optical transmittance was 90 % below 40 °C (as solution was clear) and the sample became opaque and turbid above 42 °C (<50 % transmittance). The vials in the photographs are clearly evident for the change in the transmittance in the heating and cooling cycles. Further, the plots also

revealed that the formation and clearance of turbidity in the heating and cooling cycles respectively, follow different kinetic paths. For example, in the heating cycle, the appearance of turbidity began at 40 °C and slowly completed at 70 °C. On the other hand, in the cooling cycle the change from turbid to clear solution occurred sharply at 45 °C. This suggested that self-assembly was slow process in the heating cycle whereas the reversibility was very sharp in the subsequent cooling. Thus, the lower critical solution temperature (LCST) of the PDP-TEG was assigned as 42 °C.

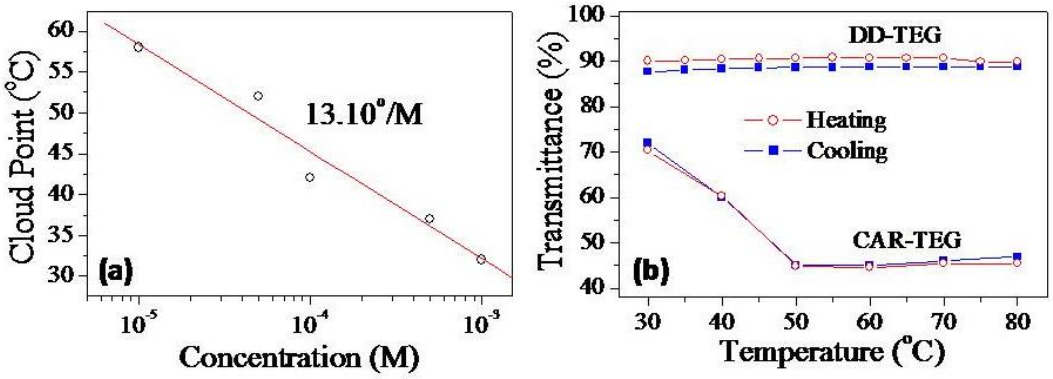

Figure.2.9.*(a) Plot of cloud point of PDP-TEG at versus concentration. (b) Optical transmittance of CAR-TEG and DD-TEG in heating and cooling cycles (10^{-4}M) in water.*

Thermo-responsive nature of the PDP-TEG at concentration ranging from $1x10^{-5}$ to $1x10^{-3}$ M was investigated and their heating and cooling cycle data are shown in figure 2.8b and 2.8c, respectively. The LCST of the PDP-TEG decreased with increase in the amphiphile concentration. At very low concentration, the PDP-TEG did not show any phase-separation phenomena. This indicated that the LCST of the amphiphile was concentration driven process. Further, the complete reversibility of the thermo-responsive behaviour of the amphiphiles was studied by measuring optical transmittance of the amphiphiles both at above and below Tcp temperatures for ten consecutive cycles. And it was observed that the thermal response of the amphiphiles was completely reversible (see figure 2.8d). The cloud points obtained for each concentration was plotted and are shown in Fig. 2.9a. The plot reveals that Tcp varied linearly with the concentration of the amphiphile (with increase in concentration from 10^{-5} M to 10^{-3} M), the cloud point decreased from 56 °C to 32 °C.

The slope of the line indicated that the cloud point changed by 13.10°/mol/L (or 0.022°/g/L) of the amphiphile concentration. Thermo-responsive PNIPAM-copolymer was found to show cloud point over concentration range as 0.51 °/g/L.[52] This suggested that the custom designed amphiphile was capable of showing thermo-responsiveness at much lower concentration (~25 times lower concentration) compared high molecular weight polymers like PNIPAM. Hence, it may be concluded that the PDP-TEG is a potential amphiphilic molecule with thermo-responsive behaviour equivalent to that of high molecular weight polymers for drug delivery applications.To study the influence of hydrophobic units on the thermo-responsive behaviour, both DD-TEG and CAR-TEG were also investigated and their optical transmittances are shown in figure 2.9b. DD-TEG did not show LCST phenomena while CAR-TEG showed very weak phase-separation. This indicated that π-π stacking of aromatic units in case of PDP-TEG and CAR-TEG is essential for LCST transition. Therefore, it suggested that the nature of the hydrophobic unit in the amphiphile structure also played crucial role in the molecular self-assembly. Thus, appropriate molecular design is essential to make the small molecular derivatives such as PDP-TEG as thermo-responsive amphiphiles. In the present case, the combination of renewable hydrophobic PDP unit, amide linkages and hydrophilic triethylene glycol monomethyl ether units provided appropriate molecular geometry for thermo-responsiveness in PDP-TEG amphiphile.

2.3.3. Shape and Size of the Amphiphile Self-assembly

To study the thermo-responsive self-organization of amphiphile in water, PDP-TEG was subjected to variable temperature dynamic light scattering (DLS) and static light scattering (SLS) studies. The DLS histograms of the aggregates at different temperatures were measured for 10^{-4} M solution and their plots are shown in figure 2.10 a. PDP-TEG showed mono-modal distributions at all the temperatures indicating the formation of homogeneous size aggregates. The stability of these nanoparticles was also investigated in different pH solution (see figure 2.10b), it was found that these nanoparticles were stable from acidic to basic

pH of 4.0 to 10.0. The hydrodynamic radius of the aggregates (half of their hydrodynamic diameter) from DLS were plotted as function of temperature and shown in figure 2.10c. The figure signified that the hydrodynamic radius of these aggregates decreased with increase in temperature. Below LCST the hydrodynamic radius of these aggregates was obtained as 110 ± 10 nm while above LCST it reduced to 45 ± 4 nm. From the plot of R_h versus the temperature, the break point was obtained as 40°C which is almost identical to the onset temperature for the phase separation (see figure 2.8a). The reversibility of the self-assembly process of the amphiphiles was further investigated by dynamic light scattering techniques (equipped with laser source, excitation 633 nm) for ten consecutive cycles. The plot of hydrodynamic diameter against number of cycles at temperature above and below LCST is shown in figure 2.11 a. The amphiphiles showed complete reversibility at temperatures both above and below LCST.

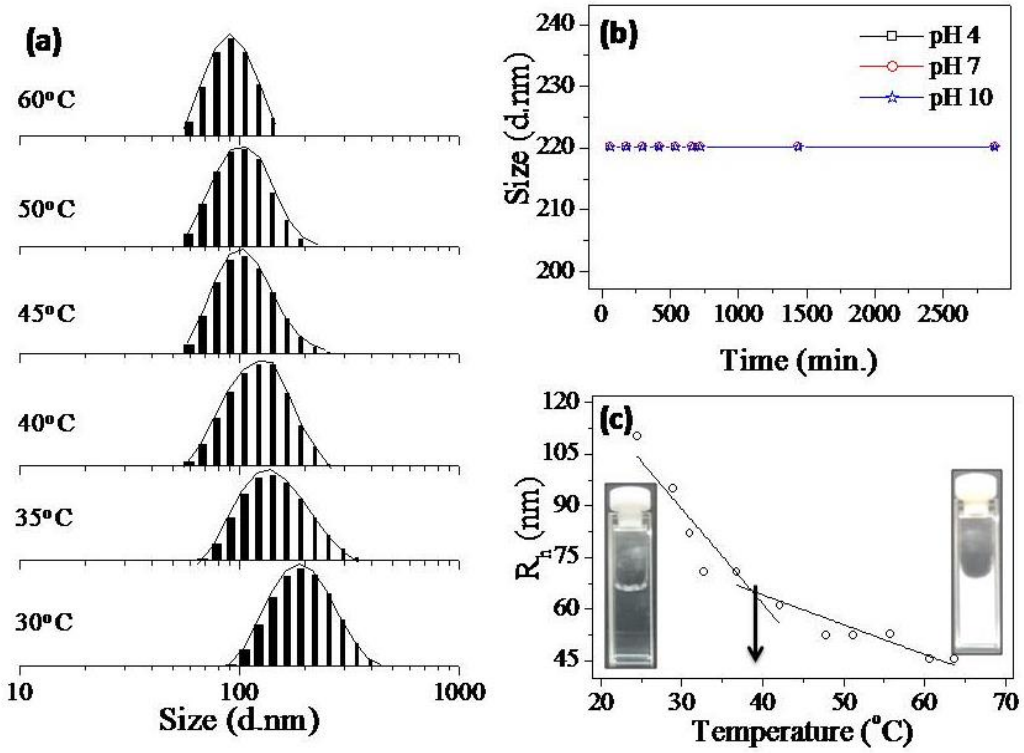

Figure 2.10 *(a) Variable temperature DLS histograms of PDP-TEG in water at 10^{-4}M. (b)Aggregate sixe of PDP-TEG vs time at different pH. (c) Plot of hydrodynamic radius versus temperature of PDP-TEG.*

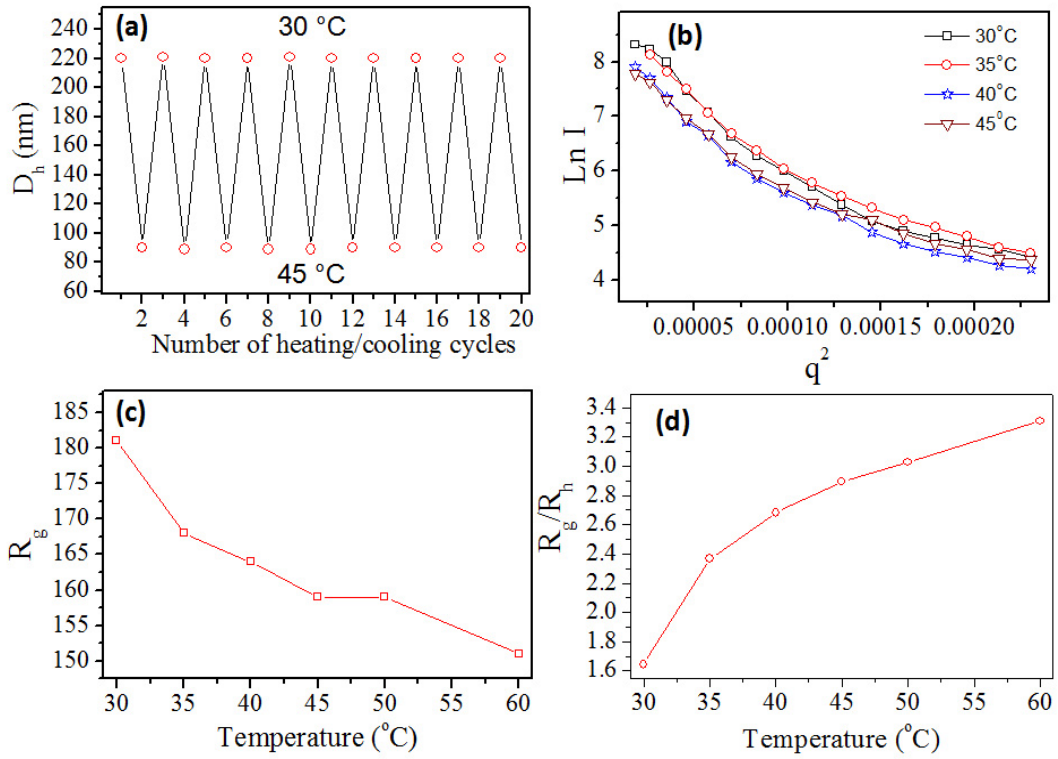

Figure 2.11*(a) Hydrodynamic diameter oscillation of the nanoparticles in the heating and cooling cycle. (b) Guinier plot of PDP-TEG in water at 10^{-4}M at various temperatures. (c) Average radius of gyration (R_g) of PDP-TEG obtained from static light scattering. (d) The plot of R_g/R_h ratio versus temperature.*

SLS measurement was carried out at 10^{-4} M solution by heating the sample in stepwise manner with an interval of 5 °C. The intensity of the scattered light obtained at various angles and at different temperature was then plotted against q^2, where q is scattering vector magnitude and the plot obtained is known as Guinier plot (see figure 2.11 b). The slope of the Guinier plot gives $(R_g)^{2/3}$ from which radius of gyration (R_g) was calculated. The plot of radius of gyration against temperature is shown in figure 2.11c. The plot revealed that with increase in temperature, the radius of gyration decreased from 180 nm to 150 nm. Utilizing R_g and R_h value obtained at various temperatures from DLS and SLS measurement, the ratio R_g / R_h was determined. The plot of R_g / R_h against temperature is shown in figure 2.11d.From the plot it is evident thatwith increase in temperature the R_g / R_h ratio increases from

1.6 to ~3.0, thereby indicating transformation from globular to rod-like structures.[53-55]

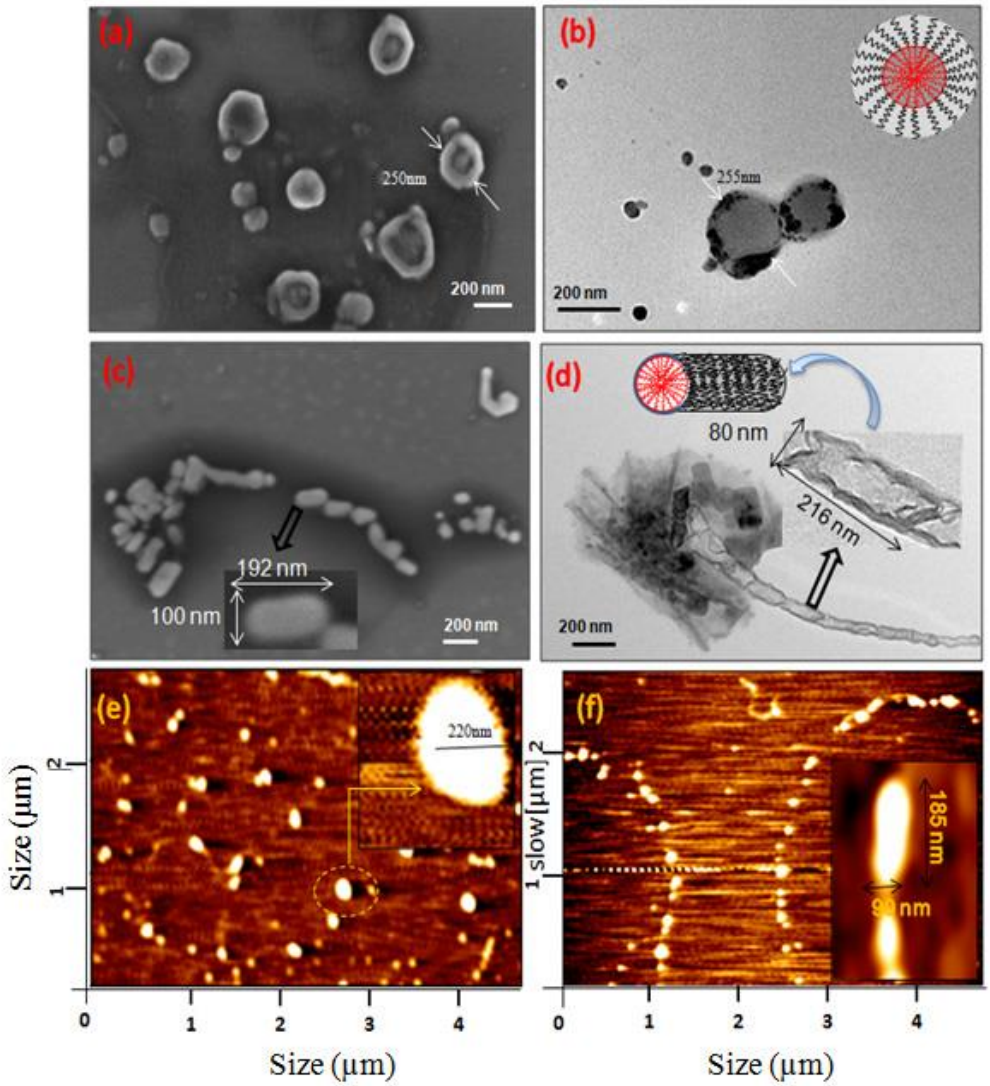

Figure 2.12. *(a) FE-SEM images of PDP-TEG at 30 ℃. (b) HR-TEM image at 30 ℃. (d) FE-SEM images of PDP-TEG at 45 ℃. (e) TEM images of PDP-TEG at 45 ℃. (e) AFM image of PDP-TEG at 30 ℃. (f) AFM image of PDP-TEG at 45 ℃.*

To visualize the shape and size of the aggregates formed by the amphiphile, the samples were subjected to field emission scanning electron microscopy (FE-SEM), high resolution transmission electron microscopy (HR-TEM), and atomic force microscopy (AFM) analysis. FESEM, HR-TEM and AFM images of PDP-TEG at 25 °C (below LCST) are given in figure 2.12. In figure 2.12a, the FE-SEM

image of the PDP-TEG showed the existence of spherical core-shell like aggregates of 250 ±17 nm diameters. [56-59] The formation of these core- shell structures of 255 ± 24 nm in diameter was further confirmed by HR-TEM (see figure 2.12b). TEM image showed hydrophobic core which was surrounded by hydrophilic shell (dark layer). Further, the AFM image (see figure 2.12e) also showed the existence of the spherical particles of 220 ± 20 nm. The images of aggregates above LCST were shown in figure 2.12c, 2.12d and 2.12f. In figure 2.12c, the aggregates showed the formation of clusters instead of isolated particles (as observed below LCST in figure 2.12a). Further, the shape of the aggregates was also transformed from spherical to rod-like structures. The formation of these rod-like nanostructures was further confirmed by HR-TEM image (see figure 2.12d). The internal parts of the rod-like structures were found to be hollow as similar to core-shell nanoparticles. AFM images in figure 2.12f also supported the formation of elongated structures above LCST. From all three images (figure 2.12c, 2.12d and 2.12f), it is very clear that the amphiphiles existed as rod-like nanoparticles above LCST and as core-shell nanoparticles below LCST.

2.3.4. Shape Transformation

To prove the existence of the in-situ shape transformation in the thermo-responsive scaffolds (see figure 2.13) in the heating and cooling cycles; the dimensions of the core shell structures were compared with the rod-like objects. In the figure 2.13, the micellar structure represents the individual micelles. The size 200 nm actually represents the aggregated micellar structures as single nanoparticles. For the above transformation, one would expect the circumference ($2\pi r$, where r= radius of core shell) of the spherical core-shell structure to be equal to the twice the lengths (L) plus the widths (W) of the nano-rods.[60] The average diameter of core-shell nanoparticles was obtained as 254 ± 35 nm, 225 ± 40 nm and 183 ± 25 nm from FE-SEM, TEM and AFM respectively. Thus, the average diameter of the core-shell nanoparticle based on all three techniques together was found to be 220 ± 36 nm (average radius = 110 ± 17 nm). The average diameter of the rod-like structure above

LCST was obtained as 94 ± 16 nm, 88 ± 18 nm and 108 ± 16 nm from FE-SEM, TEM and AFM respectively. Likewise, the length of these rod-like structures was obtained as 178 ± 37nm, 193 ± 35nm and 185 ± 16 nm from FE-SEM, TEM and AFM, respectively. All three techniques, together gave diameter and length of the rod-like structures as 97 ± 10 nm and 185 ± 8nm, respectively. The average circumference of the core-shell structure (below LCST) was calculated as $2\pi r = 0.69 \pm 0.11$ μm. This value was matching with the $2L+2D = 0.57 \pm 0.04$ μm of rod within the experimental error limit. Thus, the average sizes of the rod-like structure were in close agreement with the average diameter of the core-shell nanoparticles. This confirmed that the core-shell nanoparticles collapsed above LCST to produce rod-like structures. The resultant rod-like structures aggregated together to produce turbid solution above LCST which was completely reversible in the subsequent cooling cycle (see figure 2.8).

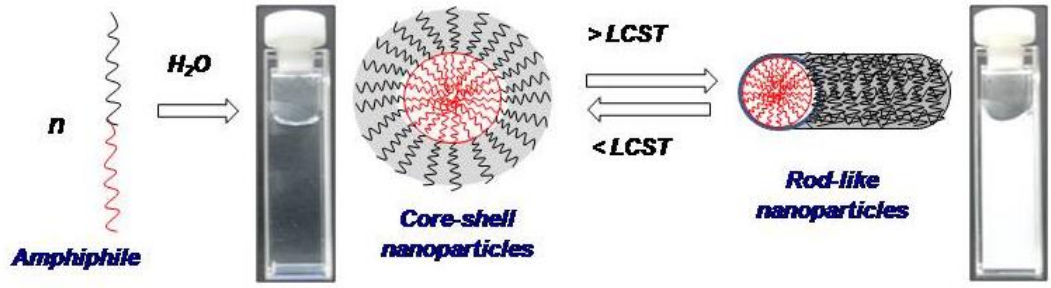

Figure 2.13. *Mechanism of shape transformation in thermo-responsive scaffolds.*

The in-situ shape transition from the hydration (below LCST) to dehydration (above LCST) state of PDP-TEG was further supported by variable-temperature ^{1}H-NMR studies. The ^{1}H-NMR spectra of PDP-TEG at various temperatures were recorded in D_2O with an interval of 10 °C from 30 to 70 °C (heating cycle). The plot of ^{1}H-NMR spectra of PDP-TEG recorded at various temperatures in the heating and cooling cycle is shown in figure 2.14a and 2.14b, respectively. Below LCST, the signals corresponding to the hydrophobic tail (1.6-0.88 ppm) and aromatic protons (7.18-6.69 ppm) of PDP in the amphiphile appeared with less intensity. This was attributed to the less exposure of the hydrophobic part of the amphiphile to aqueous

environment in core shell state.[61-63] With increase in temperature, the intensity of the signals corresponding to hydrophobic tail (1.6-0.88 ppm) and aromatic protons (7.18-6.69 ppm) were enhanced. This was attributed to breaking of hydrogen bonds of the amide-linkage with water molecules resulting in increase in chain mobility.[64,65] These signals showed complete reversibility in the subsequent cooling cycles (see figure 2.14b). Thus, below LCST, the PDP-TEG amphiphile exist in the form of core-shell nanoparticles. As temperature was increased above LCST the hydrophilic segments collapsed on the top of the hydrophobic core to produce rod-like assemblies. This type of transition would occur only if the hydrophobic segments are tightly held together in the inner core to facilitate the collapsing or un-coiling of PEG chains at the periphery of the nano-scaffolds.

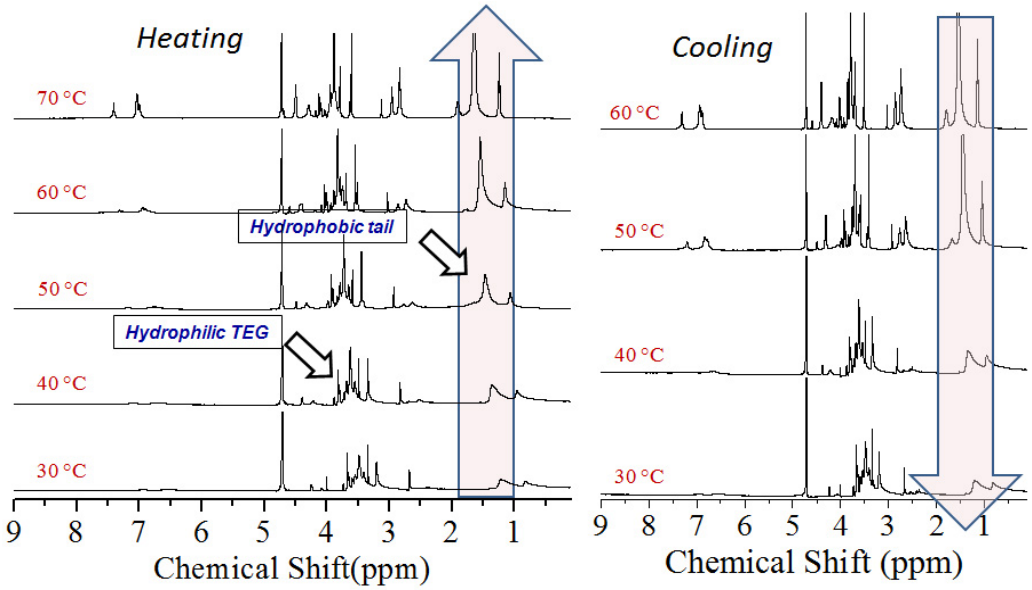

Figure 2.14. *Variable temperature ^{1}HNMR of PDP-TEG in D_2O in respective heating and cooling cycle.*

To provide evidence for the strong packing of hydrophobic PDP units, the single crystal for the compound **3** (see scheme 2.1) was obtained in dichloromethane/methanol solvent mixture (2:3 v/v). As it can be seen in figure 2.15 a and 2.15b, the terminal boc-protected amine group and the long alkyl tail were arranged in trans-confirmation with respect to each other. The three dimensional

packing of the molecules along the a-axis showed (see figure 2.15b) that the alkyl chains were extended towards each other via hydrophobic-hydrophobic interactions and were inter-digitated. While the enlarged view of the molecular packing (see figure 2.15b) revealed that the molecules were interlocked via inter-chain hydrogen bonding present between the amide linkages of the amphiphiles. Based on the morphology (FE-SEM, HR-TEM and AFM), variable temperature NMR and single crystal structure study, it may be concluded that the newly designed PDP-TEG was very unique molecule to undergo thermo-responsive phase transition from core-shell to rod-like structures.

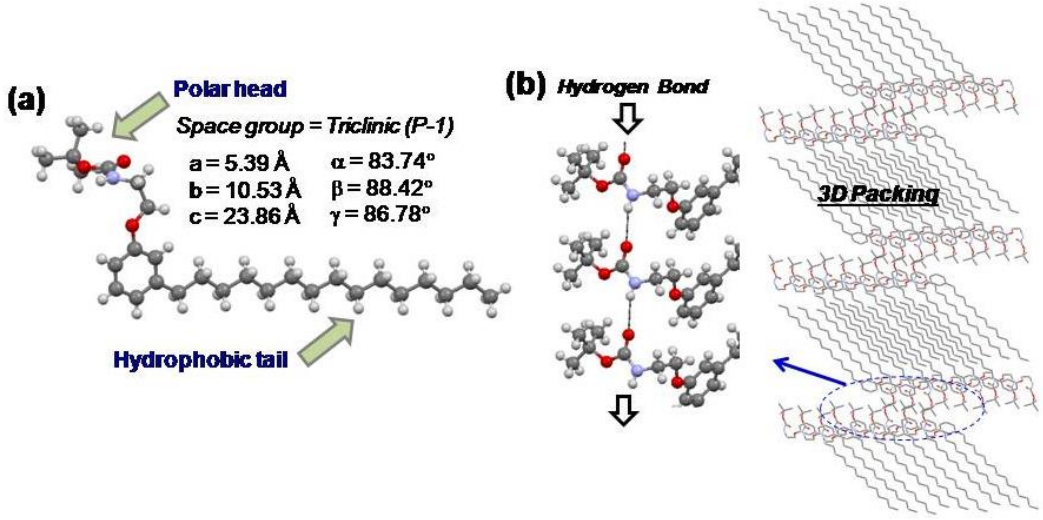

Figure 2.15*. (a) Single crystal structure of molecule 3 in scheme 2.1. (b) Three dimensional packing of molecule 3 along a-axis showing and the inter-digitations of hydrophobic tails and inter-chain hydrogen bonding.*

2.3.5. Anticancer Drug Encapsulation

The thermo-responsive amphiphile was further utilized as scaffolds for loading and delivering anticancer drug molecules. Two different hydrophobic anticancer drugs doxorubicin (DOX) and camptothecin (CPT) were chosen as drug candidates to demonstrate the proof-of-concept on the ability of the shape transformable thermo-responsive scaffold. The drugs were encapsulated in the hydrophobic interior of the core shell particle by dialysis method. The drug loading content was estimated using absorbance spectroscopy as 4.2 wt% and 1.6 wt% for

DOX and CPT, respectively. The sizes of the DOX and CPT loaded scaffolds were determined by DLS and they were found to be 220 ± 20 nm and 190 ± 20 nm, respectively (see figure2.16a and 2.16b). The sizes of the drug loaded particle was similar to that of the nascent ones (see figure 2.10a) indicating that the scaffold retained its self-organization even after the encapsulation of hydrophobic drugs. The temperature-dependent phase-transition of the DOX and CPT loaded core-shell nanoparticles were investigated and their data are given in figure 2.16c and 2.16d. The drug load scaffolds preserved the reversible self-organization in the heating cooling cycles as similar to their un-loaded core-shells. The LCST of DOX encapsulated scaffold was found to be 40 °C which was close to the nascent scaffold (42°C). On the other hand, the LCST of CPT loaded scaffolds (see figure 2.16 d) was found to be 50 °C which was 8-10° higher than that of nascent scaffold.

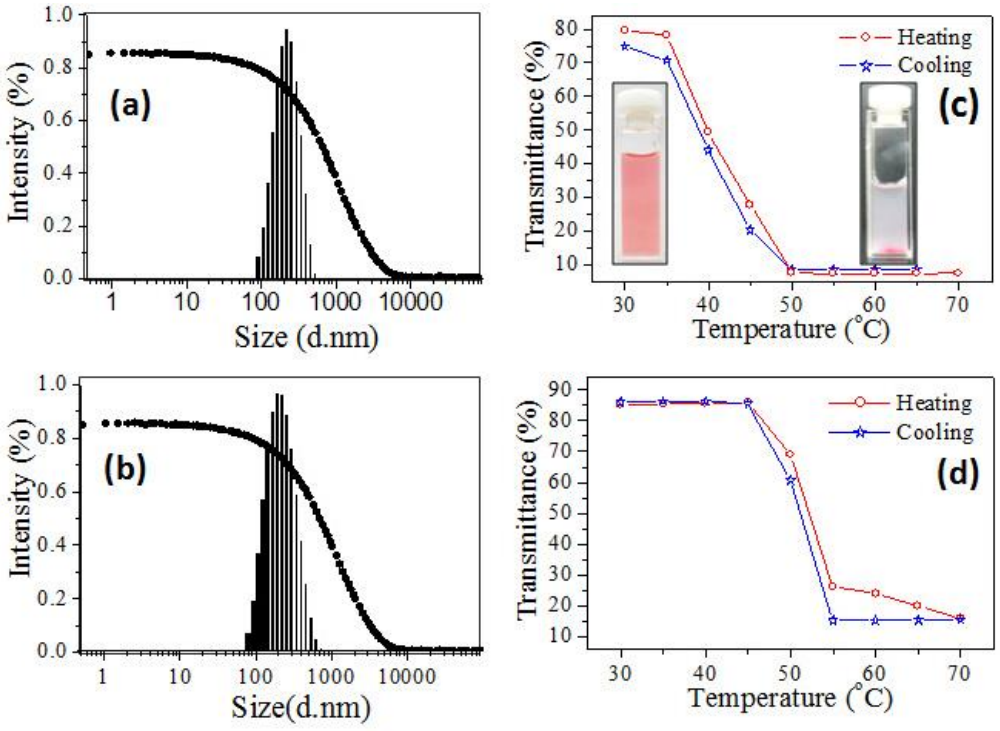

Figure 2.16. *DLS histogram of DOX (a) and CPT (b) encapsulated scaffolds. Temperature dependence of transmittance of (c) DOX loaded, (d) CPT loaded PDP-TEG in water at 10^{-4}M.*

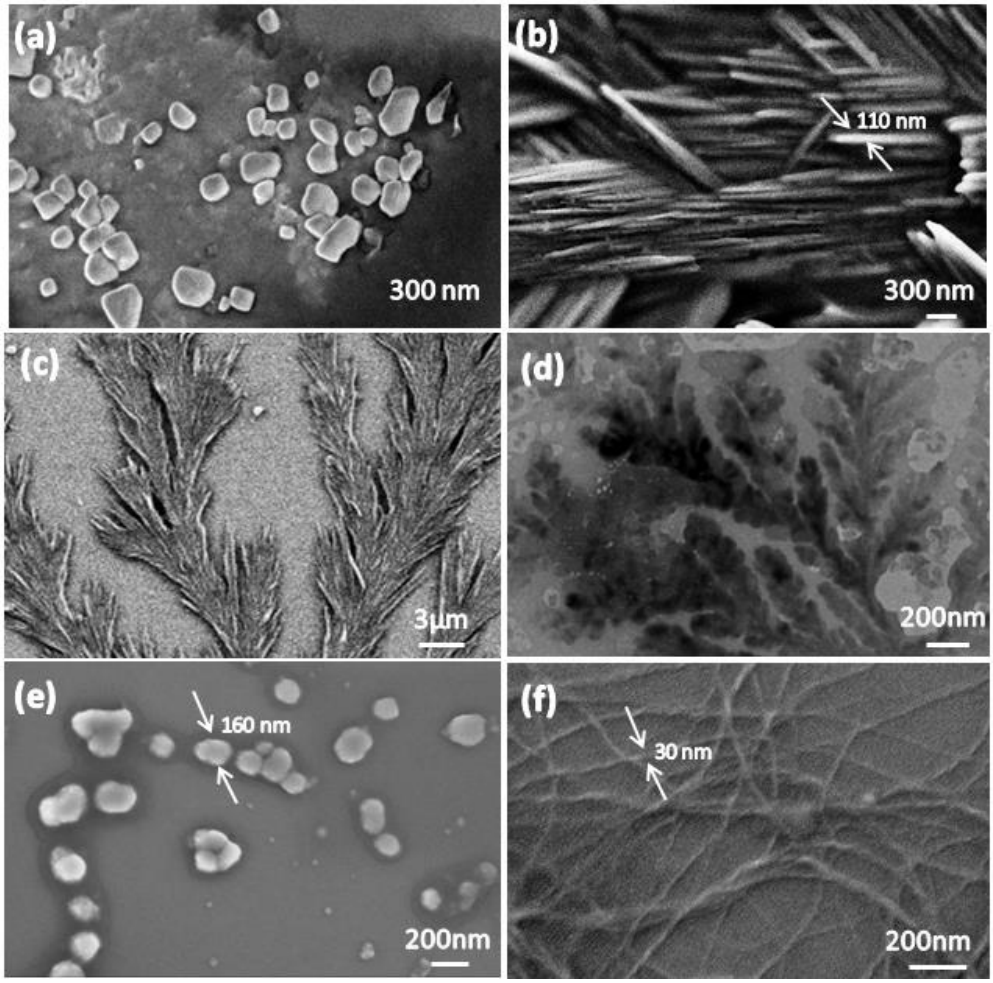

Figure 2.17. *FESEM image of DOX encapsulated PDP-TEG at 30 ^{o}C (a), 45 ^{o}C (b), and large area image at 45 ^{o}C (c) in water at 10^{-4}M. (d) TEM image of DOX encapsulated PDP-TEG at 45 ^{o}C in water at 10^{-4}M. FESEM image of CPT encapsulated PDP-TEG at 30 ^{o}C (e), and 45 ^{o}C (f) in water at 10^{-4}M.*

The morphologies of the drug loaded scaffolds are shown in figure 2.17. FE-SEM images of DOX loaded scaffold (see figure 2.17a) appeared as spherical particles with diameter of 200 ± 10 nm. Above LCST (at 45 °C), the shape of drug loaded amphiphile underwent morphological transformation from spherical to rod-like structures (see figure 2.17b). These rod-like structures were aggregated together to produce bundles which were arranged in a dendritic fashion (see larger area image figure 2.17c). In figure 2.17d, the TEM images of the DOX loaded scaffolds confirmed the existence of dendritic nature by rod-like structures. Though the CPT

loaded scaffolds appeared as spherical particles having diameter of 160 ± 10 nm below LCST (see figure 2.17e), it underwent shape transformation into nano-fibrous structures at higher temperature (see figure 2.17f). These fibrous structures are typically produced by the long range aggregation of drug plus scaffold. The difference in the morphological transformation of DOX and CPT loaded scaffolds at higher temperature can be attributed to the molecular structure of the drugs. Doxorubicin consists of five free hydroxyl group and one amino group, whereas in case of CPT only one free hydroxyl group is present. Therefore DOX interacts more strongly with the ethylene glycol units of the amphiphile thereby retaining the in-situ shape transition of nascent scaffold. On the other hand, the presence of only one free hydroxyl group leads to weak interaction with the ethylene glycol units. Hence, the nano-fibrous structures were formed in case of CPT loaded scaffold at higher temperature. Thus, it may be concluded that the DOX loaded core shell structures retained the in-situ phase transitions of nascent scaffolds whereas long nano-fibrous morphology was obtained for CPT loaded core-shells.

As both DOX and CPT are fluorescent in nature; the drug loaded nanoparticles were subjected for fluorescence microscopy images as well as photophysical studies in order to elucidate their property in free and encapsulated states. The fluorescence microscopy images of both DOX and CPT loaded nanoparticles are shown in figure 2.18a and 2.18c, respectively. Although both DOX and CPT are hydrophobic in nature, they are partially soluble in PBS (phosphate buffer saline, pH = 7.4). Absorbance and emission spectra of free DOX as well as DOX loaded nanoparticles were recorded in PBS and are shown in figure 2.18b. The absorbance and emission spectra of DOX (see figure 2.18b) did not show any variation upon encapsulation as compared to free DOX. Similarly, the absorbance and emission spectra of free CPT and CPT loaded scaffold was also recorded (see figure 2.18d) and were found to be almost identical which indicated that the properties of CPT did not change upon encapsulation. In other words, the properties of both hydrophobic drugs (DOX and CPT) did not showed any variation after being encapsulated in the hydrophobic pockets of the nanoparticles. This was further

confirmed by fluorescence lifetime of free drug as well as drug loaded nanoparticles by TCSPC techniques. The decay profile of both DOX and CPT in absence and presence of nanoparticles was collected in PBS at 558 nm and 448 nm respectively, using nano-LED laser source with 460 nm (for DOX) and 347 nm (for CPT) as excitation wavelength. The decay profiles of DOX loaded nanoparticles and free DOX is shown in figure 2.18e. Similarly decay profiles of CPT loaded nanoparticles and free CPT is shown in figure 2.18 f. Bothe the decay profiles were fitted by bi-exponential decay fits using DAS6 program and their lifetime data are summarized in table 2.2. The TCSPC lifetime values (τ_1) of DOX upon encapsulation were found to be 1.49 ns which are in close agreement with the lifetime value of free DOX (0.95 ns). Similarly, lifetime (τ_1) of CPT in loaded as well as free form was 4.66 ns and 4.59 ns respectively. The DOX and CPT retained their original structural features inside the scaffolds.

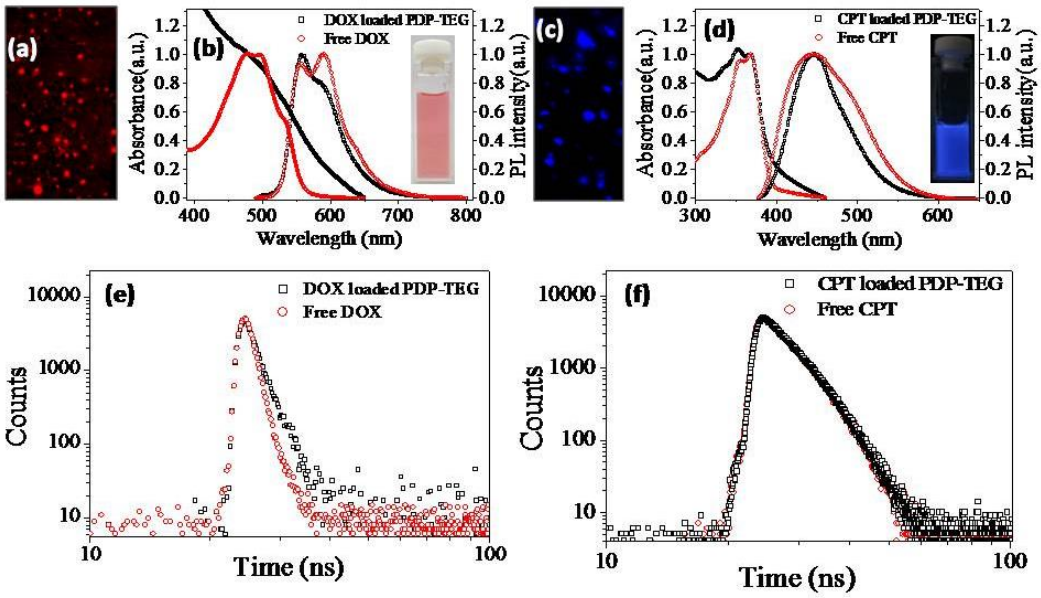

Figure 2.18.*Fluorescence microscopy images of DOX loaded scaffolds (a), and CPT loaded scaffolds (c) in PBS at 10^{-4}M. (b) Absorbance and emission spectra of free DOX and DOX loaded scaffolds. (d) Absorbance and emission spectra of free CPT and CPT loaded scaffolds.Decay profiles of (e) DOX loaded nanoparticle and free DOX, (f) CPT loaded nanoparticle and free CPT.*

Table 2.2.*Life time values of drug loaded PDP-TEG nanoparticles. The values in the brackets indicate the amplitudes.*

Drug loaded nanoparticles	**Collected at emission wavelength**		
	τ_1(ns)	**τ_2(ns)**	**χ^2**
DOX loaded nanoparticle	1.49(0.90)	5.06(0.10)	1.07
Free DOX	0.95(0.95)	2.40(0.05)	1.29
CPT loaded nanoparticle	4.66(0.57)	0.62(-0.43)	1.15
Free CPT	4.59(0.56)	0.67(-0.44)	0.99

2.3.6. *In Vitro* Drug Release Studies

Thermo-responsive drug release of DOX and CPT loaded nanoparticles were studied under physiological conditions (PBS, pH =7.4) as well as under cancer tissue environment (PBS, pH = 6.8). The drug release profile of DOX loaded scaffold at 37 °C in PBS having pH= 6.8 is shown in figure 2.19. The plot reveals that the nanoparticle was very stable and is capable of preserving the drug at pH= 6.8. Similarly, the release profile of DOX under physiological conditions (PBS, pH =7.4) was also studied (see figure 2.20a). It was observed that release profiles of the drug at pH = 7.4 or (pH= 6.8) were identical indicating that the scaffold was very stable and was also capable of preserving the drug at pH 7.4.

Further, the temperature for release studies were chosen based on the physiological temperature in cancer tissues (40-43°C), normal body temperature (37°C) and drug storage at ambient temperature (25 °C) (see figure 2.5). The drug loaded scaffolds were subjected to incubation at these three different temperatures i.e. 25°C, 37°C and 44°C. The cumulative release profiles of DOX and CPT at all the three different temperatures are shown in figure 2.20 a and 2.20 b, respectively.

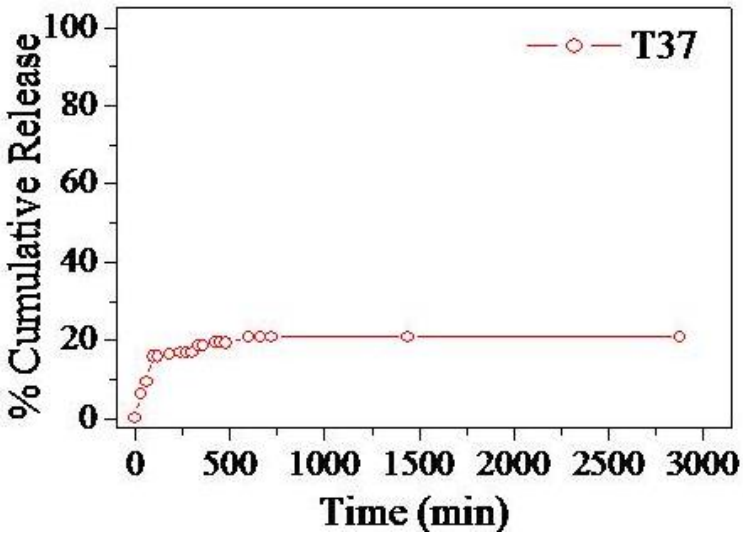

Figure 2.19. *Cumulative release profile of DOX at temperature below LCST and pH= 6.8.*

The percentage release of DOX at temperature below LCST i.e. 37°C and 25°C was less than 20%. This suggested that DOX loaded scaffold is very stable both at ambient as well as normal body temperature. At the cancer tissue temperature (above LCST at 44^{o}C), the DOX loaded scaffold showed selective release of more than 95% of the drug within 5h. At 25 °C, the CPT loaded particles (see figure 2.20b) were stable enough however, at body temperature (37 °C), more 80 % of the drug was released. At temperature above LCST (55 °C), almost 95 % of the drug was released within 5 h. This suggested that CPT loaded scaffold lost its ability to selectively release the drug at cancer tissue temperature.

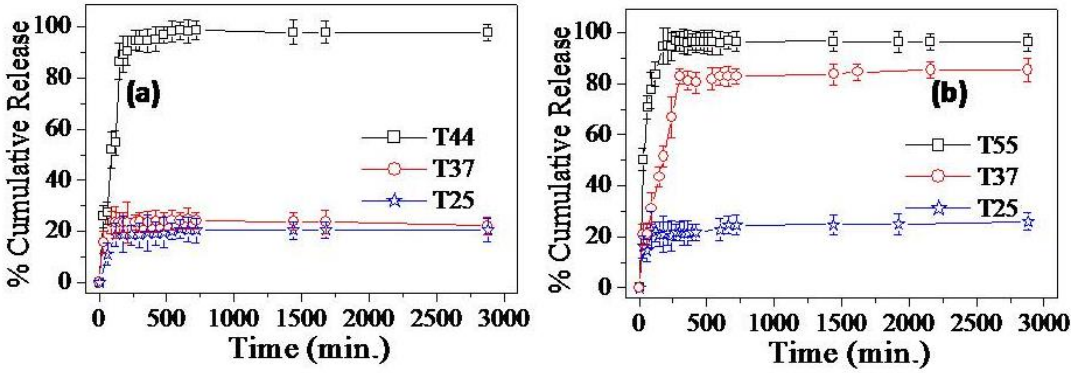

Figure 2.20.Cumulative release profile of (a) DOX and (b) CPT loaded scaffolds at temperature above and below LCST.

2.3.7. Drug Release Kinetics

The release of the drug from the polymer matrix involved several processes such as diffusion of the drug from membrane, erosion of the polymeric scaffolds and so on. Ritger and Peppas developed a semi-empirical model as given below for the drug release:[66,67]

$$\frac{M_t}{M_\infty} = kt \qquad (1)$$

$$\log\left(\frac{M_t}{M_\infty}\right) = n \log t + \log k \qquad (2)$$

where, M_t and M_∞ are the cumulative amount of drug released at time t and infinite time, respectively, *k* is a constant that depends on the structural and geometric characteristics of the polymer and *n* is the release exponent which indicates the drug release mechanism. In case of spherical particles, the value of $n = 0.43$ for Fickian diffusion and ≥ 0.85 for non-Fickian diffusion. This equation generally holds for the first 60% of the fractional drug release or for the values in the interval of $0.1<M_t/M_\infty<0.7$. This methodology was adopted by many researchers to study the drug release kinetics form micelles, vesicles and nanogels and so on. Zhuang and co-workersused the above mentioned equation to study the release mechanism of the drug from the nanogels,[68] Lecommandoux and co-workershave used the above equation to analyse the release mechanism of the drug from the polymersomes.[69] The Peppas model was currently employed by Bapurao *et al*. from our research group used the expression to analyze the mode of drug release from the polycaprolactone vesicular assemblies.[70] In the present investigation, drug release from the thermo-responsive polymer matrix was analyzed by Ritger and Peppas equation and the data are summarized in figure 2.21.

The drug release profiles were fitted to the above equation and their kinetics plots log (M_t/M_∞) against log t are shown in figure 2.21a. The rate constant k and n values are reported in the table in figure 2.21. The DOX loaded particles followed non-Fickian diffusion (n = 1.052) for selective delivery in the cancer tissue temperature. On the other hand, the CPT loaded scaffold showed unusual trend in which either non-Fickian diffusion (n = 0.824) or Fickian diffusion process (n = 0.357) occurs with respect to the normal body and cancer tissue temperatures. The difference in the release rate of DOX and CPT can be attributed to the difference in their morphology obtained at higher temperature (T > LCST). The retention of rod-like structure in DOX loaded scaffold (similar to nascent one) led to the release of DOX in controlled manner while the change in the morphology (nan-fibrous structures) in CPT loaded scaffold results burst release.

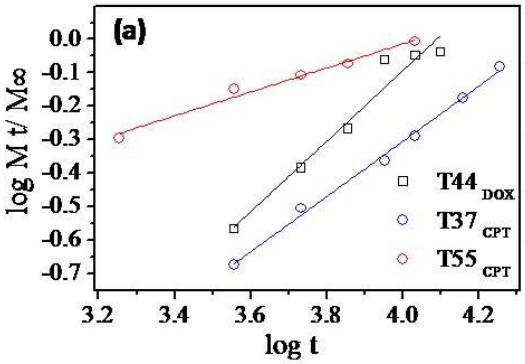

Drug loaded nanoparticles			
Parameters / Temperature	n_1	k_1	R^2
T44 DOX	1.052	49.6 μs^{-1}	0.949
T37 CPT	0.824	250.0 μs^{-1}	0.994
T55 CPT	0.357	36.0 ms	0.972

***Figure 2.21**. **(a)** Kinetic plots of DOX and CPT loaded scaffolds. Table contains the values of rate constant (k), and n of DOX and CPT releases.*

2.3.8. Cytotoxicity Studies

The cytotoxicity of the core-shell nanoparticles were investigated in cervical cancer (HeLa) cell lines using MTT assay method. The concentration of the core-shell nanoparticles was varied from 0.1µg/mL to 100.0µg/mL. The cells were incubated for 72 h at 37 °C. The histogram depicting the % cell viability data for nascent scaffold is shown in figure 2.22a. The lower concentration of the core-shell

nanoparticle showed 50 % cell viability, indicating the biocompatibility of the lower concentration of the nascent scaffold. However, the higher concentration of the scaffold was found to be toxic. Similarly, the cytotoxicity of free DOX and DOX loaded nanoparticles was tested in HeLa cell lines keeping the experimental condition identical to the nascent scaffold. The concentration of DOX was chosen according to the amount of DOX present in the nanoparticle i.e. 100.0 µg/ mL of the scaffold consists of 4.66 µg/ mL of the DOX. The drug concentration was varied from 4.66 µg/ mL to 0.00465 µg/ mL corresponding to the respective scaffold concentration. Further for comparison, the same concentration of free DOX was also employed for treatment. The % cell viability data corresponding to free DOX and DOX loaded nanoparticles in HeLa cells are shown in figure 2.22b. From figure 2.22b, it is evident that DOX loaded in nanoparticles exhibited 30 % killing at the highest concentration.This suggested that the uptake of these drug loaded nanoparticles was better. As expected, free DOX showed higher killing than the DOX present inside the nanoparticle. This trend was attributed to the fast penetrating ability of the free drug as compared to drug loaded core-shell nanoparticle in the *in vitro* studies.

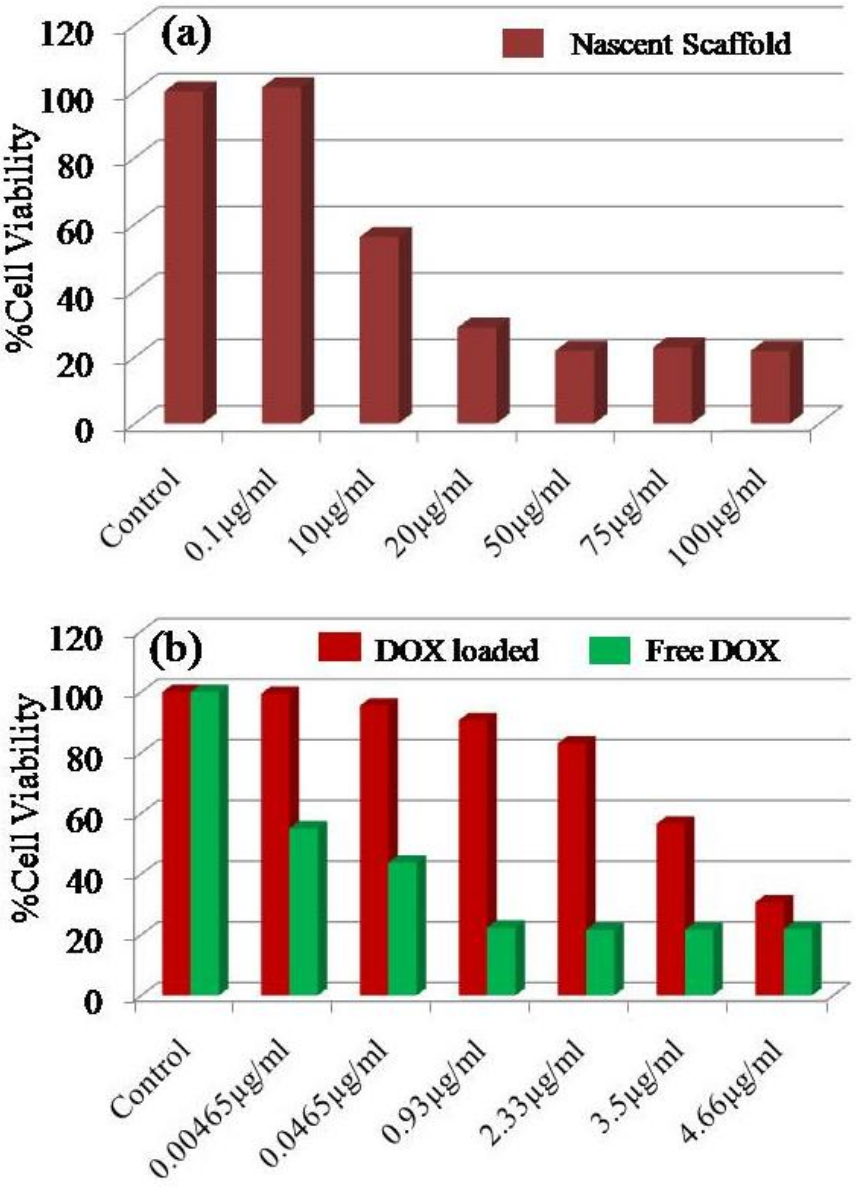

Figure 2.22. (a) *Cytotoxicity of PDP-TEG in HeLa cells at various concentrations. (b) Cytotoxicity of DOX loaded scaffold and free DOX in HeLa cells.*

Thus, the custom designed thermo-responsive amphiphile is a very potential candidate for loading and delivering anticancer drug like DOX selectively at the caner tissue temperature. The concept was successfully demonstrated based on new molecular design as well as delivering the anti-cancer drug exclusively at cancer tissue temperature. Although higher concentration of the nascent scaffold was found to be toxic, the lower concentration proves to be non-toxic in nature. However, the

cytotoxic effect of the drug loaded scaffold was less pronounced as compared to the free drug. Therefore, a further optimization of scaffold is required for the treatment of the cancer.

2.4. Conclusion

The present investigation demonstrated the design and development of in-situ shape transformable and thermo-responsive core-shell scaffolds for the first time and established their ability to load and deliver anticancer drug molecules at the cancer tissue temperature. For this purpose, a new amphiphilic molecule consisting of oligoethylene glycols and renewable resource 3-pentadecyl phenol as hydrophilic and hydrophobic units respectively was custom designed. Amide linkage was used as self-organization director to facilitate the self-assembly in aqueous medium with respect to lower critical solution temperature. The amphiphile self-assembled to produce core-shell nanoparticles at ambient temperature which underwent transformation into one dimensional rod-like assembly at temperatures closer to cancer tissue temperature. Dynamic and static light scattering confirmed the occurrence of the in-situ phase transition with respect to the R_g/R_h ratio. Morphological analysis by FE-SEM, HR-TEM and AFM provide direct evidence for the existence of amphiphilic core shell spherical morphology below LCST and rod-like structures above LCST. The shape transformation was further confirmed by carrying out detail calculation on the circumference of the core shell to that of the rod-like assemblies. Variable temperature ^{1}H-NMR studies and single crystal structures established existence of strong inter-digitations among the hydrophobic units which facilitated the thermo-responsive shape transformation. Anticancer drugs, doxorubicin (DOX) and camptothecin (CPT) were successfully loaded in the core-shell nanoparticles. These drug loaded nano-scaffolds retained their thermo-responsive molecular self-organization similar to that of their nascent amphiphiles. In vitro studies revealed that the DOX loaded scaffolds were very stable at normal body temperature (37 °C) and exclusively collapsed to release more than 90 % drugs at 44 °C which is similar to that of cancer tissue under physiological conditions. The

drug release kinetics indicated that DOX underwent non-Fickian diffusion. The MTT assay of the nascent scaffold demonstrated that lower concentration of the core-shell nanoparticle was not toxic to the cells.

2.5. References

1. Fleige, E.; Quadir, M. A.; Haag, R. *Adv. Drug Delivery. Rev.* **2012**, 64, 866-884.
2. Shim, M. S.; Kwon, Y. J. *Adv. Drug Delivery. Rev.***2012**, 64, 1046-1049.
3. Torchilin, V. P. *Nat. Rev. Drug Discov.* **2014**, 13, 813-827.
4. Crucho, C. I. C. *ChemMedChem.* **2015**, 10, 24-38.
5. Davis, M. E.; Chen, Z., Shin, D. M. *Nat. Rev.* **2008**, 7, 771-782.
6. Fang, J.; Nakamura, H.; Maeda, H. *Adv. Drug Delivery. Rev.* **2011**, 63, 136-151.
7. Maruyama, K. *Adv. Drug Delivery. Rev.***2011**, 63, 161-169.
8. Venkataraman, S.; Hedrick, J. L.; Ong, Z. Y.; Yang, C.; Ee, P. L. R.; Hammond, P.T.; Yang, Y. Y. *Adv. Drug Delivery. Rev.***2011**, 63, 1228-1246.
9. Devarajan, P. V.; Jindal, A. B.; Patil, R. R.; Mulla, F.; Gaikwad, R. V.; Samad, A. *J. Pharm. Sci*.**2010**, 9, 2576-2581.
10. Loverde, S. M.; Klein, M. L.; Discher, D. E. *Adv. Mater*.**2011**, 24, 3823-3830.
11. Champion, J.A.; Mitragotri, S. *Pharm. Res.* **2008**, 26, 244-249.
12. Doshi, N.; Mitragotri, S. *Adv. Funct. Mater.* **2009**, 19, 3843-3854.
13. Mitragotri, S.; Lahann, J. *Nat. Mat.* **2009**, 8, 15-23.
14. Frojmovic, M. M.; Milton, J. G. *Physiol. Rev.* **1982**, 62, 185-261.
15. Young, K. D. *Micrbiol. Mol. Biol. Rev.* **2006**, 70, 660-703.
16. Kolhar, P.;Doshi, N.; Mitragotri, S. *Small* **2011**, 7, 2094-2100.
17. Geng, Y.; Dalhaimer, P.; Cai, S.; Tsai, R.; Tewari, M.; Minko, T.; Denis, D. E. *Nat. Nanotechnol.* **2007**, 2, 249-255.
18. Champion, J. A.; Mitragotri, S. *Proc. Natl. Acad. Sci.* **2006**, 103, 4930-4934.
19. Gratton, S. E. A.; Ropp, P. A.; Pohlhaus, P. D.; Luft, J. C.; Madden, V. J.; Napier, M. E.; DeSimone, J. M. *Proc. Natl. Acad. Sci. USA***2008**, 105, 11613-11618.
20. Fox, M. E.; Szoka, F. C.; Frechet, J. M. *Acc. Chem. Res.* **2009**, 42, 1141-1151.
21. Chen, B.; Jerger, K.; Frechet, J. M. J.; Szoka Jr., F. C. *J. Controlled Release* **2009**, 140, 203-209.
22. Xia, Y.; Whitesides, G. M. *Angew. Chem. Int. Ed.***1998**, 37, 550-575.
23. Whitesides, G. M.; Ostuni, E.; Takayama, S.; Jiang, X.; Ingber, D. E. *Annu. Rev. Biomed. Eng.* **2001**, 3, 335-373.
24. Rolland, J. P.; Hagberg, E. C.; Denison, G. M.; Carter, K. R.; De Simone, J. M. *Angew. Chem. Int. Ed.***2004**, 43, 5796-5799.

25. Xu, S.; Nie, Z.; Seo, M.; Lewis, P.; Kumacheva, E.; Stone, H. A.; Garstecki, P.; Weibel, D. B.; Gitlin, I.; Whitesides, G. M. *Angew. Chem. Int. Ed.***2005**, 44, 724-728.
26. Dendukuri, D.; Hatton, T. A.; Doyle, P.S. *Langmuir***2007**, 23, 4669-4674.
27. Seiffert, S.; Romanowsky, M. B.; Weitz, D. A. *Langmuir***2010**, 26, 14842-14847.
28. Dendukuri, D.; Tsoi, K.; Hatton, T. A.; Doyle, P.S. *Langmuir***2005**, 21, 2113-2116.
29. Champion, J.A.; Katare, Y. K.; Mitragotri, S. *Proc. Natl. Acad. Sci.* **2007**, 104, 11901-11904.
30. Ho, C. C.; Keller, A.; Odell, J. A.; Ottewill, R. H. *Colloid Polym. Sci.***1993**, 271, 469-479.
31. Yin, Y.; Xia, Y. *Adv. Mater.* **2001**, 13, 267-271.
32. Velev, O. D.; Lenhoff, A. M.; Kaler, E. W. *Science* **2000**, 287, 2240-2243.
33. Zhang, S. *Nat. Biotec.* **2003**, 21, 1171-1178.
34. Chilkoti, A.; Dreher, M. R.; Meyer, D. E.; Raucher, D. *Adv. Drug Delivery. Rev.***2002**, 54, 613-630.
35. Wei, H.; Cheng, S.-X.; Zhang, X.-Z.; Zhuo, R.-X. *Prog. Polym. Sci.* **2009**, 34, 893-910.
36. Ge, Z.; Liu, S. *Chem. Soc. Rev.***2013**,42, 7289-7325.
37. Issels, R. D. *Eur. J. Cancer.***2008**, 44, 2546-2554.
38. Wei, H.; Zhang, X.; Cheng, C.; Cheng, S.-X.; Zhuo, R.-X. *Biomaterials* **2007**, 28, 99-107.
39. Li, Y. Y.; Zhang, X. Z.; Zhu, J. L.; Cheng, H.; Cheng S. X.; Zhuo, R.-X. *Nanotechnology* **2007**, 18, 215605-215612.
40. Liu, S. Q.; Tong, Y. W.; Yang, Y.-Y. *Biomaterials* **2005**, 26, 5064-5074.
41. Kim, D.-H.; Vitol, E. A.; Liu, J.; Balasubramanian, S.; Gosztola, D. J.; Cohen, E. E.; Novosad, V.; Rozhkova, E. A. *Langmuir* **2013**, 29, 7425-7432.
42. Chen, H.; Li, B.; Qiu, J.; Li, J.; Jin, J.; Dai, S.; Ma, Y.; Gu, Y. *Nanoscale* **2013**, 5,12409-12424.
43. Ding, J.; Zhao, L.; Li, D.; Xiao, C.; Zhuang, X.; Chen, X. *Polym. Chem.* **2013**, 4, 3345-3356.
44. Cui, Q.; Wu, F.; Wang, E. *J. Phys. Chem. B* **2011**, 115, 5913-5922.
45. Bianco-Peled, H.; Gryc, S. *Langmuir* **2004**, 20, 169-174.

46. Bae, Y. C.; Lambert, S. M.; Soane, D. S.; Prausnitz, J. M. *Macromolecules* **1991**, 24, 4403-4407.
47. Ogoshi, T.; Shiga, R.; Yamagishi, T.-a. *J. Am. Chem. Soc.***2012**, 134, 4577-4580.
48. Ogoshi, T.; Kida, K.; Yamagishi, T.-a. *J. Am. Chem. Soc.***2012**, 134, 20146-20150.
49. Betancourt, J. E.; Rivera, J. M. *J. Am. Chem. Soc.***2009**, 131, 16666-16668.
50. Yan, J.; Li, W.; Zhang, X.; Liu, K.; Wu, P.; Zhang, A. *J. Mater. Chem*.2012, **22**, 17424-17428.
51. Stolnik, S.; Illum, L.; Davis, S. S. *Adv. Drug Delivery. Rev.***1995**, 16, 195-214.
52. Roth, P. J.; Davis, T. P.; Lowe, A. B. *Macromolecules* **2012**, 45, 3221-3230.
53. Alargova, R. G.; Danov, K .D.; Kralchevsky, P. A.; Broze, G.; Mehreteab, A. *Langmuir* **1998**, 14, 4036-4049.
54. Mishic, J. R.; Fisch, M. R. *J. Chem. Phys.* **1990**, 92, 3222-3229.
55. Herzog, B.; Huber, K.; Rennie, A. R. *J. Colloid Interface Sci.* **1994**, 164, 370-381.
56. Zhao, Xiaoyong, Zhiyong Poon, Amanda C. Engler, Daniel K. Bonner, and Paula T. Hammond. Biomacromolecules 13, 2012): 1315-1322.
57. Zhao, X.; Poon, Z.; Engler, A. C.; Bonner, D. K.; Hammond, P. T. *Biomacromolecules* **2012** 13, 1315-1322.
58. Kazunori, K.; Glenn S. K.; Masayuki, Y.; Teruo, O.; Yasuhisa, S. *J. Controoled Release.***1993**, 13, 119-132.
59. Allen, C.; Maysinger, D.; Eisenberg, A.; *J. Colloid Interface Sci.* **1999**, 16, 3-27.
60. Anilkumar, P.; Jayakannan, M. *J. Phys. Chem. B* **2009**, 113, 11614-11624.
61. Cau, F.; Lacelle, S. *Macromolecules* **1996**, 29, 170-178.
62. Ma, J.-H.; Guo, C.; Tang, Y.-L.; Liu, H.-Z. *Langmuir* **2007**, 23, 9596-9605.(b)
63. Weiss, J.; Bottcher, C.; Laschewsky, A. *Soft Matter* **2011**, 7, 483-492.
64. Hrkach, J. S.; Peracchia, M. T.; Domb, A.; Lotan, N.; Langer, R. *Biomaterials* **1997**, 18, 27-30.
65. Li, Y.; Pan, S.; Zhang, W.; Du, Z. *Nanotechnology* **2009**, 20, 1-11.
66. Siepmann, J.; Peppas, N. A. *Adv. Drug Delivery. Rev.***2001**, 48, 139-157.
67. Young, C. R.; Dietzsch, C.; Cerea, M.; Farrell, T.; Fegley, K. A.; Rajabi-Siahboomi, A.; Mcginity, J. W. *Int. J. Pharmaceutics***2005**, 301, 112-120.
68. Shi, F.; Ding, J.; Xiao, C.; Zhuang, X.; He, C.; Chen, L.; Chen, X. *J. Mater. Chem.* **2012**, 22, 14168-14179.

69. Sanson, C.; Schatz, C.; Meins, J.-F. L.; Soum, A.; Thevenot, J.; Garanger, E.; Lecommandoux, S. *J. Controlled. Release* **2010,** 147, 428-435.
70. Surnar, B.; Jayakannan, M. *Biomacromolecules* **2013**, 14, 4377-4387.

Chapter 3

Thermo-responsive Polyacrylate Random Copolymers and Their Drug Delivering Capabilities

Chapter 3

Thermo-responsive Polyacrylate Random Copolymers and Their Drug Delivering Capabilities

Dual responsive polymer nano-scaffolds for administrating anticancer drugs both at the tumor site and intracellular compartments are urgently required for improving treatment in cancers. The design and development of thermo and enzyme responsive amphiphilic copolymer core-shell nano-particle for doxorubicin delivery both at extracellular and intracellular compartments has been studied. A hydrophobic acrylate monomer was tailor-made from 3-pentadecylphenol (PDP, a renewable resource) and copolymerized with oligoethylene glycol acrylate (as hydrophilic monomer) to make new classes of thermo and enzyme dual responsive polymeric amphiphiles. These amphiphilic copolymers were self-assembled to produce spherical core-shell nanoparticles in water. Upon heating, the core-shell nanoparticles underwent segregation to produce larger size aggregates above the lower critical solution temperature (LCST). The dual responsive polymer scaffold was found to be capable of loading water insoluble drug such as Doxorubicin (DOX) and Nile red dye. The drug release kinetics revealed that DOX was preserved in the core-shell assemblies at normal body temperature (below LCST, ≤ 37 ℃). At closer to cancer tissue temperature (above LCST, ~ 43℃), the polymeric scaffold underwent burst release to deliver 90 % of loaded drugs within 2 h. At the intracellular environment (pH = 7.4, 37 ℃) in the presence of esterase enzyme; the amphiphilic copolymer ruptured in slow and control rate to release > 95 % of the drugs in 12 h. Thus, both burst release of cargoes at the tumor microenvironment and control delivery at intracellular compartments were accomplished. Cytotoxicity assay of the nascent and DOX loaded polymer were carried out in breast cancer (MCF-7 cells) and cervical cancer (HeLa cells). Among the two cell lines, the DOX loaded polymers showed enhanced killing in breast cancer cells. Further, the cellular internalization of the DOX was studied by confocal and fluorescence microscopes. Thus, role of dual enzyme and thermal-responsive polymer nano-scaffold for DOX delivery in cancer cells have been demonstrated.

3.1. Introduction

Recently, intelligent drug vehicles have attracted great interests as a potential carrier for anticancer drugs or genes both in scientific and applied research areas.[1-3] These smart or intelligent vehicles deliver the chemotherapeutic agent at the desired site by taking the advantage of unusual physiochemical environments of the cancer tissues such as elevated temperature (40-43°C), low pH(4.5-6.5), over-expression of enzymes and elevated levels of glutathione.[4,5] In other words, these responsive polymeric carriers undergo disassembly in response to various intracellular stimuli such as temperature,[6-8] pH,[9-12] enzymes[13-16] or external stimuli such as temperature[17-18] and magnetic field[19-20] thereby releasing the chemotherapeutic agent (see figure 3.1). Most of the drug carriers developed till date for combating cancer, responded to single stimuli signal. Since several diseases lead to numerous physiological changes, integration of more than one stimulus in a single system will lead to delivery of the chemotherapeutic agents at the target site more effectively. Thus, development of multi/dual stimuli responsive drug carriers will increase the efficacy of chemotherapeutic agents for cancer treatment.[21]

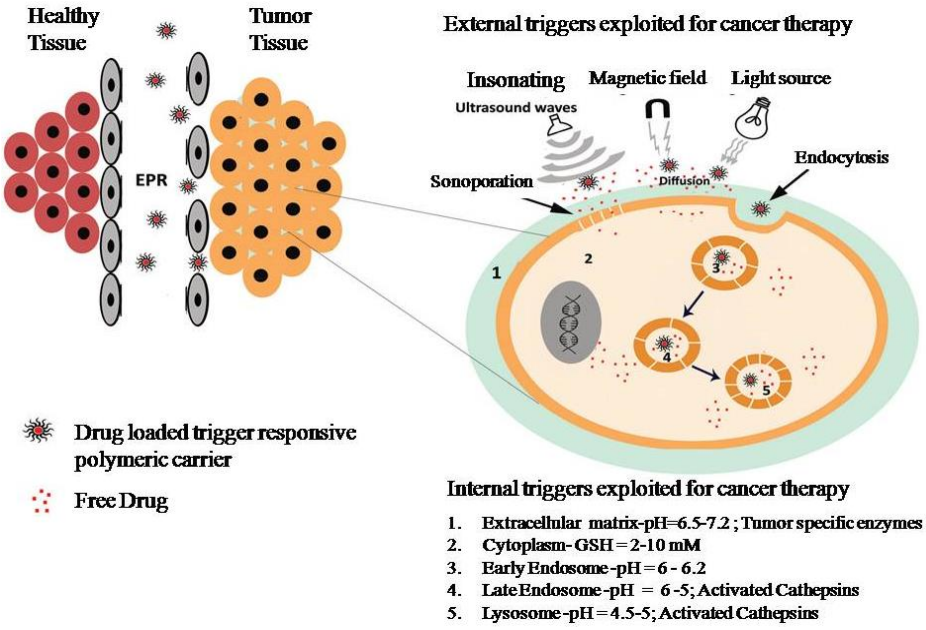

Figure 3.1.*Strategies for employing trigger responsive polymeric nanocarriers for cancer therapy (adopted from Kaur et al. Biomater. Sci.* ***2015****, 3, 955-987).*

As macromolecular carriers have advantages of passive selective accumulation of drugs at the cancer tissues through enhanced permeability and retention (EPR) effect,[22]a variety of amphiphilic block, random block and graft copolymers sensitive to different stimuli have been synthesized till date. Among various stimuli, temperature and pH have been exploited extensively for fabrication of dual responsive system since temperature and pH of the cancer tissues are slightly different (pH < 6.0 and T= 40-43 °C) compared to that of the normal tissues (pH = 7.4 and T =37 °C). [23] In order to make use of low pH of the cancer tissue environment, large number of pH responsive polymer carriers were designed with acid-labile chemical linkages such as imine,[24-25] hydrazone,[26-28] acetal[29-30] etc. At the cancer tissue environment, these chemical linkages were ruptured at the intracellular level (pH = 6.0 to 4.0) to deliver the drugs[31](see figure 3.2a).

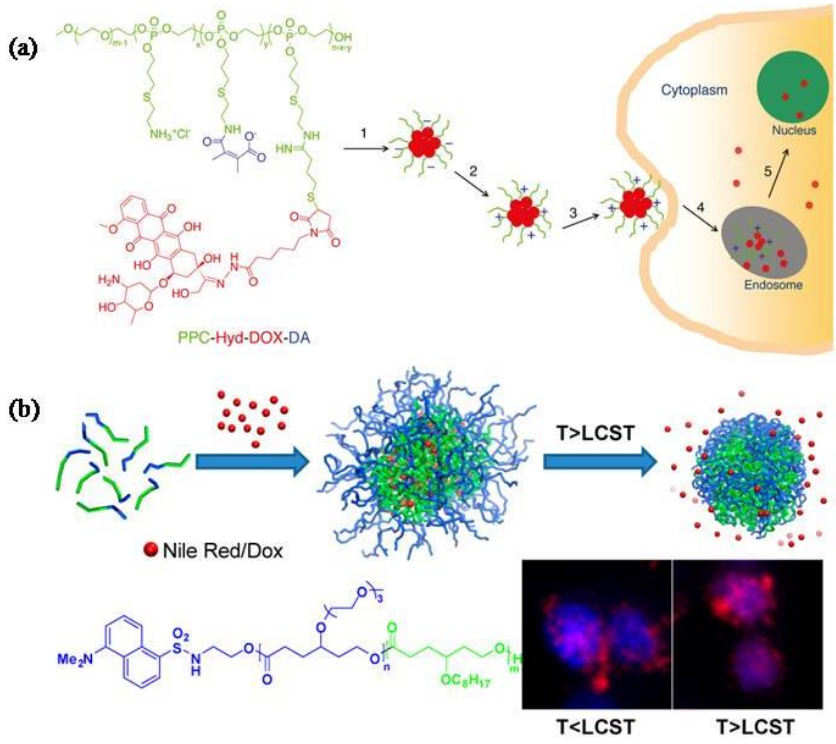

Figure 3.2. *(a) Schematic illustration of pH triggered cellular internalization and intracellular drug release of PPC-Hyd-DOX-DA having pH-sensitive hydrazone linkage (adopted from Du et al. J. Am. Chem. Soc.* ***2011****, 133, 17560-17563). (b) Temperature induced release of doxorubicin from γ-substituted poly(ε-caprolactone) micellar nanoparticle (adopted from Cheng et al. Biomacromolecules* ***2012****, 13, 2163-2173).*

The drug releasing ability of thermo-responsive polymer scaffolds are typically accompanied via precipitation or aggregation of polymer nano-assemblies in aqueous media above their lower critical solution temperature (LCST)[32] (see figure 3.2 b). Based on the LCST features in polymers; temperature-triggered disassembly technique has been developed to deliver loaded cargoes in polymer scaffolds.[33] Poly(N-isopropylacrylamide) (PNIPAM) and its copolymers are one of the most explored system as thermo-responsive polymers in literature.[34] Various anticancer drugs like doxorubicin (DOX), camptothecin, paclitaxel, cisplatin, etc were administrated using these polymersand the status of the research in these systems was recently reviewed by Wei *et al*.[35]

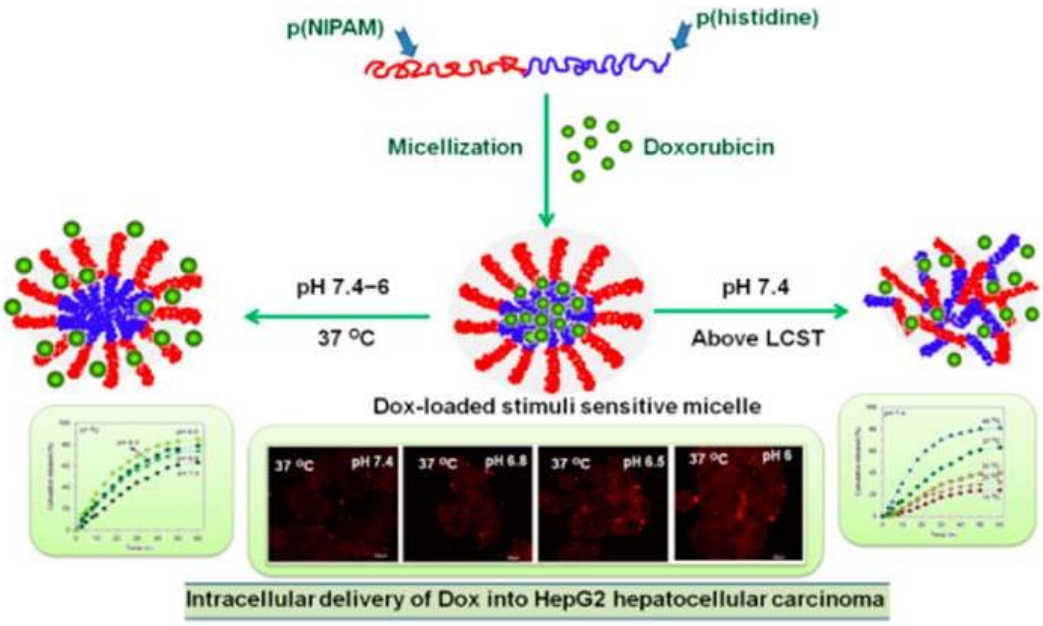

Figure 3.3.*Thermal and pH trigger release of doxorubicin (DOX) into Liver Carcinoma (adopted from Johnson et al. Biomacromolecules* ***2013****, 14, 1434-1443).*

Further, pH and thermo- dual responsive system based on PNIPAM[36-38] and polyacrylic acid[39-40] copolymers were also reported for drug delivery (see figure 3.3). Unfortunately, the LCST temperature of the PNIPAM and its copolymers were found to be ≤ 37 °C (at normal tissue temperature or below); hence, thermo-selective delivery of the drugs by these systems at cancer tissue temperature (40-43 °C) was

found to be rather difficult to achieve.[33] Stefan and coworkers had recently reported γ-substituted amphiphilic poly (ε-caprolactone) (PCL) systems[41-43] which showed enhanced drug release at 40 °C (60 %) compared to normal tissue temperature (20 %, 37 °C). These functional PCL micellar scaffolds were found to be very good candidates for delivering DOX in MCF-7 lines.[41-42] Also apart from PNIPAM and PCL, oligo(ethylene glycol) are another class of thermo-responsive polymers which exhibits phase-transition phenomena. In addition to thermo-responsive behavior, these oligo ethylene glycols are highly biocompatible. This added advantage of oligo(ethylene glycol) over PNIPAM polymer has drawn tremendous attention in recent years leading to fabrication of oligo(ethylene glycol) based smart drug carriers. Nevertheless, LCST of these oligo(ethylene glycol) are far from cancer tissue temperature. Therefore, direct application of these thermo-responsive polymers for cancer treatment is restricted. Thus, extensive efforts have been made to tune the LCST of these oligo(ethylene glycols) via macromolecular design. For instance, the ethylene glycol units are coupled with acrylic double bonds thereby further copolymerizing it with either pH or glutathione responsive unit. In other words, copolymerization approaches are being widely used to engineer these polymers for their further use as a smart polymeric system. Thus, the development of new polymer scaffolds that are capable of delivering drugs at 40 - 43 °C while being completely inert at ≤ 37 °C would be very useful to enhance the local drug concentration at cancer tissue over normal healthy tissues (see figure 3.4).

The specificity of these smart drug carriers can be further enhanced by coupling chemical or physical stimuli i.e. temperature or pH with a biochemical stimulus such as enzyme.[44,45] Incorporation of biochemical stimuli as a triggering motif in combination of physical or chemical stimuli leads to "on demand" release of therapeutic agents at the desired target due to over expression of enzymes in the diseased tissues.[23] Recently, glutathione (GSH) disulfide reductase[46-47] and phosphatase trigger[48] were also coupled with thermo-responsiveness for dual drug delivery. However, these examples did not provide any experimental evidence for

administrating anticancer drugs and their cytotoxicity in cells. Other than this example, there are no attemptsthat have been made to explore the thermo-responsive polymer for drug delivery at closer to cancer tissue temperature. In other words, the utility of biochemical stimuli (enzyme) in combination with temperature is still in its infancy. Therefore, fabrication of new self-assembled nano-carriers that, in particular, are capable of delivering drug in response to internal biological stimuli (enzyme) in combination with physical stimuli (temperature) is still a challenging task. To accomplish the above goal, here a new approach has been developed in which lysosomal enzymatic cleavage is combined with thermo-responsiveness as shown in figure 3.4. This current approach provides two advantages: (i) initial burst release of drugs at the cancer tissue (40-43°C) by thermal-stimuli and (ii) slow and controlled release of drugs by enzymatic cleavage at the intracellular compartments.

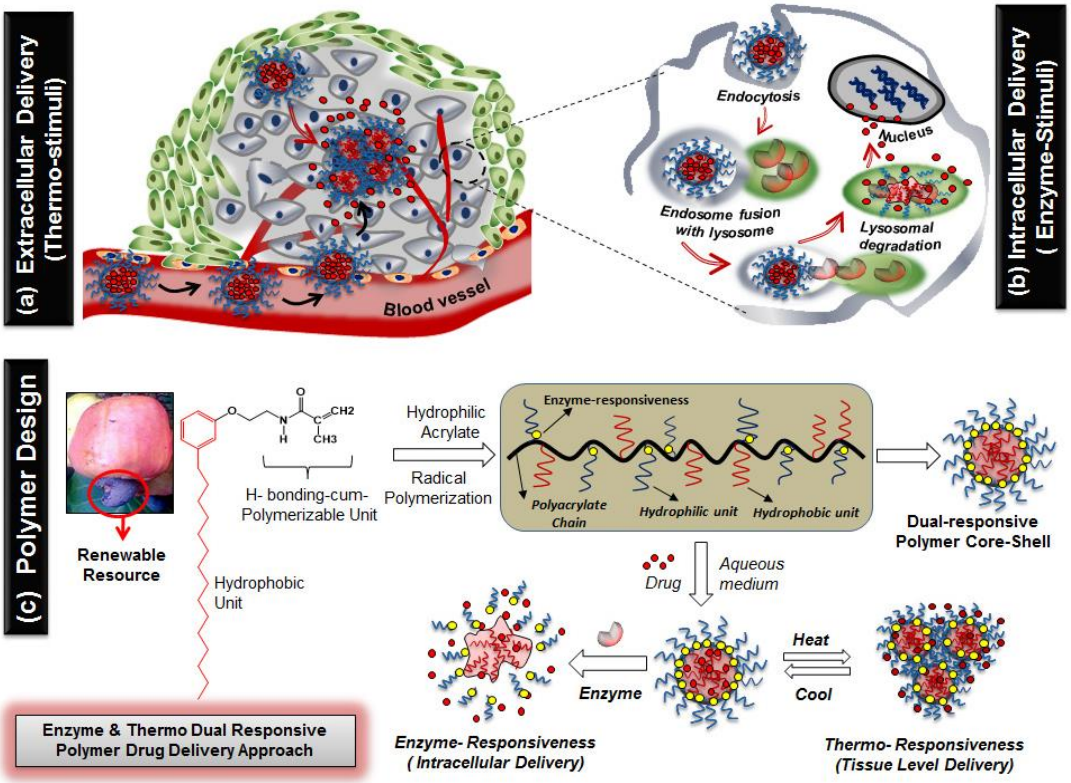

Figure 3.4.*Schematic illustration of release of anticancer drug at the tissue level by the thermal-stimuli (a) and at the intracellular compartments by enzyme-stimuli (b) Polymer design and its core-shell nanoparticle assemblies for dual responsiveness (c).*

The appropriate amphiphilic polymer structure design for having thermo- and enzyme dual responsiveness was conceived based on our earlier experience in renewable resource approach for enzyme and pH polysaccharide vesicles[49-52] and thermo-responsive small molecular amphiphiles.[53-54] Renewable resource hydrophobic unit along with PEGlated amphiphiles were found to undergo shape transformation from spherical to rod-like assemblies at cancer tissue temperature.[53] At higher PEG content, these amphiphiles were turned into super LCST system for selective binding to biomolecular anions such as adenosine triphosphate.[54] These small molecular thermo-responsive scaffolds were found to be not stable enough for loading and delivering anticancer drugs.

In this chapter new thermo- and enzyme dual responsive amphiphilic copolymer drug carrier based on the renewable resource materials were designed and their drug loading and delivering capabilities in breast and cervical cancer cells was demonstrated. For this purpose, a new hydrophobic monomer based on 3-pentadecylphenol (PDP) (from renewable resource) having methacrylamide polymerizable unit was custom designed. This monomer was copolymerized with oligoethylene glycol methacrylate under free radical polymerization to produce amphiphilic copolymers. The copolymer containing 6 % of hydrophobic amide unit in the backbone was found to produce very stable spherical **core-shell** nanoparticle at ambient conditions. Anticancer drug such as doxorubicin (DOX) was successfully encapsulated in to the dual-responsive scaffold. *In vitro* drug release studies were performed to analyze the thermo and enzyme-responsive delivery of the scaffolds. The cytotoxicity of the nascent as well as drug loaded core-shell nanoparticles was tested in breast cancer (MCF-7) and cervical cancer (HeLa) cells. Confocal and fluorescence microscopic imaging revealed the internalization of the drugs and their peri-nuclear accumulation in cells. The overall findings revealed that the core-shell polymeric design with dual thermo and enzyme-responsiveness is an excellent candidate for delivering anticancer drugs to breast cancer cells.

3.2. Experimental methods

3.2.1.Materials: 3-Pentadecylphenol, methacrylic acid, 2-ethanolamine, Boc-anhydride, triethylamine (Et_3N), triethylene glycol monomethylether, 1-ethyl-3-(3-dimethylaminopropyl) carbodiimide (EDC), diisopropyl ethylamine (DIPEA), diisopropyl azodicarboxylate (DIAD), DCC, DMAP, AIBN, were purchased from Aldrich chemicals. And all other reagents and solvents were purchased locally and purified following the standard procedure. Breast cancer cells (MCF-7) and HeLa cells were maintained in DMEM (phenol red free medium: Gibco) containing 10% (v/v) fetal bovine serum (FBS) and 1% (v/v) penicillin−streptomycin at 37 °C under a 5% CO_2 humidified atmosphere. Cells were trypsinized using 0.05% trypsin (Gibco) and seeded in 96- or 6-well (as per experiment) flat bottomed plastic plates (Costar) for all assays. Tetrazolium salt, 3-(4,5 dimethylthiazol)-2,5-diphenyl tetrazolium bromide (MTT), DMSO, and paraformaldehyde were obtained from Sigma.

3.2.2. General procedures: ^{1}H-NMR and ^{13}C-NMR spectra were recorded using 400-MHz Jeol NMR spectrophotometer in $CDCl_3$ containing small amount of TMS as internal standard. Infra-red spectra were recorded using a Thermo-Scientific Nicolet 6700FT-IR spectrometer with the solid state in KBr. The mass of the amphiphiles and all the intermediates was confirmed by using the Applied Biosystems 4800 PLUS MALDI TOF/TOF analyzer.

Size Exclusion Chromatography: The purity of the amphiphile was determined by size exclusion chromatography (SEC) using a Viscotek VE 1122 pump, ViscotekVE 3580 RI detector, and Viscotek VE 3210 UV/Vis detector in tetrahydrofuran (THF) using polystyrene as standards.

Thermal Properties of all polymers: Thermal stability of all the polymers was determined using Perkin Elmer thermal analyzer STA 6000 model at a heating rate of 10 °C/min under nitrogen atmosphere. Thermal analysis of all the polymers was performed using TA Q20 differential scanning calorimeter (DSC). The instrument was calibrated using indium standards. To remove their previous thermal history, all the polymers were heated to melt before recording their thermograms. Polymers were heated and cooled at a rate of 10 °C/min under nitrogen atmosphere.

Dynamic and Static Light Scattering Measurement: The size determination of the aqueous solution of the amphiphile was carried out by dynamic light scattering (DLS), using a NanoZS-90 apparatus utilizing 633 nm red laser (at 90° angle) from Malvern instruments.The reproducibility of the data was checked for at least three independent solutions.

Morphology analysis: FE-SEM images were recorded using Zeiss Ultra Plus scanning electron microscope. For FE-SEM analysis, the samples were prepared by drop casting on silicon wafers and coated with gold. Atomic force microscope images were recorded for drop caste samples using JPK instruments attached with Nano wizard-II setup.

Optical Transmittance measurement: Optical transmittance of amphiphile and drug loaded nanoparticles was measured using quartz cell (path length: 1 cm) with Perkin-Elmer Lambda 45 UV-Visible spectrophotometer which was equipped with temperature-controller. The sample was heated from 30 °C to 70 °C in stepwise manner with an interval of 5 °C. Similarly, cooling cycle was recorded from 70 °C to 30 °C with an interval of 5 °C.

Nile Red encapsulation: The encapsulation capability of all the copolymers was determined by using Nile red (hydrophobic dye). Nile Red (0.5 mg) and P-6 copolymer (5.0 mg) were dissolved in 1.0 mL DMSO. To it deionized water (1.0 mL) was added dropwise and the mixture was left at 25 °C with continuous stirring for 12 h. The solution was then transferred to dialysis bag (SPECTRA/POR, MWCO-500-1000) and was dialyzed against water (200 mL) for 48 h. Similarly, Nile Red was loaded in all other copolymers i.e. **P-33**, **P-27** as well as **P-TEG** (TEG-MA homopolymer). The encapsulation ability of **P-47** could not be determined as it was insoluble in water.

Preparation of P-6 core-shell nanoparticles and critical aggregation concentration (CAC): Core-shell nanoparticles were obtained by dissolving **P-6** copolymer (5.0 mg) in 1.0 mL DMSO. To it deionized water (1.0 mL) was added dropwise and the solution was then transferred to dialysis bag (SPECTRA/POR, MWCO-500-1000) and was dialyzed against water (200 mL) for 48 h. The critical aggregation concentration of the core-shell nanoparticle was determined using hydrophobic pyrene as a probe. The concentration of pyrene was fixed as 0.6 µM, while polymer concentration was varied from 0.5 mg/ mL to 0.000833 mg/ mL. In a typical experiment the required amount of pyrene probe was pipette out in 3 mL glass vials from the stock solution which was prepared in acetone. The acetone was then allowed to evaporate completely and polymer solutions of various concentrations were added to the vials containing pyrene probe. The solution was then sonicated for 1 h and was allowed to equilibrate overnight. Prior to photophysical experiments, the solutions were purged with nitrogen. The emission spectra of pyrene were recorded by using 337 nm as excitation wavelength keeping

excitation and emission slit at 2 nm. The ratio of emission intensity at 375 nm and 384 nm was calculated and was subsequently plotted against concentration of polymer. The break point in the plot of $\mathbf{I}_{375}/\mathbf{I}_{384}$ versus polymer concentration was assigned as CAC of the core-shell nanoparticle.

Doxorubicin encapsulation: The ability of the core-shell nanoparticle formed by P-6 copolymer to sequester hydrophobic drug in the inner core was determined by using Doxorubincin(DOX). DOX.HCl (0.5 mg) was neutralized with triethylamine prior to the encapsulation. DOX (0.5 mg), **P-6** copolymer (5.0 mg) were taken in DMSO (1.0 mL).To it triethylamine (1.5equivalents to DOX) and water (3.0 mL) was added and stirred at 25 °C for 12 h. The solution was then transferred to dialysis bag (SPECTRA/POR, MWCO-500-1000). It was then extensively dialyzed against deionized water (200 mL) for 48 h. The DOX encapsulated solution was filtered through 0.45µm filter and the sample was freeze-dried in lyophilizer.

Drug loading efficiency (DLE) and drug loading content (DLC) of were calculated using following equations:

DLE (%) = {weight of encapsulated CPT/ weight of CPT in feed} x 100%.

DLC (%) = {weight of CPT in nanoparticles/weight of CPT loaded nanoparticles} x 100%.

For the above purpose, approximately 1.5mg of drug loaded nanoparticles was dissolved in DMSO (2.0 mL) and their absorbance was measured to determine the DLE and DLC using their molar extinction coefficients {ε_{DOX}= 4188 (in PBS), ε_{DOX} = 7035 (in DMF)}.

***In Vitro* drug release studies:** The release profile of DOX was studied using dialysis method. Briefly, 2.0 mg of drug loaded sample was dispersed in 2.0 mL of PBS and the content was transferred in to dialysis bag, which was then immersed in 60mL of PBS and was incubated at 37 °C. Periodically; 3.0 mL of solution was withdrawn from the system and was replaced with 3.0 mL of fresh PBS solution. The aliquots obtained were then subjected to absorbance measurement and amount of DOX released was calculated. The release profile of DOX was also studied at 43 °C. Similarly, the release profile of DOX from core-shell nanoparticle formed by **P-6** copolymer in presence of esterase enzyme was also studied.

Cell Viability Assay (MTT Assay): To test the cytotoxicity of the **P-6** copolymer a cell viability assay was performed in HeLa Cell and MCF-7 cell lines using the tetrazolium salt 3-(4,5 dimethylthiazol)-2,5-diphenyl tetrazolium bromide (MTT). HeLa Cell lines (1×10^3) and MCF-7 cell (1×10^3)were seeded per well in a 96-well plate (Corning, U.S.A.) in 100 μL of DMEM with 10% FBS (fetal bovine serum) and allowed to adhere for 16 h. Prior to drug treatment, medium from cells was aspirated and various concentration of was prepared. These were added to 100 μL of DMEM with FBS in which the cells were incubated. Blank controls, DMEM with FBS in the absence of cells, were used in each experiment. All control and treated experiment wells were in triplicate. Cells were incubated for 72 h without a change in medium, and after 72 h medium were aspirated. Freshly prepared stock of MTT in sterile PBS (5 mg/mL) was diluted to50 μg/mL in 100 μL of DMEM with FBS and was added to cells. Cells were then incubated with MTT for 4 h at 37°C. Medium with MTT was then aspirated from wells and the purple formazan crystals formed as a result of reduction of MTT by mitochondrial dehydrogenase enzyme from cells were dissolved in 100μL of 100% DMSO (added per well). The absorbance from formazan crystals was immediately measured using microplate reader at 570 nm (Varioskan Flash) and is representative of the number of viable cells per well Values from the triplicates for each control and treated set were noted and their means used for calculations. The mean of the absorbance values for the blank control samples was subtracted from the average of treated samples. The values thus obtained for the control samples were equated to 100% and relative percentage values was calculated accordingly.

Cell Imaging: Breast cancer cells (MCF-7) were seeded at a density of10^5 cells on flame dried cover slips placed in a 6-well plates containing DMEM medium with 10% FBS and incubated at 37 °C for 16 h. The cells were then exposed to required concentration of DOX alone, **P-6** copolymer alone and DOX loaded nanoparticle for 8h and 12 h in a CO_2 incubator at 37 °C. After incubation, drug-containing medium was aspirated from each well, and cells were washed thrice with PBS (1 mL × 3) and fixed with 3.5% paraformaldehyde solution in PBS for 15 min at room temperature. The cells were washed thrice with PBS (1 mL) and stained with Hoechst 1:500 in 3% BSA solutions in PBS. After 1 h incubation, at roomtemperature in the dark the excess dye was washed from the plate andcells were again gently rinsed with PBS. The cover slips were mountedon slides using fluoromount mounting medium (Southern Biotech)and dried overnight at room temperature in the dark. The cells wereimaged using a LSM710 confocal microscope using the λ 405 nm(blue channel) and λ 568 nm (red channel) lasers.

3.2.3. Synthesis

Synthesis of *tert*-butyl(2-hydroxyethyl) carbamate (1): Ethanolamine (2.0 g, 32.0 mmol) was taken in the mixture of 10% Na_2CO_3 (20 mL) and THF (5 mL) and stirred at 25 °C for 10 minutes. Boc -anhydride (8.6 g, 39.0 mmol) in THF (10 mL) was added drop wise in the reaction mixture. After the addition, the content was stirred at 25 °C for 12 h. At the end of the reaction, white precipitate was observed. THF was removed by rota evaporator and the content was extracted with ethyl acetate (30 mL). The organic layer was neutralized with 5 % HCl (20 mL), dried over anhydrous sodium sulphate and the solvent was removed to obtain colorless liquid as product. It was purified by passing through silica gel column of 60-120 mesh using 10% methanol in chloroform as eluent. Yield = 4.0 g (78 %).^{1}H NMR ($CDCl_3$, 400 MHz) δ: 3.64 ppm (t, 2H, C**H**$_2$-OH), 3.23 ppm (t, 2H, C**H**$_2$-NH), 1.41 ppm (s, 9H, OC-(C**H**$_3$)$_3$, 5.25ppm (s, 1H, CH_2-N**H**). ^{13}C NMR ($CDCl_3$, 100 MHz) δ: 156.84 (**C**OO), 79.65 (O**C**-CH_3**)** 62.48 (**C**H2-OH), 43.09 (**C**H_2-NH) 28.33 (O**C**-CH_3**).** FT-IR (cm^{-1}): 3352, 2976, 2933, 2881, 1683, 1518, 1453, 1393, 1365, 1274, 1249, 1164, 1064,999,972, 900, 862, 781, 650. MALDI-TOF-MS: m/z calculated for $C_7H_{15}NO_3$: 161.11, and Found: 184.03($M^+ + Na^+$).

Synthesis of *tert*-butyl (2-(3-pentadecylphenoxy) ethyl carbamate (2): Compound **1a** (5.28 g, 32.0 mmol), 3-pentadecylphenol (10.0 g, 32 mmol) and triphenylphosphine (9.46 g, 32 mmol) was dissolved in dry tetrahydrofuran (50 mL). The reaction mixture was then kept in ice-cooled bath for 10 min under N_2 purge. Diisopropyl azodicarboxylate (6.39 mL, 32.0 mmol) was added drop wise to the reaction mixture under N_2 atmosphere and was further stirred at 25°C for 24 h. It was then purified by passing through silica gel column of 60-120 mesh using 1% ethyl acetate in hexane as eluent. Yield = 8.0 g (57.0 %).^{1}H NMR ($CDCl_3$, 400 MHz) δ: 7.19 ppm (t, 1H, Ar-**H**), 6.80-6.70 ppm (m, 3H, Ar-**H**), 5.02 ppm (s, 1H, N**H**), 4.02 ppm (t, 2H, Ar-OC**H**$_2$), 3.54 ppm (t, 2H, C**H**$_2$-N), 2.58 ppm (t, 2H, Ar-C**H**$_2$), 1.46 ppm (s, 9H, OC-C(C**H**$_3$)$_3$, 1.6-0.88 ppm (m, 29H, Aliphatic H). ^{13}C NMR ($CDCl_3$, 100 MHz) δ: 158.62(Ar-C), 155.98 (**C**O-O), 144.85, 129.29, 121.32, 114.75, 111.40 (Ar-**C**), 79.57 (O**C** $(CH_3)_3$, 67.08 (Ar-O**C**H_2), 40.26 (**C**H_2-N), 36.09, 32.00, 29.76, 26.47, 22.77, 14.20. FT-IR (cm^{-1}): 3396, 2916, 2850, 1690, 1590, 1512, 1453, 1362, 1250, 1157, 1060, 959, 866, 778, 690. MALDI-TOF-MS: m/z calculated for $C_{28}H_{49}NO_3$: 447 Found: 470 ($M^+ + Na^+$).

Synthesis of N-2(3-pentadecylphenoxy) ethyl) methacrylamide (PDP-MA): PDP-NH-Boc (7.6 g, 22.0 mmol) was dissolved in dichloromethane (15.0 mL) and to this mixture trifluoroacetic acid (40.0 mL, 522.3 mmol) was added drop wise. The contents were stirred at 25°C for 1h and then the solvent was evaporated by rotavapour. TFA was removed by adding fresh DCM (20.0 mL X 3 times) and was

evaporated by rotavapour. The content was further poured into ice-cooled diethyl ether (40.0 mL) and evaporated by rotavapour to obtain white solid as product. The white solid product was dissolved in dry dichloromethane (50.0 mL) and was purged with N_2 for 15 minutes. To it methacrylic acid (1.35 g, 16.0 mmol) was added and N_2 purging was continued further for next 15 minutes. To this reaction mixture, EDC (3.31 g, 17.0 mmol) and diisopropylethylamine (6.0 mL, 34.0 mmol) was added under N_2 atmosphere and the reaction was then left at 25 °C for 48 h with continuous stirring. It was then poured in to water (50.0 mL) and the product was extracted into chloroform. The organic layer was washed with 10% $NaHCO_3$ (25.0 mL), neutralized with 2N HCl (6.0 mL), dried over anhydrous sodium sulphate and concentrated to obtain yellow liquid as product. It was further purified by passing through silica gel column of 60-120 mesh using 15% ethyl acetate in hexane as eluent. Yield = 4.7 g (92.0 %). ^{1}H NMR ($CDCl_3$, 400 MHz) δ: 7.20 ppm (t, 1H, Ar-**H**), 6.82-6.71 ppm (m, 3H, Ar-**H**),6.27 ppm (s, 1H, N**H**), 5.72 ppm (s, 1H, C=C**H$_2$**), 5.35 ppm (s, 1H, C=C**H$_2$**), 4.09 ppm (t, 2H, Ar-OC**H**$_2$), 3.75 ppm (t, 2H, C**H**$_2$-N), 2.58 ppm (t, 2H, Ar-C**H**$_2$), 1.98 ppm (s, 3H, (C**H$_3$**)C=CH$_2$**),** 1.46 ppm (s, 9H, OC-C(C**H**$_3$)$_3$, 1.6-0.88 ppm (m, 29H, Aliphatic H). ^{13}C NMR ($CDCl_3$, 100 MHz) δ: 168.47 (NH-**C**O), 158.53, 144.86, 129.28, 121.43, 114.71,111.52, (Ar-**C**), 139.94 (CO-**C**=CH**$_2$**), 119.67 (CO C=**C**H**$_2$**), 66.69 (O**C**H$_2$-CH$_2$), 39.25(OCH$_2$-**C**H$_2$), (COO-**C**H$_2$), (C-O**C**H$_3$), (CO-**C**H$_2$-**C**H$_2$), 36.03 (Ar-**C**H$_2$), 31.93, 31.39, 29.67, 22.69, 18.62 (C=CH**$_2$C**H$_3$), 14.10. FT-IR (cm^{-1}): 3319, 3053, 2924, 1887, 1615, 1530, 1260, 1158, 1045, 865, 764. MALDI-TOF-MS: m/z calculated for $C_{28}H_{47}NO_2$: 415 Found: 438 ($M^+ + Na^+$).

Synthesis of 2-(2-(2-methoxyethoxy)ethoxy)ethyl methacrylate (TEG-MA): Triethyleneglycol monomethylether (8.6 g, 52.0 mmol), methacrylic acid (5.0 g, 58.0 mmol) were dissolved in dry dichloromethane (25 mL) under N_2 atmosphere. To the reaction mixture DCC (13.2 g, 64.0 mmol) and DMAP (0.72g, 5.9 mmol) was added under N_2 atmosphere. The reaction mixture was then stirred at 25 °C for 48 h. It was then poured in to water (20 mL) and the product was extracted into chloroform. The organic layer was then washed with 10 % $NaHCO_3$ (25.0 mL) and brine solution, dried over anhydrous sodium sulphate and was concentrated to obtain colorless liquid as product. It was purified by passing through silica gel column of 60-120 mesh using 5% ethyl acetate in hexane as eluent. Yield = 11.0 g (81.0 %).^{1}H NMR ($CDCl_3$, 400 MHz) δ: 6.07 ppm (1H, s, C=C**H$_2$**), 5.51 ppm (1H, s, C=C**H$_2$**), 4.25 ppm (t, 2H, C**H$_2$**CO-O), 3.70-3.48 ppm (s, 10H, OC**H$_2$**C**H$_2$**O), 3.32 ppm (s, 3H, CH$_2$-OC**H**$_3$), 1.88 ppm (s, 3H, (C**H$_3$**)C=CH$_2$). ^{13}C NMR ($CDCl_3$, 100 MHz) δ: 167.32 (O-**C**O-C=CH**$_2$**), 136.18 (CO-**C**=CH**$_2$**), 125.62 (CO-C=**C**H**$_2$**), 71.94

(CH_3-O-**C**H_2), 70.66-69.14 (CO-**C**H_2-**C**H_2), 59.00 (C-O**C**H_3). FT-IR (cm^{-1}): 3353, 2882, 1718, 1636, 1453, 1298, 1171, 1125, 1094, 1035, 944, 853, 662. MALDI-TOF-MS: m/z calculated for $C_{12}H_{20}O_5$: 232 Found: 255 ($M^+ + Na^+$).

Synthesis of homopolymers: Synthesis of Poly {2-(2-(2-methoxyethoxy)ethoxy)ethyl methacrylate} (P-TEG): TEG-MA (0.5 g, 2.15 mmol) was dissolved in dry DMF (1.0 mL) in 6.0 mL Schlenk flask. The mixture was degassed by two freeze-pump-thaw cycles. To this reaction mixture azo-bis isobutyronitrile (AIBN) {(0.0035 g, 0.0213 mmol (M/I = 100)} was added and the contents were once again subjected to two freeze-pump-thaw cycle. The reaction mixture was then heated in oil bath at 70 °C for 48 h. The polymer was then precipitated in cold diethyl ether and was further dried under vacuum^{1}H NMR ($CDCl_3$, 400 MHz) δ 4.10 ppm (t, 2H, C**H$_2$**CO-O), 3.66-3.57 ppm (s, 10H, OC**H$_2$**C**H$_2$**O), 3.39 ppm (s, 3H, CH_2-OC**H**$_3$), 1.65 ppm (s, 3H, (C**H$_3$**)C-CH_2), 1.04 ppm {s, 1H, (CH_3)C-C(**H**)H}, 0.88 ppm {s, 1H, (CH_3)C-C(H)**H**}. ^{13}C NMR ($CDCl_3$, 100 MHz) δ: 167.32 (O-**C**O-C-CH_2**)**, 136.18 (CO-**C**-CH_2**)**, 125.62 (CO-C-**C**H_2**)**, 71.94 (CH_3-O-**C**H_2), 70.66-69.14 (CO-**C**H_2-**C**H_2). FT-IR (cm^{-1}): 3774, 3278, 3054, 2901, 2755, 1727, 1409, 1277, 1141, 1026, 835.

Synthesis of Poly {N-2(3-pentadecylphenoxy) ethyl) methacrylamide} (P-PDP): PDP-MA **(**0.2 g, 0.48 mmol) was dissolved in dry DMF (1.0 mL) in 6.0 mL Schlenk flask. The mixture was degassed by two freeze-pump-thaw cycles. To this reaction mixture azo-bis isobutyronitrile (AIBN) (0.0008 g, 0.0049 mmol) was added and the contents were once again subjected to two freeze-pump-thaw cycle. The reaction mixture was then heated in oil bath at 70° C for 48h. The polymer was then precipitated in cold diethyl ether and was further dried under vacuum. ^{1}H NMR ($CDCl_3$, 400 MHz) δ: 7.15 ppm (t, 1H, Ar-**H**), 6.77-6.70 ppm (m, 3H, Ar-**H**), 4.04 ppm (t, 2H, Ar-OC**H**$_2$), 3.61 ppm (t, 2H, C**H**$_2$-N), 2.54 ppm (t, 2H, Ar-C**H**$_2$), 1.6-0.88 ppm (m, 29H, Aliphatic H and s, 3H, (C**H$_3$**)C-CH_2). ^{13}C NMR ($CDCl_3$, 100 MHz) δ: 172.87 (NH-**C**O), 171.60 (**C**O-O), 158.54, 144.86, 129.32, 121.36, 114.69, 111.47 (Ar-**C**), 69.07, 66.65 (Ar-O**C**H_2), 63.83 (COO-**C**H_2), 39.16 (**C**H_2-N), 36.09, 31.99, 31.49, 29.75, 29.43, 22.76, 14.19. FT-IR (cm^{-1}): 3763, 3243, 3087, 2922, 2734, 1585, 1439, 1324, 1043, 840, 699.

Synthesis of amphiphilic copolymers: Seven differentrandom block copolymers were synthesized by varying the in feed ratio of hydrophobic monomer from 10 % to 90 %. All the polymers were named as P-x (where X stands for the % incorporation of hydrophobic monomer). The details are given as: **P-47:** PDP-MA(0.5 g, 1.2

mmol) and TEG-MA (0.28 g, 1.20 mmol) was dissolved in dry DMF (1.0 mL) in 6.0 mL Schlenk flask. The mixture was degassed by two freeze-pump-thaw cycles. To this reaction mixture azo-bis isobutyronitrile (AIBN) (0.00394 g, 0.0024 mmol) was added and the contents were once again subjected to two freeze-pump-thaw cycle. The reaction mixture was then heated in oil bath at 70 °C for 48 h. The polymer was then precipitated in cold methanol, washed with hexane 2-3 times and was further dried under vacuum. ^{1}H NMR ($CDCl_3$, 400 MHz) δ: 7.14 ppm (t, 1H, Ar-**H**), 6.75-6.68 ppm (m, 3H, Ar-**H**), 4.09-3.95 ppm (t, 2H, Ar-OC**H**$_2$ and t, 2H, C**H**$_2$-N), 3.64-3.55 ppm (m, 10H, OC**H**$_2$C**H**$_2$O), 3.37 ppm (s, 3H, CH_2-OC**H**$_3$), 2.54 ppm (t, 2H, Ar-C**H**$_2$), 1.98-0.88 ppm (m, 29H, Aliphatic H and s, 3H, (C**H**$_3$)C-CH_2).^{13}C NMR ($CDCl_3$, 100 MHz) δ: 172.87 (NH-**C**O),171.60 (**C**O-O), 158.54, 144.86, 129.32, 121.36, 114.69, 111.47 (Ar-**C**), 72.00 (**C**H_2-OCH_3), 69.07, 66.65 (Ar-O**C**H_2), 39.16 (**C**H_2-N), 36.09, 31.99, 31.49, 29.75, 29.43, 22.76, 14.19. FT-IR (cm^{-1}): 3774, 3257, 2924, 2756, 1724, 1636, 1530, 1449, 1262, 1120, 965, 848, 697.

Poly {2-(2-(2-methoxyethoxy)ethoxy)ethyl methacrylate} - Poly{ N-2(3-pentadecylphenoxy) ethyl) methacrylamide(P-33): PDP-MA (0.4 g, 0.96 mmol) and TEG-MA (0.34 g, 1.44 mmol), azo-bis isobutyronitrile (AIBN) (0.00394 g, 0.0024 mmol) were used. The copolymer was precipitated in hexane (20 mL). .^{1}H NMR ($CDCl_3$, 400 MHz) δ: 7.16 ppm (t, 1H, Ar-**H**), 6.77-6.69 ppm (m, 3H, Ar-**H**), 4.09-4.06 ppm (t, 2H, Ar-OC**H**$_2$ and t, 2H, C**H**$_2$-N), 3.65-3.56 ppm (m, 10H, OC**H**$_2$C**H**$_2$O), 3.39 ppm (s, 3H, CH_2-OC**H**$_3$), 2.55 ppm (t, 2H, Ar-C**H**$_2$), 1.65-0.88 ppm (m, 29H, Aliphatic H and s, 3H, (C**H**$_3$)C-CH_2, s,2H, (CO-C-**C**H **(H),** CO-C-**CH**^{13}C NMR ($CDCl_3$, 100 MHz) δ: 171.87 (NH-**C**O),170.60 (**C**O-O), 157.54, 145.86, 129.32, 120.36, 114.69, 112.47 (Ar-**C**), 72.00 (**C**H_2-OCH_3), 69.07, 66.65 (Ar-O**C**H_2), 39.16 (**C**H_2-N), 36.09, 31.99, 31.49, 29.75, 29.43, 22.76, 14.19. FT-IR (cm^{-1}): 3777, 3071, 2904, 2755, 1721, 1308, 1120, 988, 819.

Poly {2-(2-(2-methoxyethoxy)ethoxy)ethyl methacrylate}- Poly{ N-2(3-pentadecylphenoxy) ethyl) methacrylamide(P-27): PDP-MA (0.3 g, 0.72 mmol) and TEG-MA (0.39 g, 1.68 mmol), azo-bis isobutyronitrile (AIBN) (0.00394 g, 0.0024 mmol) were used. The copolymer was purified by precipitating in hexane (20 mL). .^{1}H NMR ($CDCl_3$, 400 MHz) δ: 7.16 ppm (t, 1H, Ar-**H**), 6.76-6.69 ppm (m, 3H, Ar-**H**), 4.11-4.00 ppm (t, 2H, Ar-OC**H**$_2$ and t, 2H, C**H**$_2$-N), 3.65-3.56 ppm (m, 10H, OC**H**$_2$C**H**$_2$O), 3.39 ppm (s, 3H, CH_2-OC**H**$_3$), 2.55 ppm (t, 2H, Ar-C**H**$_2$), 1.58-0.88 ppm (m, 29H, Aliphatic H and s, 3H, (C**H**$_3$)C-CH_2, s,2H, (CO-C-**C**H **(H),** CO-C-**CH (**H**)**). ^{13}C NMR ($CDCl_3$, 100 MHz) δ: ^{13}C NMR ($CDCl_3$, 100 MHz) δ: 171.87 (NH-**C**O), 170.60 (**C**O-O), 159.54, 145.86, 130.32, 120.36, 113.69, 110.47 (Ar-**C**), 71.90 (**C**H_2-OCH_3), 69.07, 66.65 (Ar-O**C**H_2), 39.16 (C**H**$_2$-N), 36.09, 31.99, 31.49,

29.75, 29.43, 22.76, 14.19. FT-IR (cm^{-1}): 3774, 3058, 2916, 2731, 1725, 1267, 1124, 991, 825.

Poly {2-(2-(2-methoxyethoxy)ethoxy)ethyl methacrylate} - Poly{ N-2(3-pentadecylphenoxy) ethyl) methacrylamide(P-22): PDP-MA (0.1 g, 0.24 mmol) and TEG-MA (0.22 g, 0.96 mmol), azo-bis isobutyronitrile (AIBN) (0.00197 g, 0.0012 mmol) were used. The copolymer was purified by precipitating in hexane (20 mL). .^{1}H NMR ($CDCl_3$, 400 MHz) δ: 7.16 ppm (t, 1H, Ar-**H**), 6.75-6.68 ppm (m, 3H, Ar-**H**), 4.09-4.01 ppm (t, 2H, Ar-OC**H**$_2$ and t, 2H, C**H**$_2$-N), 3.65-3.56 ppm (m, 10H, OC**H**$_2$C**H**$_2$O), 3.39 ppm (s, 3H, CH_2-OC**H**$_3$), 2.55 ppm (t, 2H, Ar-C**H**$_2$), 1.68-0.88 ppm (m, 29H, Aliphatic H and s, 3H, (C**H**$_3$)C-CH_2, s,2H, (CO-C-**C**H **(H),** CO-C-**CH (**H**)**). ^{13}C NMR ($CDCl_3$, 100 MHz) δ: ^{13}C NMR ($CDCl_3$, 100 MHz) δ: 173.00 (NH-**C**O), 172.60 (**C**O-O), 157.54, 143.86, 128.92, 120.96, 113.69, 111.47 (Ar-**C**), 72.00 (**C**H_2-OCH_3), 69.07, 66.65 (Ar-O**C**H_2), 39.16 (**C**H_2-N), 36.09, 31.99, 31.49, 29.75, 29.43, 22.76, 14.19. FT-IR (cm^{-1}): 3774, 3284, 2919, 2746, 1724, 1274, 1123, 971, 822, 693.

Poly {2-(2-(2-methoxyethoxy)ethoxy)ethyl methacrylate} - Poly{ N-2(3-pentadecylphenoxy) ethyl) methacrylamide(P-6): PDP-MA (0.05 g, 0.12 mmol) and TEG-MA (0.25 g, 1.08 mmol), azo-bis isobutyronitrile (AIBN) (0.00197 g, 0.0012 mmol) were used. The copolymer was purified by precipitating in hexane (20 mL). .^{1}H NMR ($CDCl_3$, 400 MHz) δ: 7.17 ppm (t, 1H, Ar-**H**), 6.78-6.69 ppm (m, 3H, Ar-**H**), 4.10-4.04 ppm (t, 2H, Ar-OC**H**$_2$ and t, 2H, C**H**$_2$-N), 3.72-3.56 ppm (m, 10H, OC**H**$_2$C**H**$_2$O), 3.39 ppm (s, 3H, CH_2-OC**H**$_3$), 2.55 ppm (t, 2H, Ar-C**H**$_2$), 1.65-0.88 ppm (m, 29H, Aliphatic H and s, 3H, (C**H**$_3$)C-CH_2, s,2H, (CO-C-**C**H **(H),** CO-C-**CH (**H**)**). ^{13}C NMR ($CDCl_3$, 100 MHz) δ: ^{13}C NMR ($CDCl_3$, 100 MHz) δ: 172.87 (NH-**C**O), 171.60 (**C**O-O), 157.54, 145.86, 130.32, 120.36, 115.19, 111.47 (Ar-**C**), 72.00 (**C**H_2-OCH_3), 68.07, 66.55 (Ar-O**C**H_2), 38.96 (**C**H_2-N), 36.09, 31.99, 31.49, 29.75, 29.43, 22.76, 14.19. FT-IR (cm^{-1}): 3772, 3051, 2918, 2736, 1728, 1262, 1123, 1023, 856.

3.3. Results and Discussion

3.3.1. Synthesis and Characterization of Amphiphilic Polymer

A hydrophobic monomer PDP-MA was synthesized using methacrylic acid (MA) and renewable resource pentadecylphenol (PDP) via EDC/DIPEA coupling as shown in scheme 3.1. Ethanolamine was reacted with Boc-anhydride in presence of 10% Na_2CO_3 to give *tert*-butyl (2-hydroxyethyl) carbamate (**1**). The compound **1** was coupled with PDP in presence of diisopropyl azodicarboxylate and triphenylphosphine to give *tert*-butyl (2-(3-pentadecy-8-en-1-yl) phenoxy) ethyl) carbamate (**2).** The compound **2** was converted into free amine and it was then reacted with methacrylic acid in presence of EDC and diisopropylethyl amine (DIPEA) to give monomer PDP-MA. Hydrophilic monomer TEG-MA was synthesized by coupling monomethyl ether of triethylene glycol with methacrylic acid using DCC/DMAP. Both PDP-MA and TEG-MA monomers were purified by column chromatography and their structures were characterized by ^{1}H, ^{13}C-NMR, and MALDI-TOF-TOF (see figure 3.5).

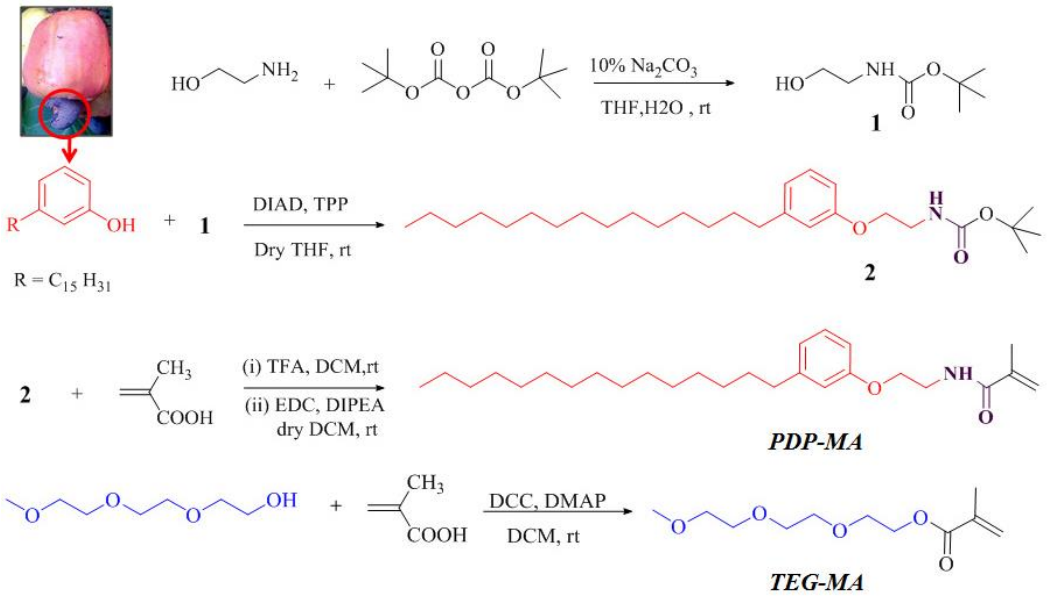

Scheme 3.1. *Synthesis of PDP-MA and TEG-MA monomers.*

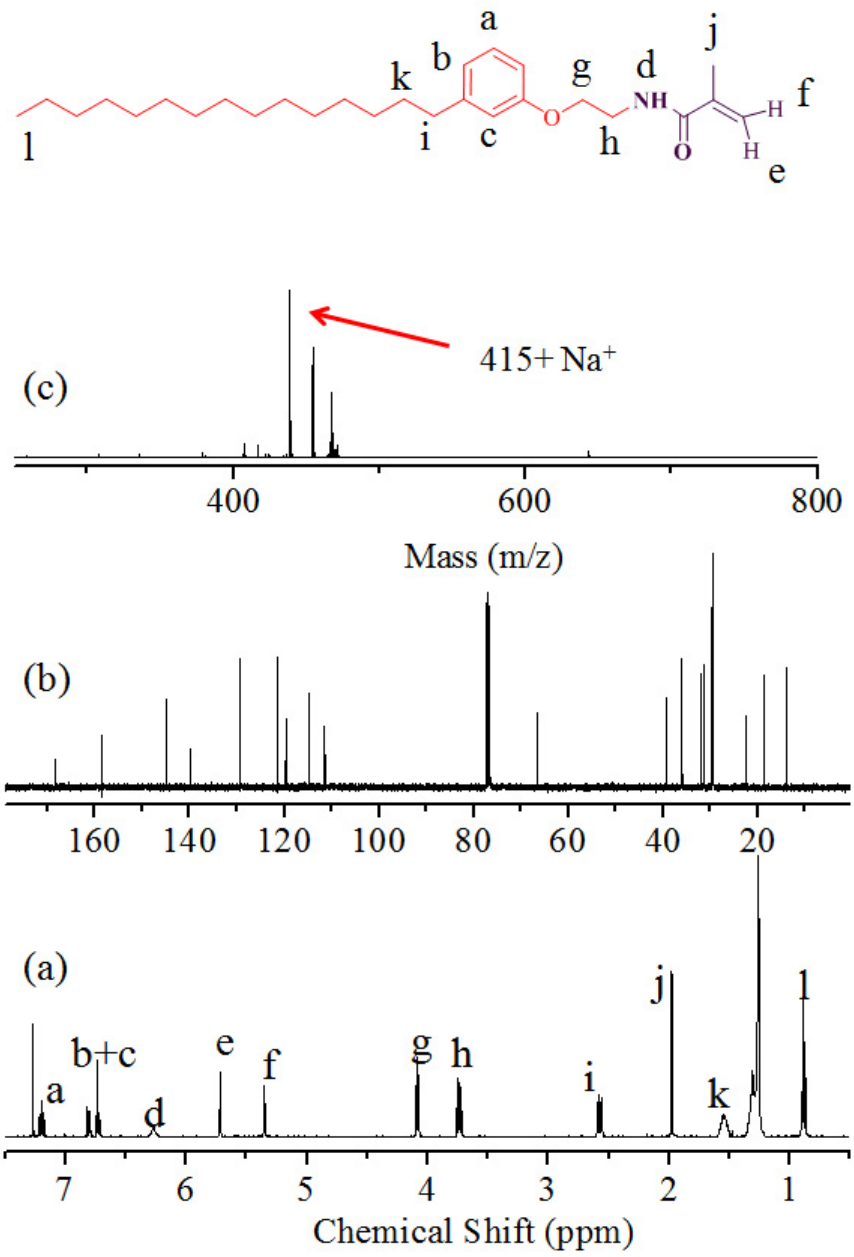

Figure 3.5*.(a) [1]H-NMR spectrum (b) [13]C-NMR spectrum (c) MALDI-TOF-TOF spectrum of PDP-MA.*

Homopolymers of PDP-MA and TEG-MA were synthesized as shown in figure 3.6 and they were named as **P-PDP** and **P-TEG**, respectively. The free radical polymerization of PDP-MA and TEG-MA monomers were carried out in dry DMF at 70 °C using AIBN as the initiator (figure 3.6). Prior to AIBN addition the polymer

solution was subjected to freeze-thaw cycle (at least two times) to make the reaction mixture oxygen free.

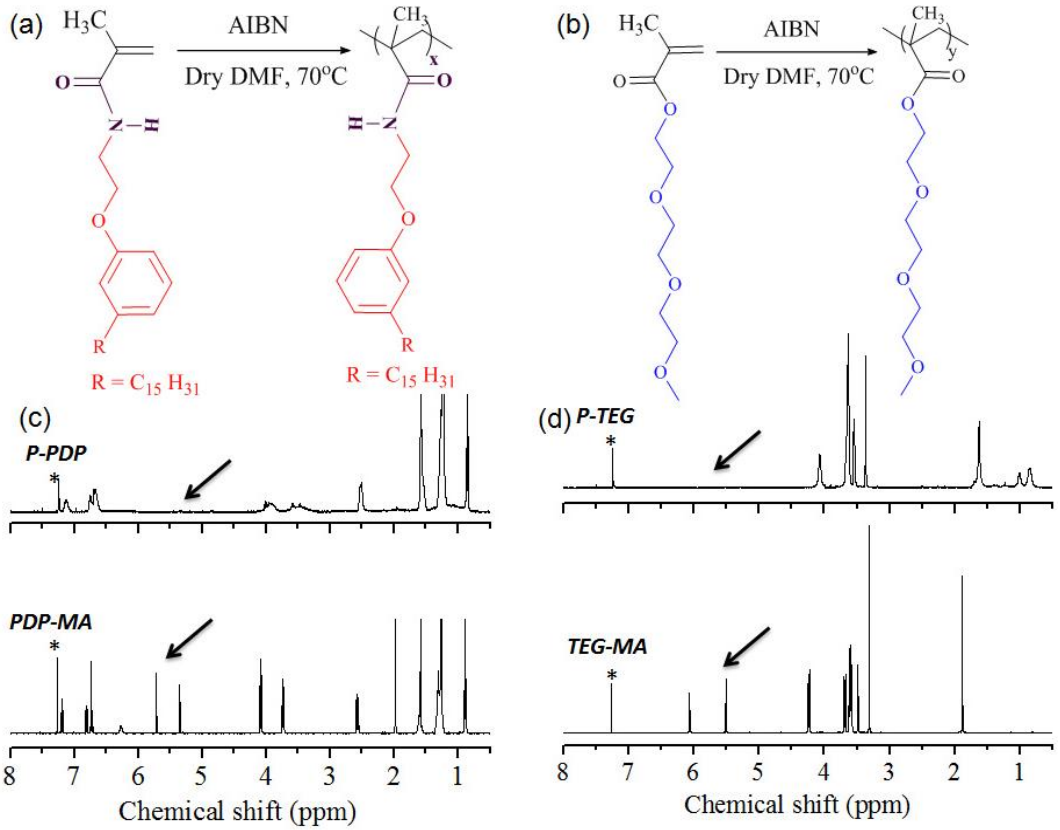

Figure 3.6 *Synthesis of homopolymers (a)P-PDP and (b)P-TEG. Comparison of* ^{1}*HNMR spectra of (c) P-PDP with PDP-MA and (d) P-TEG with TEG-MA.*

From ^{1}H NMR spectra (see figure 3.6cand 3.6d), it is clearly evident that both the monomers underwent complete conversion and the peaks corresponding to acrylic double bond in the monomers were completely disappeared in the polymer spectra. The molecular weight of the homopolymers **P-PDP** and **P-TEG** were determined by size exclusion chromatography (SEC). The SEC chromatograms of the homopolymers are shown in figure 3.8 a and their molecular weights are listed in Table 3.1. A mono-modal distribution was obtained for both the homopolymers in SEC (see figure 3.8a).

A series of amphiphilic copolymers of PDP-MA with triethylene glycol methacrylate (TEG-MA) were synthesized using AIBN as the initiator at 70 °C in

DMF (see figure 3.7 a). The mole % of PDP-MA for copolymer synthesis was varied from 10 to 90 %. The compositions of copolymers were determined by ^{1}H NMR (see figure 3.7b). These values were plotted against feed ratio and the plot is shown in seen figure 3.7c. From the plot, it is evident that with increase in feed ratio, the % incorporation increased linearly. In other words, linear relationship exists between feed ratio and % incorporation of PDP-MA monomer into the copolymer structure. At more than 50 mole % PDP-MA in feed, the polymers were obtained with low molecular weight. This trend was attributed to lower reactivity of PDP-MA monomer as compared to TEG-MA monomer in the copolymer synthesis. Thus in the present investigation, more than 50 mole % of hydrophobic monomer consisting of amide linkage could not be incorporated in the copolymer design.

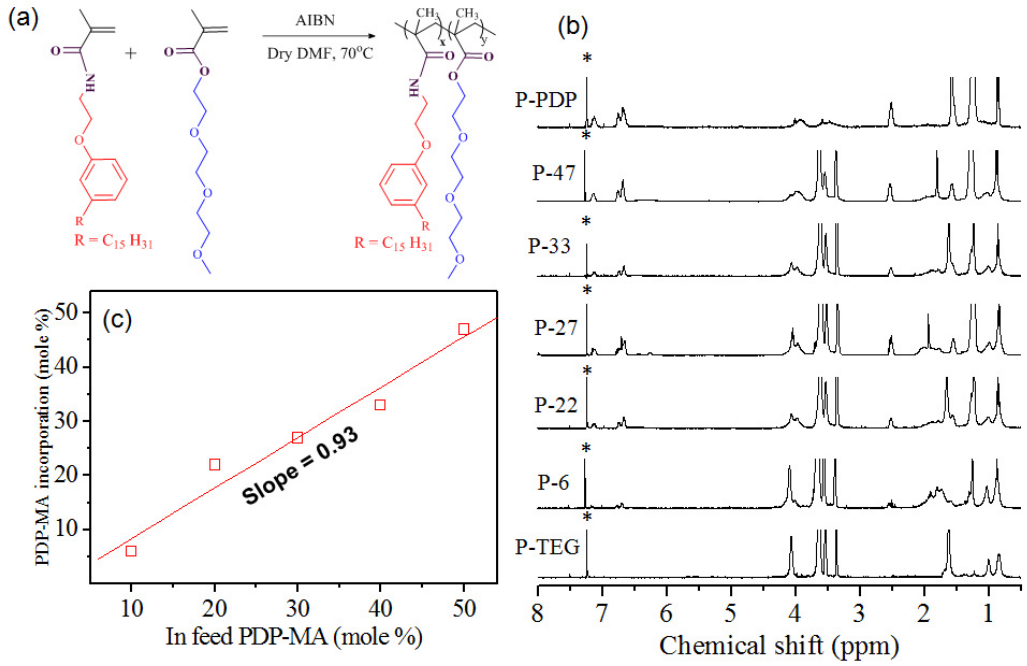

Figure 3.7*. (a) Synthesis of random copolymers (P-x).(b) ^{1}HNMR spectra of all copolymers alongwith ^{1}HNMR spectra of both the homopolymers (P-PDP and P-TEG).(c) Plot of % incorporation of PDP-MA unit in the copolymer against in feed ratio.*

From the SEC plot (see figure 3.8a and Table 3.1) it is also evident that with increase in the % incorporation of PDP-MA monomer in the copolymer structures, the SEC chromatogram shifts towards the higher molecular weight region (shown by

arrow). The molecular weights (M_w and M_n) were plotted against % incorporation of PDP-MA monomer (see figure 3.8b) and it was found that both M_w and M_n vary linearly with % incorporation. This trend indicated that the molecular weight of the copolymers increased with the increase in % incorporation of PDP-MA monomer. Since the molar mass values of the copolymers are obtained from SEC, the linear relationship between molecular weight (M_w and M_n) of the copolymers with % incorporation of PDP-MA monomer can be attributed to the combination of differences in molar mass and hydrodynamic volume of the copolymers against the polystyrene standard used. The dispersity of the copolymers varied in the range of 1.7- 2.5.

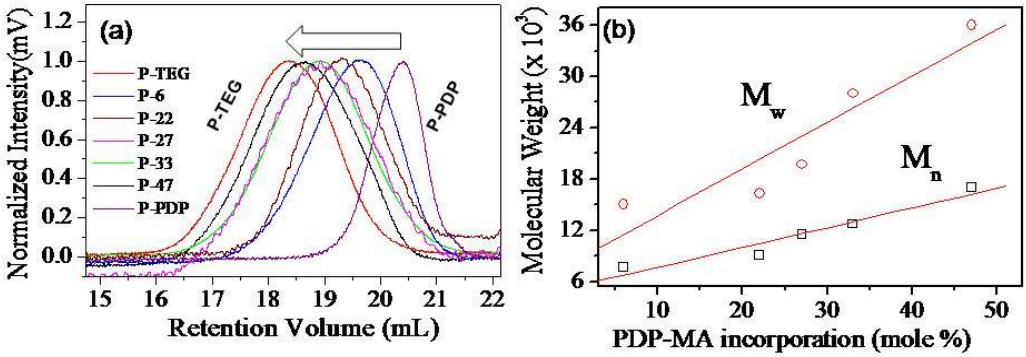

Figure 3.8*. (a) SEC chromatogram of copolymers and homopolymers. (b) Plot of M_n and M_w against PDP-MA content in copolymer structure.*

Table 3.1: Composition of the polymers and their SEC molecular weights

Polymer	Monomer in Feed (in mole %) (PDP-MA : TEG-MA)	Incorporation of PDP-MA (in mole %) (from ^{1}H NMR)	M_n (g/mol)	M_w (g/mol)	M_w/M_n
P-PDP	100:0	100	3500	5000	1.41
P-6	10:90	6.0	7700	15000	1.93
P-22	20:80	22.0	9100	16300	1.77
P-27	30:70	27.0	11500	29700	2.57
P-33	40:60	33.0	12000	28000	2.33
P-47	50:50	47.0	17700	36000	2.03
P-TEG	0:100	0	22700	46000	2.02

3.3.2. Thermal Properties of Homopolymersand Copolymers

The thermal stability of the newly synthesized homopolymers (**P-PDP and P-TEG**) and copolymers (**P-6, P-22, P-27**, **P-33 and P-47**) was analyzed by TGA and DSC. The TGA curves as well as DSC thermograms of all the homo and copolymers are shown in figure 3.9.The TGA analysis revealed that all polymers were stable up to 200 - 220 °C (see figure 3.9a). Further, from the DSC thermograms of the polymers(see figure 3.9b and 3.9c), it is evident that **P-PDP** was semi-crystalline and all other polymers were sluggish to crystallize and showed only glass transition temperature. The semi-crystalline nature of **P-PDP** was attributed to the presence of amide linkage in the polymer backbone leading to strong H-bonding interaction in the polymer structure. On the other hand, the introduction of oligoethylene glycol units in the copolymer structure disturbed the hydrogen-bond assisted packing which in turn imparts amorphous nature to the polymers.

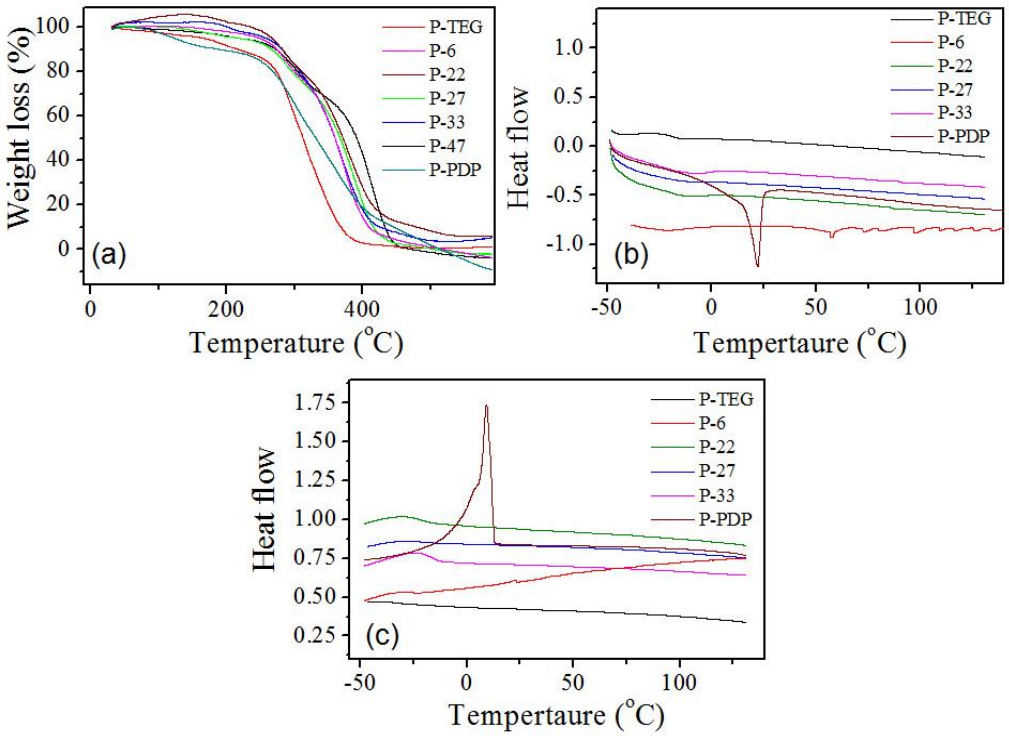

Figure 3.9*. (a) TGA profile of all the homopolymers and copolymers. DSC thermograms of all homopolymers and copolymers (b) Heating cycle and (c) Cooling cycle. The samples were recorded at 10°/min heating / cooling rates.*

3.3.3. Thermoresponsiveness of Amphiphilic Polymers

To study the thermo-responsive behaviors of the homopolymers and copolymers, their aqueous solution were subjected for optical transmittance measurement as a function of temperature using absorption spectroscopy. Prior to this, all the polymers were dialysed against water. For this purpose, 5 mg of the polymer was dissolved in DMSO and distilled water and the solution was then transferred to dialysis bag of MWCO 500-1000 and was extensively dialysed against water for 48 h. A clear solution was obtained for all the copolymers and homopolymer (see figure 3.10a). The polymer **P-PDP** and **P-47** were found to be insoluble in water. Upon heating, the aqueous solution of the polymers became turbid indicating that they were thermo-responsive in nature (see figure 3.10b). Although the polymers **P-6, P-26, P-33** and **P-TEG** showed thermo-responsiveness, the extent of turbidity in the vials varied with respect to their copolymer composition. The photograph of vials corresponding to **P-TEG**, **P-6, P-27** and **P-33** (in figure 3.10b) clearly indicated that **P-6** copolymer showed strong phase-separation compared to other polymer solutions. The reason for the thermo-responsiveness of the copolymers was attributed to the hydrophobic-hydrophilic balance in the copolymer structure.

The plot of optical transmittance of the aqueous solutions of amphiphilic copolymers are shown in figure 3.10c. The plot consists of data corresponding to heating cycles from 30 °C to 70 °C. The plot of optical transmittance as function of temperature (see figure 3.10c) revealed that **P-TEG** became opaque and turbid above 55 °C (<50% transmittance). Therefore, LCST of **P-TEG** was assigned to be 55 °C. On the other hand, the amphiphilic copolymer **P-6** (having 6% of PDP-MA monomer), underwent phase-transition at 43 °C. The other copolymers i.e. **P-27** and **P-33** exhibited frail phase-separation phenomena. This was further validated from the plot of difference in % transmittance (ΔT) as a function of % copolymer composition (see figure 3.10d). It suggested that the amount of hydrophobic

segments in the copolymer structure played crucial role in the molecular self-assembly.

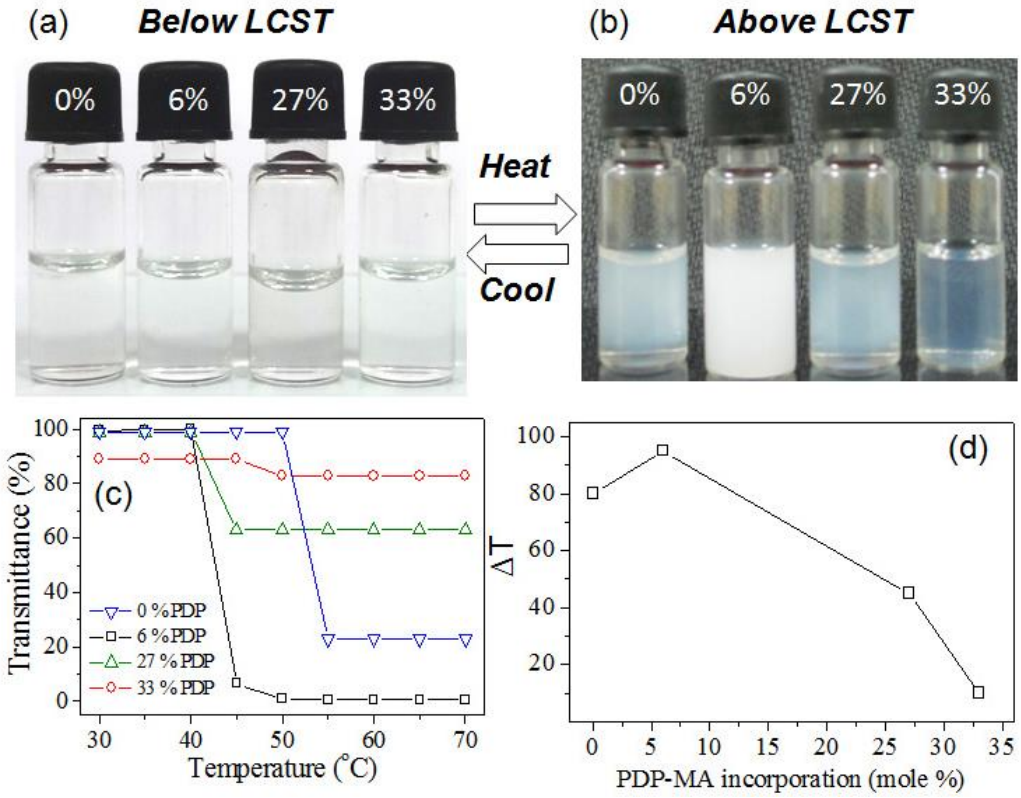

Figure 3.10*. (a) Photograph of polymer solution in vialsat25 °C (below LCST) and (b) 50 °C (above LCST). (c) Temperature dependent optical transmittance of* ***P-TEG, P-6, P-27*** *and* ***P-33*** *in water (heating cycle). (d) Plots of extent of turbidity (ΔT) versus % incorporation. From left to right the samples in the vials are corresponding to* ***P-TEG****,* ***P-6****,* ***P-27*** *and* ***P-33****, respectively.*

The LCST of hydrophilic homopolymer (P-TEG) was found to be much higher than that of cancer tissue temperature (40-43 °C) whereas the incorporation of hydrophobic segment higher than 6% in the copolymer structure leads to very weak phase-separation. In other words, 6 mole % of hydrophobic content in the copolymer structure was found to be sufficient to tune the LCST of the copolymer close to cancer tissue temperature. Therefore, an appropriate hydrophobic-hydrophilic balance is required to make these acrylate based copolymers as thermo-responsive amphiphilic polymers. In present case, combination of 6 mole % of renewable

resource based hydrophobic P-PDP unit and 94 mole % of hydrophilic triethylene glycol methacrylate unit (**P-TEG**) provided appropriate molecular geometry for thermo-responsiveness in amphiphilic copolymer structures.

The efficiency of thermo-responsive copolymers to encapsulate hydrophobic moieties was investigated using Nile Red. Nile Red is a hydrophobic dye and it is completely insoluble in water as well as it does not fluoresce in aqueous medium. Upon encapsulation in the inner hydrophobic pocket of the aggregate fluorescence gets generated indicating formation of the micellar aggregates. The copolymers **P-6, P-27, P-33** and the homopolymer **P-TEG** were employed for encapsulating Nile red. The vial in the photograph (see figure 3.11a and 3.11b) also fluoresces upon illuminating with UV light thereby, indicating that Nile Red was successfully encapsulated by the aggregates. Though all the four copolymers were capable of encapsulating Nile Red; the loading capacity of all the four was different. The dye loading content (DLC) of all the four polymers was calculated using absorption spectroscopy. DLC for **P-6, P-27, P-33** and the homopolymer **P-TEG** was found to be 0.14, 0.028, 0.047 and 0.098 wt %. Among all, the loading efficiency was higher for **P-6** copolymer which was further supported by photograph of Nile red loaded scaffolds (see figure 3.11b).

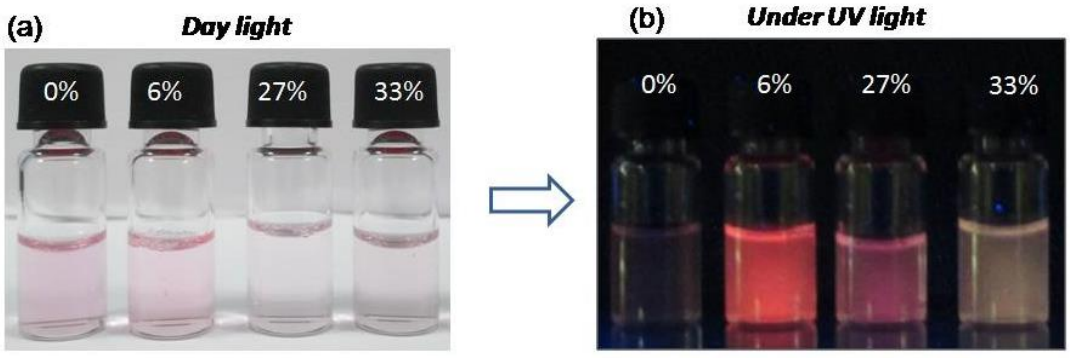

Figure 3.11 *Photograph of Nile Red loaded polymers taken in day light (a) and under exposure to UV light (b). From left to right the samples in the vials are corresponding to* ***P-TEG****,* ***P-6****,* ***P-27*** *and* ***P-33****, respectively.*

The Nile red encapsulation study also suggests that the thermo-responsive core-shell nanoparticles formed by **P-6** copolymer could also be useful for loading hydrophobic anticancer drug molecules in its inner core. Thus, amphiphilic copolymer **P-6** was chosen for further studies such as loading and delivering of anti-cancer drugs to cancer cells.

3.3.4.Size and Shape of the Polymer Self-assembly

To shed more light on the thermal-behavior of amphiphilic **P-6** copolymer, the aqueous solution of **P-6** copolymer was further subjected to optical transmittance measurement for two consecutive heating and cooling cycles from 30 °C to 70 °C (see figure 3.12a). From the plot it is evident that both heating and cooling cycle followed the same kinetic path indicating that changes in the aggregates with temperature occur at similar rates. In other words the assembly and disassembly of aggregates do not exhibit any hysteresis phenomena. The complete reversibility in the self-assembly process of **P-6** copolymer with temperature was further authenticated by measuring transmittance (%) of the copolymer in water both above and below LCST in ten consecutive heating and cooling cycles (see figure 3.12b). In ten consecutive cycles assembly-disassembly **P-6** was found to be completely reversible.

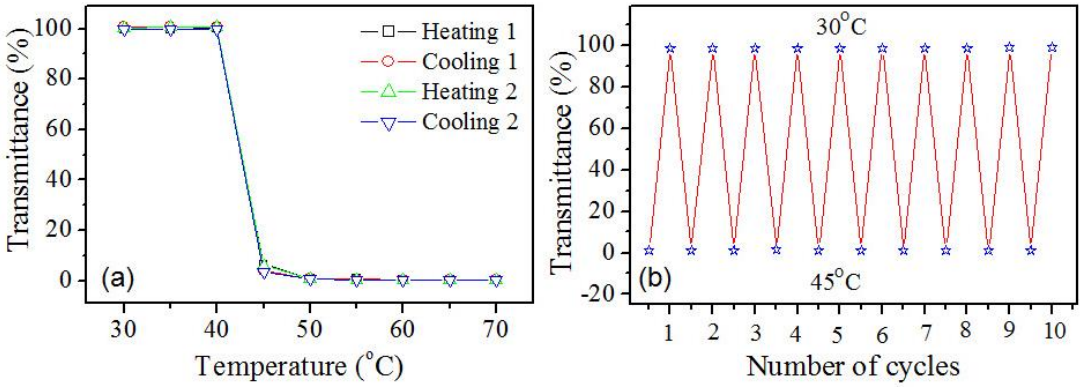

Figure 3.12. *(a) Plot of temperature dependent optical transmittance of* ***P-6****(1.0 mg/ mL) in water. (b) Reversible phase transition phenomena in ten consecutive heating and cooling cycles* ***of P-6*** *copolymer.*

Having established the phase transition temperature of **P-6** copolymer in water, the effect of pH on its LCST was also investigated. The thermo-responsive nature of **P-6** copolymer was studied in three different buffer solutions (pH = 2.0, 4.0 and 7.4) and their heating and cooling cycle data are shown in figure 3.13. In all the three pH solution i.e. 7.4, 4.0 and 2.0 the LCST of the copolymer was found to be to ~ 40 °C. Therefore the LCST value of **P-6** copolymer was retained irrespective of pH of the buffer solution varying from 2.0 to 7.4.

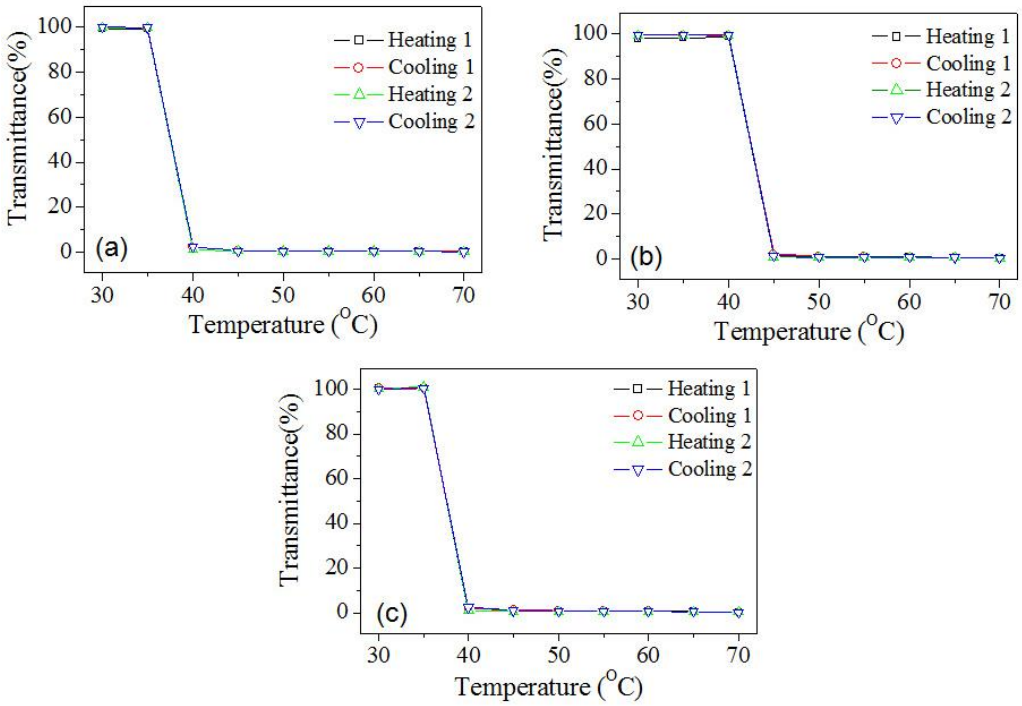

Figure 3.13*.Plot of temperature dependent optical transmittance of* ***P-6*** *copolymer (1.0 mg/ mL) in buffer of (a) pH-7.4, (b) pH-4.0 and (c) pH-2.0.*

The assembly and disassembly of the aggregates formed by **P-6** copolymer in response to temperature was studied by subjecting its aqueous solution (1.0 mg/mL) to variable temperature dynamic light scattering (DLS). The DLS histograms were recorded in the heating and cooling cycles and the plots are shown in figure 3.14a and 3.14b, respectively. The copolymer showed mono-modal distribution at all temperatures revealing that aggregates of uniform size were formed. In other words, the sizes of the aggregates were found to be homogeneous throughout the heating

cycle. Further, the hydrodynamic diameter obtained from heating and cooling cycle was plotted as a function of temperature (see figure 3.14c). The figure signifies that with increase in temperature from 30 °C to 70 °C, the hydrodynamic diameter increased from 148 ± 13 nm (below LCST) to 360 ± 30 nm (above LCST). Apart from increase in the hydrodynamic diameter a break point was also observed at 40 °C (see figure 3.14 c). The break point was identical to onset temperature for phase-separation in **P-6** copolymer (see figure 3.12 a). The reversibility of the process was further deduced from the cooling cycle data. Similar to heating cycle, cooling cycle also showed formation of homogeneous size aggregates as well as upon cooling the sizes of the aggregates returned back to its original size (see figure 3.14 b). This suggested that the temperature driven self assembly process of **P-6** copolymer was completely reversible in nature.

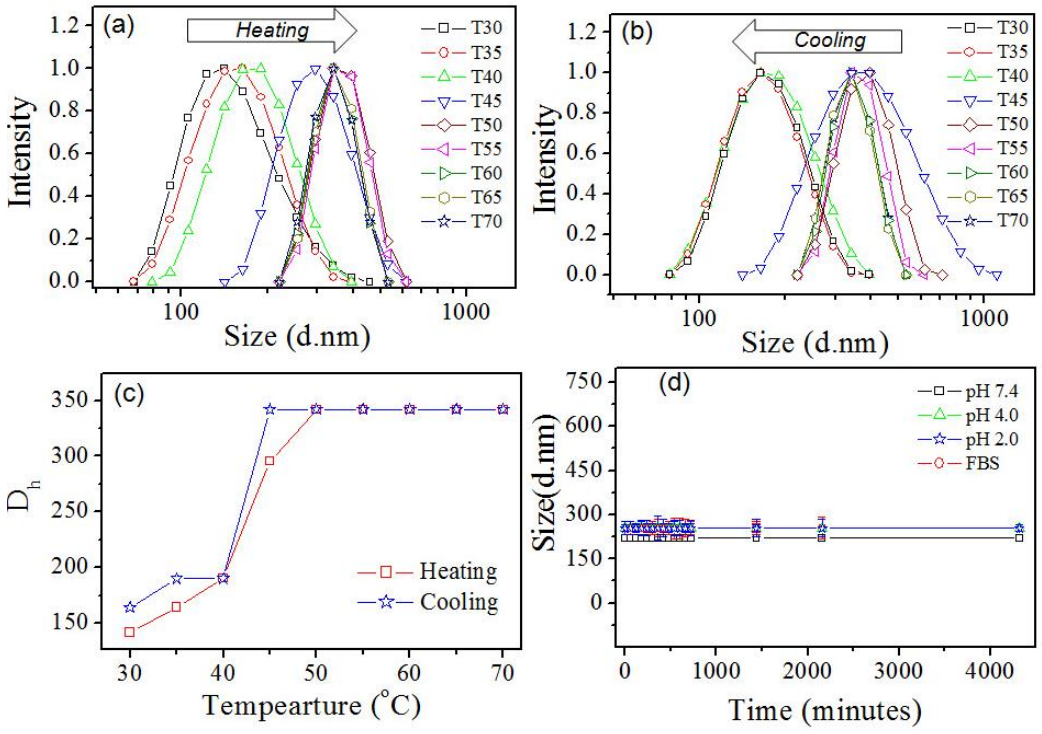

Figure 3.14*.Variable Temperature DLS histograms of* ***P-6*** *in water (1.0 mg/mL) heating cycle (a) and cooling cycle (b). (c) Plot of hydrodynamic diameter of* ***P-6*** *copolymer(1.0 mg/ mL) as function of temperature in water. (d) Plot of hydrodynamic diameter of* ***P-6*** *(1.0 mg/ mL) over time in PBS (pH 7.4), pH 4.0, pH 2.0 and in FBS.*

The stability of these aggregates was also investigated in three different pH solutions (2.0, 4.0 and 7.4) as well as in FBS (fetal bovine serum). The plots of hydrodynamic diameter of aggregates obtained at pH 7.4, pH 2.0, pH 4.0 and in FBS are shown in figure 3.14d. The size of the aggregates in FBS as well as at pH 7.4, 4.0 and 2.0 was found to be 220 nm, which is almost close to aggregates size formed in water.

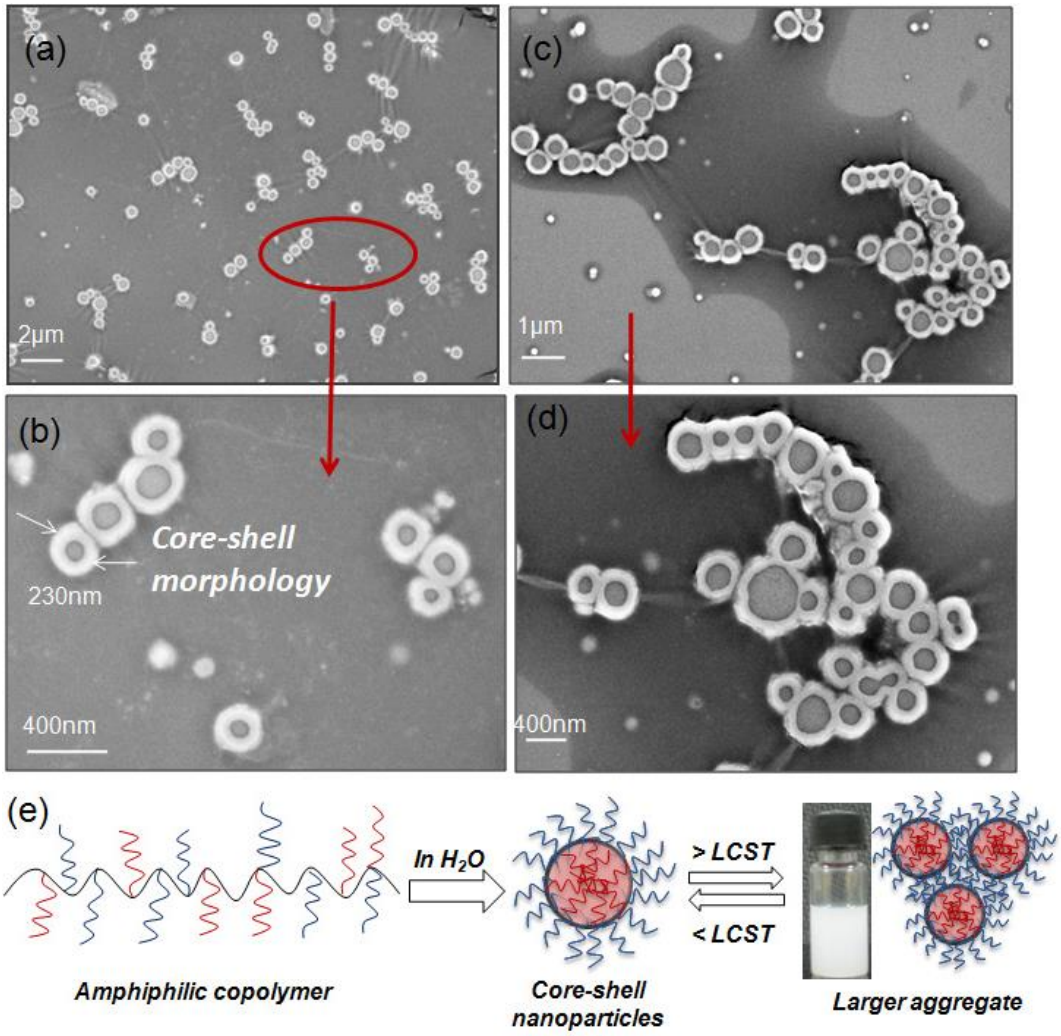

Figure 3.15. *FE-SEM images of* ***P-6*** *at 30℃ (a) and its enlarged image (b). FE-SEM images of* ***P-6*** *(c) at 45℃ and its enlarged image (d). (e) Schematic diagram depicting the mechanism involved in the temperature driven assembly-disassembly phenomena of the polymer nanoparticle.*

To visualize the shape and size of the aggregates formed by amphiphilic **P-6** copolymer, the samples were subjected to field emission scanning electron

microscope (FE-SEM) analysis. FE-SEM images of **P-6** copolymer at 30 °C (below LCST) are given in figure 3.15. In figure 3.15a, the FE-SEM image of **P-6** copolymer showed the existence of spherical hollow hydrophobic core surrounded by hydrophilic shell. In other words, **P-6** copolymer formed core-shell like nanoparticles of 230 ± 36 nm in diameter (see enlarged image figure 3.15b). The FE-SEM images of aggregates formed above LCST are shown in figure 3.15c and 3.15d. At higher temperature (above LCST) the aggregates showed the tendency to exist in the form of clusters. The enlarged FE-SEM images in figure 3.15c also supported the cluster forming tendency of aggregates above LCST. The mechanism of core-shell nanoparrticle of undergoing cluster formation at higher temperature (above LCST) is shown in figure 3.15e. Therefore, below LCST the amphiphilic **P-6** copolymer existed as isolated core-shell nanoparticles while above LCST these core-shell nanoparticles come close together leading to the formation of larger clusters.

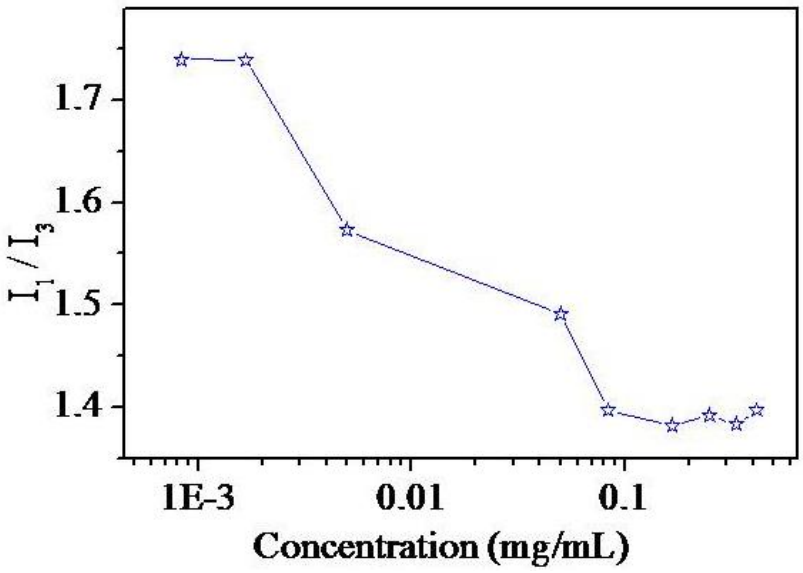

***Figure 3.16**. Plot of I_1/ I_3 as a function of polymer concentration.*

The critical aggregation concentration (CAC) of the **P-6** copolymer was estimated by using pyrene as a probe. The pyrene concentration was fixed (0.6µM) and **P-6** polymer concentration was varied from 0.833µg /mL to 0.5 mg/mL. The plot of I_1/ I_3 ratio against copolymer concentration is shown in figure 3.16. The plot

showed broad range with respect to the CAC of the core-shell nanoparticle in the range of 10.0 μg to 0.1 mg/ mL. In other words, it can be concluded that the **P-6** copolymer has stable micelle formation above 10 μg/mL to 0.1 mg/ mL. Thus, the minimum concentration required for the formation of core-shell nanoparticles is found to be 10 μg/ mL and the polymer has very good stability at low very concentration (10 μg/mL) for loading hydrophobic molecules such as pyrene. In addition, the core-shell nanoparticle once formed will remain stable even at concentration below CAC.

The tendency of the core-shell nanoparticles to undergo cluster formation at higher temperature (see figure 3.15e) was further corroborated by variable-temperature ^{1}H-NMR studies. The plot of ^{1}H-NMR spectra of PDP-TEG recorded at various temperatures in the heating and cooling cycle is shown in figure 3.17. The ^{1}H NMR spectra of amphiphilic **P-6** copolymer at various temperatures were recorded in D_2O with an interval of 10 °C from 30 to 70 °C. In the hydrated state i.e. below LCST, the intensity of the signals corresponding to the hydrophobic tail (1.23-0.88 ppm) and aromatic protons (7.14-6.67 ppm) of PDP in the copolymer structure was found to be very low. This trend was attributed to the shielding of the hydrophobic part of the copolymer from the surrounding aqueous environment indicating that it forms the core of the nanoparticle.[55-56] While,higher intensity of the signals associated with hydrophilic segment of the copolymer (3.63-3.54 ppm which corresponds to O-CH_2-CH_2 of ethylene glycol units) signified that it was exposed to water thereby, forming the outer shell of the nanoparticle. Thus, the formation of core-shell nanoparticle in hydrated state was confirmed. With increase in temperature the intensity of the signals corresponding to hydrophilic segment decreased. This decrease in signal intensity was attributed to release of hydrogen bonded water molecules from the vicinity of ethylene glycol units followed by collapsing of the hydrophilic segment. As a result, the mobility of the hydrophilic segment gets restricted, leading to decrease in the signal intensity of the shell forming unit. Therefore, in dehydrated state (above LCST) the hydrophilic segment

collapses and core-shell nanoparticles come close together forming micron size cluster. The complete reversibility from dehydrated to hydrated state was observed in subsequent cooling cycles (see figure 3.17). Thus, below LCST the amphiphilic **P-6** copolymer exist in the form of core-shell nanoparticles. As temperature was increased above LCST the hydrophilic segments collapsed on to produce micron sized clusters.

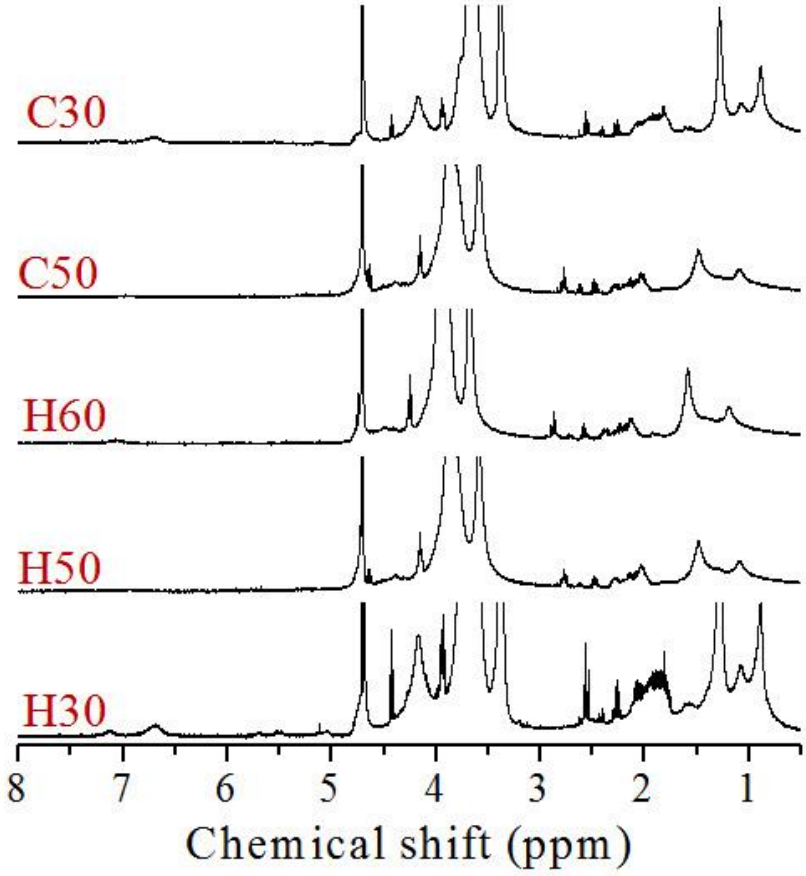

***Figure 3.17**. Variable temperature H^1 NMR of **P-6** copolymer in D_2O. H-heating and C-cooling*

3.3.5. Doxorubicin Loading in P-6 Core-Shell

To further demonstrate the ability of the thermo-responsive core-shell nanoparticles to encapsulate hydrophobic anticancer drug molecules in their hydrophobic pocket, doxorubicin (DOX) were chosen. The drug loading content of

DOX was estimated using absorption spectroscopy as 3.78 wt %. The effect of drug molecule (DOX) on the LCST of the thermo-responsive core-shell nanoparticles was further investigated by subjecting DOX loaded scaffolds for optical transmittance measurements a function of temperature. The plot of transmittance % against temperature for DOX loaded scaffold is shown in figure 3.18a. The LCST of DOX loaded scaffold was found to be ~ 43 °C, similar to that of the nascent scaffold. Further, it was also observed that in case of DOX loaded scaffold the self-assembly process during heating and cooling cycle was completely reversible in nature. In other words, the LCST value as well as reversible self-organization of the core-shell nanoparticles was retained even after encapsulation of hydrophobic drug molecules.

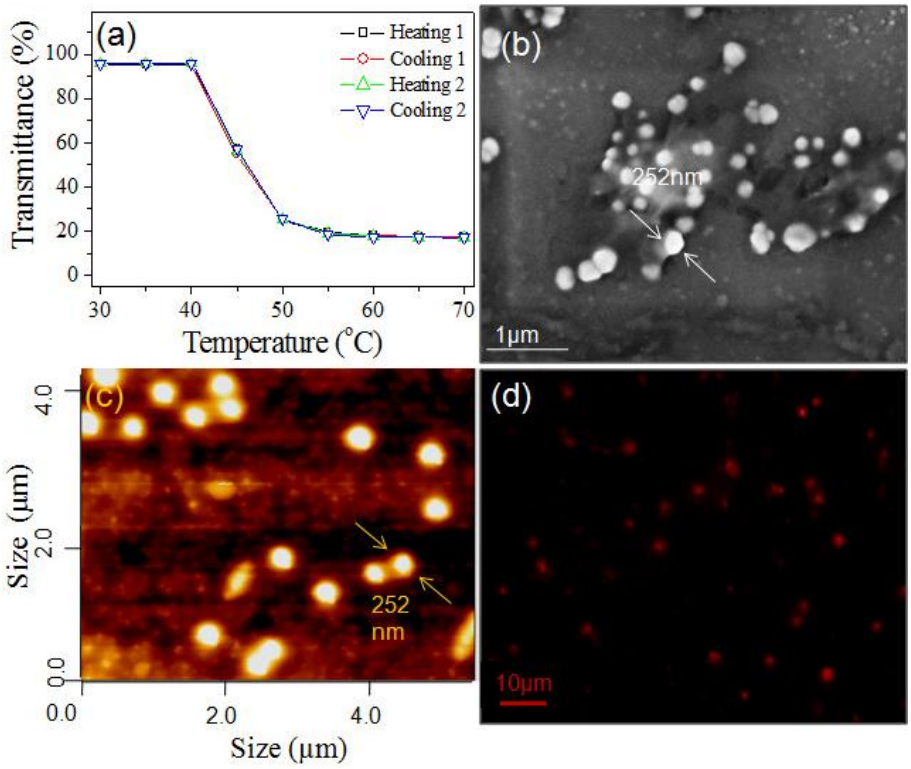

***Figure 3.18**. (a) Temperature dependent optical transmittance of DOX loaded **P-6** in water.FE-SEM image (b), AFM image (c) and Fluorescence microscopy image of DOX loaded scaffold (d).*

Having established the phase-transition temperature (LCST) of drug (DOX) loaded scaffold, the morphology of DOX loaded scaffold was further analyzed. FE-SEM, AFM and fluorescent microscopy images of DOX loaded scaffold are shown

in figures 3.18b to 3.18d. In FE-SEM image, DOX loaded scaffold (figure 3.18b) was found to be as spherical particles of 252 ± 32 nm diameter. Since the internal cavity of the core-shell particles were filled with DOX, the FE-SEM images were found to be a solid spheres unlike the cavity seen in their nascent particle (see figure 3.15). A similar trend was observed by us in the earlier thermo responsive small molecular carriers and their DOX loaded nanoparticles.[52] The formation of spherical particles of 252 ± 23 nm diameter was further confirmed by AFM image (figure 3.18c). The fluorescent microscopy image in the figure 3.18 d further authenticates the loading of DOX in the core-shell nanoparticle.

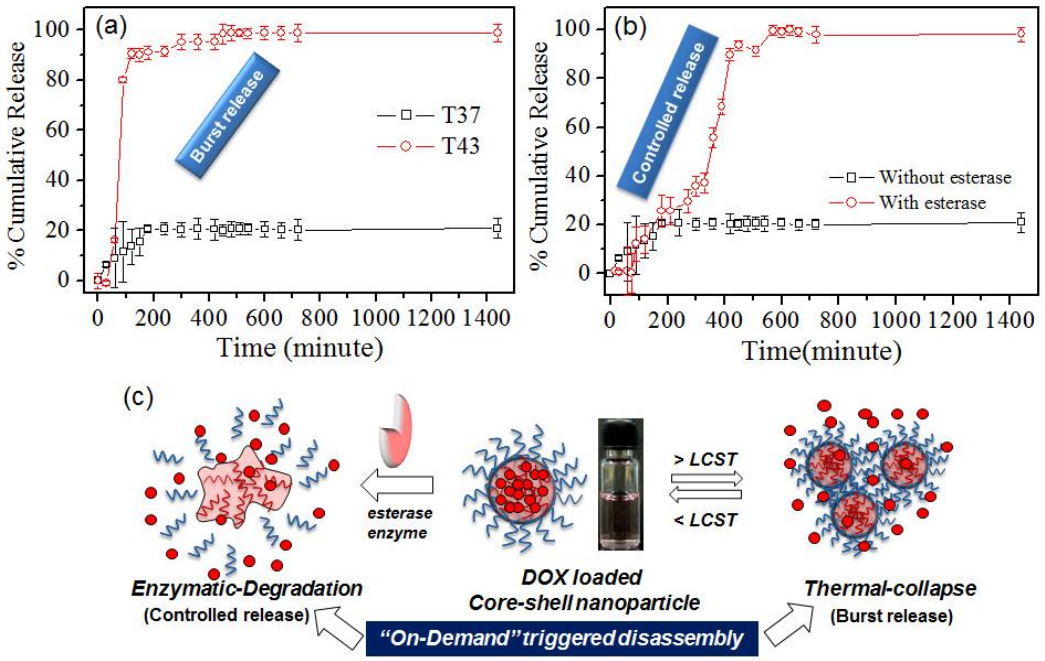

Figure 3.19. *(a) Cumulative release profile of DOX loaded scaffold using temperature as stimuli. (b) Cumulative release profile of DOX loaded scaffold using enzyme as a stimuli. (c) Schematic diagram showing release mechanism of DOX from DOX loaded scaffold in response to temperature and enzyme.*

3.3.6. *In Vitro* Drug Release Studies

Release of DOX from the polymeric nanoparticle in response to temperature were studied under physiological conditions (PBS, pH =7.4). Two different temperatures were chosen for these studies: (a) normal body temperature (37 °C)

and (b) temperature close to cancer tissue temperature (40-43 °C). The drug loaded scaffolds were incubated at 37 °C and 43 °C. The cumulative release profile of DOX loaded scaffold at 37 °C and 43 °C are shown in figure 3.19a. The percentage release of DOX from the nanoparticle at 37 °C was found to be 20 %. This signifies that DOX loaded scaffold were stable at normal body temperature (37 °C). At cancer tissue temperature (above LCST) 90 % of the drug was found to leach out within 2 h. Therefore, the DOX loaded nanoparticles were able to selectively release drug at temperature close cancer tissue. The core-shell nanoparticles formed by **P-6** copolymerapart from being thermo-responsive can also be susceptible to enzyme, as the hydrophilic segment of the copolymer consists of ester linkage. In other words, external stimuli such as esterase enzyme could also cleave the copolymer structure, causing the drug to release from the inner core of the nanoparticle. In order to investigate the enzyme-triggered drug release, the drug release kinetics using esterase enzyme as a stimulus was carried out with DOX loaded scaffold.[49,51]

Similar to thermo-responsive studies, enzyme-responsive drug release profile of DOX was also performed under physiological conditions (PBS, pH =7.4). 10 U of esterase enzyme obtained from horse liver was used to study the release behavior of DOX loaded scaffold. The nanoparticles were incubated at 37 °C in PBS (pH =7.4) and the release kinetics of DOX was studied both in presence as well as absence of esterase enzyme. The cumulative release profile of DOX loaded scaffold in absence and presence of enzyme at 37 °C in PBS (pH =7.4) are shown in figure 3.19b. In the absence of esterase enzyme, only 20 % of the drug was released while in the presence of enzyme more than 90 % of the drug from the nanoparticle was released in 12 h. This suggested that esterase enzyme chopped off the ester linkage present in the copolymer structure, thereby breaking down the self-assembly leading to release of DOX from the core-shell nanoparticle (see figure 3.19c). Additionally, the release of DOX from the core of the nanoparticle at higher temperature was found to be much faster as compared to the enzyme driven release of DOX.

3.3.7. Drug Release Kinetics

The mode of drug release from the core-shell nanoparticles was further investigated in response to temperature and enzyme, by using a semi-empirical model developed by Ritger and Peppas. The empirical equation used for determining that whether drug oozes out from the core of the nanoparticle by diffusion mechanism or by erosion of the polymeric scaffold is gives as:[57,58]

$$\log(M_t/M_\infty)=n \log t + \log k$$

where, M_t and M_∞ corresponds to cumulative amount of released drug at time t and infinite time, respectively, *k* is a constant characteristics to structure and geometry of the polymer and *n* is the release exponent. The value of *n* further provides information about drug release mechanism; for Fickian diffusion $n = 0.43$ and for non-Fickian diffusion $n \geq 0.85$.[59] The drug release profiles of DOX loaded nanoparticle obtained in response to temperature (i.e. T = 37 and T= 43) as well as esterase enzyme was fitted using the above mentioned equation. The plots of log (Mt /M∞) as a function of log t are shown in figure 3.20a. The values of constant k and n obtained are tabulated in figure 3.20.

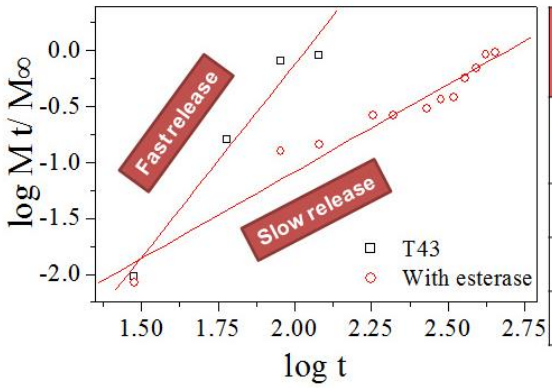

DOX loaded core-shell nanoparticles		
Parameters	*Temperature stimuli*	*Enzyme stimuli*
n_1	3.45	1.55
k_1	9.34×10^{-8}	6.36×10^{-5}
R^2	0.98	0.97

Figure 3.20. *(a) Kinetic plots of DOX loaded scaffolds. Table contains the values of constant (k), and n for release of DOX in response to temperature and enzyme.*

For temperature (above LCST) and enzyme assisted DOX release the value of *n* were found to be 3.45 and 1.55, respectively. This implies that DOX loaded nanoparticles follow non-anomalous transport mechanism to release DOX from the

core of the nanoparticle at higher temperature (above LCST) and Fickian diffusion mechanism in presence of esterase enzyme. Therefore, the custom designed acrylate based core-shell nanoparticle formed by amphiphilic **P-6** copolymer was capable of releasing DOX both in response to temperature as well as enzyme. Based on the in vitro drug release analysis; it may be concluded that the present polymer design provided new opportunity to locally enhance the drug concentration at the cancer site via burst release as well as enzymatic cleavage assisted slow release in the intracellular compartments. Thus, both burst and slow release of the DOX could be achieved via thermal and enzyme drug responsiveness in a single polymer carrier for cancer cells (see figure 3.4a).

3.3.8. Cytotoxicity Studies

The cytotoxicity of the polymeric core-shell nanoparticles were investigated both in breast cancer (MCF-7cells) and cervical cancer (HeLa) cell lines using MTT assay method. The concentration of the core-shell nanoparticles was varied from 0.01 µg/mL to 10.0 µg/mL. The cells were incubated for 72 h at 37 ° C. The histogram depicting the % cell viability data for free polymer is shown in figure 3.21a. In HeLa and MCF-7 cell lines, more than 95 % cell viability was observed indicating the biocompatibility of the nascent polymer scaffold for further drug delivery application. Similarly, the cytotoxicity of free DOX and DOX loaded nanoparticles was tested in both MCF-7 and HeLa cell lines keeping the experimental condition identical to the nascent scaffold. The concentration of DOX was chosen according to the amount of DOX present in the nanoparticle i.e. 10.0 µg/ mL of the scaffold consists of 0.378 µg/ mL of the DOX. The drug concentration was varied from 0.378 µg/ mL to 0.000378 µg/ mL corresponding to the respective scaffold concentration. Further for comparison, the same concentration of free DOX was also employed for treatment. The % cell viability data corresponding to free DOX and DOX loaded nanoparticles in MCF-7 and HeLa cells are shown in figure 3.21b and 3.21c, respectively. From figure 3.21b and 3.21c, it is evident that DOX loaded in nanoparticles exhibited 70 % killing in MCF-7 cells which was 10 % more

compared to its effect on HeLa cells. This suggested that the uptake of these drug loaded nanoparticles was better in case of breast cancer cell line (MCF-7) as compared to HeLa cells. As expected, free DOX showed higher killing in case of both HeLa and MCF-7. This trend was attributed to the fast penetrating ability of the free drug as compared to drug loaded polymeric core-shell nanoparticle in the *in vitro* studies. The effect of the drug loaded polymers may be become pronounced only at the *in vivo* analysis since the large macromolecular nano-carriers have passive selective drug accumulation through EPR effect at the cancer tissues compared to normal ones.

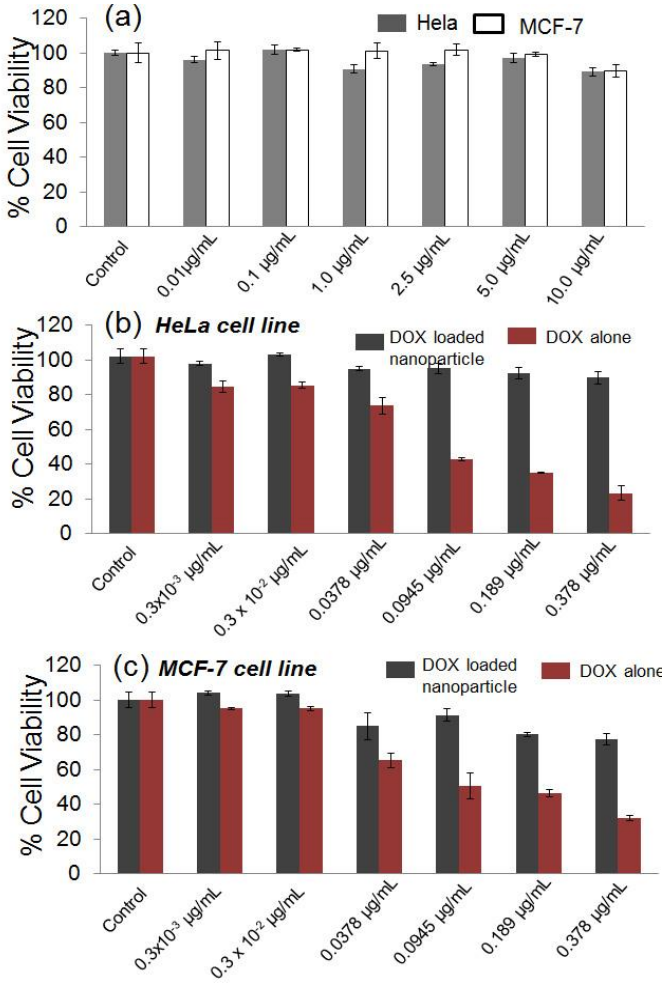

Figure 3.21. (a) *Cytotoxicity of P-6 copolymer in HeLa and MCF-7cells at various concentrations. (b) Cytotoxicity of DOX loaded scaffold and free DOX in HeLa cells. (c) Cytotoxicity of DOX loaded nanoparticle and corresponding free DOX in MCF-7 cells.*

3.3.9. Cell Imaging

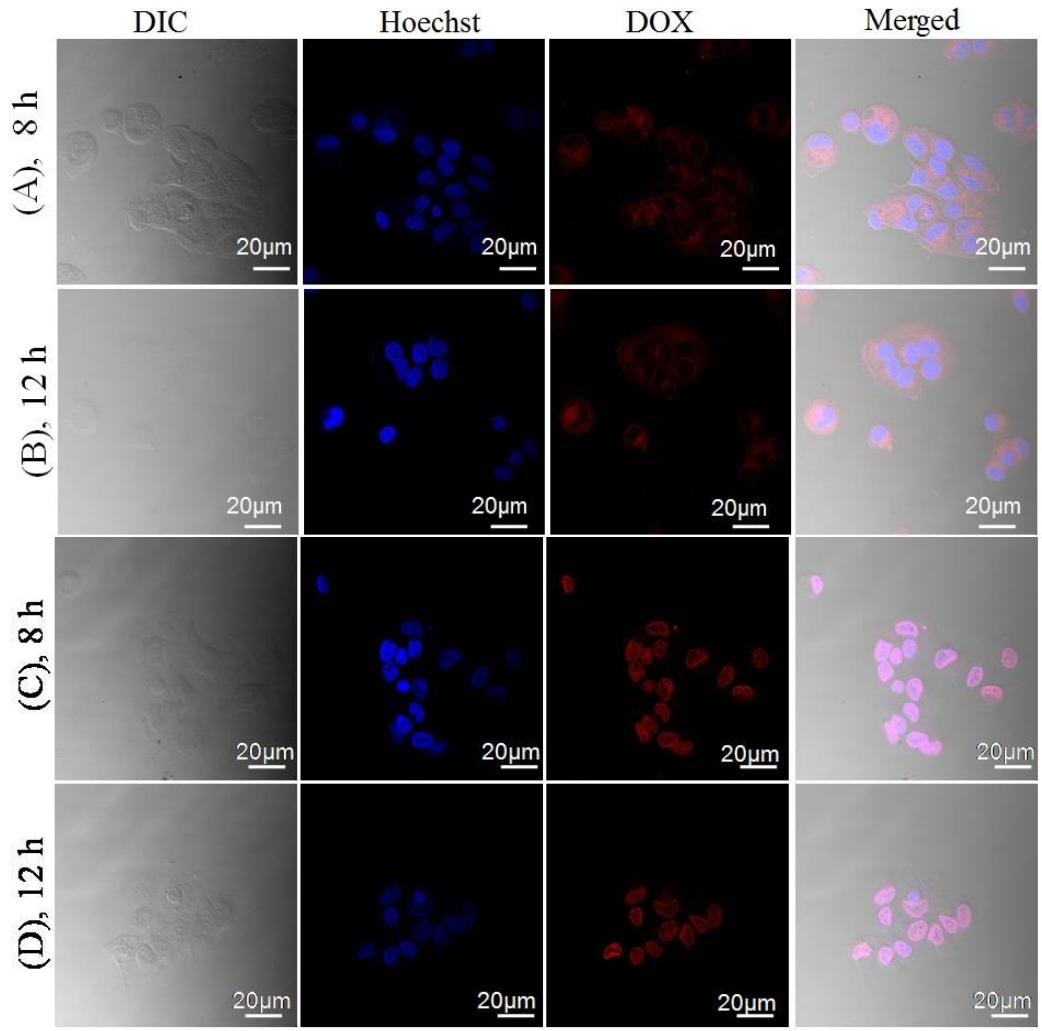

Figure 3.22. *CLSM images of MCF-7 cells incubated with DOX loaded P-6 scaffold for 8 h at 37° C (A) and 12 h at 37 °C (B). CLSM images of MCF-7 cells incubated with free DOX loaded for 8 h at 37° C (C) and 12 h at 37 °C (D).For each panel the images from left to right show differential interference contrast (DIC), staining of cell nuclei by Hoechst (blue), DOX fluorescence from within the cells, and the overlay of three images.*

The cellular internalization and intracellular release behavior of DOX loaded nanoparticles towards MCF-7 cells was monitored by confocal laser scanning microscopy (CLSM). MCF-7 cells were incubated with DOX nanoparticle and free DOX for 8 h and 12 h at 37 °C. The DOX concentration used for treatment was

0.378 µg /mL with respect to 10.0 µg /mL of the scaffold. The red DOX fluorescence which is generally observed at ~ 590 nm was monitored through the red channel (λ= 568 nm). Since, the DOX molecules have tendency to accumulate inside the cell nuclei the diffusion and accumulation of DOX in the nucleus was probed by staining with Hoechst. The blue fluorescence produced by the cell nuclei after Hoechst staining was observed through the blue channel (λ = 405 nm). The images corresponding to DOX and Hoechst fluorescence in MCF-7 cell along with the merged image are shown in figure 3.22. The images were captured in MCF-7 cells after 8 h and 12h of incubation at 37 °C are shown in figure 3.22A and 3.22 B, respectively. As shown in images 3.22A and 3.22 B, strong DOX fluorescence within the cells was observed. This can be further attributed to efficient internalization of DOX loaded nanoparticles by MCF-7 cells as well as enhanced intracellular release of DOX upon degradation of the nanoparticle inside the cell. The closer observation further reveals that the DOX-loaded nanoparticles preferentially accumulate in the perinuclear region.

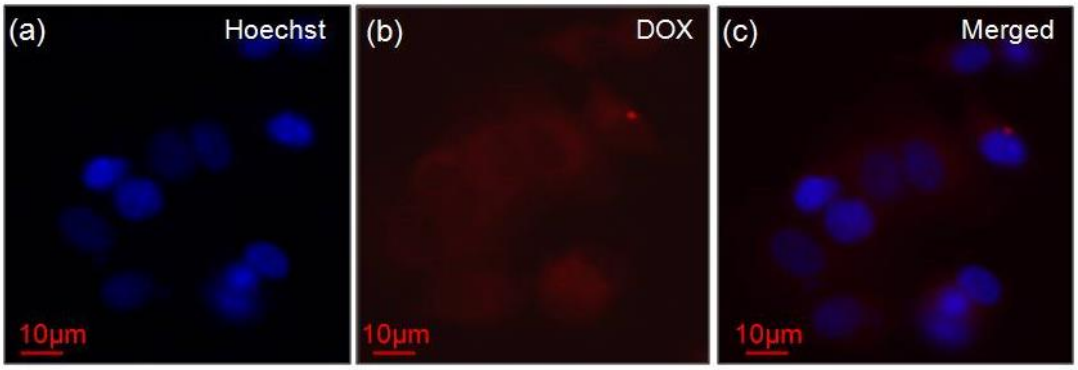

Figure 3.23*.Fluorescent microscopy images of MCF-7 cells incubated with DOX loaded core-shell nanoparticle for 4 h at 37° C. For each panel the images from* ***left*** *to right show staining of cell nuclei by Hoechst (blue), DOX fluorescence from within the cells, and the overlay of three images.*

The cellular uptake of the DOX loaded core-shell nanoparticles was also studied by using fluorescent microscopy technique. The MCF-7 cells were incubated with DOX loaded nanoparticle for 4h at 37 ° C and images are shown in figure

3.23.As shown in figure, strong DOX fluorescence from within the cells was observed (similar to confocal images). Further the fluorescent microscopy image also confirmed the perinuclear localization of DOX loaded nanoparticle inside the cells. The CLSM images of MCF-7 cell treated with free DOX showed better overlap between DOX and Hoechst staining in the nucleus (see figure 3.22 C for 12h and 3.22 D for 8 h data). This indicated that free DOX was capable of penetrating and accumulating inside nucleus. Thus, the slower penetration and less accumulation of DOX loaded polymer nanoparticle inside nucleus with respect to free DOX resulted in moderate killing effect in MCF-7 cells. The current investigation demonstrated the development of polyacrylate based thermo and enzyme responsive core-shell nanoparticles andthese polymeric scaffolds were found to be non-toxic to cells and also capable for loading and delivering drugs at the intracellular compartments. The efficacy of these engineered nanoparticles can be further enhanced by incorporating targeting ligands on to their surface leading to better uptake.

3.4. Conclusion

In summary, thermo-and enzyme dual responsive polymeric amphiphiles were designed and developed for loading anticancer drug in cancer tissue environment and intracellular compartments via burst and control release, respectively. To achieve the dual responsive characteristics, a series of new amphiphilic copolymers consisting of hydrophobic monomer based on 3-pentadecylphenol (PDP) (renewable resource) and hydrophilic monomer of oligoethylene glycol chains were chosen. Free radical polymerization of these monomers produced amphiphilic copolymers with moderate molecular weights. Among all the polymers, copolymers with 6 % of hydrophobic content exhibited maximum phase-separation phenomena with LCST temperature close to cancer tissue temperature. In aqueous medium, the copolymer was self-assembled to form core-shell nanoparticles of 230 ± 36 nm. At higher temperature (above LCST), these core-shell nanoparticles underwent segregation to produce larger size aggregates. The tendency of these core-shell nanoparticles to undergo cluster formation at higher temperature was also authenticated by light scattering techniques, electron microscopes and atomic force microscopy and variable temperature ^{1}H-NMR studies. The dual responsive core-shell polymer nanoparticles were further employed for loading DOX. The drug release kinetics of the DOX loaded nanoparticle was studied at two different temperatures at 37 °C (body temperature) and 43 °C in PBS (pH = 7.4, closer to cancer tissue temperature). Under physiological conditions only 20 % of DOX was leached which confirmed the good stability of the drug loaded core-shell nanoparticle. Above LCST, the core-shell nanoparticles underwent burst releasing of the loaded drugs > 90 % within 2 h. In the presence of esterase enzyme the controlled release of > 95 % of the drug over a period of 12 h occurred. Further kinetic parameters such as release exponent “n” and constant ‘k’ were determined, DOX release by thermo-response followed anomalous transport mechanism and the enzymatic degradation followed non-Fickian diffusion mechanism. The cytotoxicity data revealed that the nascent scaffold was not toxic to

breast cancer (MCF-7) and cervical (HeLa) cancer cells. The DOX loaded polymer nano-particles showed 25 % killing in breast cancer cells. Confocal microscopic analysis confirmed the cellular uptake of the DOX and perinuclear accumulation of drugs by nano-particles in MCF-7 cells.

3.5. References

1. Mura, S.; Nicolas, J.; Couvreur, P. *Nat. Mater.***2013**, 12, 991-1003.
2. Shim, M. S.; Kwon, Y. J. *Adv. Drug Delivery Rev*. **2012**, 64, 1046-1059.
3. Zhuang, J.; Gordon, M. R.; Ventura, J.; Li, L.; Thayumanavan, S. *Chem. Soc. Rev*. **2013**, 42, 7421-7435.
4. Ge, Z.; Liu, S. *Chem. Soc. Rev*. **2013**, 42, 7289-7325.
5. Cheng, R.; Meng, F.; Deng, Chao.; Klok, H.-A.; Zhong, Z. *Biomaterials***2013**, 34, 3647-3657.
6. Ding, J.; Zhao, L.; Li, D.; Xiao, C.; Zhuang, X.; Chen, X. *Polym. Chem*. **2013**, 4, 3345-3356.
7. Abulateefeh, S. R.; Spain, S. G.; Thurecht, K. J.; Aylott, J. W.; Chan, W. C.; Garnett, M. C.; Alexander, C *Biomater. Sci.* **2013**, 1, 434-442.
8. Li, Y.; Li, J.; Chen, B.; Chen, Q.; Zhang, G.; Liu, S., Ge, Z. *Biomacromolecules***2014**, 15, 2914-2923.
9. Chen, C.-Y.; Kim, T. H.; Wu, W.-C.; Huang, C.-M.; Wei, H.; Mount, C. W.; Tian, Y.; Jang, S.-H.; Pun, S. H.; Jen, A. K.-Y. *Biomaterials***2013**, 34, 4501-4509.
10. Du, J.-Z.; Du, X.-J.; Mao C.-Q.; Wang, J. *J. Am. Chem. Soc*. **2011**, 133, 17560-17563.
11. Quan, C.-Y.; Chen, J.-X.; Wang, H.-Y.; Li, C.; Chang, C.; Zhang X.-Z.; Zhuo, R.-X. *ACS Nano***2010**, 4, 4211-4219.
12. Surnar, B.; Jayakannan, M. *Biomacromolecules***2013**, 14, 4377-4387.
13. Molla, M. M.; Rangaduri, P.; Pavan G. M.; Thayumanavan, S. *Nanoscale* **2015**, 7, 3817-3837.
14. Harnoy, A. J.; Rosenbaum, I.; Tirosh, E.; Ebenstein, Y.; Shaharabani, R.; Beck, R.; Amir, R. J. *J. Am. Chem. Soc*. **2014**, 136, 7531-7534.
15. Hu, Q. P.; Katti, S.; Gu, Z. *Nanoscale* **2014**, 6, 12273-12286.
16. Ding, Y.; Kang, Y.; Zhang, X. *Chem. Commun*. **2015**, 51, 996-1003.
17. Roy, D.; Brooks, W. L. A.; Sumerlin,B. S. *Chem. Soc. Rev.* **2013**, 42, 7214-7243.

18. Hocine, S.; Li, M.-H. *Soft Mater*, **2013**, 9, 5839-5861.
19. Hervault, A.; Thanh, N. T. K. *Nanoscale***2014**, 6, 11553-11573.
20. Qu, Y.; Li, J.; Ren, J.; Leng, J.; Lin, C.; Shi, D. *Nanoscale***2014**, 6, 12408-12413.
21. Schattling, P.; Jochum, F. D.; Theato, P. *Polym. Chem.***2014**, 5, 25-36.
22. Fang, J.; Nakamura H.; Maeda, H. *Adv. Drug Delivery Rev*. **2011**, 63, 136-151.
23. Kaur, S.; Prasad, C.; Balakrishnan, B.; Banerjee, R. *Biomater. Sci.* **2015**, 3, 955-987.
24. Larson, N.; Ghandehari, H. **2012**, 24, 840-853.
25. Xu, X.; Flores, J. D.; McCormick, C. L. *Macromolecules***2011**, 44, 1327-1334.
26. Du, J.-Z.; Du, X.-J.; Mao, C.-Q.; Wang, J. *J. Am. Chem. Soc*. **2011**, 133, 17560-17563.
27. Kale A. A.; Torchilin, V. P. *Bioconjug. Chem.***2007**, 18, 363-370.
28. Vijayakameswara, R. N.; Mane, S. R.; Kishore, A.; Sarma, J. D.; Shunmugam, R. *Biomacromolecules***2012**, 13, 221-230.
29. Liu, R.; Zhang, Y.; Zhao, X.; Agarwal, A.; Muller, L. J.; Feng, P. *J. Am. Chem. Soc*. **2010**, 132, 1500-1501.
30. Murthy, N.; Thng, Y. X.; Schuck, S.; Xu, M. C.; Frechet, M. J. *J. Am. Chem. Soc*. **2002**, 124, 12398-12399.
31. Gao, W.; Chan, J. M.; Farokhzad, O. C. *Mol. Pharm.***2010**, 7, 1913-1920.
32. Alarcon, C. D. L. H.; Pennadam, S.; Alexander, C. *Chem. Soc. Rev*., 2005,**34**, 276-285.
33. Phillips, D. J.; Gibson, M. I. *Polym. Chem.***2015**, 6, 1033-1043.
34. Oh, K. T.; Yin, H.; Lee, E. S.; Bae, Y. H. *J. Mater. Chem.* **2007**, 17, 3987-4001.
35. Wei, H.; Cheng, S.-X.; Zhang, X.-Z.; Zhuo, R.-X. *Prog. Polym. Sci*. **2009**, 34, 893-910.

36. Soppimath, K. S.; Liu, L.-H.; Seow, W. Y.; Liu, S.-Q.; Powell, R.; Chan, P.; Yang,Y. Y. *Adv. Funct. Mater.***2007**, 17 355-362.
37. Johnson, R. P.; Jeong, Y.-I.; John, J. V.; Chung, C.-W.; Kang, D. H.; Selvaraj, M.; Suh H.; Kim, I. *Biomacromolecules***2013**, 14, 1434-1443.
38. Li, W.; Li, J.; Gao, J.; Li, B.; Xia, Y.; Meng, Y.; Yu, Y.; Chen, H.; Dai, J.; Wang, H.; Guo, Y. *Biomaterials***2011**, 32, 3832-3844.
39. Liu, J.; Detrembleur, C.; Debuigne, A.; Gillet, M.-C. D. P.; Mornet, S.; L. Elst, V.; Laurent, S.; Labrugere, C.; Duguet, E.; Jerome, C. *Nanoscale***2013**, 5, 11464-11477.
40. Jiang, H.; Lu, G.; Feng, C.; Li, Y.; Huang, X. *Polym. Chem.***2013**, 4, 3876-3844.
41. Cheng, Y.; Hao, J.; Lee, L. A.; Biewer, M. C.; Wang, Q.; Stefan, M. C. *Biomacromolecules***2012**, 13, 2163-2173.
42. Rainbolt, E. R.; Miller, J. B.; Washington, K. E.; Senevirathne, S. A.; Biewer, M. C.; Siegwart, D. J.; Stefan, M. C. *J. Mater. Chem. B* **2015**, 3, 1779-1787.
43. Rainbolt, E. R.; Washington, K. E.; Biewer, M. C.; Stefan, M. C. *J. Mater. Chem. B* **2013**, 1, 6532-6537.
44. Hu, Q.; Katti, P. S.; Gu, Z. *Nanoscale***2014**, 6, 12273-12286..
45. Anderson, T. L.; Thompson, D. H.; Kaasgaard, T. *Mol. Membr. Biol.***2010**, 27, 353-363.
46. Zhunag, J.; Chacko, R.; Amado, D. F.; Wang, H.; Thayumanavan, S. *ACS Macro Lett.***2014**, 3, 1-5.
47. Miao, K.; Li, H.; Zhao, Y. *Polym. Chem.***2014**, 5, 3335-3345.
48. Caponi, P.-F.; Qiu, X.-P., Vilela, F.; Winnik, F. M.; Ulijn, R. V. *Polym. Chem.***2011**, 2, 306-308.
49. Pramod, P. S.; Katamura, C.; Chapaker, S.; Balasubramaniam, N.; Jayakannan, M. *Biomacromolecules***2012**, 13, 3627-3640.
50. Pramod, P. S.; Shah, R.; Sonali, C.; Balasubramanian, N.; Jayakannan, M. *Nanoscale***2014**, 6, 11841-11855.
51. Pramod, P. S.; Shah, R.; Jayakannan, M. *Nanoscale***2015**, 7, 6636-6652.

52. Sridhar, U.; Pramod, P. S.; Jayakannan, M. *RSC Advances***2013, 3, 21237–21241.**
53. Kashyap, S.; Jayakannan, M. *J. Mater. Chem. B* **2014**, 2, 4142-4152.
54. Kashyap, S.; Jayakannan, M. *J. Mater. Chem. B* **2015**, 3, 957-967.
55. Yao, X.; Chen, D.; Jiang, M. *J. Phys. Chem. B***2004**, 108, 5225-5229.
56. Huang, R.; Chen, D.; Jiang, M. *J. Mater. Chem. B* **2010**, 20, 9988-9994
57. Yang, Y. Q.; Guo, X. D.; Lin, W. J.; Zhang, L. J.; Zhang, C. Y.; Qian, Y. *Soft Matter,* **2012**, 8, 454-464.
58. Siepmann, J.; Peppas, N. A. *Adv. Drug Delivery. Rev.***2001**, 48, 139-157.
59. Young, C. R.; Dietzsch, C.; Cerea, M.; Farrell, T.; Fegley, K. A.; Rajabi-Siahboomi, A.; Mcginity, J. W. *Int. J. Pharmaceutics***2005**, 301, 112-120.

Chapter 4

Super LCST Thermo-responsive Nanoparticle Assembly for ATP Binding through Hofmeister Effect

Chapter4

Super LCST Thermo-responsive Nanoparticle Assembly for ATP Binding through Hofmeister Effect

Super LCST thermo-responsive amphiphilic nanoparticle assembly was developed for detection of adenosine triphosphate (ATP) through Hofmeister effect. For this purpose, a new diblock molecular was designed based on hydrophilic polyethylene glycol and renewable resource 3-pendadecylphenol as hydrophobic unit. The amphiphile self-assembled as 150 nm micellar nanoparticle and showed super lower critical solution temperature (LCST) above 90 ℃. The amphiphile followed the "Hofmeister effect" for anion series and it exhibited high selectivity for the recognition of ATP over its adenosine precursors such as ADP, AMP and inorganic phosphate (Pi). The preferential binding for ATP is attributed to the encapsulation in the hydrophobic pocket and modification of hydration shell at the periphery of the amphiphilic nanoparticles.Electron and atomic force microscopes and dynamic light scattering techniques confirmed the size and shape of the amphiphilic assembly and its ATP complexes. Isothermal calorimetric experiments were carried out to determine the binding constants for the amphiphilic nanoparticle binding to ATP. The amphiphilic nanoparticle binding to ATP was found to be an endothermic process and showed binding constant three times higher compared to its precursor Pi. The cytotoxicity of the super LCST amphiphile was studied. The amphiphile was found to be non-toxic in nature. In a nut-shell, the super LCST amphiphile selectively binds to ATP over its precursors ADP, AMP and inorganic phosphate (Pi) at temperature close to cancer tissue temperature.

4.1. Introduction

Specific ion effect also widely known as "*Hofmeister effect*" was pioneered by Franz Hofmeister in 1888. It was originally related to ability of salts to precipitate or crystallize out proteins from the aqueous solutions.[1,2,3] The anions had much more pronounced effect on the precipitation of the proteins as compared to cations.[4,5] On the basis of their ability to 'salt in' and 'salt out' proteins from the aqueous solution, anions were ranked by Franz Hofmeister (also known as Hofmeister series) which is given as:[6,7,8]

The highly solvated anions present on the left end of the series exhibit strong interaction with the water molecules. As a result, they withdraw water molecules from the vicinity of the proteins and organize them around themselves leading to the salting-out of proteins. Hence, these anions were termed as water "structure maker" or kosmotropes. While ions on the right end of the series were termed as water "structure breaker' or chaotrope as they were less efficient in assembling water molecules around themselves; resulting in hydration of the protein molecules.[9,10]Apart from this very basic hypothesis of "making" and "breaking" of hydrogen bond between anion and water molecules (see figure 4.1) several other hypotheses have been proposed in order to understand the mechanism of the Hofmeister effect. For instance, Ninham and co-workers anticipated dispersion forces to be major contributing factor for the Hofmeister effect.[11,12,13] Several theories and experimental methods were developed to address the mechanism of the Hofmeister effect.[14,15,16]

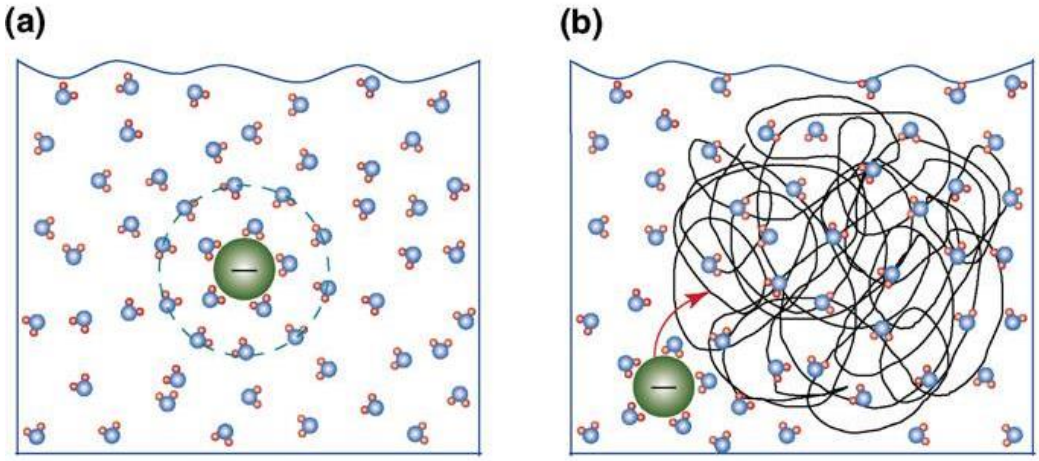

Figure 4.1. *Anions and water structure. (a) Organized water beyond an anion' first hydration shell would be needed for structure-making and breakingeffects to occur. (b) The direct interaction of an anion with a macromolecule in aqueous solution. The relative sizes of water molecules, macromolecules, and the anion are not generally to scale. However, the relative size of the anion with respect to the water molecules is approximately correct for* $SO4^{2-}$ *(adopted from Curr. Opin. Chem. Biol.* ***2006****, 10, 658-663).*

Hofmeister effect has not only been employed for understanding the physical behavior of proteins in aqueous solution. Instead it has been expanded to the macromolecular system.[17,18] The influence of anions on thermo-responsive polymers is found to be of immense importance regarding fundamental understanding of polymer chain folding and crystallization in the aqueous environment.[10] Likewise, the influence of these 'salting out' and 'salting in' anions on the phase-transition temperature (LCST) of thermo-responsive polymers has been extensively studied,[19, 20] since the ions present in the biological fluids such as chloride, phosphate, bicarbonate, etc can influence the efficacy of various thermo-responsive nano-carriers (micelles, nanoparticles and vesicles etc)(see figure 4.2). However, there are

no efforts under taken to study the role of Hofmeister effect for the binding (or sensing) of biologically important anionic species such as adenosine phosphates.

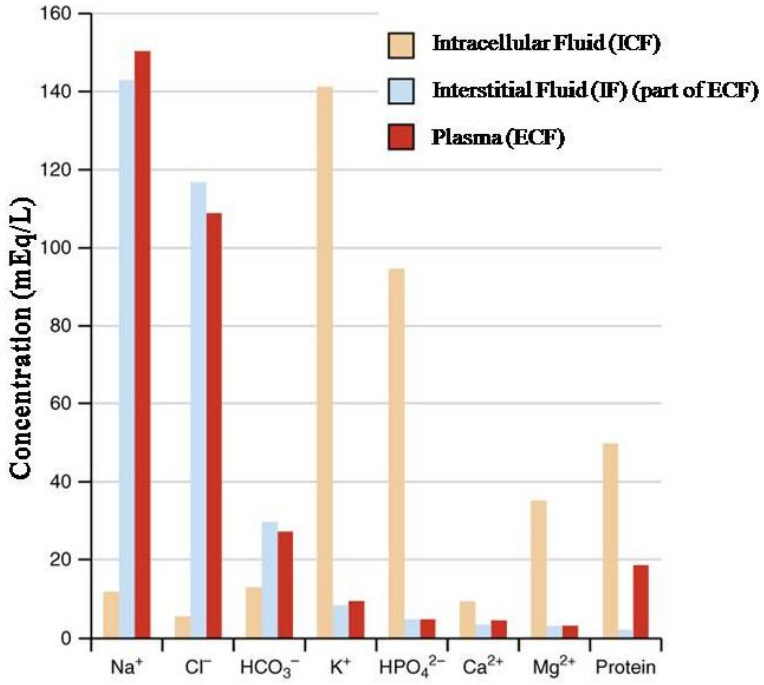

Figure 4.2. *The concentration of various cation and anions in the body fluid(electrolyte composition of body fluid).*

Poly(N-isopropylacrylamide) (PNIPAM)[18,21] and elastin-like polypeptides (ELPs) [22,23,24] are some of the most extensively studied thermo-responsive commercial polymer for Hofmeister effect.[10] Elegant prior work had established that the ions exhibiting this 'salting out' and 'salting in' behavior changes the phase-transition temperature (LCST) of PNIPAM polymer. Wei et al. recently reviewed the anticancer drug loading and delivering capabilities of PNIPAM to cancer cells.[25] Hofmeister effect was also employed to understand enzymatic activity,[26,27,28,29] peptide self-assembly,[30] fluorescent polyacrylates,[31] polyacrylate hydrogels,[32,33] guest-host interactions,[34] cationic polythiophenes,[35] O-acylcholines,[36] cationic gemini surfactants[37] and PEO-PPO-PEO triblocks.[38] These studies emphasized the importance of Hofmeister effect in the self-assemblies of organic materials and polymers.

Hofmeister effect of biological phosphate anions is very important to be studied since the phosphate anions are ubiquitous in biological systems and are of paramount importance in intra- and extracellular signaling and ion transport.[39] Of all the phosphate derivatives, ATP (adenosine triphosphate) which is a multifunctional nucleotide is of immense importance as it serves as the molecular currency for intracellular energy generation (see figure 4.3). Apart from being involved as the energy currency of the cell it also functions as a signaling molecule in the extracellular environments[40,41] (see figure 4.3).

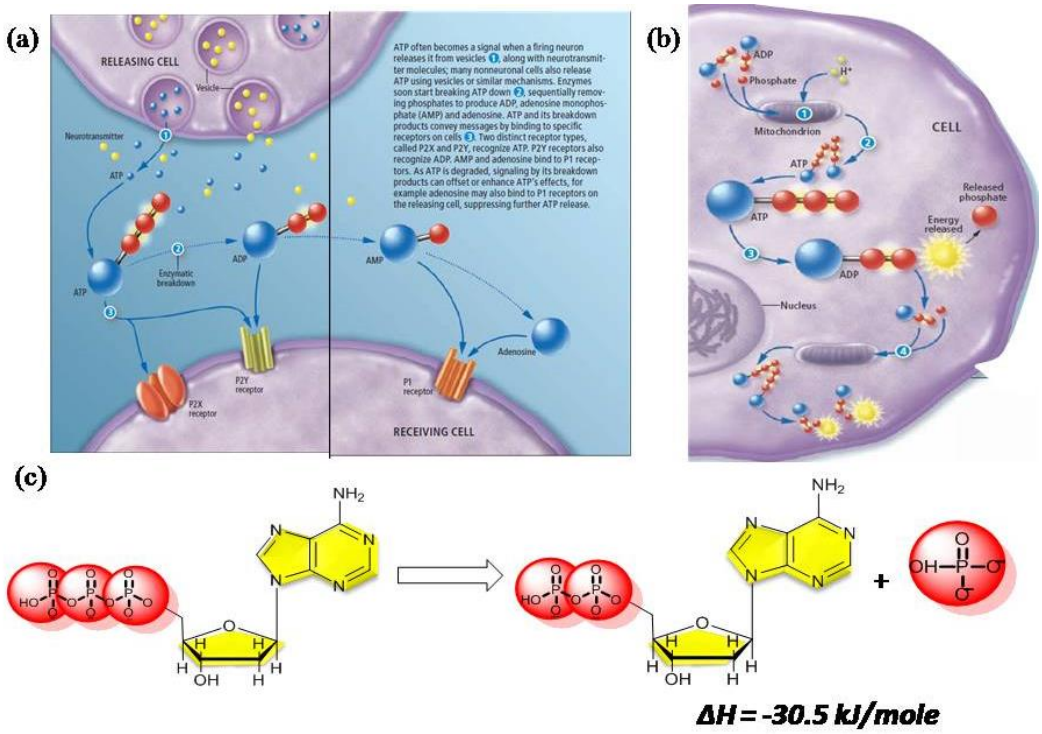

Figure 4.3. *ATP as (a)signaling molecule and (b)molecular energy currency of cell (c)Mechanism of ATP hydrolysis into ADP and inorganic phosphate (Pi) (adopted from Khakh et al. Sci. Am.* ***2009****, 301, 84-92).*

Extracellular ATP are found to play vital roles in several biochemical pathways such as platelet function, neurotransmission, signal transduction, vasodilatation, and muscle contraction.[42]Recent studies revealed that under the physiological condition, the concentration of extracellular ATP was found to be much higher in cancer tissues compared to normal tisues.[43,44] For extracellular ATP administration studies at tumor sites, the concentration of ATP are typically varied

from 1 to 5 mM to trigger apoptosis or programmed cell death.[45,46] The enhancement in extracellular ATP concentration in cancer tissues are generally promoted by release of ATP from cytoplasm mediated via several plasma membrane receptors such as ABC transporters, P2X7 receptors, connexins etc.[47]

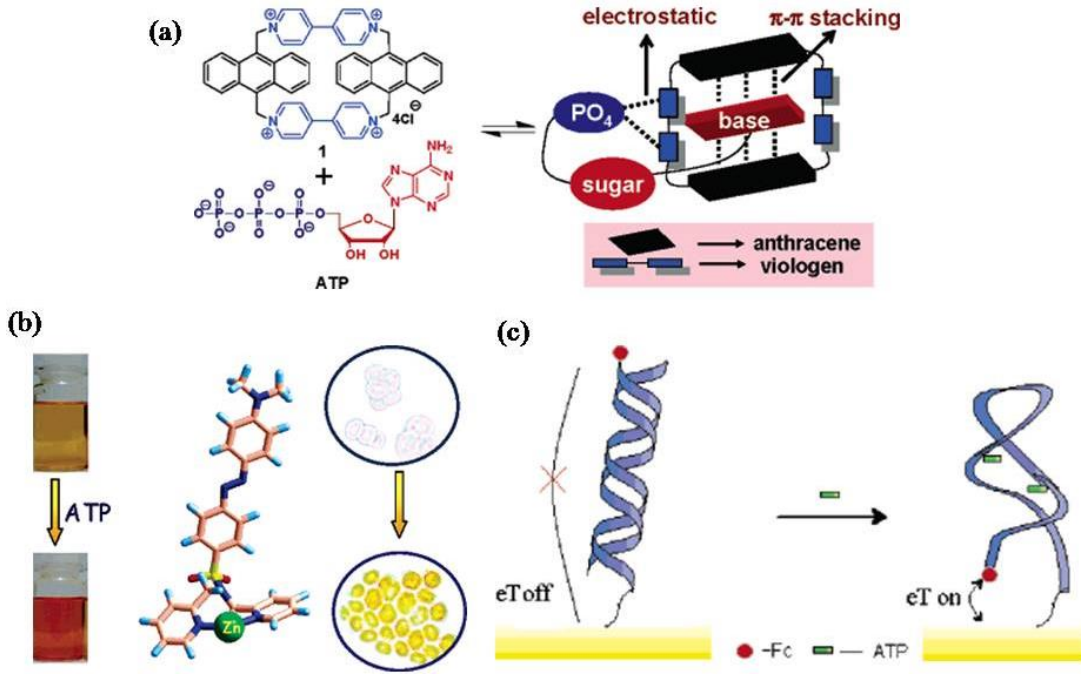

Figure 4.4. *(a) Recognition of ATP using cyclic anthracene through guest-host interaction(adopted from Neelakandan et al. Org. Lett.**2005**, 7, 5765-5768).(b) A colorimetric sensor for ATP (adopted from Jose et al. Org. Lett.**2007**, 9, 1979-1982). (c) A target responsive electrochemical aptamer switch for ATP detection (adopted from Zhou et al. J. Am. Chem. Soc.**2007**, 129, 1042-1043).*

Various optical chromophores were developed to recognize ATP through colorimetric changes[48,49] or fluorescence techniques[50-53] and this topic was recently reviewed by Zhou et al.[54]Among the various probes cholic acid based fluorescent chemosensor,[52] naphthalimide coupled dipicolylamine-Zn complex,[53] Zn free polydiacetylenes[51] and host-guest interaction based on cyclic anthracene derivatives[48](see figure 4.4a) were worth mentioning. Aptamer hybridized silica nanoparticle (see figure 4.4c) and ATP functionalized gold nanoparticles was also reported for sensing ATP (see figure4.4b).[55,56] However, sensing or binding of ATP through Hofmeister effect by the thermo-responsive is not attempted till date.

The uncontrolled cell division and fast growth makes the cancer tissue environment (42-44 °C; pH= 6.5 to 5.5) much different than normal tissues (37 °C and pH = 7.4).[57] Thermochemotherapy, a drug administration concept is recently developed to enhance the cytotoxicity of the anticancer drugs at least three times by applying temperature between to 40.5 °C to 43.5°C.[58] Thus, developing thermo-responsive drug carriers that could disassemble either at abnormal tissue temperature (40- 43 °C) or external stimuli of heat in the thermochemotherapy would enhance the efficacy of the cancer treatment.[59] Additionally, the porous network and defective lymphatic drainage in cancer tissues allow the accumulation of larger size macromolecular or self-assembled polymer particles (150-250 nm) through the enhanced permeability and retention (EPR) effect.[60,61] The existing thermo-responsive materials such as PNIPAM would support the EPR effect; however, it cannot be used for ATP binding since its LCST is less than 37 °C.[25] Hence, the above multi-task problem could be addressed only with the design of new thermo-responsive scaffold having "*super LCST characteristics*" to withstand the Hofmeister effect of anions at cancer tissue temperature (42-43°C).

In general, ATP binding showed interference with its precursors such as ADP, AMP and Pi (inorganic phosphate); thus, the new scaffold should have preferential selectivity for detection of ATP among its other anionic precursors. In the previous two chapters, both the small molecule and polymeric scaffold even upon being thermo-responsive in nature could not be employed for studying the influence of the biologically relevant anions since they lose their thermal responsive characteristics in presence of anions. Thus, the new material design requires the following criteria: (i) *super LCST characteristics* for recognizing ATP through *Hofmeister effect*, (ii) it should show selective binding towards ATP over its other precursors in aqueous medium and (iii) it should have ability to self-organize into nano-size objects so that it can penetrate through cancer tissues via *EPR* effect. This concept is schematically shown in figure 4.5.

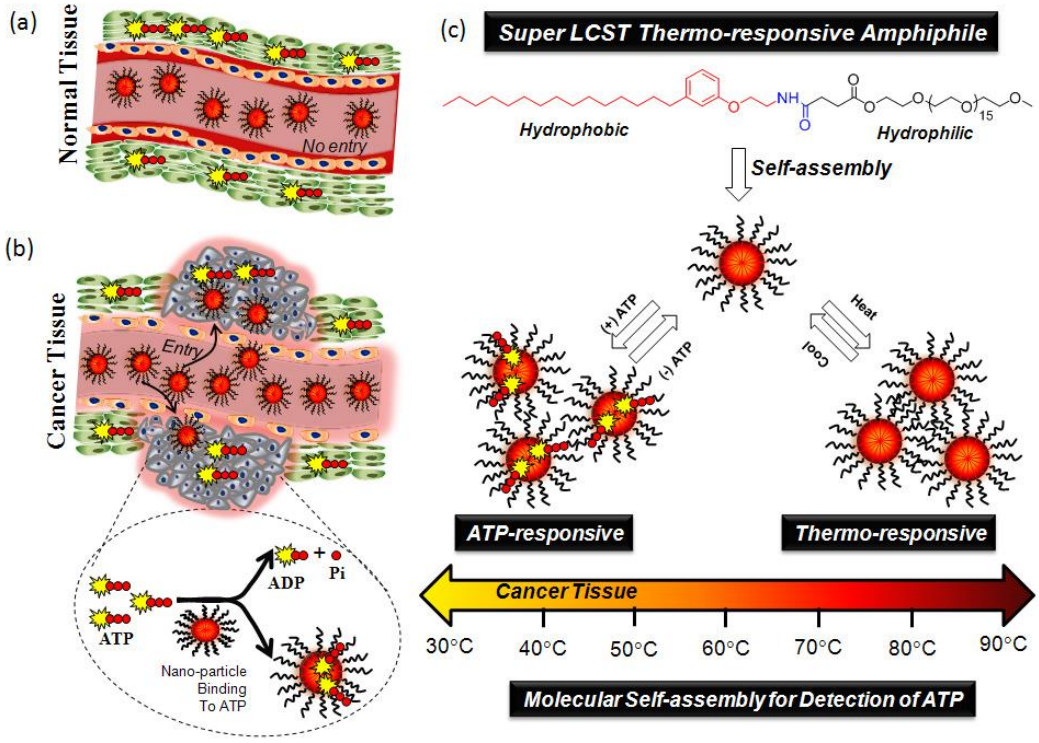

Figure 4.5. *Thermo-responsive amphiphilic nanoparticle entry at normal tissue (a) and cancer tissue (b) environment. The expanded part in figure b demonstrate the ATP pathways for hydrolysis and binding to nanoparticle. (c) A di-block molecular design for the super LCST amphiphile* ***1*** *and the self-assembly of the amphiphilic nanoparticle towards ATP.*

In this chapter a *super LCST thermo-responsive amphiphilic nano-scaffold*was developed and was used as a tool to recognize and bind ATP is reported. New di-block amphiphile was designed with hydrogen bonded amide linkage that connect both side with hydrophobic unit based on renewable resource 3-pentadecyl phenol (PDP) and polyethylene glycol chains as hydrophilic part. PDP was chosen in the present investigation since it was found to be an efficient hydrophobic unit for producing polysaccharide vesicles,[62-64] multi-vesicularbodies[65] and shape transformable thermo-responsive core-shell nanoparticles[66] in our earlier works. Thus, the selection of hydrophobic PDP unit with appropriate PEG chain length has facilitated the designing of thermo-responsive amphiphile that showed highest LCST

> 90° C (named as *super LCST amphiphile*). This thermo-responsive scaffold followed typical Hofmeister series and exhibited preferential binding towards ATP at 42-44 °C. Dynamic light scattering, electron and atomic force microscopes provided direct evidence for the mechanism of nano-particle driven ATP detection. Further, isothermal calorimetric experiments were also carried out to determine the association constants for the selective binding of thermo-responsive nanoparticle to ATP.

4.2. Experimental Methods

4.2.1: Materials: 3-Pentadecylphenol, 2-ethanolamine, succinicanhydride, Boc-anhydride, triethylamine (Et_3N), polyethylene glycol monomethylether (MW=750), 1-ethyl-3-(3- dimethylaminopropyl) carbodiimide (EDC), diisopropyl ethylamine (DIPEA), diisopropyl azodicarboxylate (DIAD) were purchased from Aldrich chemicals. And all other reagents and solvents were purchased locally and purified following the standard procedure. The *tert*-butyl (2-hydroxyethyl) carbamate was synthesized using our earlier procedure reported in chapter 2.

4.2.2: General procedures: ^{1}H-NMR and ^{13}C-NMR spectra were recorded using 400-MHz Jeol NMR spectrophotometer in $CDCl_3$ containing TMS as internal standard. Infra-red spectra were recorded using a Thermo-Scientific Nicolet 6700FT-IR spectrometer with the solid state in KBr. The mass of the amphiphiles and all the intermediates was confirmed by using the Applied Biosystems 4800 PLUS MALDI TOF/TOF analyzer.

Size Exclusion Chromatography: The purity of the amphiphile was determined by size exclusion chromatography (SEC) using a Viscotek VE 1122 pump, ViscotekVE 3580 RI detector, and Viscotek VE 3210 UV/Vis detector in tetrahydrofuran (THF) using polystyrene as standards. The optical transmittance measurement was done by a Perkin-Elmer Lambda 45 UV-Visible spectrophotometer.

Dynamic and Static Light Scattering Measurement: The size determination of the aqueous solution of the amphiphile was carried out by dynamic light scattering (DLS), using a Nano ZS-90 apparatus utilizing 633 nm red laser (at 90° angle) from Malvern instruments.The reproducibility of the data was checked for at least three independent solutions.

Morphology analysis: FE-SEM images were recorded using Zeiss Ultra Plus scanning electron microscope. For FE-SEM analysis, the samples were prepared by drop casting on silicon wafers and coated with gold.TEM images were recorded using a Technai-300 instrument by drop casting the sample on Formvar-coated copper grid. Atomic force microscope images were recorded for drop casted samples using JPK instruments attached with Nano wizard-II setup.

Optical Transmittance measurement: Optical transmittance of PDP-PEG750 was measured at 500nm using quartz cell (path length: 1cm) with Perkin-Elmer Lambda 45 UV-Visible spectrophotometer which was equipped with temperature-controller. The heating cycle was recorded by heating the sample continuously from 30 °C to

90°C. Similarly, cooling cycle was recorded from 90 °C to 30 °C. The heating and cooling cycles were maintained at 10 °/min rate using peltier heating/cooling source.

Isothermal Titration Calorimetry (ITC): The titrations of ATP and inorganic phosphate anion with the scaffold (PDP-PEG-750) were performed at 25 °C using iTC200 microcalorimeter (MicroCal Inc.). In the case of these experiments, ATP and inorganic phosphate anion was titrated into scaffold solution. Both the solution in the injection syringe and the one in the ITC cell were prepared in water. Two blank titrations were also performed; (i) titration of water with the same ATP and Pi solution and (ii) titration of the amphiphile with water. The stoichiometries of substrate binding (n) and binding constant (Ka) of amphiphile **1** with ATP and Pi were obtained after subtracting the blank titrations. The stirring speed used was 1000rpm, and the reference power was set at 0.5 μcal/s for all the titrations. The volume of the ITC200 cell was 0.200 mL while that of syringe was 0.040 mL.

Cell Viability Assay (MTT Assay). To test the cytotoxicity of the amphiphile **1**a cell viability assay was performed in Hela Cell lines using the tetrazolium salt, 3-(4,5dimethylthiazol)-2,5-diphenyl tetrazolium bromide (MTT). Hela Cell lines (1 × 103) were seeded per well in a 96- well plate (Corning, U.S.A.) in 100 μL of DMEM with 10% FBS (fetalbovine serum) and allowed to adhere for 12 h and 24 h. Prior to drug treatment, medium from cells was aspirated and various concentration of amphiphile **1** was prepared. These were added to 100 μL of DMEM with FBS in which the cells were incubated. Blank controls, DMEM with FBS in the absence of cells, were used in each experiment. All control and treated experiment wells were in triplicate. Cells were incubated for 12 and 24 h without a change in medium, and after 12 and 24 h, amphiphile **1** medium was aspirated. Freshly prepared stock of MTT in sterile PBS (5 mg/mL) was diluted to 50 μg/mL in 100 μL of DMEM with FBS and was added to cells. Cells were then incubated with MTT for 4 h at 37°C. Medium with MTT was then aspirated from wells and the purple formazan crystals formed as a result of reduction of MTT by mitochondrial dehydrogenase enzyme from cells were dissolved in 100μL of 100% DMSO (added per well). The absorbance from formazan crystals was immediately measured using microplate reader at 570 nm (Varioskan Flash) and is representative of the number of viable cells per well. Values from the triplicates for each control and treated set were noted and their means used for calculations. The mean of the absorbance values for the blank control samples was subtracted from the average of treated samples. The values thus obtained for the control samples were equated to 100% and relative percentage values for amphiphile **1** was calculated accordingly.

4.2.3. Synthesis

Synthesis of PEG750-COOH (PEG-Acid): Poly(ethylene glycol) MW 750 monomethylether (10.0 g, 13.0 mmol) and succinic anhydride (1.6 g, 16.0 mmol) were dissolved in dry dichloromethane (60 mL) and was purged with N_2 for 10 min. To this reaction mixture, Et_3N (1.85 mL, 13.0 mmol) was added drop wise. Immediately after the addition of Et_3N the reaction mixture started to boil vigorously. The reaction proceeded at 25°C for 48 h with continuous stirring under N_2 atmosphere. The reaction mixture was poured in to water (100 mL) and was neutralized with 2N concentrated HCl (2.0 mL). The organic layer was washed with brine solution, dried over anhydrous sodium sulphate andconcentrated to obtain yellow liquid as product. It was purified by passing through silica gel column of 60-120 mesh using 50% methanol in chloroform as eluent. Yield = 6.0g (66.0 %).^{1}H NMR ($CDCl_3$, 400 MHz) δ: 4.14 ppm (t, 2H, CO-OC**H$_2$**), 3.56-3.50 ppm (s, 66H, OC**H$_2$**C**H$_2$**O), 3.23 ppm (s, 3H, CH_2-OC**H**$_3$), 2.52 ppm (s, 4H, CO-C**H**$_2$-C**H**$_2$). ^{13}C NMR ($CDCl_3$, 100 MHz) δ: 177.05 (**C**OOH), 171.88 (**C**OO-CH_2), 70.56 (O**C**H_2-**C**H_2-O), 69.93 (COO-**C**H_2), 58.51 (C-O**C**H_3), 28.45 (CO-**C**H_2-**C**H_2). FT-IR (cm^{-1}): 3448, 2875, 1727, 1649, 1453, 1349, 1286, 1247, 1202, 1087, 947, 842, 677, 622. MALDI-TOF-MS: m/z calculated for $C_{39}H_{76}O_{21}$: 880 and found: 903 ($M^+ + Na^+$).

Synthesis of *tert*-butyl(2-(3-pentadecylphenoxy)ethyl carbamate (PDP-NH-Boc): *tert*-Butyl(2-hydroxyethyl) carbamate(3.7 g, 23.0 mmol), 3-pentadecylphenol (7.0 g, 23.0 mmol) and triphenylphosphine (6.6 g, 25.0 mmol) was dissolved in dry tetrahydrofuran (20 mL). The contents were then placed in ice-cooled bath for 10 min with continuous N_2purge. To this ice-cooled reaction mixture, diisopropyl azodicarboxylate (4.47 mL, 23.0mmol) was added drop wise under N_2 atmosphere. The reaction mixture was further stirred at 25°C for 24 h. It was purified by passing through silica gel column of 60-120 mesh using 1% ethyl acetate in hexane as eluent. Yield = 8.0 g (66.0 %).^{1}H NMR ($CDCl_3$, 400 MHz) δ: 7.19 ppm (t, 1H, Ar-**H**), 6.80-6.70 ppm (m, 3H, Ar-**H**),5.02 ppm (s, 1H, N**H**), 4.02 ppm (t, 2H, Ar-OC**H$_2$**), 3.54 ppm (t, 2H, C**H**$_2$-N), 2.58 ppm (t, 2H, Ar-C**H**$_2$), 1.46 ppm (s, 9H, OC-C(C**H**$_3$)$_3$, 1.6-0.88 ppm (m, 29H, Aliphatic H). ^{13}C NMR ($CDCl_3$, 100 MHz) δ: 158.62(Ar-C), 155.98 (**C**O-O), 144.85, 129.29, 121.32, 114.75, 111.40 (Ar-**C**), 79.57 (O**C** $(CH_3)_3$, 67.08 (Ar-O**C**H_2), 40.26(**C**H_2-N), 36.09, 32.00, 29.76, 26.47, 22.77, 14.20. FT-IR (cm^{-1}): 3396, 2916, 2850, 1690, 1590, 1512, 1453, 1362, 1250, 1157, 1060, 95, 866, 778, 690.MALDI-TOF-MS: m/z calculated for $C_{28}H_{49}NO_3$: 447and found: 470($M^+ + Na^+$).

Synthesis of 2-(2-(2-methoxyethoxy)ethoxy)ethyl 4-oxo-4-((2-(3-pentadecylphenoxy)ethyl)amino)butanoate (amphiphile 1): PDP-NH-Boc (2.0 g, 44.0 mmol) was dissolved in dichloromethane (5.0 mL) and to this mixture

trifluoroacetic acid (10.0 mL, 129.7 mmol) was added drop wise. The contents were stirred at 25°C for 1h and then the solvent was evaporated by rotavapour. TFA was removed by adding fresh DCM (10.0 mL X 3 times) and was evaporated by rotavapour. The content was further poured into ice-cooled diethyl ether (15.0 ml) and evaporated by rotavapour to obtain white solid as product. The white solid product (1.34 g, 3.8 mmol) was dissolved in dry dichloromethane (20.0 ml) and was purged with N_2 for 15 minutes. To it PEG-Acid (3.0 g, 3.5 mmol) was added and N_2 purging was continued further for next 15 minutes. To this reaction mixture, EDC (0.81 g, 4.2 mmol) and diisopropylethylamine (1.4 mL, 7.8 mmol) was added under N_2atmosphere and the reaction was then left at 25 °C for 48 h with continuous stirring. It was then poured in to water (30.0 mL) and the product was extracted into chloroform. The organic layer was washed with 10% $NaHCO_3$ (30.0 mL), neutralized with 2N HCl (6.0 mL), dried over anhydrous sodium sulphate and concentrated to obtain yellow liquid as product. It was further purified by passing through silica gel column of 60-120 mesh using 5% methanol in chloroform as eluent. Yield = 2.27 g (54.0%).^{1}H NMR ($CDCl_3$, 400 MHz) δ: 7.18 ppm (t, 1H, Ar-**H**), 6.80-6.70 ppm (m, 3H, Ar-**H**),6.24 (CO-N**H**), 4.24 ppm (t, 2H,COO-C**H**$_2$), 4.02 ppm (t, 2H, Ar-OC**H**$_2$), 3.69-3.66 ppm (m, 75H, O-C**H**$_2$-C**H**$_2$),3.56 ppm (t, 2H, C**H**$_2$-N), 3.38 ppm (s, 3H, CH_2-OC**H**$_3$), 2.70 ppm (t, 2H, Ar-C**H**$_2$), 2.57 ppm (t, 2H, NH-CO-C**H**$_2$), 2.51 ppm (t, 2H, C**H**$_2$-COO), 1.6-0.88 ppm (m, 29H, Aliphatic H). ^{13}C NMR ($CDCl_3$, 100 MHz) δ: 172.87(NH-**C**O),171.60(**C**O-O), 158.54, 144.86, 129.32, 121.36, 114.69, 111.47 (Ar-C), 72.00 (**C**H_2-OCH_3), 70.64 (O-**C**H_2-**C**H_2), 69.07, 66.65(Ar-OCH_2), 63.83 (COO-**C**H_2), 59.11(O-CH_3), 39.16(C**H**$_2$-N), 36.09, 31.99, 31.49, 29.75, 29.43, 22.76, 14.19. FT-IR (cm^{-1}): 3374, 2916, 2878, 1735, 1651, 1599, 1551, 1460, 1347, 1278, 1244, 1103, 955, 846, 784, 751, 697.MALDI-TOF-MS: m/z calculated for $C_{62}H_{115}NO_{21}$: 1121 and found: 1144 ($M^+ + Na^+$).

4.3. Results and Discussion

4.3.1. Synthesis and Characterization of Amphiphile 1

An amphiphilic molecule was synthesized from poly(ethylene glycol) monomethyl ether MW= 750 g/mol as hydrophilic part and renewable resource pentadecyl phenol (PDP) as the hydrophobic unit as shown in scheme 4.1. Succinic anhydride was ring opened with PEG in presence of Et_3N which act as a base to give PEG-Acid. *tert*-Butyl (2-hydroxyethyl) carbamate was coupled with PDP in presence of diisopropyl azodicarboxylate and triphenylphosphine to give *tert*-butyl (2-(3-pentadecy-8-en-1-yl) phenoxy) ethyl) carbamate (PDP-NH-Boc). The carbamate was then treated with trifluoroacetic acid (TFA) to give 2-(3-pentadecy-8-en-1-yl) phenoxy) ethanamine which was further coupled with PEG-acid in presence of EDC and diisopropylethyl amine (DIPEA) to give amphiphile **1**.

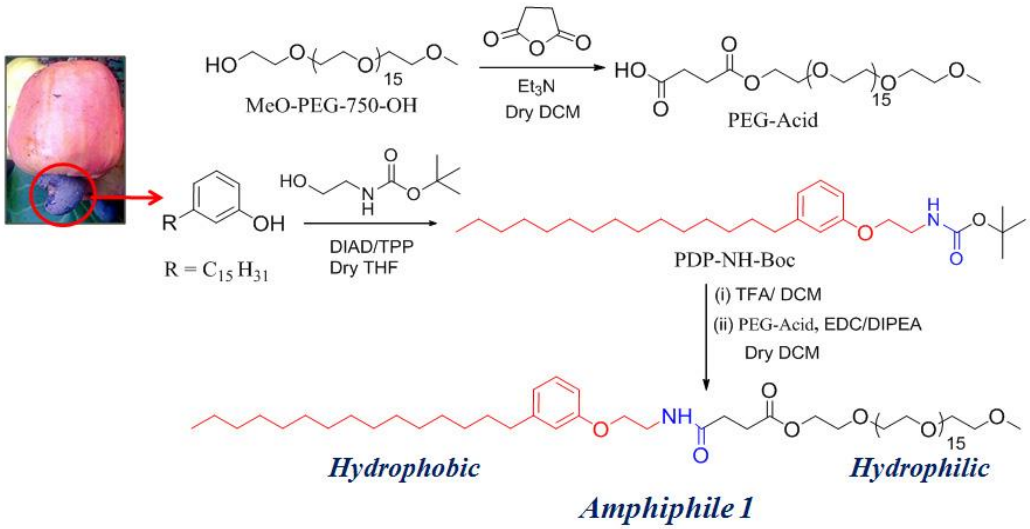

Scheme 4.1. *Synthesis of thermo-responsive amphiphile **1**.*

The structure of amphiphile **1** was characterized by ^{1}H and ^{13}C-NMR and MALDI-TOF-TOF. Figure 4.6 shows the ^{1}H-NMR, ^{13}C NMR spectra of amphiphile **1**. The aromatic peak corresponding to type a protons in amphiphile **1**appears as a triplet at 7.18 ppm and type b and c as a multiplet at 6.80-6.72 ppm. At 6.24 ppm a broad N**H** peak was visible. Two triplets for COOC$\mathbf{H}_2$ protons (type e) and Ar-OC$\mathbf{H}_2$ protons (type f) appeared at 4.23 ppm and 4.02 ppm, respectively. Peaks corresponding to all

the ethylene glycol protons (type g, h) a multiplet appeared in the range of 3.69-3.55 ppm. A triplet corresponding to C**H**$_2$-N at 3.56 ppm gets merged with oligotheylene peaks. Singlet appears for the O-C**H**$_3$ proton (type j) at 3.38 ppm. A triplet appears for the NH-CO-C**H**$_2$- protons (type k) at 2.57 ppm. Triplet appears for the Ar-C**H**$_2$ protons at 2.51 ppm. All alkyl protons appear at 1.50-0.88 ppm. All the other intermediates were similarly characterised and the detailed analysis has been given earlier in the experimental section.

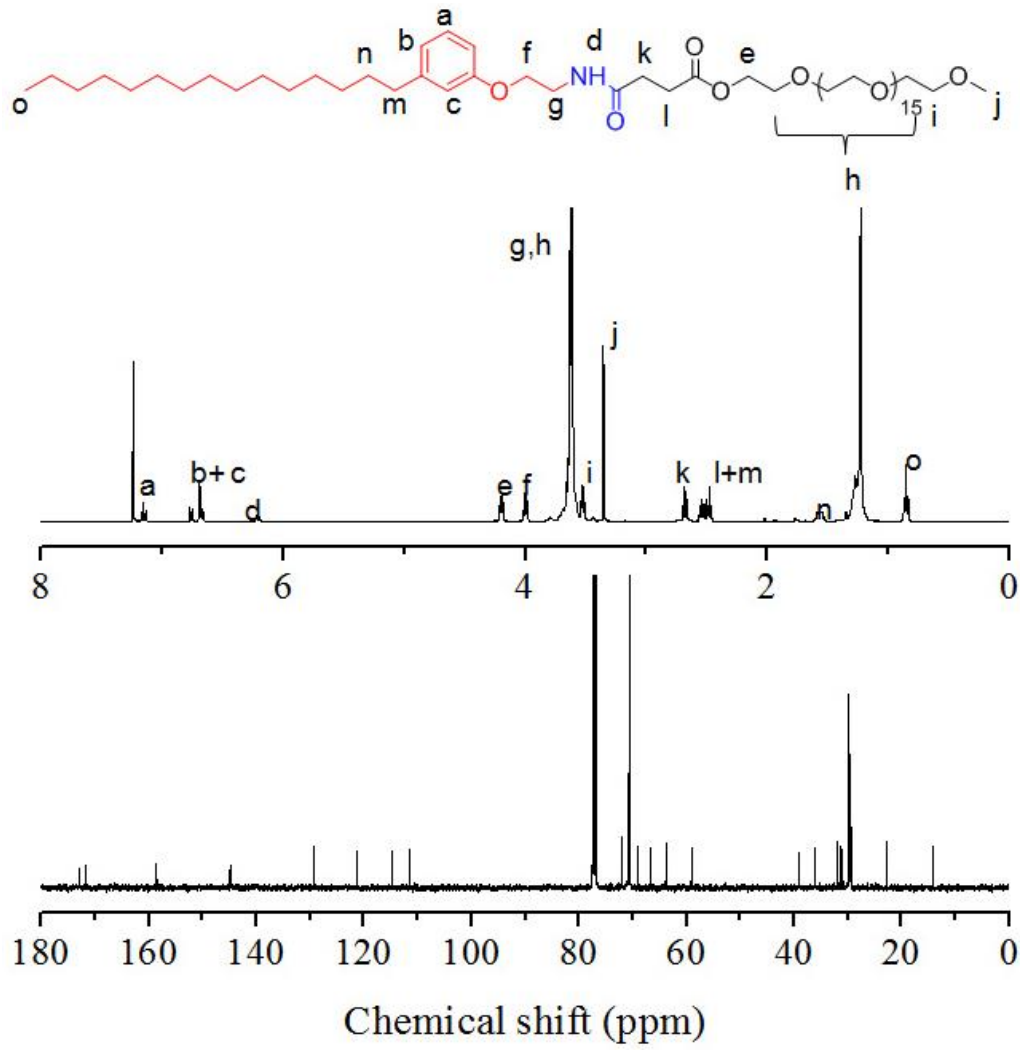

Figure 4.6. *(a) ^{1}H-NMR spectrum (b) ^{13}C-NMR spectrum of amphiphile* ***1.***

Further, amphiphile **1** was also characterized using MALDI-TOF-TOF. The MALDI-TOF-TOF spectrum of amphiphile **1** is shown in figure 4.7a. The spectrum

showed distribution of mass peaks in the range of m/z = 900 to 1500 (see figure 4.7a). The mass differences between the adjacent peaks were obtained as 44 a.m.u with respect to the distribution in the PEG chains in the diblock amphiphile **1**. The mass of each peak was calculated using the formula: (44.05) n + 461+ 23, where 44.05 is the repeating unit mass of PEG units and 461 and 23 are corresponding to the mass of hydrophobic unit and sodium ion, respectively. The mass of the peak corresponding to n = 15 is shown by arrow.

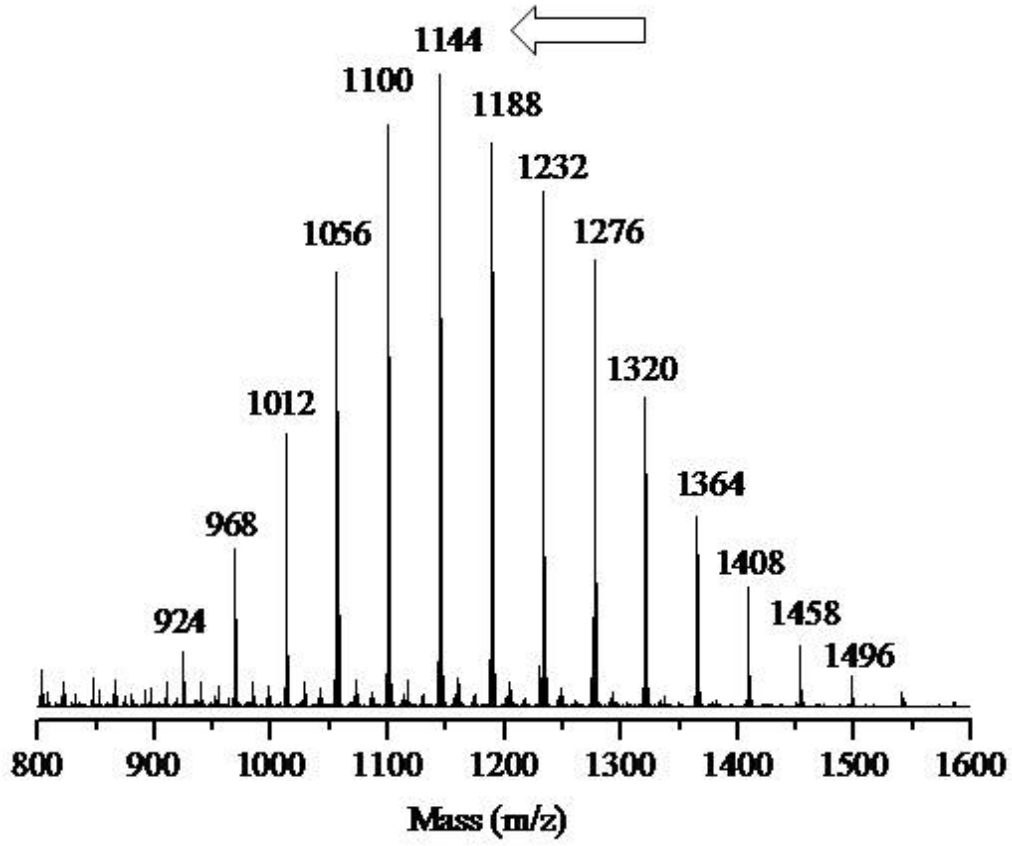

Figure 4.7. *MALDI-TOF spectrum of amphiphile **1** and the repeating unit mass for the peak at n=15 is shown by arrow.*

4.3.2. Thermo-responsive Behavior of Amphiphile 1

The thermo-responsive behavior of the amphiphile **1** was studied by optical transmittance measurement as a function of temperature using absorbance spectrophotometer. The plots of optical transmittance in the heating and cooling

cycles are shown in figure 4.8a. The plot revealed that the transmittance of the aqueous solution of amphiphile **1** decreases from 97 % to 10 % at 92 ^{o}C (LCST). From the plot it is also evident that both heating and cooling cycle followed the same kinetic path indicating that changes in the aggregates with temperature occur at similar rates. In other words the assembly and disassembly of aggregates do not exhibit the hysteresis phenomena.The temperature-driven self-assembly was further studied by subjecting the aqueous solution of amphiphile**1** (10^{-4} M) to variable temperature dynamic light scattering (DLS). The DLS histograms recorded for amphiphile **1** in the heating and cooling cycles are shown in figure 4.8b and 4.8c, respectively. Amphiphile **1** showed mono-modal distribution indicating the formation of uniform size aggregates in water.Further, it showed sharp increase in the hydrodynamic diameter from 140 ± 30 nm (below LCST) to 600 ± 30nm with respect to the formation of larger aggregates above LCST.

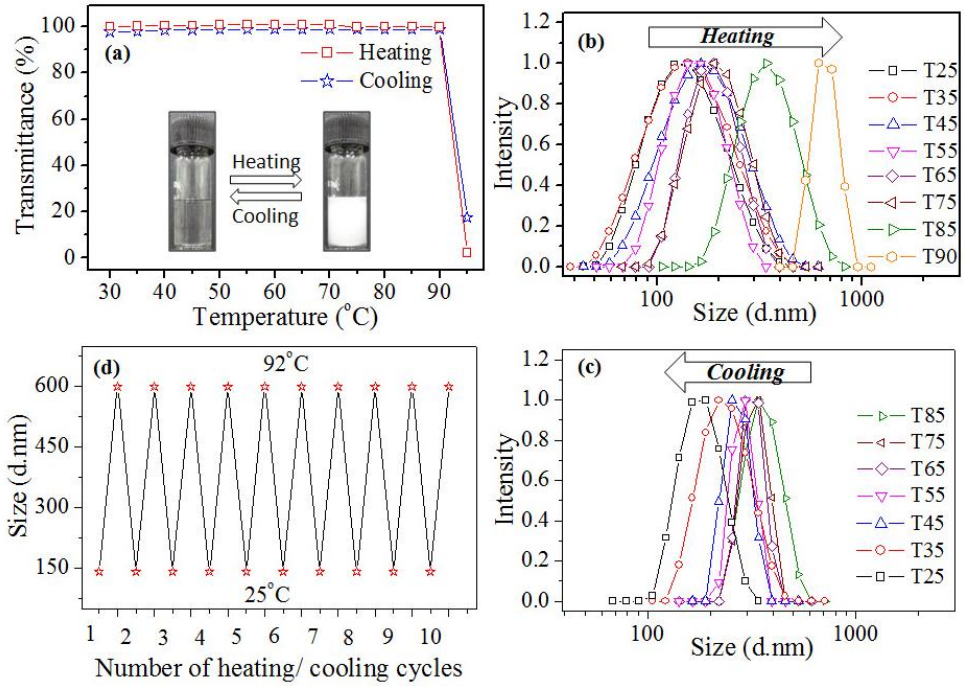

Figure 4.8. *(a)Temperature dependent optical transmittance of amphiphile **1** in water in heating and cooling cycle. DLS histogram of amphiphile **1** in the heating (b) and cooling (c) cycles. (d) Hydrodynamic diameter oscillation of the nanoparticles in consecutive ten heating and cooling cycle. The concentration of amphiphile **1** is 10^{-4}M.*

The reversibility of the thermo-responsive self-assembly process was further inferred from the cooling cycle (see figure 4.8c). It is important to mention that the DLS histograms are broad at the low temperature; however, it became very narrow while approaching the LCST temperature (see figure 4.8b). On the other hand, in the subsequent cooling cycle (see figure 4.8c), the DLS histograms retained the narrow distribution at room temperature also. The reversibility of the amphiphile self-assembly was further confirmed byrepetitive scanning in the continuous heating and cooling cycles. The plot of size of the amphiphile above and below LCST for ten consecutive cycles is shown in figure 4.8d. The size of the aggregates varied from 140± 20 nm to 600± 35 nm with perfect reproducibility. This implies that temperature induced self-assembly process in the amphiphile **1** was completely reversible; however, the dis-assembly occurred more uniformly as compared to the self-assembling process in the cooling and heating cycles, respectively.

4.3.3. Shape and Size of the Self-Assembled Amphiphile 1

To visualize the size and shape of the nano-aggregates, the amphiphile **1** was subjected to field emission-scanning electron microscopy (FE-SEM), high resolution transmission electron microscopy (HR-TEM) and atomic force microscopy (AFM) analysis. In figure 4.9a, the FE-SEM image of amphiphile **1** showed the formation of spherical shape particles of 170 ± 22 nm in diameter. The HR-TEM image of these particles confirmed that these spherical aggregates (150 ± 20 nm in size) are hardspheres with respect to micellar nanoparticles (see figure 4.9b). AFM image of amphiphile **1** also confirmed the existence of spherical nanoparticles of 130 ± 25 nm (see figure 4.9c). HR-TEM image of the nano-aggregates above LCST is shown in figure 4.9d. Above LCST, the nanoparticles of size 140±20 nm were found to form clusters together as larger aggregates. The sizes of the nano-particulate assemblies below and above LCST from the microscope images matched very well with their solution aggregates in DLS (see figure 4.8b and 4.8c).

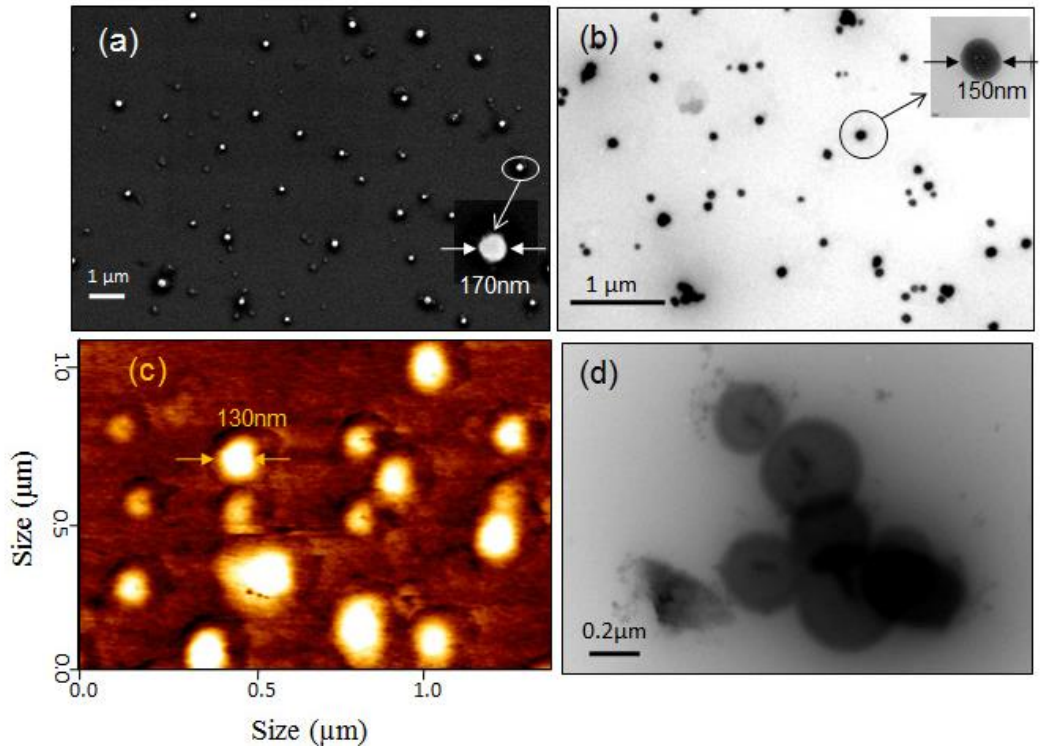

Figure 4.9. *(a) FE-SEM image, (b) HR-TEM image and (c) AFM image of amphiphile* ***1*** *below LCST (25 ℃). (d) HR-TEM of amphiphile* ***1*** *above LCST at 90 ℃. The concentration of amphiphile* ***1*** *is* 10^{-4} *M for the imaging*.

4.3.4.Critical Micellar Concentration of Amphiphile 1

The critical micellar concentration (CMC) of the amphiphile was determined using Nile Red as a fluorescent probe. Nile Red is a hydrophobic dye which is insoluble in water and displays no fluorescence in aqueous medium. Once it has been sequestrated in the hydrophobic core, the fluorescence gets generated which can be used as an indicator of formation of the micellar aggregates (see figure 4.10). The concentration of Nile red was kept constant (0.2 µM) while concentration of amphiphile **1** was varied from 1.0 µM from 1.0 mM (see figure 4.10a). The plot reveals that the emission intensity increases with increase in the scaffold concentration. Further, the emission intensity of the Nile red was plotted against the amphiphile concentration (see inset figure in 4.10a). The plot showed a gradualincrease in the emission intensity with respect to scaffold concentration and a

break point at $1.0x10^{-5}$ M was observed indicating that CMC of the amphiphile **1** is $1.0x10^{-5}$ M. The Nile red encapsulation study also suggested that the thermo-responsive micellar assemblies could be useful for loading diverse hydrophobic molecules in its inner core including anticancer drug molecules.

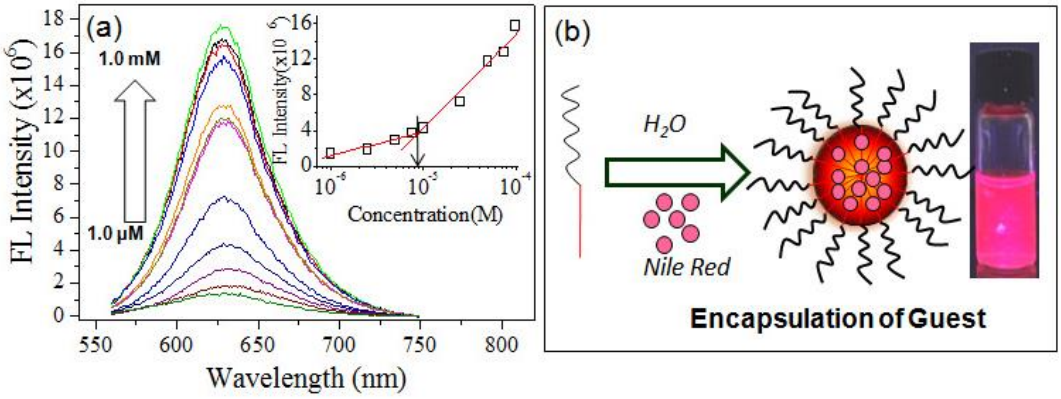

Figure 4.10.*(a) Fluorescence spectra of Nile red (0.2 µM) encapsulated at concentration of amphiphile* ***1*** *from 1.0 µM to 1.0 mM.* ***Inset figure show the plot of the emission intensity versus concentration of amphiphile 1 with a break point for CAC. (b) Schematic representation of Nile Red encapsulated micellar-nanoparticle of amphiphile 1 and photographs of vial represents the Nile red loaded scaffold in water.***

4.3.5. Hofmeister effect of Amphiphile 1

Three anion sources were chosen to investigate the Hofmeister effect on the LCST of amphiphile **1**: NaSCN, a strong chaotrope (water "structure breaker"), NaCl and Na_2SO_4, a strong kosmotrope (water "structure maker"). The plot of transmittance (%) as the function of temperature at various concentrations of NaCl, Na_2SO_4 and NaSCN is shown in figure 4.11a, 4.11b, 4.11c respectively. The transitions are appeared in two phases and this behavior is attributed to: (i) initial fast binding of anions to the nano-particles and (ii) followed by the diffusion controlled slow binding process due the precipitation of the amphiphile. At the initial stage, the homogeneous environment facilitates the fast binding whereas the heterogeneous precipitation at the secondary stage became diffusion process. The onset of the cloud point in heating cycle is termed as turbidity 'turn-on temperature' while the

temperature at which turbidity gets cleared off completely is termed as 'turn-off temperature'.

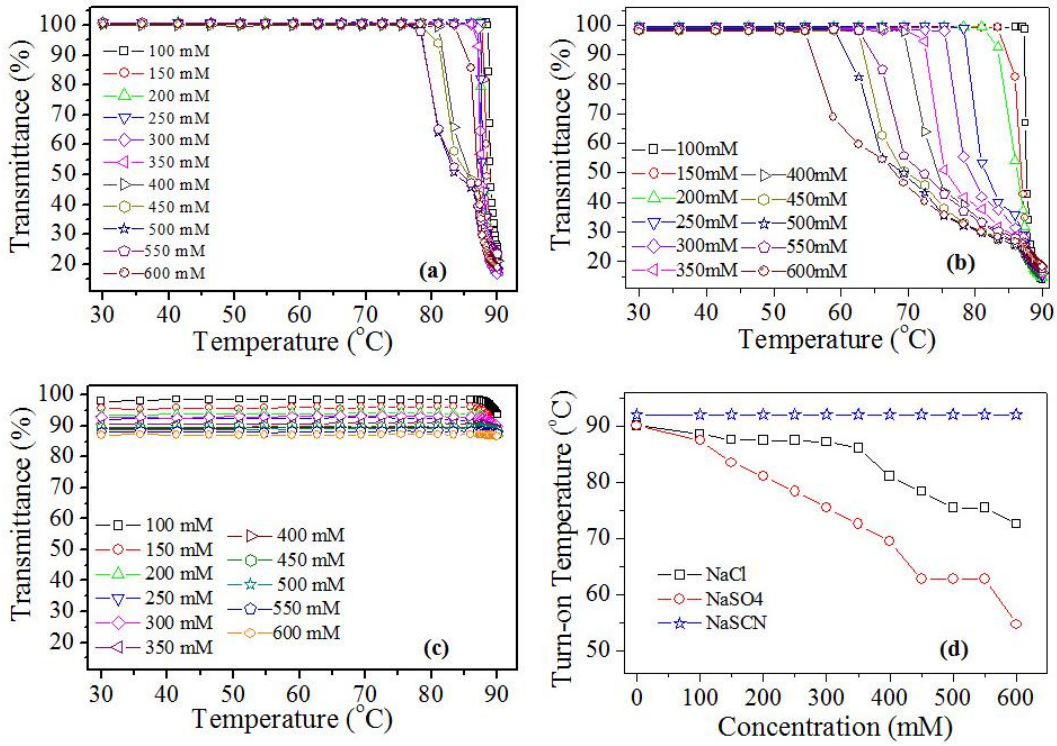

Figure 4.11. *(a) Temperature dependent transmittance of amphiphile **1** with various concentration of NaCl (a), Na_2SO_4 (b) and NaSCN(c). (d) Turn-on temperature at various concentrations of NaSCN, NaCl and Na_2SO_4.*

The 'turn-on temperature' for Na_2SO_4, NaCl and NaSCN is plotted against concentration (see figure 4.11d). From the plot it is evident that with increase in the concentration of the SO_4^{2-}anion from 100 mM to 600 mM the onset of the cloud point (LCST) of the amphiphile decreases from 90 ^oC to 50 ^oC. Thus, the LCST changes by 40 ^oC in presence of SO_4^{2-}anion. On the other hand, when the concentration of Cl^- anion was increased from 100 mM to 600 mM the LCST of the amphiphile changed only by 15 ^oC while in the presence of SCN^- anion does not lead to any change in the LCST value of PDP-PEG 750 (see figure 4.11d). In other words, the LCST value of the amphiphile can not be measured in presence of SCN^- anion as it is a chaotrope which leads to increase in the LCST value. And as the

LCST of the amphiphile was found to be 92 ^{o}C, further increase in the LCST value in presence of SCN^- anion will cross the boiling point of the water. On the other hand, the SO_4^{2-}anion showed higher salting out compared to Cl^- ions. This indicates that amphiphile **1** has less affinity towards Cl^- anion. At very high concentration (above 500 mM), large amount of precipitation occurred and the error became very high. This is one of the main reasons that the Hofmeister effect could not be studied for more than 600 mM salt concentration. The lowering of the LCST from 90 ^{o}C to 55 ^{o}C in presence of the sulphate ion was attributed to the binding of anions towards the amide and PEG-chains which altered the hydration shell in the micellar assemblies. The reduction in the hydration induces the precipitation of the PEG chains on the periphery of the nano-particulate assemblies which results in the turbidity. During precipitation, many nano-particles come together as a result of nucleation followed by growth. This process is evident from the DLS (figure 4.8) and HR-TEM image as shown in figure 4.9. This experiment confirmed that the newly designed thermo-responsive amphiphile **1** showed binding towards anions and followed the Hofmeister series.

4.3.6. ATP Binding

Biological anions such as adenosine triphosphate (ATP) and its precursors ADP (adenosine diphosphate), AMP (adenosine monophosphate) and inorganic phosphate (Pi) were chosen to test the binding abilities of the thermo-responsive nano-scaffold. Under physiological conditions, ATP ecto-nuclotidase hydrolyzes the ATP into ADP and Pi with release of 30.5 kJ/mole of energy which is further utilized for several biological processes (see figure 4.3c). The amphiphile **1** was subjected to optical transmittance measurement with variable concentration of nucleotides. The plot of % transmittance obtained in presence of ATP in heating and cooling cycle is shown in figure 4.12a and 4.12b, respectively. From the heating cycle (see figure 4.12a), it is evident that with increase in concentration of ATP the LCST of the nano-particulate assembly significantly reduced. This is attributed to the tendency of ATP to alter the hydration shell at the periphery of the nanoparticle which results in the

precipitation of PEG chains (as similar to SO_4^{2-} ions). In the subsequent cooling cycle (see figure 4.12b), the amphiphile+ ATP complex showed slow disassembly process and the complex was stable up to 42-44 °C at the higher concentration of ATP. The reason for this stable assembly is hydrophobic interaction as well as π-π staking between the aromatic units of the amphiphile and tha ATP molecule. The formation of this stable assembly implies that the large accumulation of ATP at the cancer tissue could retain the amphiphile **1**+ATP complex in stable form. Similarly, optical transmittance of amphiphile **1** was recorded in presence of ATP precursors also i.e. ADP, AMP and inorganic phosphate (Pi).

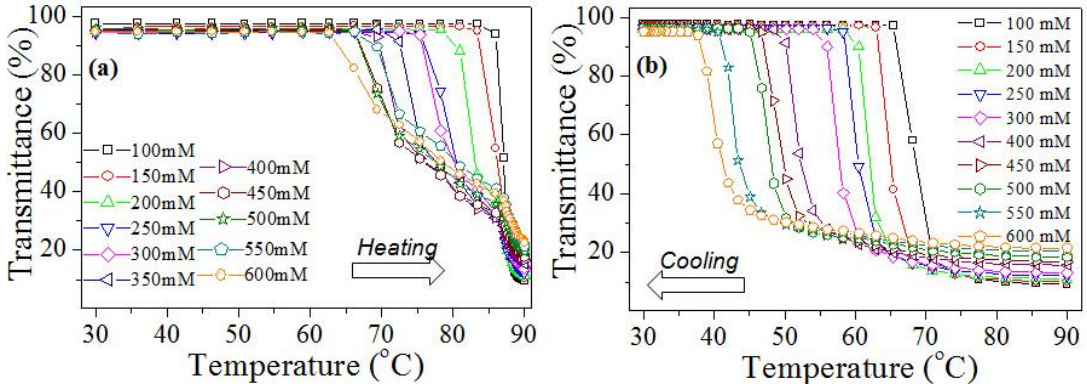

Figure 4.12. *Temperature dependent optical transmittance of amphiphile **1** in water at various concentration of ATP in the heating (a) and (b) cooling cycle.*

The plot of % transmittance obtained in presence of Pi in corresponding heating and cooling cycle are shown in figure 4.13a and 4.13b, respectively. From the heating cycle data (figure 4.13a), it is evident that the LCST of amphiphile **1** decreases from 90 °C to 70 °C with the increase in the concentration of inorganic phosphate anion from 100 mM to 600 mM. Thus, LCST of amphiphile **1** gets lower down by 20 °C. Further, upon comparing the heating and cooling cycle data one can deduce that both heating and cooling process do not follow the same kinetic path.On the other hand, the LCST of the amphiphile **1** changes only by 15 °C with increase in the concentration of ADP from 100 mM to 600 mM (see figure 4.13c), thereby indicating that amphiphile **1** has low affinity towards ADP. Likewise, upon increasing the concentration of AMP from 100 mM to 600 mM the LCST of the

amphiphile **1** changes by only 5 °C(see figure 4.13d). Therefore, presence of AMP does not lead to remarkable changes in the LCST of the amphiphile **1**. Therefore, among all the nucleotides ATP had more pronounced effect as compared to ADP, AMP and Pi.

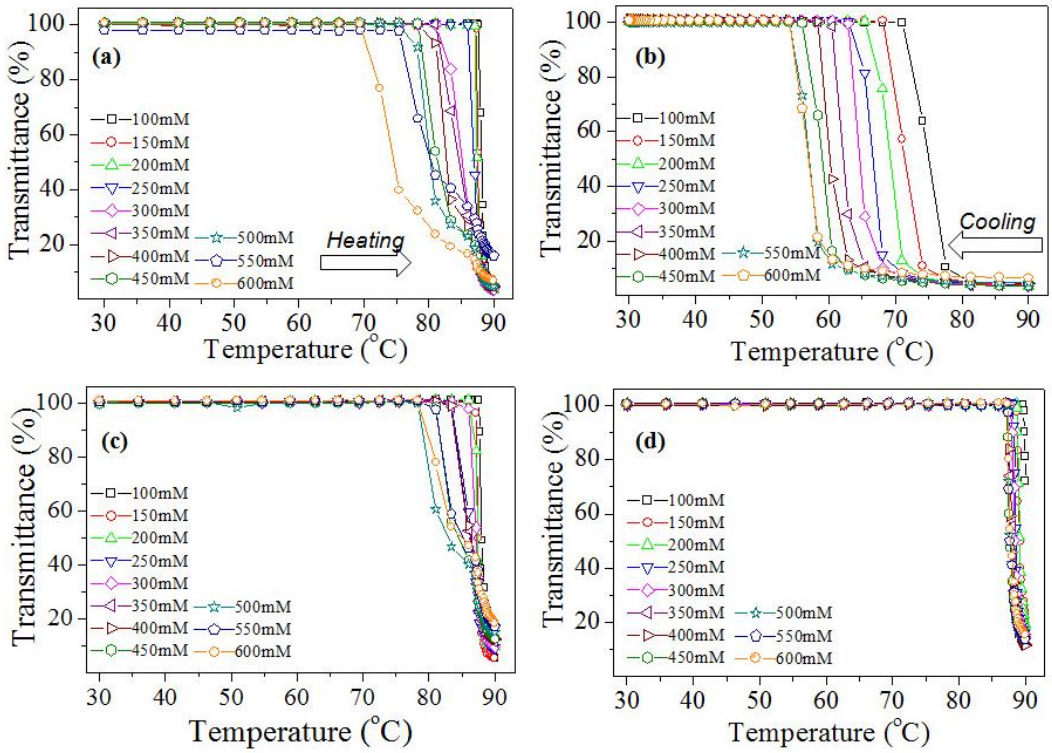

Figure 4.13. *Temperature dependent optical transmittance of amphiphile **1** in water at various concentration of Pi in the heating (a) and (b) cooling cycle. %Transmittance of amphiphile **1**(10^{-4} M) at various concentrations of Adenosine diphosphate (ADP) (c) and Adenosine monophosphate (AMP)(d).*

The ATP binding studies was further subjected to variable temperature dynamic light scattering (DLS) measurement for fixed concentrations of ATP (300 mM) and scaffold (see figure 4.14a and 4.14b). The hydrodynamic diameter from the heating and cooling cycle was plotted against temperature and is shown in figure 4.14c. From the heating cycle, it is evident that the size of the aggregates increased gradually from 300 nm to 1.7 μm with the increase in temperature. The increase in size is attributed to the combination of ATP encapsulation as well as aggregation of nanoparticles at higher temperature. On the other hand, in the cooling cycle the size

of the aggregates did not change much and retained the size in the micrometer range. This indicates that the complex formation between the ATP and nanoparticle produced larger size aggregates in the heating cycle; however, they did not dis-assemble into its individual nano-particle + ATP in the subsequent cooling. This implies that once the nanoparticles bind to ATP, it would not disassociate or release the ATP molecule immediately (see figure 4.5b). It is also important to note that the scaffold alone did not show any larger change in the size in the heating/cooling cycles (see figure 4.8b and 4.8c); thus, the non-occurrence of dis-assembly observed

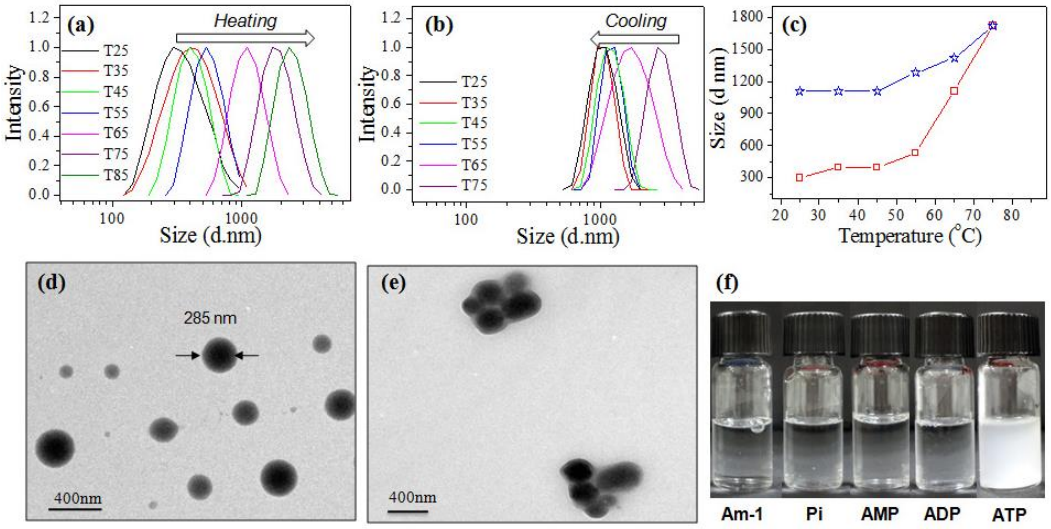

in figure 4.14a to 4.14c are corresponding to the formation of stable ATP+ scaffold.

Figure 4.14. *Temperature dependent DLS histogram of amphiphile **1** in water in presence of adenosine triphosphate (ATP) (300 mM) in the heating cycle(a) and cooling cycle(b). (c) Plot of hydrodynamic diameter against temperature in the heating and cooling cycles. HR-TEM image of ATP-amphiphile **1** complex in water below LCST (d) and above LCST (e). (f) Photograph of amphiphile **1** with ATP AMP, ADP and Pi in water at 45 °C temperature. The concentration of amphiphile **1** is 10^{-4}M and the concentrations of analytes are 300 mM.*

Further, the aggregation phenomenon of the nanoparticle in presence of ATP was validated by subjecting the scaffold+ATP complex to HR-TEM analysis. The HR-TEM images of the nano-aggregates showed the scaffold + ATP complex as individual nanoparticle below LCST (see figure 4.14d). Above LCST, the nanoparticles were assembled together to produce micro-meter size aggregates (see

figure 4.14e). This morphological assembly was further evident from the observation in the % transmittance and DLS (see figure 4.14a and 4.14b). The photographs of vials containing scaffold with ATP, ADP, AMP and Pi at 45 °C are shown in figure 4.14f. Only the ATP+ scaffold complex showed the turbidity at 45 °C indicating that nanoparticle assembly has preferential binding towards ATP compared to other nucleotides.

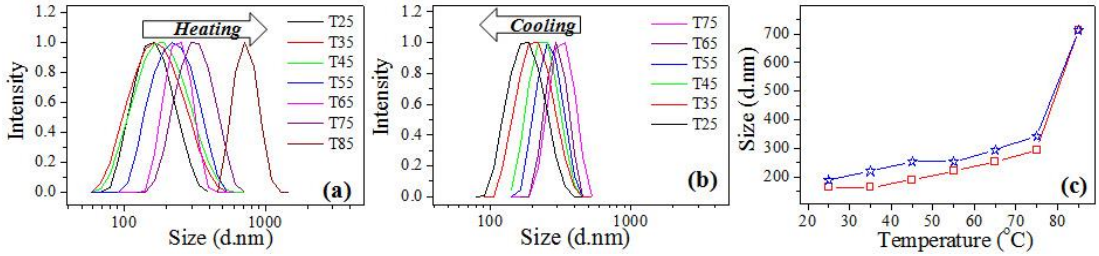

Figure 4.15. *Temperature dependent DLS data of amphiphile* ***1****(10^{-4} M) complexed with Pi (300 mM) (a) heating cycle (b) cooling cycle. (c)Plot of hydrodynamic diameter of amphiphile* ***1*** *against temperature obtained from heating and cooling cycle of Pi.*

This is further supported by variable temperature DLS analysis of scaffold in presence of Pi .The plot of hydrodynamic diameter ofamphiphile **1** in presence of Pi (300mM) obtained at various temperatures in heating and cooling cycle is shown in figure 4.15a and 4.15b, respectively. The size of the aggregates increases from 250 nm to 750 nm upon heating (see figure 4.15a) while in the cooling cycle (see figure 4.15b) it completely reverts back to its original size. This suggests that the complex formed between the scaffold and Pi is not stable unlike its ATP complex. ADP and AMP did not show any remarkable changes in the LCST of the nanoparticle (see figure 4.13c and 4.13d). These control experiments confirmed that thermo-responsive nanoparticle has preferential binding towards ATP.

The unique characteristics of present thermo-responsive nanoparticle of undergoing complexation with ATP exclusively at cancer tissue temperature was further validated by subjecting another thermo-responsive short amphiphile having triethylene glycol (TEG) as hydrophilic unit (in the place of PEG chains), reported in chapter 2 (**PDP-TEG**) and thermo-responsive polymeric scaffold with 6 % of

hydrophilic content in the copolymer structure i.e. **P-6** copolymer, reported in chapter 3 for the anion studies. The structure of both **PDP-TEG** and **P-6** copolymer are given in figure 4.16. The % transmittance plot of **PDP-TEG** in absence and presence of ATP is shown in figure 4.16a and 4.16b, respectively. Similarly, % transmittance plot of **P-6** copolymer in absence and presence of ATP is shown in figure 4.16c and 4.16d, respectively. Both the shorter amphiphile i.e. **PDP-TEG** and the polymeric scaffold **P-6** copolymer has LCST of 42 °C which is much lower compared to the LCST of amphiphile **1** (90 °C) (see figure 4.16aand 4.16c).

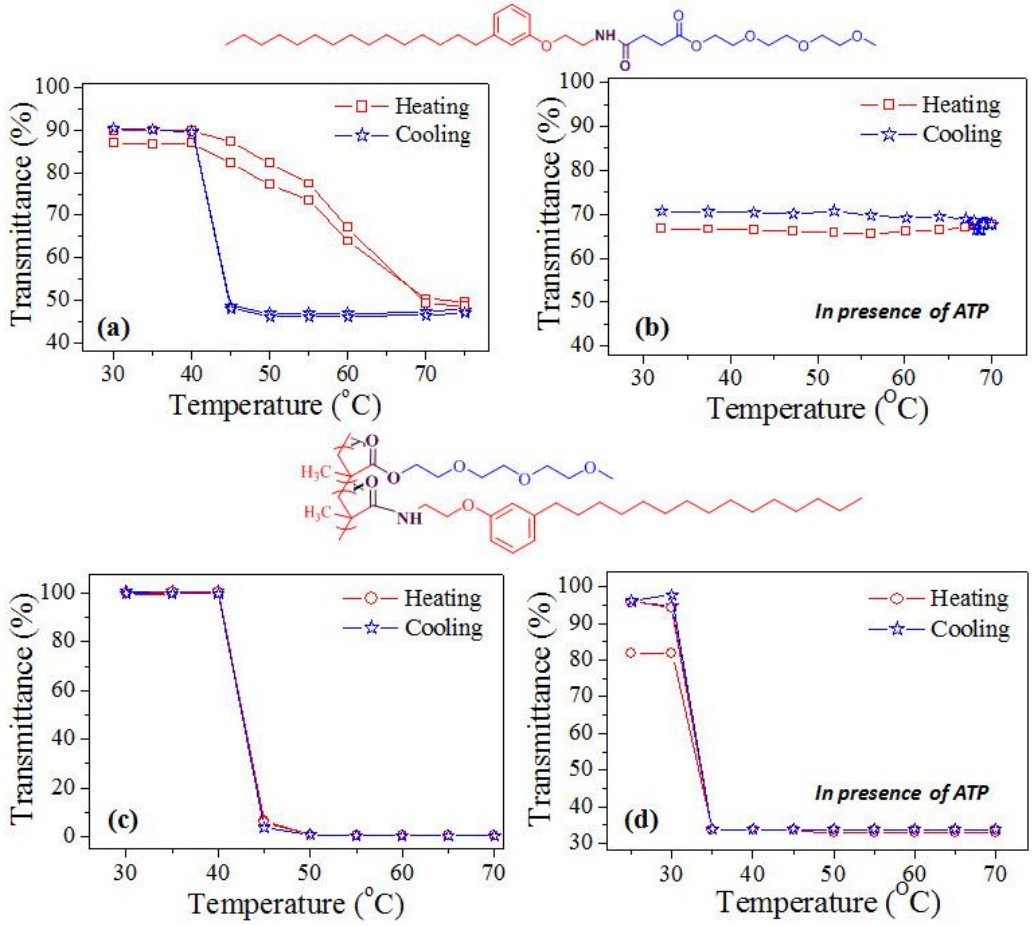

Figure 4.16.*%Transmittance of thermo-responsive diblock having triethylene glycol (PDP-TEG) (a) absence of anions (b) presence of ATP (100mM). %Transmittance of thermo-responsive diblock having 6 % of ethylene glycol in the **P-6** copolymer structure (c) absence of anions (d) presence of ATP (100mM). The plot of **PDP-TEG** and **P-6** copolymer was taken from earlier chapters for comparison purpose.*

This indicates that the super LCST nature of the amphiphile arose from the long PEG-lated chains in the amphiphiles design strategy (see scheme 4.1). Surprisingly, upon binding to the anionsthe short amphiphile **PDP-TEG** lost its LCST behaviors, whereas the LCST of the polymeric scaffold lowers down to 30 °C (below cancer tissue temperature). This clearly supports the structure of the thermo-responsive material is very crucial to study Hofmeister effect towards anions. In the present case, the super LCST amphiphile **1** provided appropriate hydrophilic and hydrophobic balance for the above purpose. Recently, Cremer and co-workers had reported that the LCST of the PNIPAM and elastic-like peptide decreased upon complexation with the anions by 10-11 ° in presence of SO_4^{2-}anion.[18]In present case, the LCST of amphiphile **1** decreased by 35 ^oC upon binding to SO_4^{2-}anion. It suggested that the amphiphile **1** experienced Hofmeister effect as equivalent to that of high molecular weight thermo-responsive PNIPAM. Thus, the amphiphile **1** has appropriate molecular design with super LCST characteristics for binding or sensing anions in a larger temperature window from 90 °C to 30°C.

In order to shed more light on the selectivity of the amphiphile **1** towards ATP, the difference in turn-on and turn-off turbidity temperature of scaffold in presence of ATP, ADP, AMP and Pi were plotted and are shown in figure 4.17a and 4.17b. The plot of turn-on temperature as a function of concentration reveals that affinity of the amphiphile **1** was significantly more towards ATP as compared to ADP, AMP and Pi. The 'turn-off temperature' plot revealed that ATP could bring down the scaffold LCST to 45 ^oC. On the other hand in case of Pi it comes only up to 70 ^oC. This suggests that the nanoparticle is efficient to bind ATP over its precursors. The reason for the efficient binding of ATP towards the amphiphile was attributed to the occupation of ATP in the micellar scaffold. ATP has three phosphate anionic groups which are hydrophilic and well separated from the hydrophobic adenosine+sugar units (see figure 4.3c).

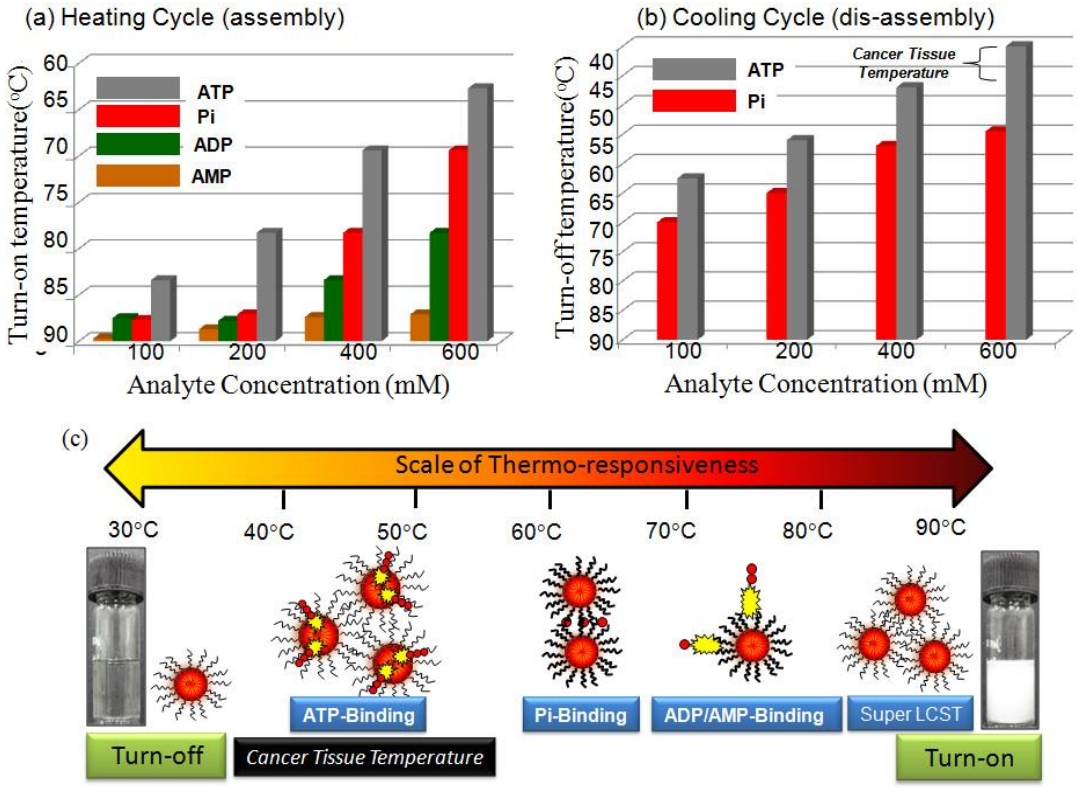

Figure 4.17. *(a) Plot of Turn-on temperature of amphiphile* ***1*** *as a function of concentration of ATP, ADP, AMP and Pi. (b) Plot of Turn-off temperature of amphiphile* ***1*** *as a function of concentration of ATP and Pi. (c) Temperature-sensing scale of amphiphile* ***1*** *for the ATP, ADP, AMP and Pi.*

Recently, Wang *et al.*[67] and Liu et al.[68] had independently reported the ATP anion binding to the polymer nanoparticle or liposomes were found to be driven by host and guest interactions through hydrophobic inner core of the nano-assemblies. Further, it was found that ADP and AMP were found to lack perfect guest geometry to occupy the hydrophobic host pocket.[48] Thus, in the present case, during the complexation with the amphiphile the ATP hydrophobic part could penetrate into the hydrophobic core of the micellar nanoparticle through like-like interactions. These geometrical arrangements provide better contact between the ATP hydrophilic phosphate groups towards the amide and PEG chains in the micellar exterior shell (see figure 4.17c). This arrangement gives the ATP aromatic core in the hydrophobic pocket of the nano-particle and the anion projecting towards the amide and PEG chains to maximize the Hofmeister effect. As a result, ATP anion induced maximum

influence on the hydration of the amphiphilic scaffold through Hofmeister effect that reduces the LCST of the ATP+ scaffold complex. However, in the case of inorganic Pi, the inorganic anion could easy diffuse compared to AMP and ADP in hydroshell of PEG-lated chains at the nanoparticle exterior to induce Hofmeister effect significantly.

Further to estimate the detection dynamic range of ATP binding, the concentration of amphiphile was fixed as 10^{-4} M and the ATP concentration was varied from 10mM to 100 mM (see figure 4.18). The plots showed that the change in the LCST phenomena could be detected in transmittance mode at minimum [ATP] = 100 mM. This mechanism is further supported by the large increase in the size of the amphiphilic scaffold in the nascent form compared to that of ATP+ scaffold. For example, the sizes of the scaffold doubled from 140 nm to 300 nm upon binding to ATP at 25 °C (see figure 4.8b and 4.14a for 25 °C). This large increase in the size in the scaffold is attributed to the encapsulation of ATP in the micellar core of the amphiphilic self-assembly. On the other hand ADP and AMP have inadequate hydrophilic and hydrophobic balance. Thus, the shape specific encapsulation towards the micellar nanoparticle is not effective to show Hofmeister effect.

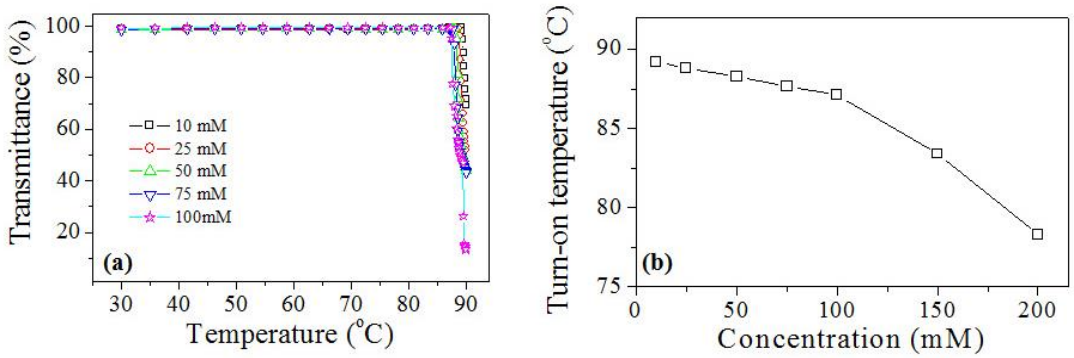

Figure 4.18. *(a) Plot of % transmittance of amphiphile* ***1*** *in presence of 10mM to 100 mMof ATP. (b) Plot of turn-on temperature of amphiphile* ***1*** *in presence of various concentration of ATP.*

Inorganic phosphates affect the scaffold like any other kosmotropes (like sulphate anions) and this was supported by no change in the size of the micellar

assemblies after binding to Pi (see figure 4.15c). Hence, the ATP complexation towards the nano-particle assembly is natural choice for maximizing the Hofmeister effect though host-guest interactions. The temperature ranges at which ATP, ADP, AMP and Pi are active on the amphiphilic scaffold are shown in the scale with their possible self-assembled structures in figure 4.17c.

4.3.7. Cytotoxicity Studies of Amphiphile 1

The cyctotoxicity of the super LCST amphiphile **1** towards the cancer tissue was checked in Hela cell lines at 37 ° C using MTT assay. The cells were treated for 12 and 24 h and the data are shown in figure 4.19. The cells showed more than 85 % cell viability below 1 μg/mL. At higher amphiphile concentration (5 and 10 μg/mL), the cells showed 75 % viability. For most of the drug delivery research, the polymer or scaffold concentration are typically used < 1.0 μg/mL; thus, the new renewable resource based LCST amphiphile may be very useful biomaterials.

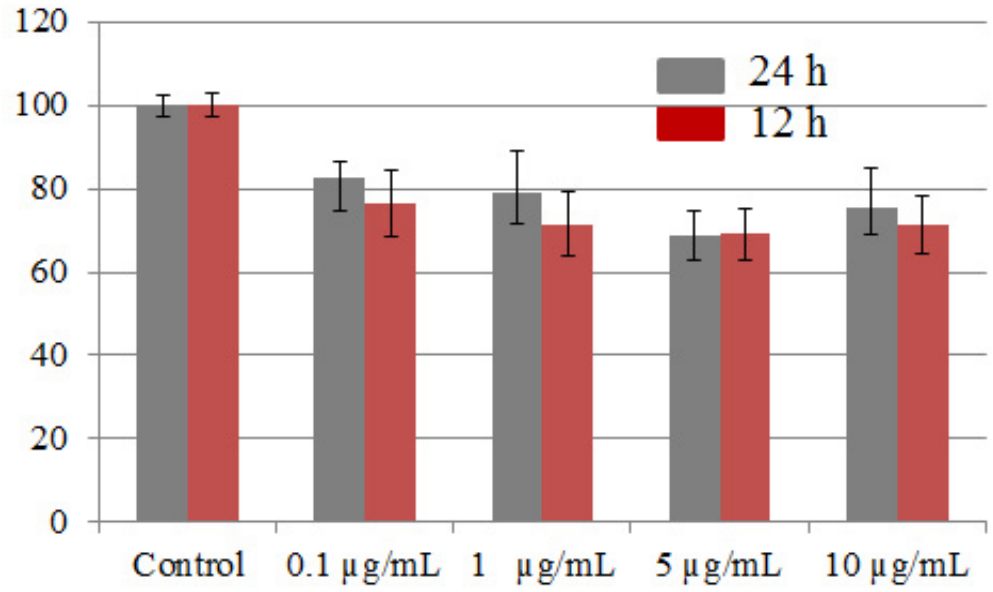

Figure 4.19. *Cytotoxicity data of amphiphile **1** at various concentrations in MTT assay after24 and 12h.*

4.3.8. Isothermal Calorimetry and Binding Constants

Isothermal titration calorimetry (ITC) technique directly measures the heat of the complexation (enthalpy, ΔH), the stoichiometry of substrate binding (n), and the binding constant (Ka). The binding efficiency of ATP and its close interfering anion Pi (based on figure 4.17b) with the scaffold was further evaluated by ITC and the data are provided in figure 4.20. The titration of ATP with the nanoparticle displayed endothermic curves (see figure 4.20a) while exothermic curves were obtained for titration of phosphate anion (see figure 4.20b). Further, the binding constant for the ATP and phosphate anion complexation with the nanoparticle was found to be 2230 M^{-1} and 719 M^{-1}, respectively. The three times higher binding constant for the ATP towards the scaffold indicate that the ATP binding was stronger than inorganic phosphate anion.

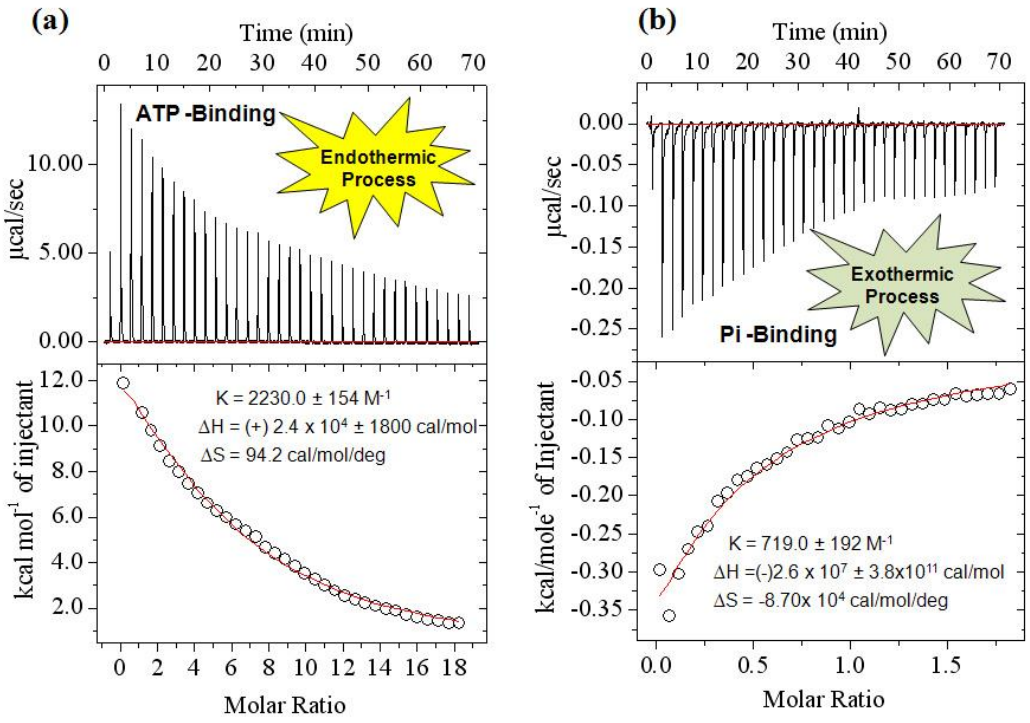

Figure 4.20. *(a) Isothermal calorimetric titration curves for the binding of amphiphile* ***1*** *(0.1 mM) with ATP (10 mM) at 25 °C. (b) Calorimetric curves for the binding of amphiphile* ***1*** *(1 mM) with Pi (10 mM) at 25 °C.*

Earlier ITC reports for ATP binding to poly (dC) (double stranded DNA made up of cytosine)[69] and 3-phophoglycerate kinase[70] showed binding constants of 2.45 x 10^4 M^{-1} and 3.5x 10^3 M^{-1}, respectively. The binding constant of ATP-nanoparticle complex in the present case has value similar to that of above examples. Hence, it can be said that the affinity of thermo-responsive nanoparticles towards ATP was very good as similar to that of DNA and proteins. Further, the ATP binding to the amphiphilic scaffold is endothermic in nature; thus binding of ATP to the amphiphile **1** upon heating is thermodynamically more favoured as compared to Pi. In other words, the main driving force for ATP binding is entropic gain due to release of water molecules from the vicinity of the aggregates. Therefore, it was natural choice for thermodynamically binding to the high temperature environment of the cancer tissue compared to normal tissues. Additionally, the amphiphile nano-particle has encapsulation capabilities for hydrophobic dye and this concept may be expanded to load and deliver water insoluble anticancer drugs. This may provide additional advantage of simultaneous binding of ATP and also delivering the drugs to the cancer tissue temperature. Based, on above studies, it may be summarized that the newly developed thermo-responsive amphiphilic nanoparticle could be useful for targeting the ATP as trigger and also as carrier for drugs to the cancer tissue.

4.4. Conclusion

In conclusion, a new thermo-responsive molecular assembly was developed to detect and bind to ATP in aqueous medium. The amphiphilic molecule was designed with appropriate hydrophilic polyethylene glycol (PEG 750) unit and renewable resource 3-pentadecylphenol hydrophobic part to produce the *super LCST amphiphile* for more than 90 °C in water. The amphiphile **1** self-assembled as 150 nm micellar nano-particles in water at ambient conditions and its hydrophobic pocket was capable of loading water insoluble dyes like Nile red. Dynamic light scattering techniques, electron and atomic force microscopes confirmed that the self-assembled structures exist in the form of spherical nano-particles. The amphiphile **1** showed selective phase separation for anions such as sulphates and chlorides (salting-out) following the Hofmeister series. Hofmeister effect of the amphiphile **1** was explored for binding to anionic biomolecules ATP and its precursors ADP, AMP and Pi. The amphiphile **1** showed high preferential binding towards ATP over its precursors ADP, AMP and Pi. Isothermal calorimetric experiments further confirmed the ATP binding and it estimated three times higher binding constant for ATP towards the amphiphile **1** as compared to Pi. Endothermic nature of the ATP binding to amphiphile **1** could provide advantages for selective binding at cancer tissue temperature (42-44 °C) which is higher as compared to normal tissues (37 °C). Therefore, the present thermo-responsive scaffold has high affinity for binding to ATP.

4.5. References

1. Kunz, W.; Henle, J.; Ninham, B.W. *Curr. Opin. Collo.Int.Sci.* **2004**, 10, 19-37.
2. Crevenna, A.H.; Naredi-Rainer, N.; Lamb, D. C.; Wedlich-Soldner, R.; Dzubiella, J. *Biophys. J.***2012**, 102, 907-915.
3. Zhang, Y.; Cremer, P. S. *Proc. Natl. Acad. Sci.* ***2009***, 106, 15249-15253.
4. Okur, H. I.; Kherb, J.; Cremer, P. S. *J. Am. Chem. Soc.* **2013**, 135, 5062-5067.
5. Kunz, W. *Curr. Opin. Collo.Int.Sci.* **2010**, 15, 34-39.
6. Bostrom, M.; Williams, D. R. M.; Ninham, B. W. *Biophys. J.***2003**, 85, 686-694.
7. Nostro, P. L.; Ninham, B. W. *Chem. Rev.* **2012**, 112, 2286-2322.
8. Bostrom, M.; Williams, D. R. M.; Ninham, B. W. *Curr. Opin. Collo.Int.Sci.* **2004**, 9, 48-52.
9. Zhang, Y.; Cremer, P. S. *Annu. Rev. Phys. Chem.* **2010**, 61, 63-83.
10. Zhang, Y.; Cremer, P. S. *Curr. Opin. Chem. Biol.* **2006**, 10, 658-663.
11. Parsons, D. F.; Bostrom, M.; Nostro, P. L.; Ninham, B. W. *Phys. Chem. Chem. Phys.* **2011**, 13, 12352-12367.
12. Nostro, P. L.; Ninham, B. W.; Milani, S. A.; Nostro, L.; Pesavento, G.; Baglioni, P. *Biophys. Chem.* **2006**, 124, 208-213.
13. Bostrom, M.; Williams, D. R. M.; Ninham, B. W. *Phys.Rev. Lett.* **2001**, 87, 168103.
14. Xie, W. J.; Gao, Y. Q. *J. Phys. Chem. Lett.* **2013,**4, 4247-4252.
15. Salis, A.; Ninham, B. W. *Chem. Soc. Rev.* **2014**, 43, 7358-7377.
16. Gurau, M.C.; Lim, S.-M.; Castellana, E. T.; Albertorio, F.; Kataoka, S.; Cremer, P. S. *J. Am. Chem. Soc.* **2004**, 126, 10522-10523.
17. Chen, X.; Yang, T.; Kataoka, S.; Cremer, P. S. J. *Am. Chem. Soc.* **2007**, 129, 12272-12279.
18. Zhang, Y.; Furyk, S.; Bergbreiter, D. E.; Cremer, P. S. *J. Am. Chem. Soc.* **2005**, 127, 14505-14510.
19. Thormann, E. *RSC Adv.* **2012**, 2, 8297-8305.
20. Freitag, R.; Garret-Flaudy, F. *Langmuir* **2002**, 18, 3434-3440.

21. Zhang, Y.; Furyk, S.; Sagle, L. B.; Cho, Y.; Bergbreiter, D. E.; Cremer, P. S. *J. Phys. Chem. C* **2007**, 111, 8916-8924.

22. Cho, Y.; Zhang, Y.; Christensen, T.; Sagle, L. B.; Chilkoti, A.; Cremer, P. S. *J. Phys. Chem. B* **2008**, 112, 13765-13771.

23. Kherb, J.; Flores, S. C.; Cremer, P. S. *J. Phys. Chem. B* **2012**, 116, 7389-7397.

24. Rembert, K. B.; Paterova, J.; Heyda, J.; Hilty, C.; Jungwirth, P.; Cremer, P. S. *J. Am. Chem. Soc.* **2012**, 134, 10039-10046.

25.Wei, H.; Cheng, S.-X.; Zhang, X.-Z.; Zhuo, R.-X. *Prog. Polym. Sci.* **2009**, 34, 893-910.

26. Pinna, M. C.; Bauduin, P.; Touraud, D.; Monduzzi, M.; Ninham, B. W.; Kunz, W. *J Phys. Chem. B* **2005**, 109, 16511-16514.

27. Pinna, M. C.; Salis, A.; Monduzzi, M.; Nninham, B. W. *J Phys. Chem. B* **2005**, 109, 5406-5408.

28. Bauduin, P.; Nohmie, F.; Touraud, D.; Neueder, R.; Kunz, W.; Ninham, B. W. *J Mol. Liq* **2006**, 123, 14-19.

29. Vrbka, F.; Jungwirth, P.; Bauduin, P.; Touraud, D.; Kunz, W. *J. Phys. Chem. B***2006**, 110, 7036-7043.

30. Paterova, J.; Rembert, K. B.; Heyda, J.; Kurra, Y.; Okur, H. I.; Liu, W. R. Hilty, C.; Cremer, P. S.; Jungwirth, P. *J. Phys. Chem. B***2013**,117, 8150-8158.

31. Magnusson, J. P.; Khan, A.; Pasparakis, G.; Saeed, A. O.; Wang, W.; Alexander, C. *J. Am. Chem. Soc.* **2008**, 130, 10852-10853.

32. Swann. J. M. G.; Bras, W.; Topham, P. D.; Howse, J. R.; Ryan, A. J. *Langmuir* **2010**, 26, 10191-10197.

33. Li, L.; Ryu, J.-H.; Thayumanavan, S. *Langmuir* **2013**, 29, 50-55.

34. Gibb, C. L. D.; Gibb, B. C. *J. Am. Chem. Soc.* **2011**,133, 7344-7347.

35. Qiu, M.; Long, S.; Li, B.; Yan, L.; Xie, W.; Niu, Y.; Wang, X.; Guo, Q.; Xia, A. *J. Phys. Chem. C* **2013**,117, 21870-21878.

36. Tarafdar, P. K.; Reddy, S. T.; Swamy, M. J. *J. Phys. Chem. B* **2013**, 117, 9900-9909.

37. Manet, S.; Karpichev, Y.; Dedovets, D.; Oda, R. *Langmuir* **2013**, 29, 3518-3526.

38. Deyerle, B. A.; Zhang, Y. *Langmuir* **2011**, 27, 9203-9210.

39. Schwiebert, E. M.; Zsembery, A. *Biochim. Biophys. Acta* **2003**,1615, 7-32.

40. Khakh, B. S.; Burnstock, G. *Sci. Am.* **2009**, 301, 84-92.

41. Burnstock, G. *Trends Pharmacol Sci.* **2006**, 27, 166-176.

42. Junger, W. G. *Nat. rev. Immunol.* **2011**, 11, 201-212.

43. Ohta, A.; Gorelik, E.; Prasad, S. J.; Ronchese, F.; Lukashev, D.; Wong, M. K. K.; Huang, X.; Caldwell, S.; Liu, K.; Smith, P.; Chen, J.-F.; Jackson, E. K.; Apasov, S.; Abrams, S.; Sitkovsky, M. *Proc. Natl. Acad. Sci.* **2006**, 103, 13132-13137.

44. Pellagatti, P.; Raffaghello, L.; Bianchi, G.; Piccardi, F.; Pistoia, V.; Virgillio, F. D. *PloS ONE* **2008**, 3, e2599.

45. Zheng, L.M.; Ztchlinsky, A.; Liu, C.-C.; Ojcius, D. M.; Young, J. D.-E. *J. Cell Bio.* **1991**, 112, 279-288.

46. Wen, L. T.; Knowles, A. L. *Br.J. Pharmacol.* **2003**,140, 1009-1018.

47. Virgillio, F. D. *Cancer. Res.* **2012**, 72, 5441-5447.

48. Neelakandan, P. P.; Hariharan, M.; Ramaiah, D. *Org. Lett.*, **2005**, 7, 5765-5768.

49. Jose, D. A.; Mishra, S.; Ghosh, A.; Shrivastav, A.; Mishra, S. K.; Das, A. *Org. Lett.*, **2007**, 9, 1979-1982.

50. Kaur, J.; Singh, P. *Chem. Commun.* **2011**, 47, 4472-4474.

51. Jeon, H.; Lee, S.; Li, Y.; Park, S.; Yoon, J. *J.Mater. Chem.***2012**, 22, 3795-3799.

52. Wang, H.; Chan, W.-H. *Org. Bimol. Chem.* **2008**, 6, 162-168.

53. Moro, A. J.; Cywinski, P. J.; Korsten, S.; Mohr, G. J. *Chem. Comm.* **2010**, 46, 1085-1087.

54. Zhou, Y.; Xu, Z.; Yoon, J. *Chem. Soc. Rev.*,**2011**, 40, 2222-2235.

55. Wang. Y.; Wang, Y.; Liu, B. *Nanotechnology***2008**, 19,415605.

56. Zhou, X.; Song, S.; Zhang, J.; Pan, D.; Wang, L.; Fan, C. *J. Am. Chem. Soc.*, **2007**, 129, 1042-1043.

57. Ge, Z.; Liu, S. *Chem. Soc. Rev.***2013**, 42, 7289 – 7325.

58. Issels, R. D. *Eur. J. Cancer***2008**, 44, 2546-2554.

59. Kong, G.; Barun, R. D; Dewhirst, M. W. *Cancer Res.* **2000**, 60, 4440-4445.

60. Fang, J.; Nakamura, H.; Maeda, H. *Adv. Drug Delivery. Rev.* **2011**,63, 136-151.

61. Maruyama, K. *Adv. Drug Delivery. Rev.* **2011**,63, 161-169.

62. Pramod, P. S.; Katamura, C.; Chapaker, S.; Balasubramaniam, N.; Jayakannan, M. *Biomacromolecules***2012**, 13, 3627-3640

63. Pramod, P. S.; Shah, R. Chapaker, S.; Balasubramanian, N.; Jayakannan, M. *Nanoscale***2014**, 6, 11841-11855.

64. Sridhar, U.; Pramod, P. S.; Jayakannan, M.*RSC Advances***2013,** 3, 21237 – 21241.

65. Kashyap, S.; Jayakannan, M. *J. Phys. Chem. B***2012**, 116, 9820-9831

66. Kashyap, S.; Jayakannan, M. *J. Mater. Chem. B* **2014**, 2, 4142-4152.

67. Wang, C.; Chen, Q.; Wang, Z.; Wang, X. *Angew. Chem. Int. Ed.* **2010**, 49, 8612-8615.

68. Liu, J.; Morikawa, M.-a.; Kimizuka, N. *J. Am. Chem. Soc.* **2011**, 133, 17370-17374.

69. Borgan, A. P.; Widger, W. R.; Bensadek, D.; Garcia, I. R; Gaskell, S. J.; Kohn, H. *J. Am. Chem. Soc.* **2005**, 127, 2741-2751.

70. Flachner, B.; Kovari, Z.; Varga, A.; Gugolya, Z; Vonderviszt, F.; Szabo, G. N.; Vas, M. *Biochemistry* **2004**, 473, 3436-3449.

Chapter 5

Amphiphilic Amphiphiles Sorting into Multivesicular Bodies and their Encapsulation Capabilities

Chapter 5

Amphiphilic Amphiphiles Sorting into Multivesicular Bodies and Their Encapsulation Capabilities

Synthetic macromolecular amphiphiles sorting into multivesicular bodies (MVB)s and their fluorophore encapsulation pathways were reported. Renewable resource based amphiphiles having hydrophobic units and flexible hydrophilic polyethylene glycols (PEG) were custom designed for the above purpose. Single crystal structure was resolved to prove the existence of the strong inter-molecular interactions and the formation of uni-lamellar layer-like self-assemblies. These amphiphilic AB amphiphiles underwent selective vesicular fission either by outward budding or inward invagination to produce small uni-lamellar vesicles (SUV)s or MVBs, respectively. Self-organization parameters such as relative volume (v_e) and reduced area difference (Δa_o) were determined based on theoretical models and very good correlation with the experimental results was established for the synthetic-MVBs. Pyrene was encapsulated to study the mechanistic aspects of the MVB formations. An un-usual non-linear trend was observed in the pyrene dynamic excimer formation with respect to the sorting of diblock membrane into MVBs. Strong inter-molecular interaction was found to be a critical deciding factor in synthetic diblock membranes to facilitate MVBs. The drug loading and delivering capabilities of both MVBs and SUVs was studied under physiological conditions (pH = 7.4, PBS). The DOX release kinetics was further studied in presence of esterase enzyme for determining the susceptibility of ester linkages in both SUVs and MVBs. MVBs showed two step DOX release profile both in absence and presence of esterase enzyme. Thus, the encapsulation capabilities of MVBs were found to be very unique in that the molecules were trapped uniformly throughout the hydrophobic layer of both outer and inner vesicular structures. In a nut-shell, the synthetic amphiphiles based MVBs as a potential vectors for drug delivery was demonstrated.

5.1. Introduction

Molecular self-organization is a powerful tool to assemble molecules or polymer chains in a particular nano or micron sized object under certain conditions and later disassociate into individual components using desired external stimuli such as concentration, pH or temperature.[1] The self-assembled polymer-drug conjugates are typically produced via reversible hydrogen bonding, hydrophilic/hydrophobic or ion- interactions between the small or short chain drug molecules with the larger cavity provided by the polymers.[2] The self-organized polymer-drug form will be administrated inside the cell and upon un-zipping, the drug components will be disassociated from the assembly and released to particular target.[3] The biocompatible polymer components will be easily washed away from the bio-system without inducing toxicity to other living cells (see figure 5.1.).

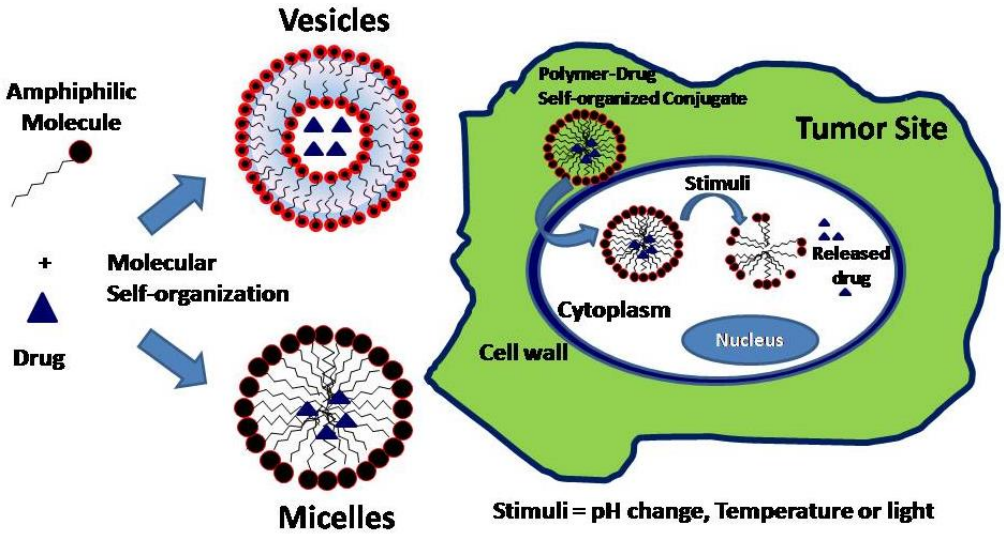

Figure 5.1. *Molecular self-organized approach for controlled drug delivery.*

Since most of the biological processes are associated with; (i) change in the concentration of species either inside or outside the cells, (ii) change in the acidic, neutral or basic environment (stomach and intestine) and (iii) variation in the temperature in a target site (tumor cells and normal cells), the self-assembly is a powerful tool for controlled drug delivery application.[4] Polymeric micelles,[5,6,7] vesicles,[8] liposomes,[9] and nanogels have been developed as drug delivery vehicles.

High molecular weight polymers can significantly improve therapeutic efficacy due to the enhanced permeability and retention effect,[10,11] however, making well-defined molecular architecture for encapsulation of drug delivery is a challenging problem. Additionally, the low loading of active drug within self-assembled systems and inefficient release of drug from the vehicle into the cytoplasm, results in a requirement for new polymer designs. Therefore, designing new self-assembled polymeric carriers is an important and required research for controlled drug delivery in biological systems.

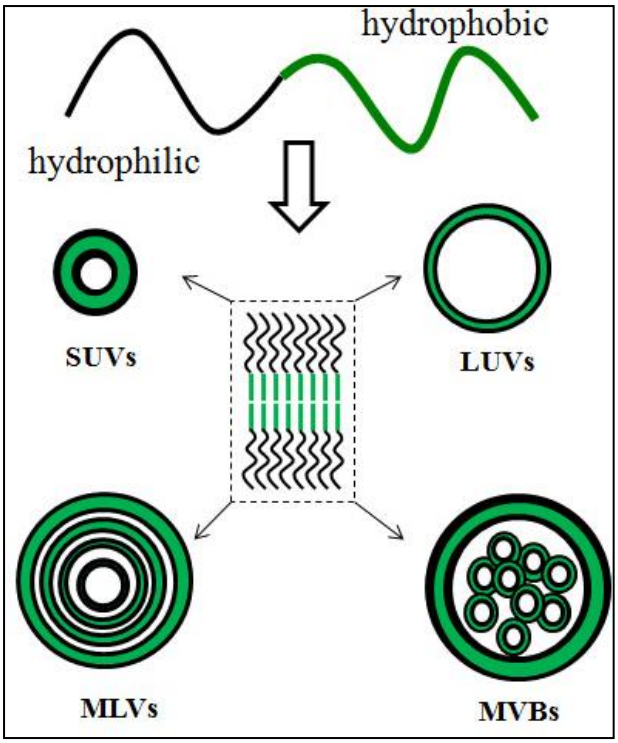

Figure 5.2. *Various self-assembled structure formed by block copolymers.*

Amphiphilic molecules have the tendency to undergo self-organization via hydrophilic or hydrophobic interactions with the solvent molecules in which there are embedded. Both small and polymeric amphiphiles undergo self-organization to form stable nano or micron-sized micelles or vesicles.[12,13] The formation of micelles and vesicles by small molecule amphiphiles consisting of polar head and hydrophobic tail are well understood. However, optimizing the hydrophilicity and types of functional groups (like carboxylic, amides, cationic or anionic) in the

polymer chain and self-organize them in solvents (mostly in water) is a very challenging task. Apart from formation of conventional micelles and vesicles amphiphilic block or graft copolymers can also form could various other self-assembled structures such as small uni-lamellar vesicle (SUVs), large uni-lamellar vesicles (LUVs), multi-lamellar vesicles (MLVs) and multi-vesicular bodies (MVBs) (see figure 5.2).

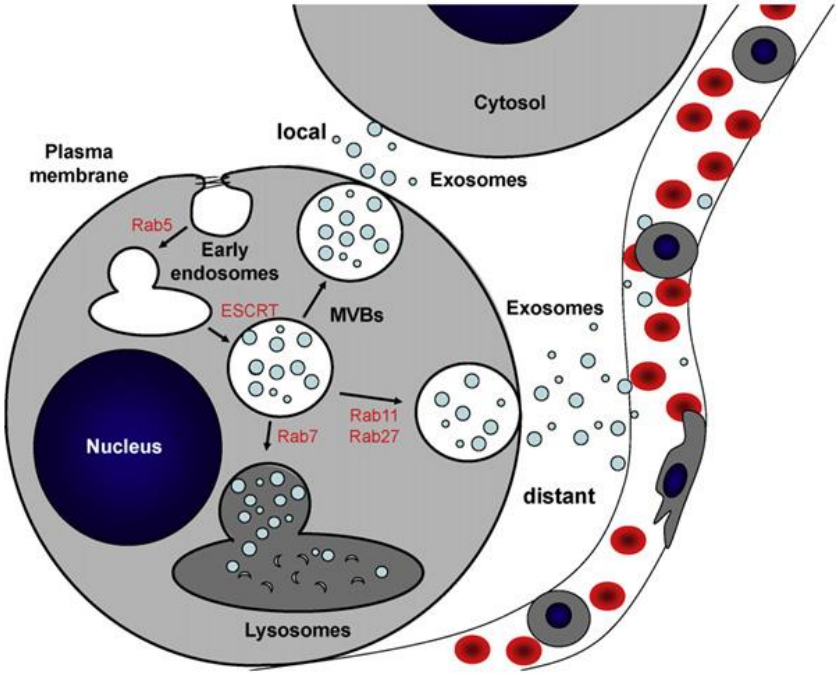

Figure 5.3. *Members of the ESCRT complexes mediate multi-vesicular body (MVB) formation. MVBs can either fuse with lysosomes to degrade their cargo, or with the plasma membrane to release their intraluminal vesicles as exosomes. Exosomes can locally mediate intercellular signaling or at distantsites when secreted into the blood stream (adopted from Ludwig et al. Int. J. Biochem. Cell B,2012, 44, 11-15).*

Among, all the vesicular structures, multivesicular bodies (MVB)s have gained tremendous importance since they are very important key-intermediates in the regulation of several physiological processes under tightly controlled signaling pathways across the biological cell membranes.[14,15] MVBs are formed in the biogenesis of the liposomal organelles in which portions of the diblock membrane invaginate into small intraluminal vesicles (ILVs) and subsequently released into the

lumen[16] (see figure 5.3). MVBs areidentified to play a crucial role as cargo-transport machinery via complicated multi-step process in the functioning of human immunodeficiency virus (HIVs) and down regulation of receptors and transporters in enveloped viruses of plasma membranes.[17,18] Though, the evolution of MVBs *in vivo* is still under debate, recent *in vitro* studies revealed that ubiquitin directed endosomal sorting complex responsible for transport (ESCRT) protein account for these un-usual cell machinery.[19,20] The ILVs produced by the sorting of diblock membrane has unique advantages in that these small internal vesicles were perfectly protected by the sorting membrane; as a result these nano-objects were less susceptible to external stimuli such as pH and temperature, etc.[21] Therefore, MVBs behave as storage vesicles of cargo (drug/gene) which have to be delivered to the internal part of the animal cells. Synthetic macromolecules based vesicular self-assemblies were also reported in single and multi component phospholipids,[22,23] metal ion-amphiphilic ligand interactions,[24] charge-transfer complexes,[25] light-responsive guest-host complexes,[26] dendritic[27] and hyperbranched[28] polymers and so on. Despite significant advances made in producing small uni-lamellar vesicles (SUVs),[29,30,31,32] giant uni-lamellar vesicles (GUVs)[33,34,35] and multi-lamellar vesicles (MLVs)[36,37] in liposome and synthetic macromolecules;[38,39,40,41,42] mimicking of MVBs in synthetic membranes are far from reality. Bio-mimicking of MVBs in synthetic vesicles is an important task[43,44,45,46,47] which could further fuel the creation of complex membrane models and their encapsulation capabilities resembling cell membranes which have potential applications in the chemistry-biology interface.

The present investigation is emphasized on mimicking of multivesicular bodies (MVBs) in bio-inspired synthetic AB diblock membranes. Custom designed renewable resource based amphiphilic AB-amphiphiles formed uni-lamellar structures in water and they subsequently self-organized either as SUVs or MVBs depending upon their hydrophilic content(see figure 5.4). Single crystal structure was resolved for the amphiphilic building blocks to confirm the origin of uni-lamellar packing in the vesicular structures. Further, theoretical calculations were performed

to determine two important structural parameters: reduced volume (ν) and reduced area difference (Δa_0) of the synthetic diblock membrane. A direct correlation between theoretical calculation and experimental results were achieved and it was found that inward invagination and outward budding of diblock membranes exclusively produced MVBs or SUVs, respectively. Additionally, the mechanistic aspect of MVBs formation was studied using pyrene encapsulation in water. The detailed photophysical experiments revealed that the diblock membranes showed unusual non-linear trend in the excimer formation with their self-organization in water. MVB formation was facilitated by the strong inter-molecular interactions in the membrane. The loading and delivery of DOX both in SUVs and MVBs revealed that DOX loaded MVBs were more stable under physiological conditions as compared to SUVs. Also, DOX was released from MVBs in two steps both in absence and in presence of enzyme. However, the release kinetics of DOX was much faster in presence of enzyme than in absence of enzyme.

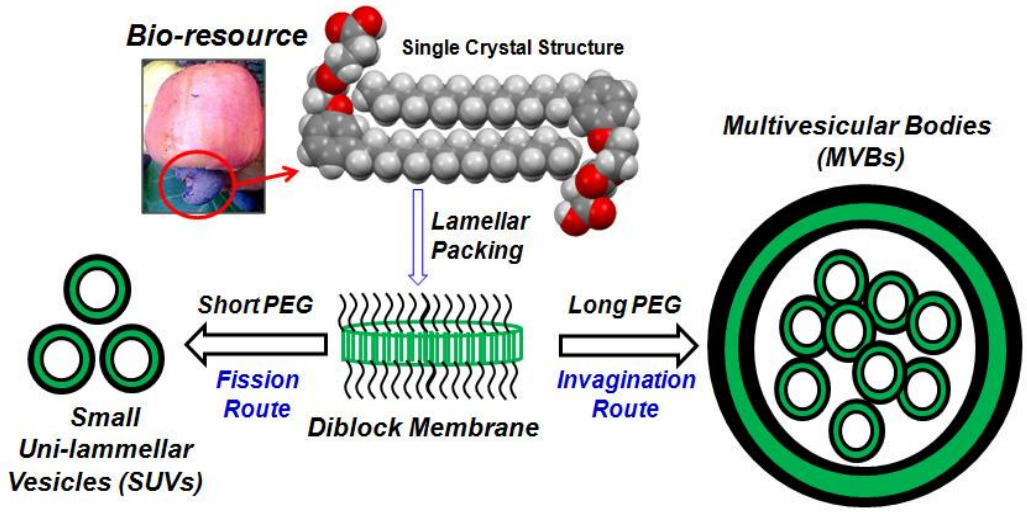

Figure 5.4.*Synthetic diblock membranes sorting into MVBS and SUVs.*

5.2. Experimental Methods

5.2.1. Materials: 3-Pentadecylphenol, 2-bromoethanol, succinicanhydride, triethylamine, triethyleneglycolmonomethylether, polyethylene glycol monomethylether (M_n=750), dicyclohexylcarbodiimide, 4-dimethylamino pyridine were purchased from Aldrich chemicals. NaOH and all other reagents and solvents were purchased locally and purified following the standard procedures.

5.2.2. General procedures: ^{1}H-NMR and ^{13}C-NMR spectra were recorded using 400-MHz Jeol NMR spectrometer in $CDCl_3$ containing small amount of TMS as internal standard. Infra-red spectra were recorded using a Thermo-Scientific Nicolet 6700FT-IR spectrometer with the solid state in KBr. The mass of all the diblock polymers was confirmed by using the Applied Biosystems 4800 PLUS MALDI TOF/TOF analyzer.

Dynamic and Static Light Scattering Measurement: The size determination of the aqueous solution (1.0 mg/mL) of the amphiphile was carried out by dynamic light scattering (DLS), using a Nano ZS-90 apparatus utilizing 633 nm red laser (at 90° angle) from Malvern instruments.For this purpose, 5.0 mg of the A-B amphiphiles were doissolved in 5.0mL of ditilled water. It was then extensively dialyzed (SPECTRA/POR, MWCO-500-1000) against deionized water (200 mL) for 48 h. The solution was filtered through 0.45 μm filter and the aqueous solutions (1.0 mg/mL) of the samples were subjected to dynamic light scattering (DLS) analysis. The reproducibility of the data was checked for at least three independent solutions.

Morphology analysis: Atomic force microscope images were recorded for drop caste samples using JPK instruments attached with Nanowizard-II setup. AFM is also attached with Zeiss inverted optical microscope. TEM images were recorded using a Technai-300 instrument.

Thermal Properties of all samples: Thermal stability of all the amphiphiles was determined using Perkin Elmer thermal analyzer STA 6000 model at a heating rate of 10° C/min under nitrogen atmosphere. Thermal analysis of all the amphiphiles was performed using TA Q20 differential scanning calorimeter (DSC). The instrument was calibrated using indium standards. To remove their previous thermal history, all the samples were heated to melt before recording their thermograms. Samples were heated and cooled at a rate of 10° C/min under nitrogen atmosphere.

Single Crystal X-Ray Analysis: Single crystals were subjected to data collection at 100 K on Bruker APEX duo CCD-X ray diffractometer equipped with graphite monochromator Mo Ka radiation(λ=0.71073 Å). The frames were integrated with

Bruker APEX software package. The structures were solved by direct methods and refined using SHELX S v97 programs. The crystallographic parameters for PDP-Acid molecule have been summarized in table 5.1.Crystal structures were visualized using Mercury 3.0 software.

Table 5.1: Unit cell parameters for PDP-Acid molecule.

Compound	**PDP-Acid**
Formula	$C_{27}H_{44}O_5$
Recrystn solv	DCM/MeOH
Molwt	448
Colour, habit	Colourless, needle
temp(K)	100
System	Triclinic
space group	P-1
a, (Å)	10.79
b, (Å)	20.28
c, (Å)	24.74
α, (deg)	85.30
β, (deg)	85.82
γ, (deg)	75.68
V, Å^3	522.44
d $_{cacl}$,g cm^{-1}	1.141
μ(mm^{-1})	0.08
GOF	0.952
no. of unique reflections	4032
Reflections collected	11205
θ range	1.34 to 24.04
No. of refined parameters	1161
R_1 (on F, I>2σ (I))	0.0972
wR_2 (on F^2, all data)	0.3195

Photophysical Characterization: The absorption and emission studies were done by a Perkin-Elmer Lambda 45 UV-Visible spectrophotometer and SPEX Flurolog HORIBA JOBIN VYON fluorescence spectrophotometer with a 450W Xe lamp asthe excitation source at room temperature. The excitation spectra are collected at 395nm and 476nm (pyrene emission wavelength) and the emission spectra are recorded by exciting at the excitation maxima. The pyrene samples were purged with N_2 gas for at least 15-20 minutes prior to photophysical experiments. Fluorescence intensity decays were collected by time correlated single photon counting technique (TCSPC) setup from Horiba Jobin Yvon., using NanoLED-339 for pyrene as sample excitation source.

Doxorubicin and CPT encapsulation: The ability of these core-shell nanoparticles to encapsulate hydrophobic molecules in the hydrophobic inner core was determined by using DOX. DOX.HCl (0.5 mg) was neutralized with triethylamine prior to the encapsulation. DOX (0.5 mg), PDP- TEG (SUVs) (5.0 mg) were taken in DMSO (1.0 mL). To it triethylamine (1.5 equivalents to DOX) and water (3.0 mL) was added and stirred at 25°C for 12 h. It was then extensively dialyzed (SPECTRA/POR, MWCO-500-1000) against deionized water (200 mL) for 48 h. The DOX encapsulated solution was filtered through 0.45 µm filter and the sample was freeze-dried in lyophilizer. Similar procedure was followed for encapsulating DOX in PDP-PEG 750 (MVBs). Drug loading efficiency (DLE) and drug loading content (DLC) of both the samples were calculated using following equations:

DLE (%) = {weight of encapsulated DOX/ weight of DOX in feed}x 100%.

DLC (%) = {weight of DOX in nanoparticles/weight of DOX loaded nanoparticles} x 100%.

For the above purpose, approximately 1.5 mg of drug loaded nanoparticles was dissolved in DMSO (2.0 mL) and their absorbance was measured to determine the DLE and DLC using their molar extinction coefficients {ε_{DOX}= 4188 (in PBS), ε_{DOX} = 7035 (in DMF)}.

***In Vitro* drug release studies:** The release profile of DOX was studied using dialysis method. Briefly, 3.0 mg of drug loaded sample was dispersed in 3.0 mL of PBS and the content was transferred in to dialysis bag, which was then immersed in 100mL of PBS and was incubated at 37°C. Periodically; 3.0 mL of solution was withdrawn from the system and was replaced with 3.0 mL of fresh PBS solution. The aliquots obtained were then subjected to absorbance measurement and amount of DOX released was calculated. Similarly, the release profile of DOX from MVBs in presence of esterase enzyme was also studied.

5.2.3. Synthesis

Synthesis of 2-(3-pentadecylphenoxy)ethanol (1a): Sodium hydroxide (3.5 g, 88.0 mmol) was dissolved in ethanol-water mixture (1:1 v/v, 100 mL) in 250 mL flask and was purged with nitrogen for 10 minutes. 3-Pentadecylphenol (12.0 g 40.0 mmol) was added into the reaction mixture and the content was refluxed for 30 minutes at 100°C. It was cooled and then freshly distilled 2-bromoethanol (6.4 g, 80 mmol) was added drop wise. The reaction mixture was then refluxed for 24 h under nitrogen atmosphere. It was poured into water (100 mL), extracted with ethyl acetate and washed subsequently with 5% NaOH solution and brine. The organic layer was dried over anhydrous sodium sulphate, filtered and evaporated to obtain pale yellow solid as product. It was purified by passing through silica gel column of 60-120 mesh using 3% ethyl acetate in hexane as eluent. Yield = 7.6 g (55.0 %). ^{1}H NMR ($CDCl_3$, 400 MHz) δ: 7.17 ppm (t, 1H, Ar-**H**), 6.75 ppm (m, 3H, Ar-**H**), 4.08 ppm (t, 2H, Ar-OC**H$_2$**), 3.95 ppm (t, 2H, C**H$_2$**-OH), 2.57 ppm (t, 2H, Ar-C**H$_2$**), 1.6-0.88 ppm (m, 29H, Aliphatic H). ^{13}C NMR ($CDCl_3$, 100 MHz) δ: 158.66, 144.87, 129.31, 121.42, 114.89, 111.51 (Ar-**C**), 66.07 (Ar-O**C**H_2), 61.64 (**C**H_2-OH), 36.11, 32.02, 31.50, 29.78, 29.62, 29.46, 22.80, 14.22. FT-IR (cm^{-1}): 3369, 3293, 2912, 2848, 1593, 1457, 1357, 1264, 1172, 1087, 1047, 958, 898, 785, 697 and 598. MALDI-TOF-MS: m/z calculated for $C_{23}H_{40}O_2$ (MW=348.56): Theoretical: 387.56, Found: 387.19 (M^++K^+).

Synthesis of (E)-2-(3-(pentadec-8-en-1-yl)phenoxy)ethanol (1b): Cardanol (10.0 g, 33.0 mmol) and 2-bromoethanol (6.2 g, 49.5mmol) were reacted in the presence of NaOH (2.64 g, 66.0mmol) in ethanol -water mixture (1:1 v/v, 100 mL) as described for **1a**. It was purified by passing through silica gel column of 60-120 mesh using 3% ethyl acetate in hexane as eluent. Yield = 6.0 g (53.0 %).^{1}H NMR ($CDCl_3$, 400 MHz) δ: 7.18 ppm (t, 1H, Ar-**H**), 6.79 ppm (m, 3H, Ar-**H**), 4.08 ppm (t, 2H, Ar-OC**H$_2$**), 5.34 ppm (d, C**H**=C**H),** 3.96 ppm (t, 2H, C**H$_2$**-OH), 2.57 ppm (t, 2H, Ar-C**H$_2$**), 1.6-0.88 ppm (m, 29H, Aliphatic H). ^{13}C NMR ($CDCl_3$, 100 MHz) δ: 158.66, 144.87, 129.31, 121.42, 114.89, 111.51 (Ar-**C),** 66.07 (Ar-O**C**H_2), 61.64 (**C**H_2-OH), 36.11, 32.02, 31.50, 29.78, 29.62, 29.46, 22.80, and 14.22. FT-IR (cm^{-1}): 3370, 2923, 2854, 1569, 1487, 1449, 1373, 1258, 1159, 1078, 1048, 964, 899, 874, 777, 725, 694, 609.MALDI-TOF-MS: m/z calculated for $C_{23}H_{38}O_2$ (MW=346.55): Theoretical: 385.55, Found: 385.15 (M^++K^+).

Synthesis of 4-oxo-4-(2-(3-pentadecylphenoxy)ethoxy)butanoicacid (2a)-PDP-COOH: Compound **1a** (4.0 g, 11.4mmol) and succinic anhydride (1.4 g, 13.8 mmol) was taken in dichloromethane (50 mL) in a 100 mL flask. Triethylamine (1.5 mL, 11.4 mmol) was added drop wise and the reaction started immediately followed by vigorous boiling. The reaction mixture was stirred at 30 °C for 24 h. It was poured in

100 mL of water, neutralized with 2N concentrated HCl (2 drops). The crude solid was filtered and further purified by crystallization from hot methanol. Yield = 3.3g (64.0 %). ^{1}H NMR ($CDCl_3$, 400 MHz) δ: 7.18 ppm (t, 1H, Ar-**H**), 6.78 ppm (m, 3H, Ar-**H**), 4.45 ppm (t, 2H, Ar-OC**H$_2$**), 4.16 ppm (t, 2H, C**H**$_2$-O), 2.68 ppm (s, 4H, CO-C**H**$_2$-C**H**$_2$), 2.56 ppm (t, 2H, Ar-C**H**$_2$), 1.6-0.88 ppm (m, 29H, Aliphatic H). ^{13}C NMR ($CDCl_3$, 100 MHz) δ: 177.82 (**C**O-OH), 172.11 (O-**C**O) 158.38, 144.75, 129.19, 121.38, 114.85, 111.41 (Ar-**C**), 65.63 (Ar-O**C**H$_2$), 63.26 (**C**H$_2$-O), 36.0, 31.91, 31.38, 29.67, 29.35, 28.77, 28.71, 22.68, and 14.11. FT-IR (cm^{-1}): 2918, 2848, 1738, 1700, 1581, 1454, 1396, 1293, 1233, 1172, 1081, 938, 864, 784, 687, 572. MALDI-TOF-MS: m/z calculated for $C_{27}H_{44}O_5$ (Mw-448.64) : theoretical: 487.64 , Found: 487.17 (M^++K^+).

Synthesis of (E)-4-oxo-4-(2-(3-(pentadec-8-en-1-yl)phenoxy)ethoxy)butanoic acid (2b)-CAR-COOH: Compound **1b** (6.0 g, 17.0 mmol) was reacted with succinic anhydride (2.1 g, 2.0 mmol), in the presence of Et_3N (1.7 g, 17.3 mmol) in dichloromethane (60.0 mL) as described for **2a**. It was purified by passing through silica gel column of 60-120 mesh using 8% ethyl acetate in hexane as eluent Yield = 4.0 g (52 %). ^{1}H NMR ($CDCl_3$, 400 MHz) δ: 7.17 ppm (t, 1H, Ar-**H**), 6.79 ppm (m, 3H, Ar-**H**), 5.34 ppm (d, C**H**=C**H),** 4.46 ppm (t, 2H, Ar-OC**H$_2$**), 4.16 ppm (t, 2H, C**H**$_2$-O), 2.68 ppm (t, 2H, Ar-C**H**$_2$),2.56 ppm (t, 2H, Ar-C**H**$_2$), 1.6-0.88 ppm (m, 29H, Aliphatic H). ^{13}C NMR ($CDCl_3$, 100 MHz) δ: 178.04 (**C**O-OH), 172.13 (O-**C**O) 158.34, 144.64, 129.8, 129.15, 121.32, 114.81, 111.37 (Ar-**C**), 65.58 (Ar-O**C**H$_2$), 63.22 (**C**H$_2$-O), 35.93, 31.32, 29.67, 29.35, 29.26, 29.16, 28.79, 28.67, 27.15, 22.70 and 14.07. FT-IR (cm^{-1}): 2916, 2851, 1726, 1589, 1444, 1250, 1169, 1063, 966, 780, 691, 611. MALDI-TOF-MS: m/z calculated for $C_{27}H_{42}O_5$ (MW= 446.62): Theoretical: 485.62, Found: 485.16 (M^+ + Na^+).

Synthesis of 2-(2-(2-methoxyethoxy)ethoxy)ethyl (2-(3-pentadecylphenoxy)ethyl) succinate (PDP-TEG): Compound **2a** (5.0 g, 11.1 mmol), triethylene glycol monomethyl ether (2.2 g, 13.3 mmol) and 4-dimethylamino pyridine (0.1 g, 1.1 mmol) were dissolved in dry dichloromethane (50 mL) under N_2 atmosphere. The reaction mixture was cooled and stirred at 5 °C for 10 minutes. To this ice-cooled mixture, dicyclohexylcarbodiimide (2.8 g, 13.3 mmol) was added and stirring was continued for 10 minutes at 5 °C. The reaction continued for 24h at 25 °C under N_2 atmosphere. The solvent was evaporated and the solid mass was dissolved in ethyl acetate (200 mL). The white precipitate of DCU obtained was filtered using G3-sintered funnel. The filtrate was washed with water (200 mL), neutralized with 2N HCl (2 mL), washed with 5% Na_2CO_3 solution (100 mL) and dried over anhydrous sodium sulphate. The solvent was evaporated to obtain yellow liquid as product. It was further purified by passing through silica gel column using 25% ethyl acetate in

hexane as eluent. Further, it was purified by dialysis against water using semi-permeable membrane (MWCO-1,000). Yield = 2.1g (3.00 %). ^{1}H NMR ($CDCl_3$, 400 MHz) δ: 7.18 ppm (t, 1H, Ar-**H**), 6.73 ppm (m, 3H, Ar-**H**), 4.44 ppm (t, 2H, Ar-OC**H$_2$**), 4.24 ppm (t, 2H, O-C**H$_2$**-CH_2) 4.15 ppm (t, 2H, C**H**$_2$-O), 3.38 ppm (s, 3H, O-C**H**$_3$), 3.65 ppm (t, 8H,C**H**2-O-C**H**$_2$), 3.56 ppm (t, 2H, C**H**$_2$-OCH_3) 2.66 ppm (s, 4H, CO-C**H**$_2$-C**H**$_2$), 2.58 ppm (t, 2H, Ar-C**H**$_2$), 1.59-0.88 ppm (m, 29H, Aliphatic H). ^{13}C NMR ($CDCl_3$, 100 MHz) δ: 172.22 (O-**C**O) 158.36, 144.70, 129.14, 121.31, 114.79, 111.37 (Ar-**C**), 71.85 (C-OCH_3), 70.5-68.9 (O-CH_2-CH_2O), 65.6 (Ar-O**C**H_2), 63.82 (CH_2-O), 58.98 (O-CH_3), 35.96, 31.87, 31.36, 29.64, 29.55, 29.47, 29.37, 29.31, 28.91, 22.64, and 14.09.FT-IR (cm^{-1}): 2920, 2857, 1738, 1588, 1451, 1351, 1253, 1149, 1104, 857, 784, 696, 572. MALDI-TOF-MS: m/z calculated for $C_{34}H_{58}O_8$ (MW=594.82): Theoretical: 617.82, Found: 617.46 ($M^+ + Na^+$).

Synthesis of 2,5,8,11,14,17,20,23,26,29,32,35,38,41,44,47,50-heptadecaoxadopentacontan-52-yl(2-(3-pentadecylphenoxy)ethyl)succinate (PDP-PEG750): Compound **2a** (1.0g, 2.2mmol), polyethylene glycol monomethyl ether (M_n=750) (2.0 g, 2.6mmol),4-dimethylamino pyridine (0.3 g, 0.2mmol) was reacted with dicyclohexylcarbodiimide (0.5 g, 2.6mmol) as described for **PDP-TEG**. . It was further purified by passing through silica gel column using 20% methanol in dichloromethane as eluent. The product was repetitively washed with n-hexane to remove the un-reacted PEG-750 and further purified by dialysis against water using semi-permeable membrane (MWCO-1,000). Yield = 1.5 g (35 %).^{1}H NMR ($CDCl_3$, 400 MHz) δ: 7.15 ppm (t, 1H, Ar-**H**), 6.69 ppm (m, 3H, Ar-**H**), 4.40 ppm (t, 2H, Ar-OC**H$_2$**), 4.19 ppm (t, 2H, O-C**H$_2$**-CH_2), 4.12 ppm (t, 2H, C**H**$_2$-O), 3.65-3.59 ppm (s, 32H,C**H**2-O-C**H**$_2$), 3.34 ppm (s, 3H, O-C**H**$_3$), 2.64 ppm (s, 4H, CO-C**H**$_2$-C**H**$_2$), 2.53 ppm (t, 2H, Ar-C**H**$_2$), 1.55-0.88 ppm (m, 29H, Aliphatic H). ^{13}C NMR ($CDCl_3$, 100 MHz) δ: 172.25 (O-**C**O) 158.39, 144.73, 129.18, 121.32, 114.80, 111.41 (Ar-**C**), 71.88 (C-OCH_3), 70.5-69.0 (O-CH_2-CH_2O), 65.64 (Ar-O**C**H_2), 63.85 (**C**H_2-O), 59.01 (O-**C**H_3), 31.94, 31.47, 30.08, 29.67, 29.58, 29.34, 22.67 and 14.10. FT-IR (cm^{-1}): 2920, 2857, 1735, 1650, 1595, 1457, 1349, 1247, 1096, 947, 853, 697, 567. MALDI-TOF-MS: m/z calculated for $C_{62}H_{114}O_{22}$, Theoretical: 1233, Found: 1234.07 ($M^+ + Na^+$).

Synthesis of (E)-2,5,8,11,14,17,20,23,26,29,32,35,38,41,44,47,50-heptadecaoxadopentacontan-52-yl(2-(3-(pentadec-8-en-1-yl)phenoxy)ethyl) succinate (CAR-PEG750): Compound **2b** (6.0 g, 17.0 mmol), polyethyleneglycolmonomethyl ether (M_n= 750, 12.1g, 16.0mmol), 4-dimethylamino pyridine (0.2 g, 1.3mmol), was reacted with dicyclohexylcarbodiimide (3.3 g, 16mmol) as described for **PDP-TEG**. . It was further purified by passing through silica gel column using 15% methanol in dichloromethane as eluent. The crude

product was repetitively washed with n-hexane to remove the unreacted PEG-750 and further purified by dialysis against water using semi-permeable membrane (MWCO-1,000). Yield = 2.1 g (13 %). ^{1}H NMR ($CDCl_3$, 400 MHz) δ: 7.14 ppm (t, 1H, Ar-**H**), 6.74 ppm (m, 3H, Ar-**H**), 5.28 ppm (d, C**H**=C**H),** 4.39 ppm (t, 2H, Ar-OC**H$_2$**),4.19 ppm (t, 2H, O-C**H$_2$**-CH_2), 4.08 ppm (t, 2H, C**H**$_2$-O), 3.59 ppm (s, 32H,C**H**2-O-C**H**$_2$), 3.32 ppm (s, 3H, O-C**H**$_3$), 2.62 ppm (s, 4H, CO-C**H**$_2$-C**H**$_2$), 2.50 ppm (t, 2H, Ar-C**H**$_2$), 1.55-0.88 ppm (m, 29H, Aliphatic H). ^{13}C NMR ($CDCl_3$, 100 MHz) δ: 172.25 (O-CO) 158.39, 144.73, 129.18, 121.32, 114.80, 111.39 (Ar-**C**), 71.88 (C-OCH_3), 70.5-69.0 (O-CH_2-CH_2O), 65.64 (Ar-O**C**H_2), 63.85 (**C**H_2-O), 59.01 (O-**C**H_3), 31.94, 31.47, 30.08, 29.67, 29.58, 29.34, 22.67, and 14.10. FT-IR (cm^{-1}): 2928, 2866, 1738, 1657, 1593, 1537, 1454, 1347, 1244, 1093, 947, 849, 792, 696, 568. MALDI-TOF-MS: m/z calculated for $C_{62}H_{112}O_{22}$, Theoretical: 1143 Found: 1143.99 ($M^+ + Na^+$).

5.3. Results and Discussions

5.3.1. Synthesis and Characterization of Amphiphiles

Two naturally available plant based long tailed phenolic compounds such as cardanol (contains ω-unsaturated alkyl chain) and its saturated analogue 3-pentadecylphenol were chosen as the hydrophobic units for the AB diblock design (see scheme-5.1). Both cardanol and 3-pentadecylphenol are the main constituents of cashew nut shell liquid which are produced as plant based industrial waste. 3-Pentadecylphenol was reacted with 2-bromoethanol in presence of NaOH as a base to give 2-(3-pentadecylphenoxy)ethanol (**1a**). Succinic anhydride was ring opened with **1a** in presence of Et_3N as base to give 4-oxo-4-(2-(3-pentadecylphenoxy)ethoxy)butanoic acid (**2a**). The compound **2a** was further coupled with triethylene glycol monomethyl ether (TEG) and polyethylene glycol (PEG-750) monomethyl ether to produce two A-B amphiphiles of PDP-TEG and PDP-PEG-750, respectively (PDP- represents pentadecylphenol as hydrophobic part). Cardanol was converted into **2b** (as described for **2a)** andreacted with PEG-750 monomethyl ether to obtain CAR-PEG-750 diblock (CAR- represents cardanol as hydrophobic part). The amphiphiles were purified (by column chromatography and dialysis using semi-permeable membrane).

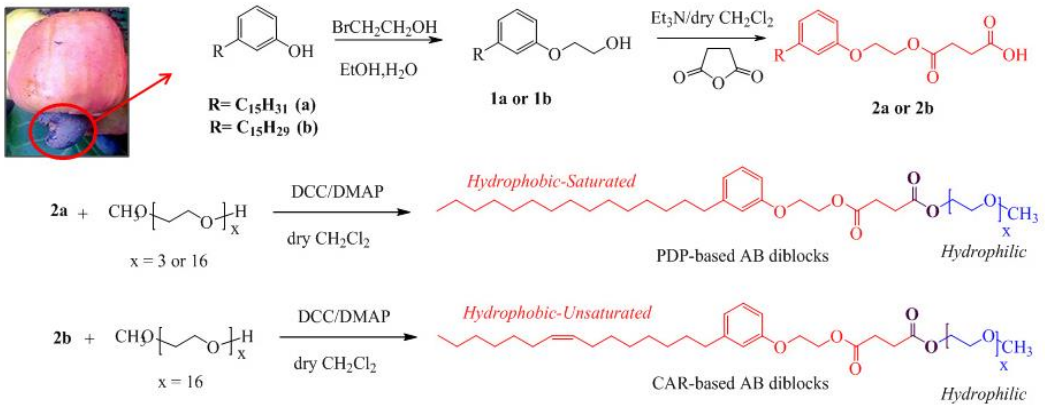

Scheme 5.1.*Synthesis of Renewable Resource Based AB amphiphiles.*

The structure of amphiphiles was characterized by ^{1}H and ^{13}C-NMR and MALDI-TOF-TOF. Figure 5.5 shows the ^{1}H NMR, and ^{13}C NMR spectra of PDP-

PEG750. The Ar-H (type a) in PDP-PEG750 appears as a triplet at 7.15 ppm and type b, and c as a multiplet at 6.67 ppm. Two triplet appears for the Ar-OCH_2-CH_2 protons (type d) and Ar-OCH_2-OCH_2 protons (type f) at 4.40 ppm and 4.11 ppm respectively. A triplet appears for the CO-O-CH_2 proton (type e) at 4.19 ppm. A multiplet appears for the all the ethylene glycol protons (type h) at 3.64-3.59 ppm. Singlet appears for the O-CH_3 proton (type h) at 3.34 ppm. A singlet appears for the CO-CH_2-CH_2-CO protons (type i) at 2.64 ppm. Triplet appears for the Ar-CH_2 protons at 2.53 ppm. All alkyl protons appear at 1.55-0.82 ppm. In ^{13}C NMR spectrum the signal for carbonyl carbon atoms appears at 172.25 ppm. Signals for all the aromatic carbon appears in the range of 110-160 ppm and signals for all alkyl carbon appears in the range of 10 – 50 ppm. The intensity of the signal at 70.50 ppm gets intensified for every carbon atom added to the ethylene glycol unit.

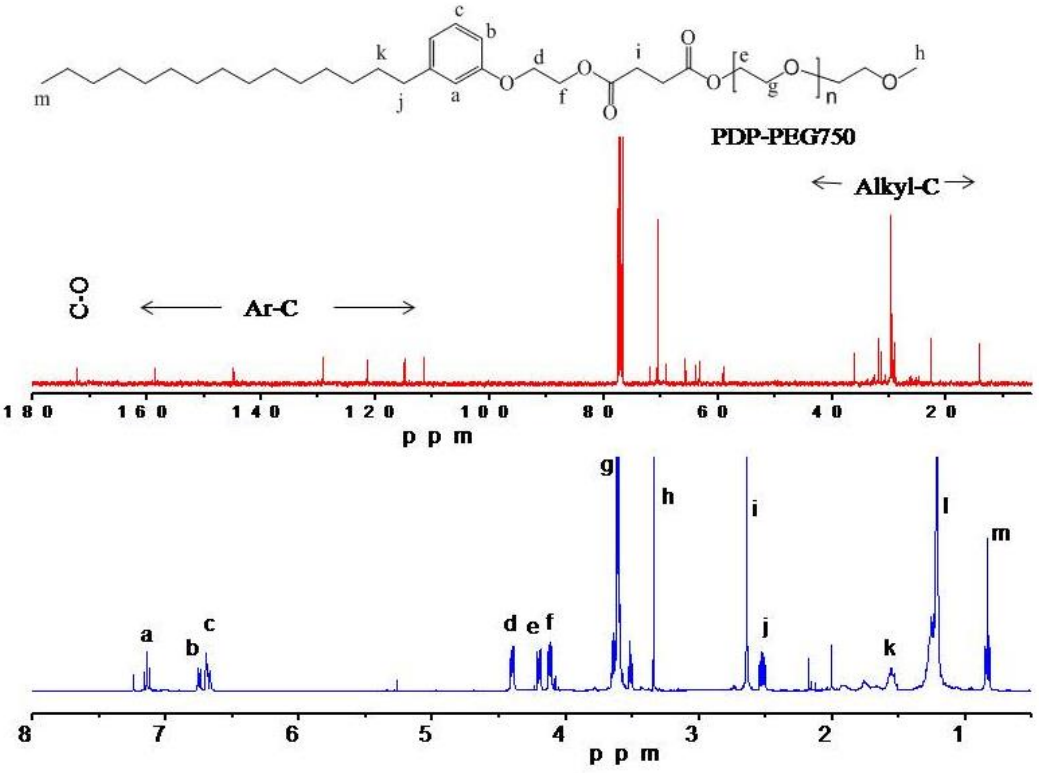

Figure 5.5. *(a) ^{1}H-NMR spectrum (b) ^{13}C-NMR spectrum of PDP-PEG 750.*

The MALDI-TOF spectra of the PEG-750 and its corresponding A-B diblock containing PDP are shown in figure 5.6. MALDI-TOF spectra of PEG750 shows

adistribution of mass peaks in the range of m/z = 400 to 1200, having a difference of 44 a.m.u between each mass peak, corresponding to the mass of repeating unit present in PEG750. All the mass peaks in the spectrum corresponds to sodium ions of PEG chains and the mass of each peak was calculated using the formula: $(44.05)_n$ + 31 + 23, where 44.05 is the mass of repeating unit, n-corresponds to the number of repeating unit present, 31 is the mass of OMe group and 23 is the mass of sodium ion.

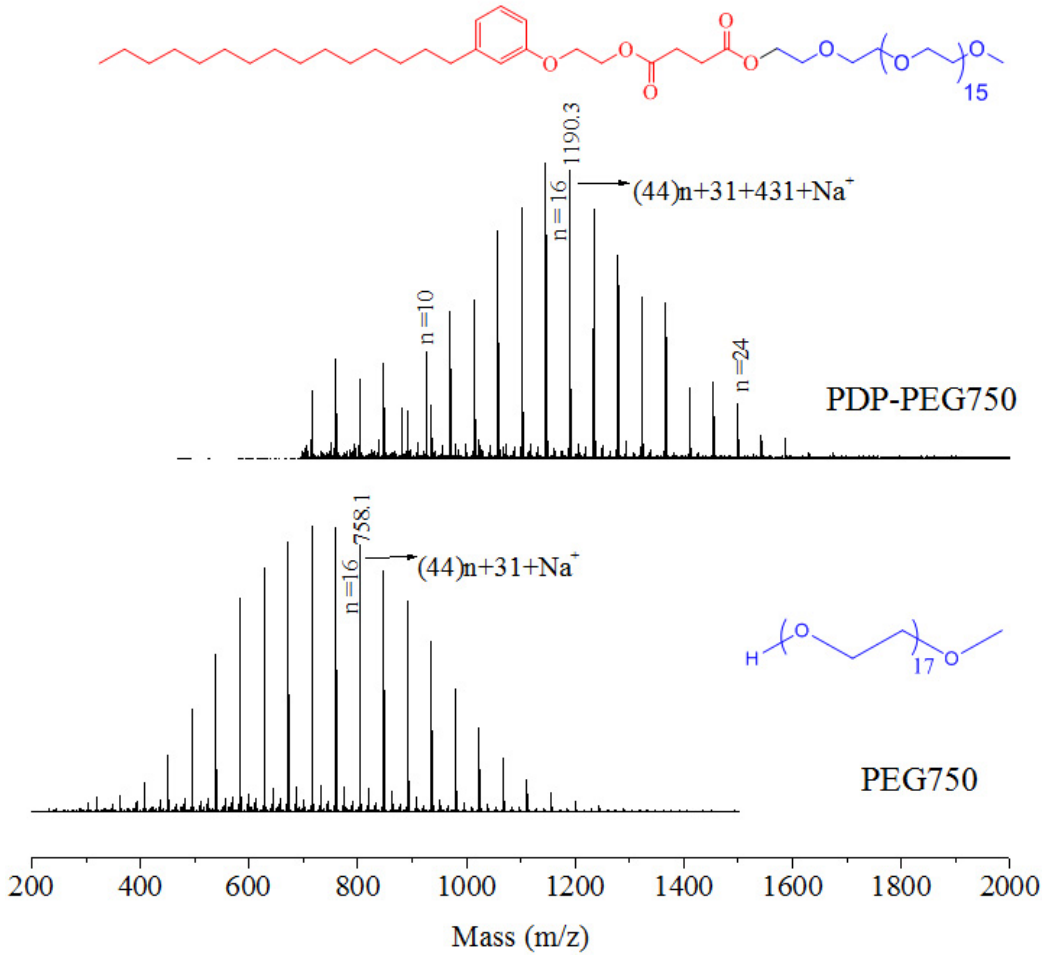

Figure 5.6. *MALDI-TOF spectrum of PDP-PEG 750 and PEG-750 and the repeating unit mass for the peak at n=16 in both the cases is shown by arrow.*

Whereas MALDI-TOF spectrum of PDP-PEG750 shows a distribution of mass peaks in the range of m/z = 800 to 1600. Thus a shift in the spectrum can be observed by 400amu approximately, which corresponds to the mass of PDP-COOH,

thereby confirming the formation of PDP-PEG750. In this case mass of each peak was calculated using the formula: $(44.05)_n + 431 + 31 + 23$, where 44.05 is the mass of repeating unit, n-corresponds to the no. of repeating unit present, 431 is the mass of PDP-COOH, 31 is the mass of OMe group and 23 is the mass of sodium ion.

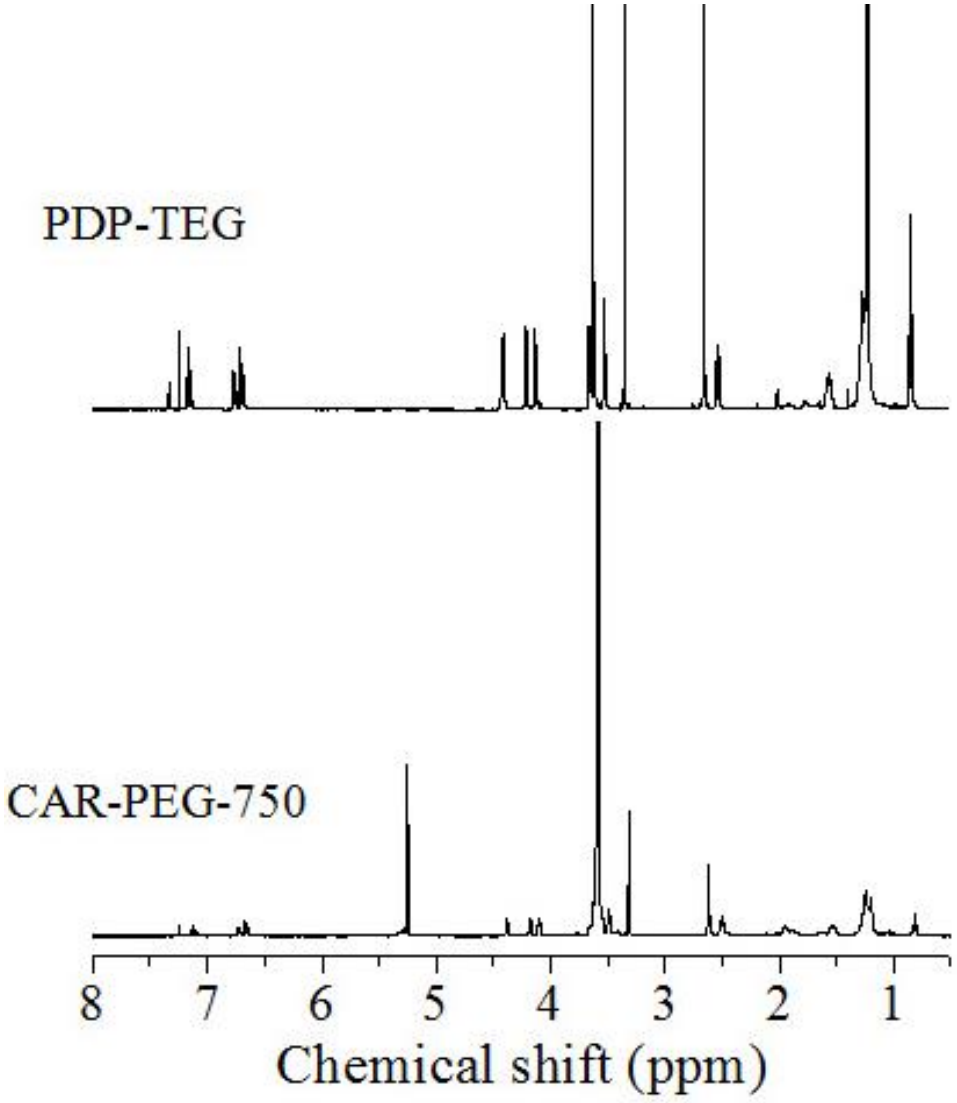

Figure 5.7. *^{1}H-NMR spectrum of PDP-TEG and CAR-PEG-750.*

All other amphiphiles were also characterised by ^{1}H and ^{13}C-NMR and MALDI-TOF-TOF. The^{1}H-NMRspectrumof PDP-TEG and CAR-PEG-750 are shown in figure 5.7.

5.3.2. Shape and Size of the Self-Assembled Amphiphiles

The current molecular design provides two categories of A-B amphiphiles to study their self-assembly in water: (i) fixed hydrophobic units (PDP alkyl units) with variable hydrophilic PEG chain length (PDP-TEG and PDP-PEG-750) and (ii) variable hydrophobic units (PDP, and CAR) with fixed hydrophilic PEG-750 chains (PDP-PEG-750 and CAR-PEG-750). To determine the self-assembled structures formed by the A-B amphiphiles, 5.0 mg of the A-B amphiphiles were doissolved in 5.0mL of ditilled water. It was then extensively dialyzed (SPECTRA/POR, MWCO-500-1000) against deionized water (200 mL) for 48 h. The solution was filtered through 0.45 µm filter and the aqueous solutions (1.0 mg/mL) of the samples were subjected to dynamic light scattering (DLS) analysis.

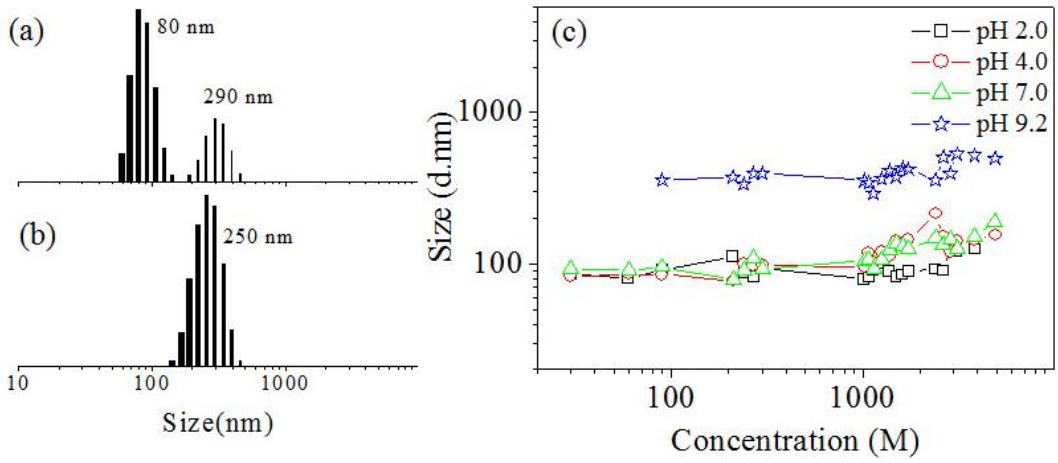

Figure 5.8. *DLS histograms of AB amphiphiles in PDP-PEG-750 (a) and PDP-TEG (b) in PBS at 10^{-5}M. (c)Aggregate size of PDP-PEG750 vs concentration at various pH.*

DLS histograms recorded for PDP-PEG-750 and PDP-TEG blocks in PBS (phosphate buffer saline, pH = 7.4) at $1x10^{-5}$ M are shown in figure 5.8a and 5.8b. PDP-PEG-750 showed a broad distribution with the formation of aggregates with sizes ranging from 80-300 nm. PDP-TEG showed narrow distribution with the formation of uniform size aggregates of 200-250 nm in water. The formation of these nano- sized aggregates may be explained on the basis of hydrophilic-hydrophobic interaction between the molecules as they come close together in water. Upon

monitoring the aggregate size for 5 days at various pH it was found that these aggregates were stable at pH- 2.0, 4.0 and 7.0(see figure 5.8c). While at pH- 9.2 their size increases after 90 minutes indicating that these aggregates are stable in acidic and neutral pH but undergoes swelling in basic condition. Thus, these nano-aggregates were found to be stable under longer storage (5 days) and at both acidic–to-neutral pH.

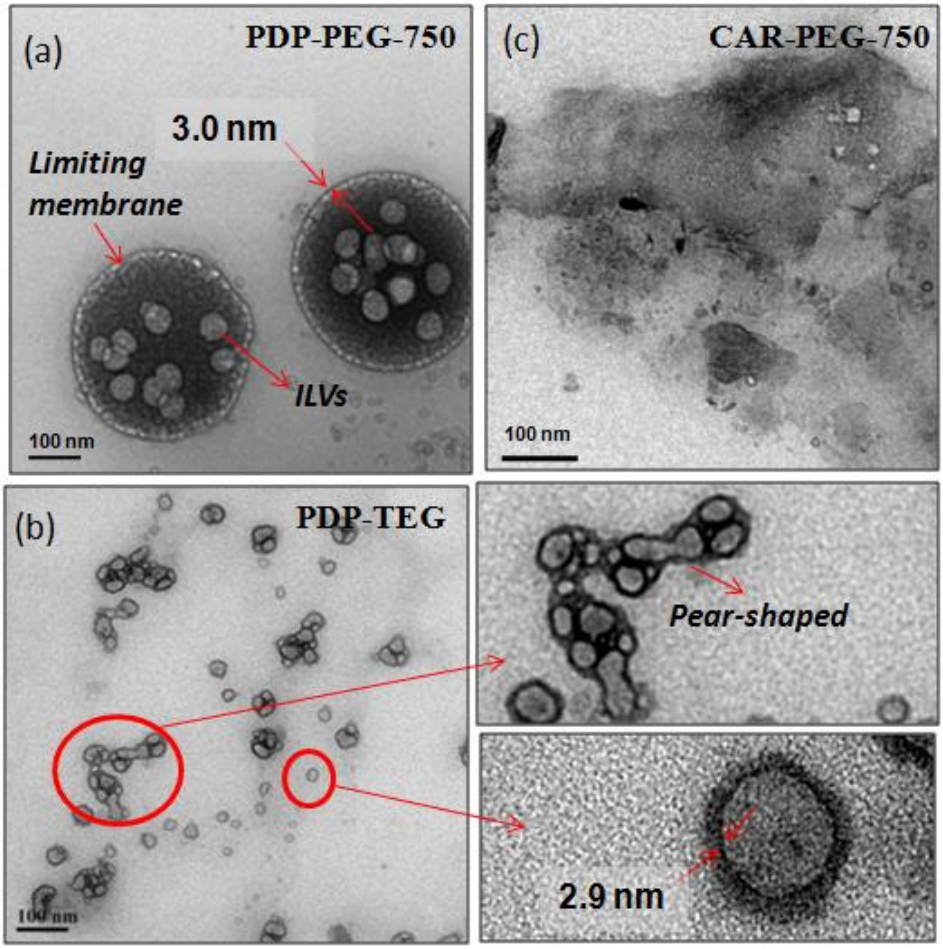

Figure 5.9. *HR-TEM images of PDP-PEG-750 (a), PDP-TEG (b) and CAR-PEG-750 (c).*

To visualize the size and shape of the A-B diblock nano-aggregates, the samples were subjected to high resolution transmission electron microscope (TEM) analysis. HR-TEM images of PDP-PEG750 and PDP-TEG are given in figure 5.9a and 5.9b, respectively. The morphology of PDP-PEG750 was found to be identical to

multivesicular bodies (MVBs) consisting of spherical shaped diblock membrane which accommodated 10±4 intra-luminal vesicles (ILVs) of ~ 45-50 nm in diameter. Both the diblock membrane and ILVs were found to have identical wall thickness (~3.0 nm) which further supported the sorting of ILVs from the same diblock membrane. The enlarged portion of the PDP-PEG-750 vesicles clearly showed the appearance of dark hydrophilic layer covered by hydrophilic corona at the outer surface. On the other hand, the PDP-TEG block with short hydrophilic PEG chain showed the formation of isolated small uni-lamellar vesicles (SUVs) of 40 nm diameter with wall thickness ~ 2.9 nm. The enlarged section of figure 5.9b confirmed the existence of SUVs as aggregated compound vesicles. This is in confirmation with the existence of large aggregates for PDP-TEG observed in the DLS data (figure 5.8b).[48] Further, TEM analysis was carried out for theunsaturated hydrophobic block CAR-PEG-750 (see figure 5.9c). From the image it is evident that it did not show any controlled self-organization in water; as a result, no definite morphology was observed (see figure 5.9c). Hence, both the nature of the hydrophobic units (saturated or unsaturated chain) and length of the PEG chain played a crucial role in the molecular self-assembly of A-B amphiphiles in water.

Further, images of pear-shaped vesicles which were yet to be split into individual SUVs were also clearly visible. The TEM image of PDP-TEG also indicates the presence of pear-shaped vesicle was uniformly distributed throughout the sample(see figure 5.10). Atomic force microscopic analysis of the amphiphiles confirmed spherical shape of the vesicles and the size of the vesicles matched with that of TEM (see figure 5.11).

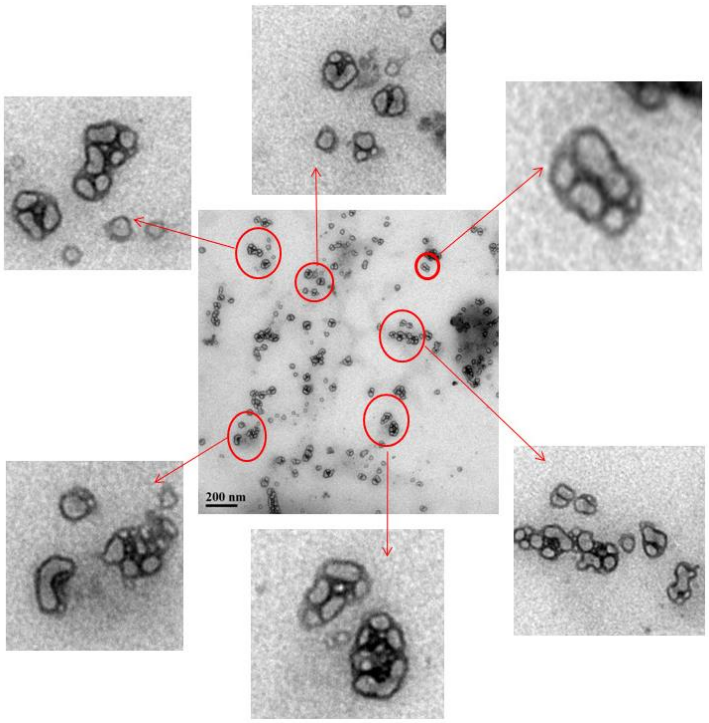

Figure 5.10.*HR-TEM images of SUVs form PDP-TEG in phosphate buffer saline (PBS).*

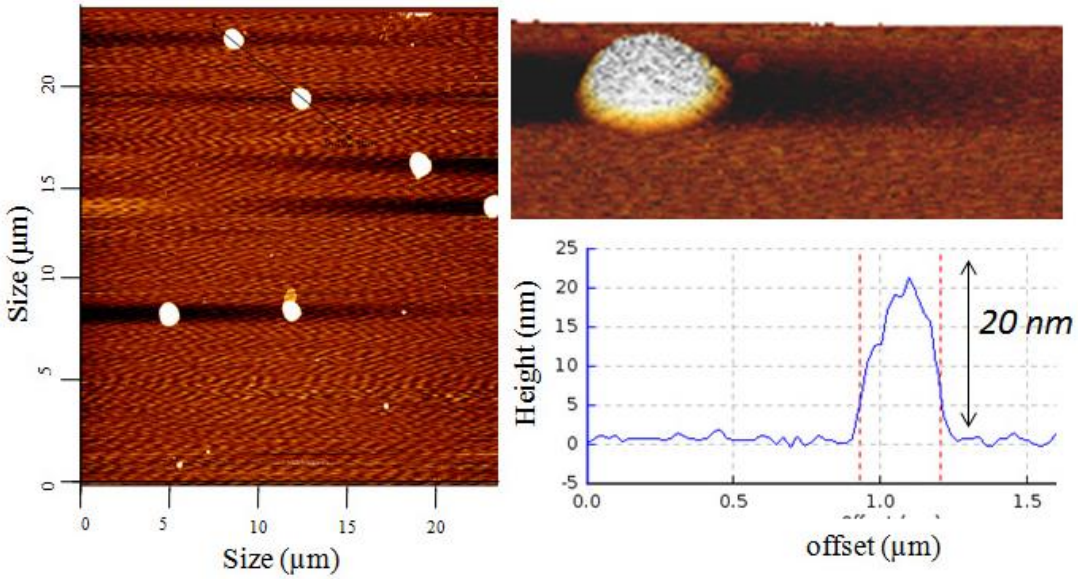

Figure 5.11.AFM image of PDP-PEG750 at neutral pH(7.4).

The packing of surfactant molecules into self-assembled objects like lamellar arrangements were typically validated by utilizing their single crystal structures.

Unfortunately, most of the surfactant molecules are typically liquids or low melting solids and very difficult to obtain single crystal data to trace their molecular interactions. Recently, Smith *et al.* had successfully grown single crystals for sodium dodecyl sulfate and established the correlation between the molecular packing with its uni-lamellar self-organization.[49,50] However, crystallographic evidence for the micelle or vesicular packing of amphiphiles is very rare in the literature. In order to understand the nature of the chain packing in the vesicular structures produced in the current investigation, single crystal X-ray structure of the hydrophobic PDP-unit was resolved. A-B amphiphiles were liquid-like in nature and did not form crystals. Interestingly, good quality single crystals were grown for their synthetic intermediate compound **2a** (see scheme 5.1) in dichloromethane/methanol solvent mixture (2:3 v/v). The molecule **2a** has same features of hydrophobic part as in the AB blocks, and therefore, it could be presumed that its crystal structure could provide direct information on the packing of PDP units in the vesicle. Single crystal X-ray structure of **2a** is shown in figure 5.12 and other details are given in the experimental section.

The molecule **2a** crystallized in triclinic lattice in the space group of P-1 and their unit cell parameters were determined as: a = 10.795, b = 20.28, c = 24.74, α = 85.30, β = 85.82, γ = 75.68 with R-factor 9.43. The pentadecyl chains in the molecule **2a** were organized in all trans-conformations which were separated from the hydrophobic carboxylic functional group (to which PEG chains were connected in the AB di-blocks). The three dimensional packing of the molecules along the a-axis showed the perfect lamellar sheet formation. The alkyl chains were projected towards each other via like interactions and inter-digitated to form hydrophobic layer of thickness 29.2 Å (or 2.92 nm, see figure 5.12). The wall thickness of the vesicles in SUVs and MVBs were (~ 3.00 nm, from TEM images) almost identical to the inter-digitized hydrophobic layer distance (~2.92 nm, from the crystal structure) indicating that the thin hydrophobic walls in the vesicles were constituted by long tails in the PDP units. Based on the crystal packing, it may be concluded that the vesicles (MVBs and SUVs) were typically uni-lamellar in nature. This is for the first

time that such a good correlation has been proposed between the wall thicknesses of the vesicles and their chemical structure using single crystal analysis. It is very important to mention that the formation of lamellar structures in the vesicular assemblies were elucidated based on the two independent techniques like single crystal structure and the morphological analysis by HR-TEM. However, more experimental and theoretical studies are required to confirm the above model. The identical wall thickness of the SUVs or MVBs suggested that the AB amphiphiles initially would have undergone similar self-organization in water to produce diblock membranes of same thickness; however, their budding patterns could have varied at a later stage for the exclusive formation of MVBs (or SUVs).

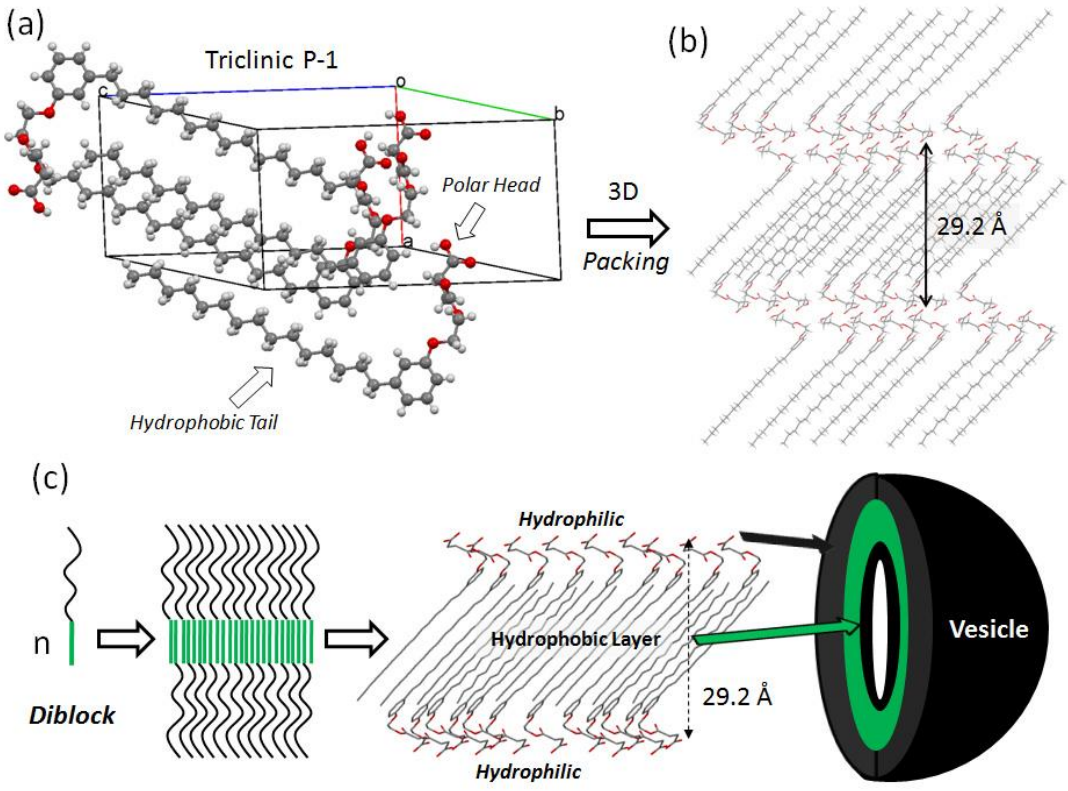

Figure 5.12. *Single crystal structure of compound 2a. Unit cell (a) and the three dimensional packing of molecules along the a-axis (b). The packing diagram represents the uni-lamellar formation and its spherical vesicle (c).*

5.3.3. Theoretical Calculation

Based on the theoretical model, the evolution of vesicles were typically involved in two- consecutive steps: (i) AB diblock with hydrophilic and hydrophobic unit undergo self-organization in water to produce disk like large diblock membrane with radius of R_D and (ii) in order to minimize the membrane-elastic strain energy, these diblock membranes undergo closure to produce larger vesicles of radius R_m (wher $R_{m=}R_D/2$).[51] The schematic representation of the vesicle formation is shown in figure 5.13.More often, these large vesicles further undergo shape change to reduce the bending energy; as a result, the mother vesicles deformed into either pear-shaped vesicle or stomatocyte with respect to their inward or out-ward curvatures, respectively.[52] Two important parameters determine the nature of the curvature and they are: reduced volume (ν) and reduced area difference (Δa_0) which are defined as

$$\nu = V / [4/3\ \pi\ R_m^3] \qquad (1) \qquad \text{and}$$

$$\Delta a_o = \Delta A / [8\pi D R_m] \qquad (2)$$

where, V is the volume of the vesicle, D is the bi-layer thickness and $\Delta A = 2DM$ where M is the mean-curvature of the vesicle. The reduced volume ν and Δa_o are kept at maximum (equal to 1) which corresponds to the most stable spherical shape of vesicles.[53] The value of $\Delta a_o > 1$ and $\Delta a_0 < 1$ represents the outward and inward curvature of the mother vesicle, respectively. In the event these deformed mother vesicles (stomatocyte or pear-shaped) underwent further transformation into smaller vesicles, the ν is replaced by relative volume[17d] ν_e, which is represented as

$$\nu_e = ½[\Delta a_0\ [3-(\Delta a_0)^2] \qquad (3)$$

In the case of SUV formation via membrane fission from pear-shaped vesicle, the mean curvature represented as $M=4\pi\ (R_1+R_2)$ where R_1 and R_2 are the radii of the SUVs. Substituting M in eqns. (2) results, $\Delta a = [R_1 + R_2]/ R_m$. In the case of inward invagination and subsequent splitting from the diblock membrane (for MVBs formation), the mean curvature became, $M = 4\pi\ (R_1-R_2)$. Substituting M in

this case in eqn. (2) results, $\Delta a = [R_1 - R_2]/ R_m$ for the generation of intra-luminal vesicle in MVBs. Based on these theoretical model, the 'ν_e' and Δa_o were determined for PDP-TEG and PDP-PEG-750 blocks and values are shown in the table in figure 5.13. The radii of the mother vesicle (R_m) and the disk like diblock membrane bi-layer (R_D) were calculated from the surface area of the SUVs or MVBs and the values are summarized in the table in figure 5.13. The ν_e values were found to be almost similar in both PDP-TEG (0.85± 0.06) and PDP-PEG-750 blocks (0.85± 0.09), which indicated that the extent of bi-layer closure to spherical mother vesicles was almost identical in both blocks.[52,53]On the other hand, Δa_o were obtained differently as 0.70±0.29 and 1.33±0.03 for PDP-PEG-750 and PDP-TEG, respectively. For PDP-TEG, the larger Δa_o values (> 1) confirmed the outward budding of membrane into pear-shaped deformed vesicles (as shown in figures 5.9b and 5.13). The lower Δa_o (< 1) values supported the deformation of diblock membrane into stomatocyte in the PDP-PEG-750 block (see figure 5.13). The inward invagination of stomatocyte in PDP-PEG-750 (see figure 5.9a) produced MVBs in synthetic-diblock membrane as observed in biological cells.

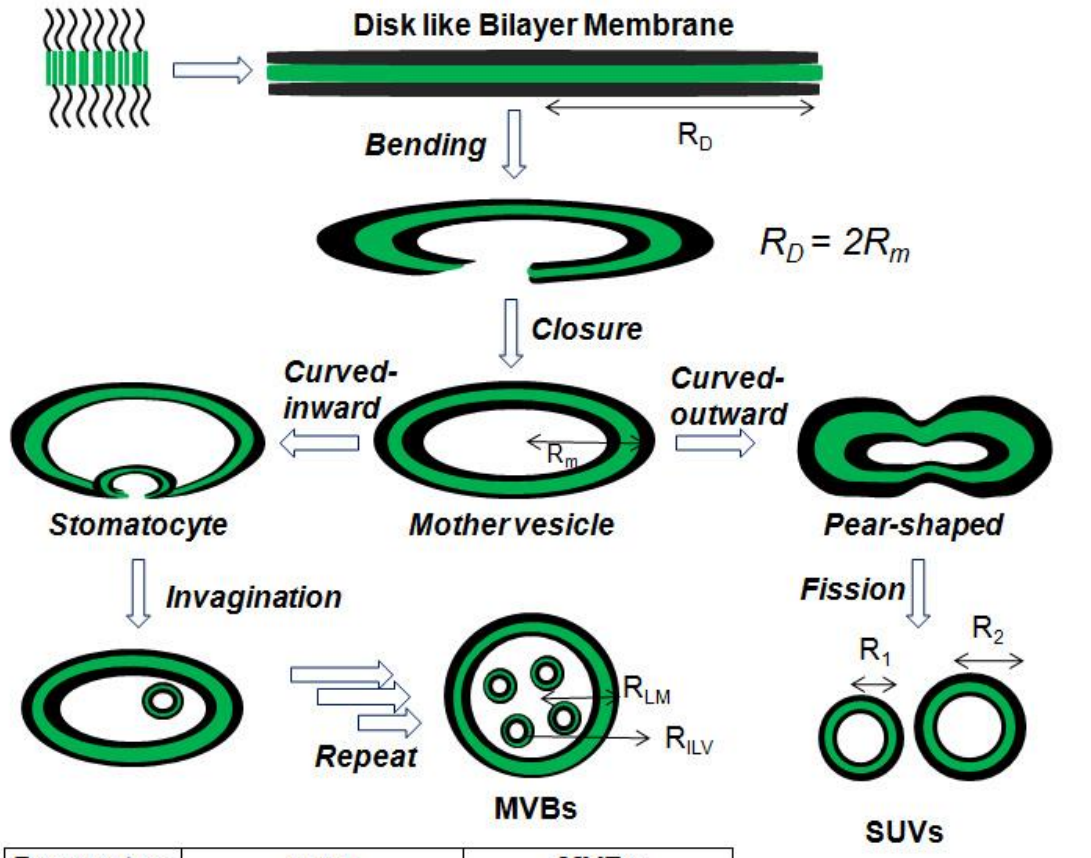

Parameters	SUVs	MVBs
R_D	48±7.2 nm	396 ± 22.5.0 nm
R_m	24±4.3 nm	198 ± 22.6 nm
Surface area	7.28 x10^3 ± 2.2x10^3nm^2	4.96x10^3±2.1x10^3nm^2
Δa_o	1.33±0.03	0.70 ±0.29
υ_e	0.85±0.06	0.85 ±0.09

Figure 5.13. *Evolution of MVBs and SUVs from diblock membrane and their structural parameters determined based on theoretical model.*

The comparison of R_D (or R_m) values among the AB amphiphiles indicated that the size of the self-organized bi-layer (or mother vesicle) produced by the short hydrophilic block (PDP-TEG) was 1/8 times smaller compared to that of its long PEG chain counterpart PDP-PEG-750. Further, the ratio of the surface area between the large diblock membrane vesicle ($4\pi R_{LD}$, which accommodated the small vesicles) and the intra-luminal vesicles ($\sum 4\pi R_i$) were calculated. The ratio was obtained as 3:1 (see table in figure 5.13) which indicated that during the mulivesicular bodies' formation, the diblock membrane underwent inward invagination upto 25 % of its original surface area until it formed stable spherical vesicle. The repetitive invagination (more than 10 times as seen in the present case) produced MVBs which were only possible if the stability of the uni-lamellar diblock membrane was very high in water.

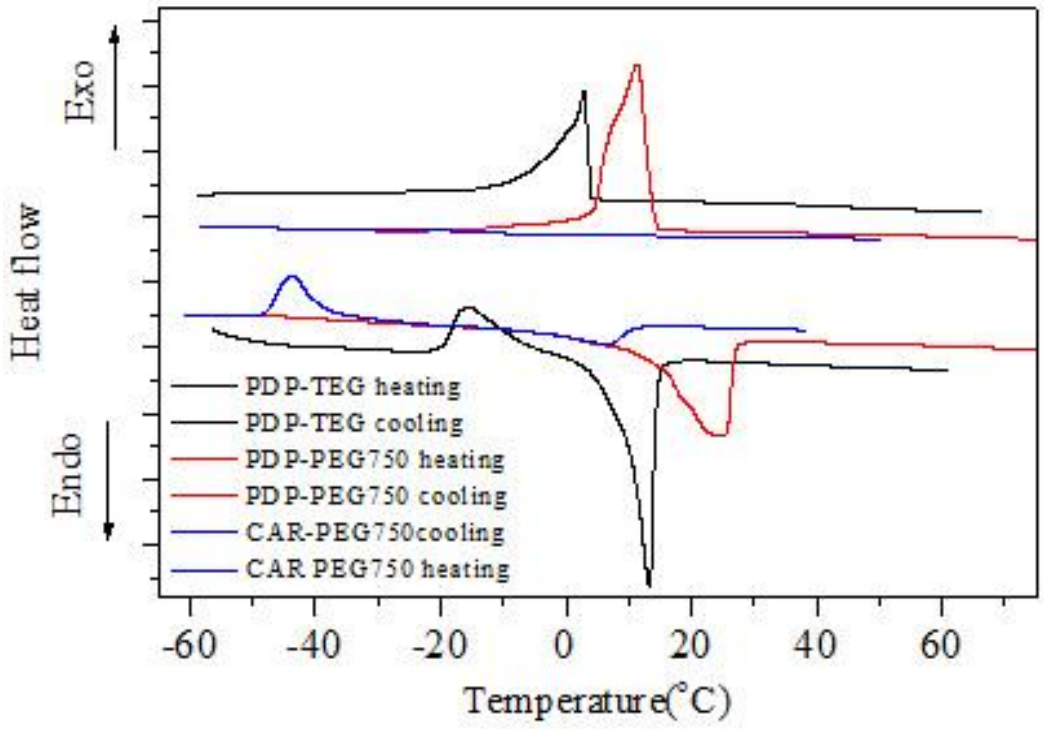

Figure 5.14. *DSC thermograms and Enthalpies of transitions for PDP-TEG, PDP-PEG750 and CAR-PEG750.*

To test the packing abilities of AB amphiphiles, they were subjected to differential scanning calorimetric analysis (DSC) (see figure 5.14). The enthalpies of

the crystallization and melting transitions (kJ/mol) of the AB block having long PEG-750 units were obtained almost 3-4 times higher than that of its short triethyleglycol counterpart (see table 5.2). Typically, strongly packed chains showed higher crystallinity and needed higher energy for melting and released more heat during crystallization. Hence, it can be confirmed that the longer PEG chain facilitated higher order of packing in the AB amphiphiles.

Table 5.2. *Enthalpy values of transitions for all the AB amphiphiles.*

Sample	Heating cycle				Cooling cycle	
	T_m(K)	ΔH_m(kJ/mole)	T_{cc}(K)	ΔH_{cc}(kJ/mole)	T_c(K)	ΔH_c(kJ/mole)
PDP-COOH	355.83	75.04	344.36	19.60	310.95	39.0
PDPTEG	286.35	35.50	257.01	15.92	275.95	24.40
PDP-PEG750	298.11	87.95	_	_	284.28	109.08
CAR-PEG750	27.76	16.19	229.56	22.90	_	_
PEG750	300.81	77.3	-	-	290.79	89.4

Further, it was very clear from the enthalpies that the PDP-PEG-750 block has much higher enthalpies than their individual counterparts: PDP-acid and PEG-750 (see table 5.2). This provides direct evidence for the strong packing of amphiphiles via cooperative structural effects which lacked in their individual hydrophilic or hydrophobic parts alone. The strong inter-molecular interaction in PDP-PEG-750 blocks produced larger diblock membrane (eight times bigger in size) which further underwent inward invagination to produce MVBs as noticed in the biological cell membranes. On the other hand, the shorter hydrophilic content (PDP-TEG) produced small and loosely packed membrane which preferred outward

budding to from SUVs (as seen in many synthetic examples). Thus, a very good correlation between the theory and experimental results were established in the mechanistic aspects of SUVs and MVBs. The above studies revealed that strong uni-lamellar packing was essential for synthetic membranes to form MVBs. PDP-PEG-750 is a unique bio-mimicking synthetic block which produced exclusively MVBs through inward invagination mechanism.

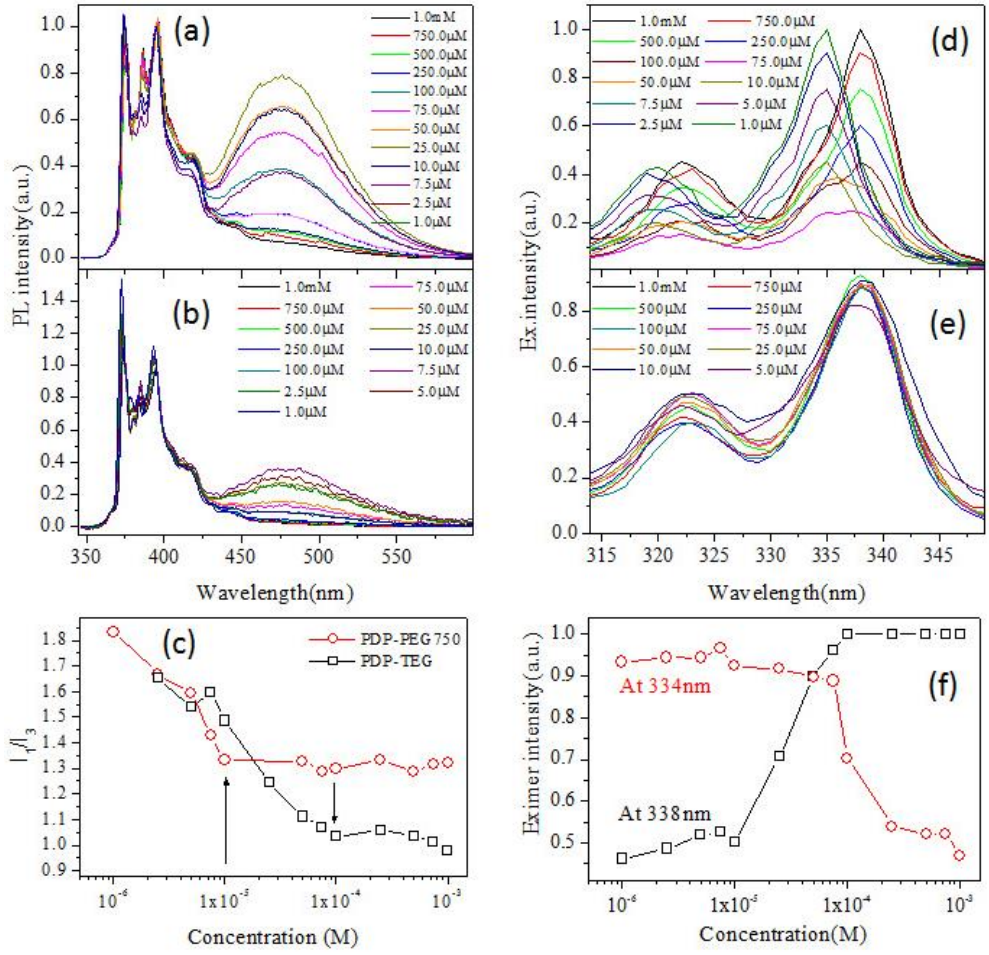

Figure 5.15.*Emission spectra of pyrene at various concentrations of PDP-TEG (a) and PDP-PEG-750 (b) in PBS (excited at 337 nm). Plot of I_1/I_3 versus the concentration of blocks (c). Excitation spectra of pyrene collected at monomer (d) and excimer emission (e) at various concentration of PDP-TEG. Plots of excitation intensity versus the concentration of PDP-TEG (f).*

Since the structure of SUVs were identical to the thermo-responsive amphiphile PDP-TEG (having amide-linkage) mentioned in the previous chapter 2,

so before pyrene encapsulation the aqueous solution of SUVs were subjected to heating. This ester molecule did not shows LCST behaviour. In other words, although PDP-TEG molecule with ester linkage was capable of forming small unilamellar vesicle, replacement of amide linkage with ester linkage leads to loss of thermo-responsive behavior. This suggests that amide plays a crucial role in thermo-responsive behavior of the amphiphiles. Thus, appropriate molecular design is essential to make the small molecular derivatives such as PDP-TEG as thermo-responsive amphiphiles.

5.3.4. Pyrene Encapsulation Studies

Fluorophore encapsulations provide direct evidence for mechanistic aspects of vesicle formation in water.[54, 55, 56,57, 58] Pyrene was chosen as fluorophore for the above purpose because of its well-known emission characteristics and its preferential occupation only at the hydrophobic layer of the vesicles. Pyrene encapsulation resembles the hydrophobic drug loading in vesicles for therapeutics, and therefore, the encapsulation studies in the synthetic MVBs might provide insight into the MVB formation mechanism as well as their potential future applications. The concentration of pyrene was fixed as 0.6 µM and the concentrations of the A-B amphiphiles were varied from 10^{-3}M to 10^{-6} M in water.[59] The emission spectra of blocks are shown in figure 5.15a and 5.15b. PDP-TEG showed sharp emission peaks with respect to its monomer emission (360- 420 nm) and additionally a broad excimer emission with maxima at 475 nm.[54, 55] The emission spectra of PDP-PEG-750 also showed the formation of excimer; however, the intensity was relatively less.

In general, pyrene does not form excimer at 0.6 µM since all molecules are completely isolated in water at this low probe concentration.[56,57] Therefore, the appearance of excimer in the presence of A-B amphiphiles (in water) was direct evidence for the encapsulation of pyrene molecules in the self-organized structure. The I_1/I_3 ratio of the monomer emission peaks were plotted against the concentration of the A-B di blocks (see in figure 5.15c). The I_1/I_3 value were obtained in the range of $1 < I_1/I_3 < 1.5$ which indicated the encapsulation of pyrenes in the hydrophobic

layer of the vesicles.[56] The break point in the I_1/I_3 plots was the direct measure of their critical vesicular concentration (CVC) and the CVCs of the PDP-TEG and PDP-PEG-750 were obtained as $1.0x10^{-4}$M and $1.0x10^{-5}$ M, respectively. Excitation spectra of the pyrene molecules collected at both monomer and excimer emission are shown in figures 5.15d and 5.15e, respectively. In figure 5.15d, two peaks appeared at 334 nm and 338 nm which were characteristics of pyrene monomer absorption in the hydrophilic and hydrophobic environment, respectively.[57] The excitation spectra shifted towards higher wavelength with the increase in the concentration of the di-block with a clear isosbectic point at 336 nm. This confirmed the encapsulation of more pyrene molecules in the hydrophobic layer of the diblock membrane with increase in the diblock concentration in water.

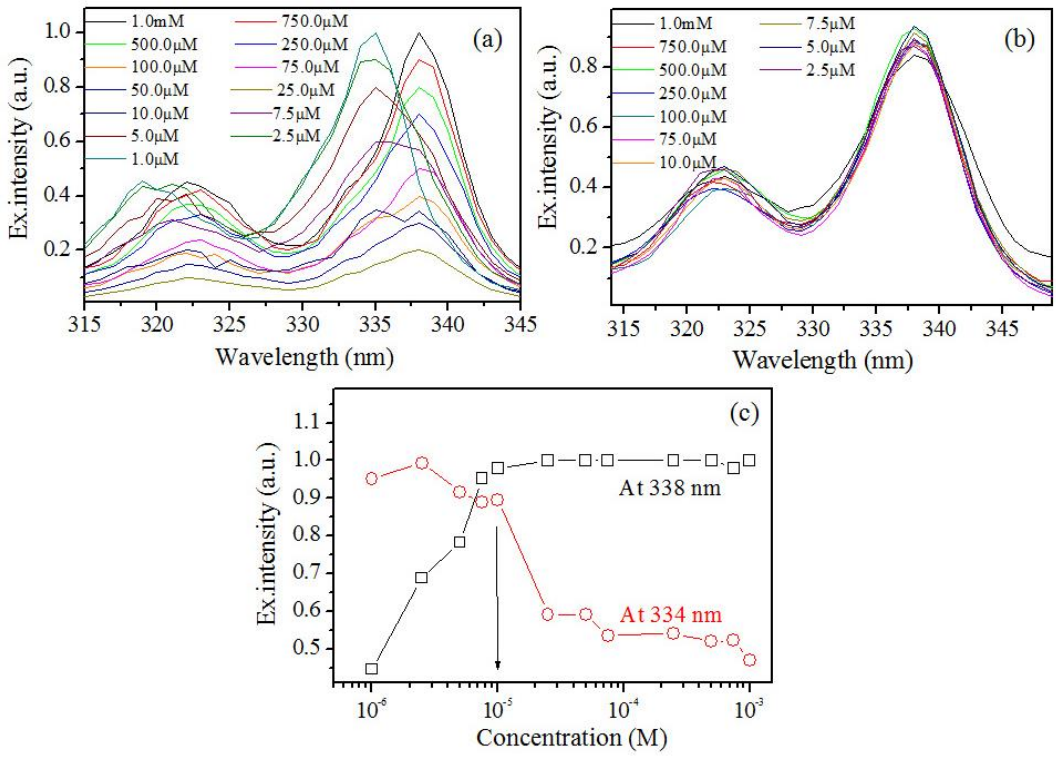

Figure 5.16. *Excitation spectra of PDP-PEG750 collected at monomer emission (a) and excimer emission (b).Excitation intensity at 334 nm and 338 nm (c).*

A similar observation was also found for the pyrene encapsulation in PDP-PEG-750 blocks (see figure 5.16). The plots of excitation intensity at 334 nm and 338 nm versus the concentration of the blocks showed break points at $1.0x10^{-4}$M and

$1.0x10^{-5}$ M for PDP-TEG (see figure 5.15f) and PDP-PEG-750 (see figure 5.16c), respectively. These break points were exactly same as that of the CVC values obtained based on I_1/I_3 ratio (see figure 5.15c). The one order magnitude difference in CVC values among the amphiphiles confirmed that the molecular self-organization of PDP-PEG-750 block (10^{-5} M) was stronger compared to that of PDP-TEG (10^{-4} M). These results were in accordance with the trend observed in DSC data and theoretical calculation, which once again confirmed the need for strong inter-chain interactions in the diblock membranes for MVBs in synthetic macromolecules.

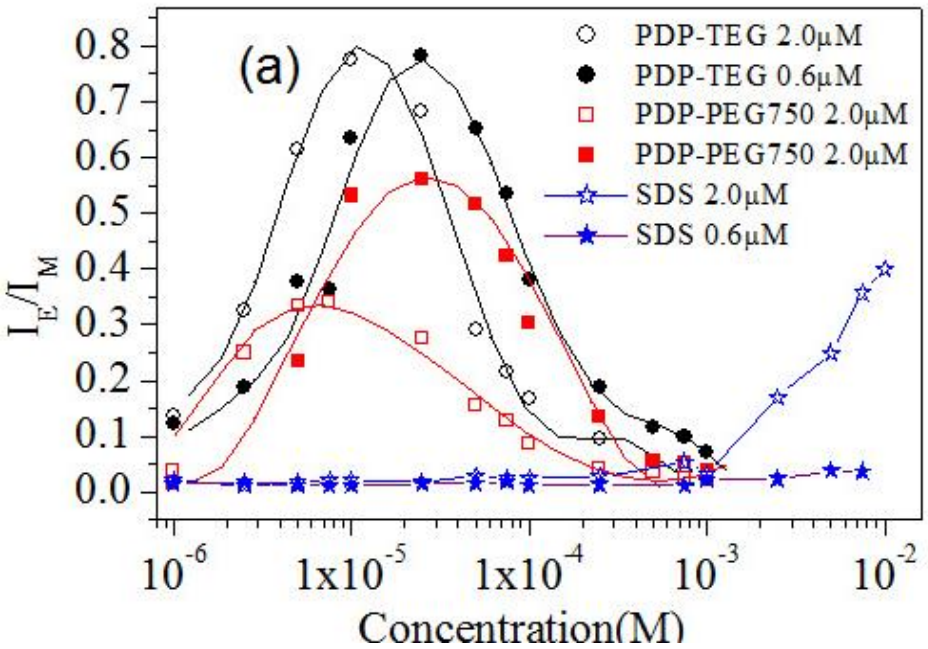

Figure 5.17. *Plot of I_E/I_M versus the concentration of the di-blocks and SDS.*

Dynamic excimers are formed between excited state monomer and ground state pyrene during the photo-excitation process. The excitation spectra collected at the excimer emission showed absorption at 338 nm with respect to pyrene monomer in ground state. This is the direct proof for the formation of pyrene dynamic excimer during their encapsulation in the hydrophobic layer of diblock membranes.[54] The intensities of the dynamic excimer emission were found to be highly sensitive to the concentration of the AB blocks in the solution. The ratio of PL intensities of excimer to monomer (I_E /I_M) was plotted against the concentration of the di blocks and shown

in figure 5.17. The plots showed an unusual nonlinear trend with the concentration of AB amphiphiles in water. The intensity of the dynamic excimer emission initially increased with the increase in the diblock concentration, reached a maximum and then decreased with further increase in di-block concentration. The magnitude of the intensity ratio (in Y-axis) was much higher for PDP-TEG blocks compared to that of its long PEG-chain block (PDP-PEG-750). This confirmed that the SUVs formation (from PDP-TEG) accompanied by strong pyrene excimer formation compared to that of the MVBs (from PDP-PEG-750). The comparison of I_E /I_M plots in figure 5.17 and figure 5.15c (also figure 5.15f), indicated that both the enhancement in the pyrene dynamic excimer formation and also its disappearance occurred much below their CVC of the amphiphiles.

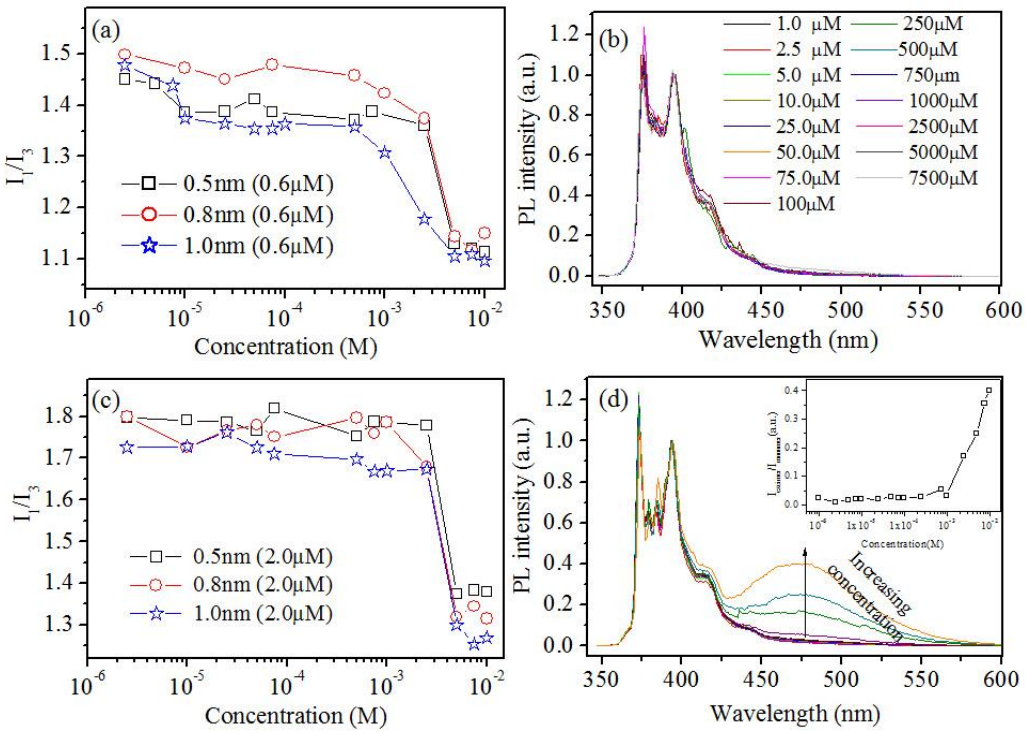

Figure 5.18. *Pyrene encapsulation in SDS micelles in PBS. (a)The I_1/I_3 values were obtained using different slit widths 1.0 nm, 0.8 nm and 0.5 nm at 0.6 μM of pyrene. (b)Emmision spectra of SDS at 0.6 μM of pyrene. (c) The I_1/I_3 values were obtained using different slit widths 1.0 nm, 0.8 nm and 0.5 nm at 2.0 μM of pyrene. (d) Emmision spectra of SDS at 2.0 μM of pyrene.*

To prove the unusual excimer formation of pyrene in the vesicular structure, a control experiment was carried out for pyrene encapsulation in sodium dodecyl sulfate (SDS) in PBS under identical conditions. Two concentration of pyrene (0.6 μM and 2.0 μM) were chosen for the encapsulation studies in SDS in PBS to determine their I_1/I_3 values with viable slit widths of 1.0 nm, 0.8 nm and 0.5 nm (see figure 5.18). For 0.6 μM of pyrene, I_1/I_3 values were obtained as I_1/I_3 = 1.5 below CMC and I_1/I_3 = 1.1 above CMC.[56] At higher pyrene concentration (2.0 μM), I_1/I_3 values were obtained as I_1/I_3 = 1.8 below CMC and I_1/I_3 = 1.2 above CMC.[60,61] In order to compare the encapsulation ability of of pyrene in the amphiphiles with SDS, 2.0 μM of pyrene was also encapsulated in the PDP-TEG and PDP-PEG-750 and their data are given in figure 5.19.

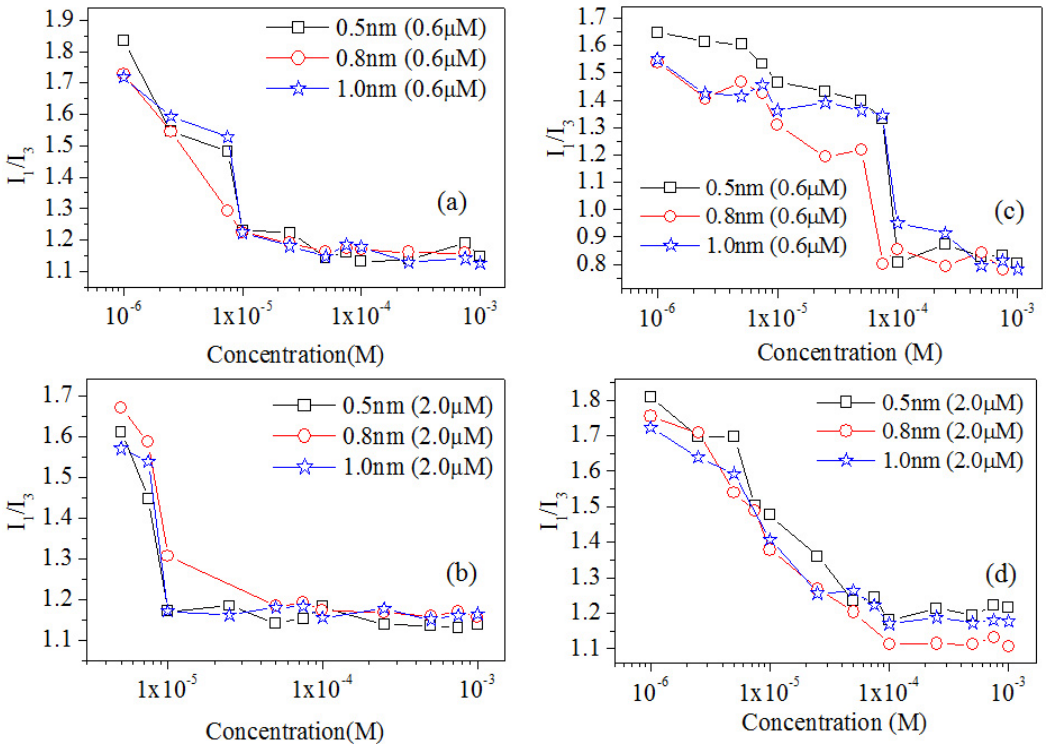

Figure 5.19.*Pyrene encapsulation in PDP-TEG and PDP-PEG-750s in PBS. (a)The I_1/I_3 values were obtained for PDP-PEG-750 using different slit widths 1.0 nm, 0.8 nm and 0.5 nm at (a) 0.6 μM (b) 2.0 μM of pyrene.(c) The I_1/I_3 values were obtained for PDP-TEG using different slit widths 1.0 nm, 0.8 nm and 0.5 nm at (c)0.6 μM (d) 2.0 μM of pyrene.*

In all the cases the I_1/I_3 values increase with the decrease in slid widths and also showed non-linear trend with clear CMC (or CVC). Further, to compare the excimer formation ability of pyrene in SDS with the new amphiphiles, the I_E /I_M ratios were plotted for both 0.6 μM and 2.0 μM concentration (see figure 5.17). At lower concentration (0.6 μM), the pyrene molecules did not form excimer at the all the concentration of SDS (see figure 5.18). On the other hand, excimer formation was observed for 2.0 μM concentration of pyrene in SDS above CMC. On the other hand, the newly designed amphiphiles PDP-TEG and PDP-PEG-750 pyrene excimer formation for both 0.6 μM and 2.0 μM of pyrene. Further, the newly designed amphiphiles followed as unusual trend in the excimer formation with maxima below CVC. The reason for this trend may be attributed to the variation in the self-organization behavior of vesicular structure formation and encapsulation of pyrene in the new amphiphiles compared to that of the SDS micelles.

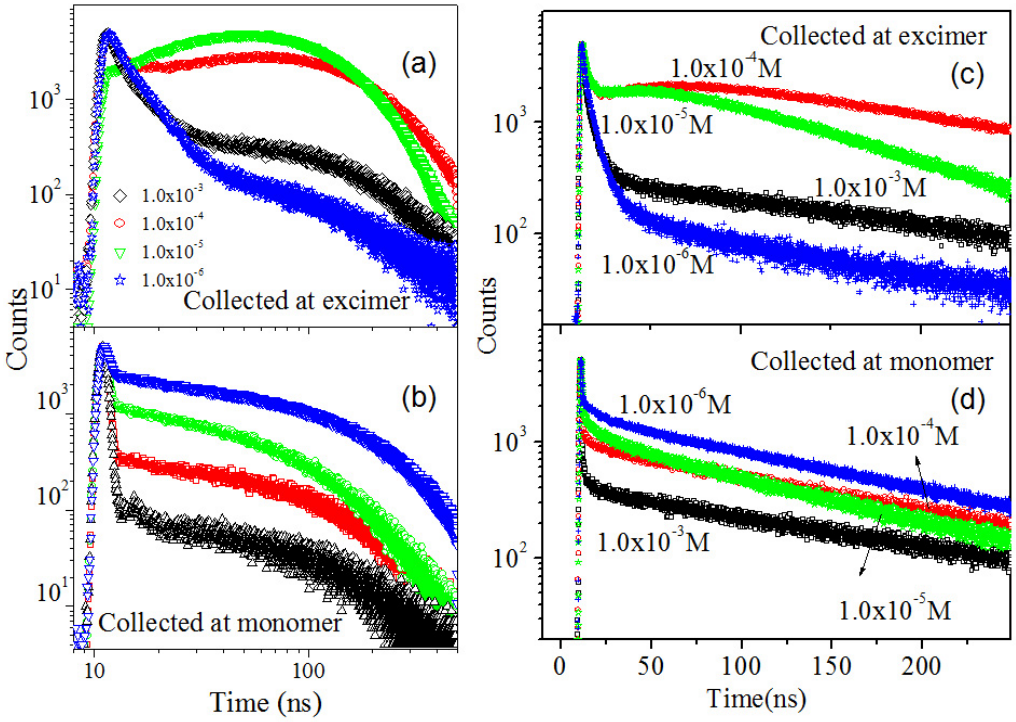

Figure 5.20. *TCSPC fluorescent decay profiles of pyrene encapsulated in PDP-TEG collected at excimer (a) and monomer (b) emission. TCSPC fluorescent decay profiles of pyrene encapsulated in PDP-PEG-750 collected at excimer (c) and monomer (d) emission (excited with 337 nm LED laser source).*

To further confirm these unusual excimer trends, fluorescent decay profiles of pyrene were investigated by TCSPC techniques. The fluorescent decay profiles were collected at both monomer emission (at 375 nm) and excimer emission (at 475 nm) using a nano-LED laser source with 339 nm excitation wavelength. Pyrene fluorescent decay profiles at different PDP-TEG concentration (from 10^{-3} to 10^{-6}M) are shown in figure 5.20a and 5.20b. Similarly, the decay profiles of pyrene at different PDP-PEG-750 concentration were obtained (see figure 5.20c and 5.20d). The decay profiles were fitted by bi- or tri-exponential decay fits and the lifetime data for both PDP-TEG and PDP-PEG-750 are shown in table -5.3. The initial building up of the decay curve at $1x10^{-5}$ M is the typical nature of the dynamic pyrene excimer formation.[62,63] The decay profile of pyrene collected at monomer emission (see figure 5.20b) showed drastic change with the increase in the AB diblock concentration in water. This trend was attributed to the self-quenching of pyrene monomers while the diblock membranes approached towards the CVC.[64] Hence, the encapsulation of pyrene molecules in the hydrophobic layer of the diblock membrane occurred in a step-wise manner which primarily controlled by self-organization of A-B amphiphiles in water. Although the excimer decay appeared to show a pronounced rise time, it seemed that the decays did not go down to zero at t = 0, which was a condition for excimer formation by diffusion.

All excimer decays showed a short decay time observed often when pyrene aggregates were present, but at diblock concentrations of 10^{-5} M and 10^{-4} M where pyrene was concentrated in a few hydrophobic domains, excimer was also formed by diffusion.[54] This was demonstrated in table-5.3 by normalizing the pre-exponential factors and calculated the *A*E-/*A*E+ ratios where the ratio of the sum of the negative pre-exponential factors divided by that of the positive pre-exponential factors, namely the *A*E-/*A*E+ ratio. The monomer decays showed a very short decay time (τ_1< 0.1 ns) due to residual light scattering. It is worth noting that longer decay times were obtained for the monomer and excimer decays for the PDP-PEG750 samples.

Long decay times indicate that quenching of pyrene by oxygen in the air was hindered in the tightly packed PDP-PEG750 vesicle membranes.

Table5.3. *Fluorescence decay life time data for PDP-TEG block. The values in the parenthesis are corresponding to amplitude of the exponential decay times.*

PDP-TEG								
Concentration of A-B diblock	**Collected at excimer emission**				A_E/A_{E+}	**Collected at Monomer emission**		
	τ_1 (ns)	**τ_2 (ns)**	**τ_3 (ns)**	**χ^2**		**τ_1 (ns)**	**τ_2 (ns)**	**χ^2**
$1.0x10^{-3}$ M	0.9 (0.01)	4.6 (0.14)	157.0 (0.85)	1.16	0	0.003 (100)	112 (0.0)	1.17
$1.0x10^{-4}$ M	2.2 (0.01)	41.0 (-0.25)	121.0 (0.99)	1.2	-0.25	19.7 (12.0)	120.0 (88.0)	1.12
$1.0x10^{-5}$ M	30.0 (-0.22)	51.2 (-0.03)	72.0 (1.00)	1.13	-0.25	5.98 (37.6)	135.0 (62.3)	1.08
$1.0x10^{-6}$ M	1.3 (0.16)	5.8 (0.41)	104 (0.43)	1.09	0	9.73 (2.1)	138 (97.8)	1.07
PDP-PEG-750								
$1.0x10^{-3}$ M	1.1 (0.09)	5.4 (0.15)	190.0 (0.76)	1.01	0	0.003 (100)	112 (0.0)	1.17
$1.0x10^{-4}$ M	2.7 (0.02)	41.7 (-0.18)	154.0 (0.98)	1.16	-0.25	19.7 (12.0)	120.0 (88.0)	1.12
$1.0x10^{-5}$ M	2.7 (0.04)	29.6 (-0.22)	85.0 (0.96)	1.17	-0.25	5.98 (37.6)	135.0 (62.3)	1.08
$1.0x10^{-6}$ M	1.9 (0.12)	61.0 (0.28)	110 (0.60)	1.11	0	9.73 (2.1)	138 (97.8)	1.07

In order to explain the trend in the I_E/I_M ratio of pyrene chromophore in the SUVs and MVBs (in figure 5.17), the models developed by Cuniberti et al.[65] and Duhamel co-workers[66,67,68] for pyrene labelled polymers were utilized. The I_E/I_M ratio was correlated to excimer formation parameters as shown in equation 4:

$$I_E / I_M = \kappa [\phi^\circ_E / \phi^\circ_M] \tau_M k_1[Py]_{loc} \quad (4)$$

where κ is a constant that depends on the geometry and sensitivity of the spectrofluorometer, ϕ°_E and ϕ°_M are the fluorescence quantum yields of the pyrene monomer and excimer, respectively; τ_M is the natural lifetime of the pyrene

monomer. The other two parameters k_1 and $[Py]_{loc}$ represent the rate constant of excimer formation and the local pyrene concentration, respectively. Since the parametersκ, $\phi^{\circ}_{E,}$ ϕ°_{M} andτ_M are constants and do not vary with the types of the amphiphiles (either PDP-TEG and PDP-PEG-750), it may be assumed that the trend in the I_E /I_M ratio in figure 6a was directly influenced by k_1 and$[Py]_{loc.}$[69]As illustrated by the Duhamel co-workers, the values k_1 could be experimentally determined by the expression: $k_1 = \{1/\langle\tau\rangle\} - \{1/\tau_M\}$, where $\langle\tau\rangle = \sum a_i\tau_i / \sum a_i$ is corresponding to the number average life time for those pyrenes form excimer via diffusion.[70,71] The rate constant k_1 for the excimer formation was calculated based on excimer life times (see table 5.3) and using the pyrene monomer life time, τ_M = 168 ns as in earlier reported.[58] The excimer rate constant values aregiven in the tables 5.4

Table5.4.*Excimer formation rate constant calculations for PDP-TEG and PDP-PEG-750.*

PDP-TEG						
Concentration	$\sum a_i \tau_i$	$\sum a_i$	$\langle\tau\rangle = \sum a_i \tau_i/\sum a_i$	$1/\langle\tau\rangle$	$1/\tau_M$	$k_1=1/\langle\tau\rangle - 1/\tau_M$
1×10^{-3} M	134.103	1	134.10×10^{-9}	7.46×10^{6}	5.95×10^{6}	1.51
1×10^{-4} M	109.562	0.75	146.03×10^{-9}	6.847×10^{6}	5.95×10^{6}	0.897
1×10^{-5} M	63.864	0.75	85.152×10^{-9}	11.7×10^{6}	5.95×10^{6}	5.75
1×10^{-6} M	47.306	1	47.306×10^{-9}	52.1×10^{6}	5.95×10^{6}	15.15
PDP-PEG-750						
1×10^{-3} M	144.909	1	144.90×10^{-9}	6.90×10^{6}	5.95×10^{6}	0.95
1×10^{-4} M	143.47	0.82	174.96×10^{-9}	5.715×10^{6}	5.95×10^{6}	-0.24
1×10^{-5} M	75.196	0.78	96.405×10^{-9}	10.3×10^{6}	5.95×10^{6}	4.35
1×10^{-6} M	83.308	1	83.308×10^{-9}	12.0×10^{6}	5.95×10^{6}	6.05

The excimer formation rate constant k_1 was plotted against the concentration of the PDP-TEG and PDP-PEG-750 and shown in figure 5.21. Two observations are very clear from these plots. First, the excimer rate constants decreased with the increase in the di-block concentration. This trend was attributed to the hindrance caused for the free diffusion of pyrene monomer by amphiphiles. Secondly, at low di-block concentration (below 10^{-5}M), the excimer rate constant for the PDP-TEG was found to be almost two times higher than that of PDP-PEG-750. This was attributed to the difference in the rigidity of the diblock membranes. The PDP-PEG-750 was found to be much more rigid compared to the PDP-TEG (evident from DSC data, table 5.2), and therefore, the more rigid polymer chains provide less possibility for the pyrene monomer diffusion in the encapsulated membrane layer. Therefore, the larger variation in extent of I_E /I_M ratio (Y-axis) at lower diblock concentrations infigure 5.17 was directly controlled by the rigidity of the di-block membranes.

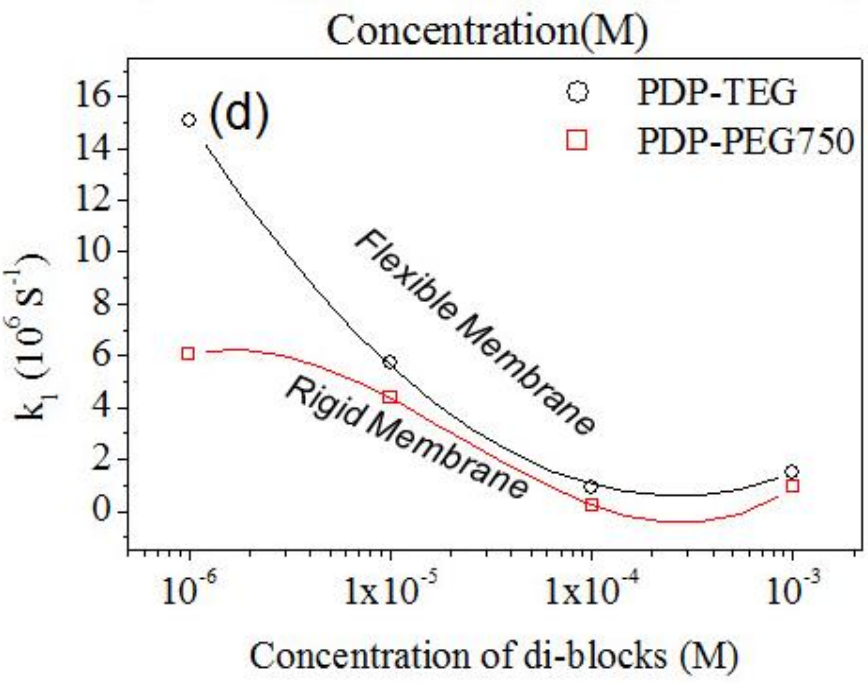

Figure 5.21. *Plots of excimer formation rate constant (k_1) versus the concentration of the amphiphiles (d).*

Typically, the rigid backbone are tightly packed and expected to hinder the diffusion of the pyrene monomers in the hydrophobic vesicular layer. As a result, the

MVBs were produced by the PDP-PEG-750 showed feeble pyrene excimer emission due to the less probability for the overlap of the excited pyrene with ground state monomers. On the other hand, in the more flexible PDP-TEG (produced SUVs), the excimer formation was promoted by the close vicinity of the pyrene molecules. It is also important to mention that the I_E /I_M ratio (in equation 4) was also influenced by the local pyrene concentration $[Py]_{loc}$. In the present case, due to the non-availability of theoretical model it is very difficult to determine the $[Py]_{loc}$ using the the known expressions for the pyrene substituted polymers.[66] Since, the surface area of the MVBs and SUVs are significant different (see figure 5.13), one may anticipate that utilization of more pyrene molecules may show significant difference in their encapsulation capabilities. For example, the surface area of MVBS are eight time higher than that of SUVs, and therefore, more pyrene molecules could be accommodated in the MVBs compared to latter. To check this hypothesis, two concentrations of pyrene molecules were utilized for the encapsulation (0.6 μM and 2.0 μM) (see excimer peaksfigure 5.22a and 5.22b).

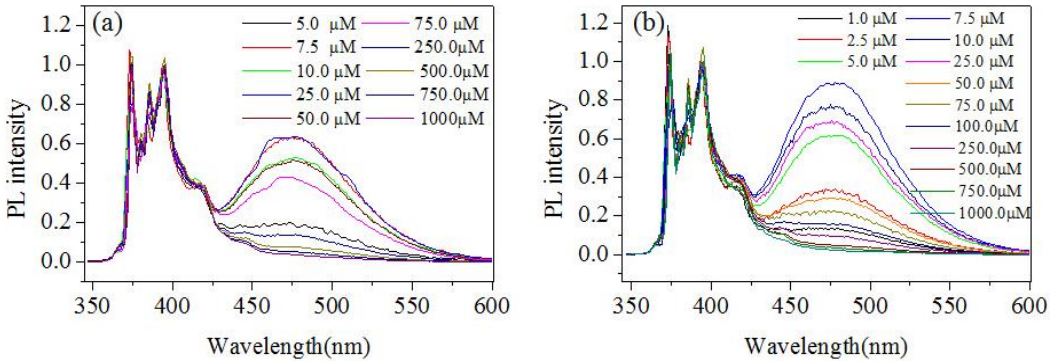

Figure 5.22. *Emission spectra of PDP-PEG-750 (a)and PDP-TEG(b) using 2.0 μM pyrene in PBS. Excitationa nd emision slit widths are 1.0 nm.*

With increase in the pyrene concentration from 0.6 μM and 2.0 μM, the $[Py]_{loc}$ concentration was also expected to increase in the vesicular membrance upon more encapsulation. The I_E /I_M ratio increased almost twice in PDP-PEG-750 with increase in the loading of pyrene from 0.6 μM at 2.0 μM in the feed. Interestingly, the I_E /I_M ratio did not show any major changes in the PDP-TEG which was

attributed to the availability of low surface area of its vesicular membranes. Hence, it the increase in the I_E /I_M ratio in PDP-PEG-750 at higher pyrene incorporation may be attributed to the increase in the $[Py]_{loc}$ concentration. Nevertheless, in the preset investigation, the difference in the encapsulations of pyrene molecules into SUVs orMVBs were demonstrated very well by detailed photophysical studies. These studies revealed that rigid diblock membrane PDP-PEG-750 (mother of MVBs) distributed the pyrene molecules uniformly in the larger hydrophobic layer. This observation could be very useful for encapsulation of hydrophobic guest molecules like pyrene (or drugs) could be in the MVBs for future applications in loading and delivering of polyaromatic molecules for therapeutics in polymer based drug deliveries.

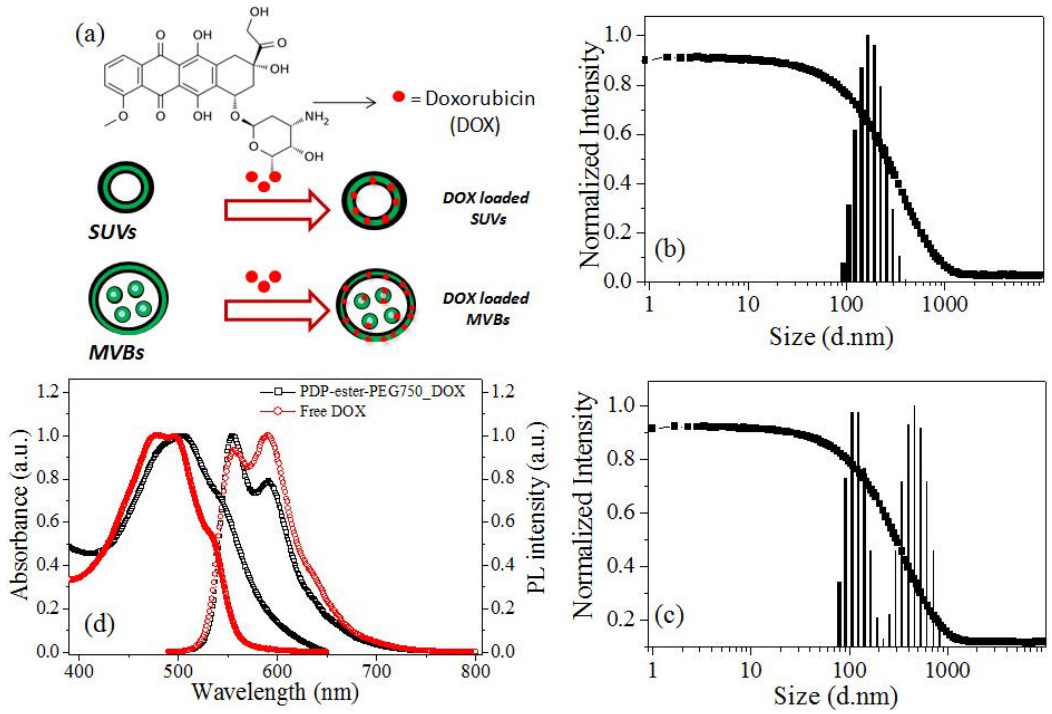

Figure 5.23.*(a) Schematic representation of encapsulation of hydrophobic anti-cancer drug, doxorubicin in SUVs and MVBs. DLS histogram of DOX loaded (b) SUVs and (c) MVBs. (d) Absorbance and emission spectra of free DOX and DOX loaded MVBs.*

5.3.5. Anticancer Drug Encapsulation

In order to understand the drug encapsulation capabilities of MVBs and SUVs, anticancer drugs doxorubicin was encapsulated in the hydrophobic layer of the vesicles. The drugs were encapsulated in the hydrophobic layer of the both MVBs and SUVs by dialysis method. The drug loading content was estimated using absorbance spectroscopy as 2.3wt% and 0.6 wt% for MVB and SUV, respectively. The sizes of the DOX loaded SUVs and MVBs were determined by DLS. The size of DOX loaded SUVs was found to be 170 nm. On the other hand, DOX loaded MVBs showed bimodal distribution having vesicles of sizes 105nm and 450nm (see figure 5.23b and 5.23c). The sizes of the drug loaded vesicles was similar to that of the nascent ones (see figure 5.8a) indicating that the scaffold retained its self-organization even after the encapsulation of hydrophobic drugs. As DOX is fluorescent in nature; the drug loaded vesicles were subjected for photophysical studies in order to elucidate their property in free and encapsulated states. Absorbance and emission spectra of free DOX as well as DOX loaded MVBs were recorded in water and are shown in figure 5.23d. The absorbance and emission spectra of DOX (see figure 5.23d) did not show any variation upon encapsulation as compared to free DOX.

5.3.6. *In vitro* Drug Release Studies

Further, drug release of DOX loaded vesicles were studied under physiological conditions (PBS, pH =7.4). DOX loaded MVBs and SUVs were incubated at 37 °C in PBS (pH =7.4) and the release kinetics of DOX in both the cases was studied. The cumulative release profile of DOX loaded MVBs and SUVs at 37 °C in PBS having pH= 7.4 are shown in figure 5.24a and 5.24 b, respectively. The percentage release of DOX at in case of SUVs reaches 90 % within 8h. This indicates that SUVs are not stable under physiological conditions (see figure 5.24 a). On the other hand, release of DOX in case of MVBs occurred in two steps. In first step, 30% of DOX was released in 2h, which reaches 60 % in second step i.e. 12h. Thus, it suggests that DOX is present in both outer bigger vesicles as well as in intra-

luminal vesicles. And since, first the DOX is released from the outer vesicles and then from the inner intra-luminal vesicles two steps were observed in the release profile of MVBs (see figure 5.24b).

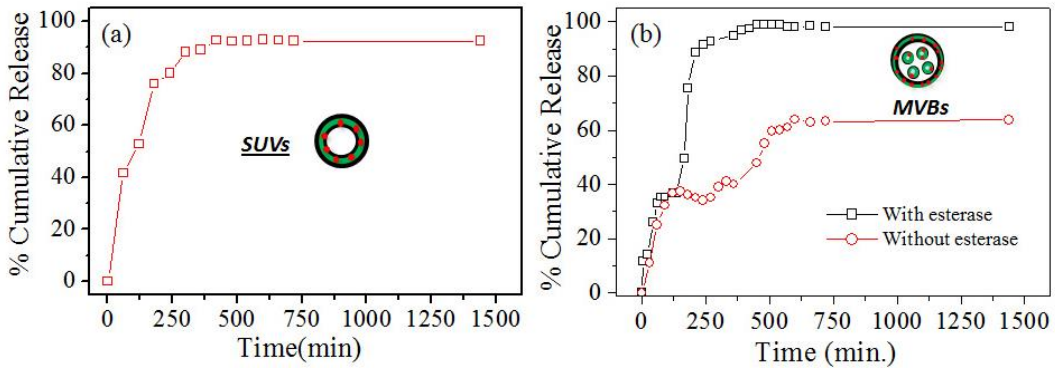

Figure 5.24.*Cumulative release profile of DOX loaded (a) SUVs and (b) MVBs scaffolds under physiological conditions (PBS, pH =7.4). The cumulative release profile of MVBs were also carried out in presence and absence of esterase enzyme.*

Similarly, enzyme-responsive drug release profile of DOX in case of MVBs was also performed under physiological conditions (PBS, pH =7.4). 10 U of esterase enzyme obtained from horse liver was used to study the release behavior of DOX loaded scaffold. DOX loaded MVBs were incubated at 37 °C in PBS (pH =7.4) and the cumulative release profile of DOX loaded scaffold in presence of enzyme at 37 °C in PBS (pH =7.4) are shown in figure 5.24b. In the presence of esterase enzyme also, the release profile showed two steps. In the initial first step only 30 % of the drug was released in 2h (similar to drug release profile in absence of esterase enzyme), which was followed by release of more than 90 % of the drug from the MVBs in 8h (see figure 5.24b). This suggested that ester linkage present in the outer bilayer was first exposed to esterase enzyme. As a result ester linkage gets chopped off which in turn leads to breaking down of the self-assembly leading to release of DOX from the MVBs. Subsequently, the ester linkage present in the hydrophobic bilayer of the inner intra-luminal vesicles was chopped off by the enzyme and the DOX was released. Thus, it was found that release of DOX from the MVBs was release enzyme-driven process.

5.4. Conclusion

In conclusion, new classes of AB diblock amphiphilic block copolymers based on renewable resource hydrophobic rigid unit and different hydrophilic PEG content were designed for mimicking MVBs in synthetic macromolecules. The rigid hydrophobic units formed very stable unilamellar through inter-digitation of alkyl tails which was confirmed by single crystal structures. Longer PEG-750 chain induced strong inter-chain packing in the diblock membrane; as a result of which they underwent inward curvature to form stomatocytes wchich further invaginated to produce MVBs containing almost ten intraluminal vesicles of 45-50 nm in diameter. Amphiphiles with short TEG hydrophilic units produced smaller unilamellar vesicles(SUVs) through outward budding. Theoretical models were adopted to determine the structural parameters such as relative volume (v_e) and reduced area difference (Δa_o) and very good correlation between the theory and experimental results were obtained. The difference in the diblock molecular self-organization was further confirmed by the DSC analysis and determination of their critical vesicular association (CVC). Pyrene encapsulation studies showed unusual non-linear trend in the dynamic excimer formation of the self-organized amphiphiles. Controlled experiments were also carried out for SDS and pyrene to trace the factors which govern the vesicular membrane formation of the custom designed amphiphiles. The drug loading and delivering capabilities of both MVBs and SUVs were determined. Both loaded doxorubicin successfully in their hydrophobic layer. Further the drug release kinetics of DOX from both SUVs and MVBs were studied in presence and absence of esterase enzymes. And it was found that SUVs were not stable under physiological conditions since it released more that 90 % of the DOX at pH = 7.4. On the other hand, MVBs showed two step DOX release profile both in absence and presence of esterase enzyme. The encapsulation capabilities of MVBs were found to be very unique in that the molecules were trapped uniformly throughout the hydrophobic layer of both outer and inner vesicular structures However, both SUVs and MVBs were not thermo-responsive in nature. Thus, replacement of amide linkage with ester bonds leads to loss of thermo-responsive behavior.

5.5. References

1. Klaikherd, A.; Nagamani, C.; Thayumanavan, S. *J. Am. Chem. Soc.***2009**, 131, 4830–4838.
2. Zhang, S. *Nat. Biotec.* **2003**, 21, 1171-1178.
3. Orive, G.; Hernandez, R. M.; Gascon, A. R.; Domınguez-Gily, A.; Pedraz, J. L. *Curr. Opin. Biotec.* **2003**, 14, 659-664.
4. Ge, Z.; Liu, S. Chem. Soc. Rev. 2013, 42, 7289-7325.
5. Jones, M.-C.; Leroux, J.-C. *Eur. J. Pharm. Biopharm.* **1999**, 48, 101-111.
6. Ahmad, Z.; Shah, A.; Siddiq, M.; Kraatz, H.-B. *RSC Adv.* **2014**, 4, 17028-17038.
7. Kwon, G.; Okano, T. *Adv. Drug Deliv. Rev.***1996**, 21, 107-116.
8. Lee, J. S.; Feijen, J. *J. Control. Release* **2012**,161, 473-483.
9. Malam, Y.; Loizidou, M.; Seifalian,A. M. *Trends Pharmacol. Sci.* **2009**,30, 592-599.
10. Fang, J.; Nakamura, H.; Maeda, H. *Adv. Drug Delivery. Rev.* **2011**, 63, 136-151.
11. Maruyama, K. *Adv. Drug Delivery. Rev.***2011**, 63, 161-169.
12. Ringsdorf, H.; Schlarb, B.; Venzmer, J. *Angew. Chem. Int. Ed.***1988**, 27, 113–158.
13. Wang, C; Wang, Z.; Zhang, X. *Acc. Chem. Res.***2012**, 45, 608-618.
14. Gibbings, D. J.; Ciaudo, C.; Erhardt, M.; Voinnet, O. *Nature Cell Biol*. **2009**, *11*, 1143-1149.
15. Raiborg, C.; Rusten, T. E.; Stenmark, H. *Curr. Opin. Cell Biol.* **2003**, *15*, 446-455.
16. Hurley, J. H.; Boura, E.; Carlson, L. A.; Rozycki. B. *Cell* **2010**, 143, 875-887
17. Davies, B. A.; Lee, J. R. E.; Oestreich, A. J.; Katzmann, D. J. *Chem. Rev*. **2009**, *109*, 1575-1586.
18. Tran, J. H.; Chen, C. J.; Emr, S.; Schekman, R. *Proc. Natl. Acad. Sci.* **2009**, *106*, 17395-17400.
19. Wollert, T.; Hurley, J.H. *Nature*, **2010**, *464*, 864-869

20. Babst, M. *Curr. Opin. Cell Biol.* **2011**, *23*, 452-457.
21. Ludwig, A. K.; Geibel, B.*Int. J. Biochem. Cell Biol.* **2012**, *44*, 11-15. (b) Lassic, D. D.; *Biochem. J.* **1988**, 256, 1-11.
22. Murakami, Y.; Nakano, A.; Fukuya, K. *J. Am. Chem. Soc*., **1980**, *102*, 4253-4254.
23. Boyer, C.; Zasadzinski, J. A. *ACS Nano*., **2007**, *3*, 176-182.
24. Richard, A.; Marchi-Artzner, V.; Lalloz, M-N.; Brienne, M-J.; Artzner, F.; Gulik-Krzywicki, T.; Guedeau-Boudeville, M-A.; Lehn, J-M. *Proc. Nat. Acad. Sci.*,**2004**, *101*, 15279-15284.
25. Jeon, Y. J.; Bharadwaj, P. K.; Choi, S. W.; Lee, J. W.; Kim, K. *Angew. Chem. Int. Ed.***2002**, *41*, 4474-4476.
26. Nalluri, S. K. M.; Ravoo, B. J. *Angew. Chem. Int. Ed.***2010**, *49*, 5371-5374.
27. Azagarsamy, M. A.; Sokkalingam, P.; Thayumanavan, S. *J. Am. Chem. Soc*., **2009**, *131*, 14184-14185.
28. Tao, W.; Liu, Y.; Jiang, B.; Yu, S.; Haung, W.; Zhou, Y.; Yan, D. *J. Am. Chem. Soc*., **2012**, *134*, 762-764.
29. Balachandran, V. S.; Jadhav, S. R.; Pradhan, P.; Carlo, S. D.; John, G.*Angew. Chem. Int. Ed.* **2010**, *49, 9509-9512.*
30. Koback, M. A.; Keating, C. D.*J. Am. Chem. Soc.***2011**, *133*, 9545-9555.
31. Meledandri, C.J.; Perlo, J.; Farrher, E.; Brougham, D.F.; Anoardo, E. *J. Phys. Chem. B***2009**, *113*, 15532-15540.
32. Mahabir, S.; Wan, W.; Katsaras, J.; Nieh, M.P. *J. Phys. Chem. B***2010**, *114*, 5729-5735.
33. Tanaka, T.; Yamazaki,M.*Langmuir*, **2004**, *20*, 5160-5164.
34. Zhou, Y.; Yan, D.*Angew. Chem. Int. Ed.* **2005**, *44*, 3223-3226.
35. Cans, Koback, A. S.; M. A.; Keating, C. D. *J. Am. Chem. Soc.***2008**, *130*, 7400-7406.
36. Ghosh, S.; Reches, M.; Gazit, E.; Verma, S. *Angew. Chem. Int. Ed.* **2007**, *46*, 2002-2004.
37. Ghosh, S.; Verma, S.*Chem. Eur. J.* **2008**, *14*, 1415-1419.

38. Barbetta, A.; Pucci, C.; Tardani, F.; Andreozzi, P.; Mesa, C. L. *J. Phys. Chem. B***2011**, *115*, 12751-12758.
39. Scholtysek, P.; Achilles, A.; Hoffmann, C.V.; Lechner, B.D.; Meister, A.; Tschierske, C.; Saalwachter, K.; Edwards, K.; Blume, A. *J. Phys. Chem. B***2012**, *116*, 4871-4878.
40. Smith, A.E.; Xu, X.; York, S. E. K.; Savin, D.A.; McCormick, C.L. *Macromolecules***2010**, *43*,1210-1217.
41. Sun, V. Z.; Deming, T. J.; Kamei, D. T. *Biomacromolecules***2011**, *12*, 10-13.
42. Chen, Z. X.; Su, X. X.; Deng, S. P. *J. Phys. Chem. B***2011**, *115*, 1798-1806.
43. Chiu, H. C.; Lin, Y. W.; Huang, Y. F.; Chuang, C. K.; Chern, C. S.*Angew. Chem. Int. Ed.* **2008**, *47*, 1875-1878.
44. Gao, W. P.; Bai, Y.; Chen, E. Q.; Li, Z. C.; Han, B. Y.; Yang, W. T.; Zhou, Q. F.*Macromolecules*, **2006**, *39*, 4894-4898.
45. Lorenceau, E.; Utada, A. S.; Link, D. R.; Cristobal, G.; Joniact, M.; Weitz, D. A. *Langmuir*, **2005**, *21*, 9183-9186.
46. Pozzi, G.; Birault, V.; Werner, B.; Dannenmuller, O.; Nakatani, Y.; Ourisson, G.; Terakawa, S. *Angew. Chem. Int.Ed. Engl.* **1996**, *35*, 177-180.
47. Meeuwissen, S. A.; Kim, K. T.; Chen, Y.; Pochan, D. J.; van Hest, J. C. M. *Angew. Chem. Int. Ed.*,**2011**, *50*, 7070-7073.
48. Jin, Q.; Liu, G.; Liu, X.; Ji, J. *Soft Matter*, **2010**, *6*, 5589-5595.
49. Smith, L. A.; Hammond, R. B.; Roberts, K. J.; Machin, D.; McLeod, G. *J. Mol. Struct.***2000**, *554*, 173-182.
50. Smith, L. A.; Thomson, G. B.; Roberts, K. J.; Machin, D.; McLeod, G. *Crys. Growth Design*, **2005**, *5*, 2164-2172.
51. Antoneitti, M.; Forster, S. *Adv.Mater*. **2003**, *15*, 1323-1333.
52. Seifert, U.; Berndl, K.; Lipowsky, R. *Phys. Rev. A* **1991**, *44*, 1182-1202.
53. Mui, B. L. S.; Dobereiner, H. G.; Madden, T. D.; Cullis, P. R.*Biophys. J.* **1995**, *69*, 930-941.
54. Winnik, F. M.*Chem. Rev.* **1993**, *93*, 587-614.

55. Baig, C. K.; Duhamel, J.; Fung, S. Y.; Bezaire, J.; Chen, P. *J. Am. Chem. Soc.* **2004**, *126*, 7522-7532.
56. Kalyanasundaram, K.; Thomas, J. K. *J. Am. Chem. Soc.* **1977**, *99*, 2039-2044.
57. Kawaguchi, S.; Yekta, A.; Duhamel, J.; Winnik, M. A. *J. Phys. Chem.* **1994**, *98*, 7891-7898.
58. Duhamel, J.; Yekta, A.; Winnik, M. A. *J. Phys. Chem*. **1993**, *97*, 2759-2763.
59. Changez, Kang, M.; N. G.; Lee, C.H.; Lee, J. S. *Small*, **2010**, *6*, 63-68.
60. Dong, D. C.; Winnik, M. A. *Photochem. Photobio*,**1982**, *35*, 17-21.
61. Dong, D. C.; Winnik, M. A. *Can. J. Chem*. **1984**, *62*, 2560-2565.
62. Costa, T.; Melo, J. S. S. D.; Castro, C. S.; Gago, S.; Pillinger, M.; Goncalves, I. S. *J. Phys. Chem.B.* **2010**, *114*, 12439-12447.
63. Kaushlendra, K.; Deepak, V. D.; Asha, S. K. *J. Polym. Sci. Part A: Polym. Chem.***2011**, *49*, 1678-1690.
64. Vanderkooi, J. M.; Callis, J. B. *Biochemistry*, **1974**, *19*, 4000-4006.
65. Cuniberti, C.; Perico, A. *Eur. Polym. J*. **1980**, *16*, 887-893.
66. Duhamel, J. *Acc. Chem. Res*. 2006, 39, 953-960.
67. Yip, J.; Duhamel, J.; Qiu, X. P.; Winnik, F. M. *Can. J. Chem*. **2011**, *89*, 163-172.
68. Teertstra, S. J.; Lin, W. Y.; Gautheir, M.; Ingratta, M.; Duhamel, J. *Polymer*, **2009**, *50*, 5456-5466.
69. Ingratta, M.; Hollinger, J.; Duhamel, J. *J. Am. Chem.Soc*. **2008**, *130*, 9420-9428.
70. Ingratta, M.; Duhamel, J. *J. Phys. Chem. B*. **2008**, *112*, 9209-9218.
71. Yip, J.; Duhamel, J.; Bahun, G. J.; Adronov, A. *J. Phys. Chem. B.***2010**, *114*, 10254-10

Summary and Future Directions

The thesis entitled **"*Thermo-Responsive Small and Polymeric Amphiphiles for Drug Delivery*"** deals with design and development of thermo-responsive small and polymeric amphiphilic molecules from renewable resource Cashew Nut Shell liquid (CNSL) based pentadecyl phenol (PDP) conjugated to highly biocompatible and biodegradable oligoethylene glycol for targeted drug delivery. The thesis is focused to develop small amphiphilic molecule based shape tunable core-shell nanoparticles in order to understand the drug loading and delivering mechanisms of thermo-responsive nanocarriers in tumor microenvironment. The knowledge gained from small amphiphile based thermo-responsive nanocarriers was utilized to design polymeric nanovehicles sensitive temperature and enzyme. Efforts were also put to study the effect of anions present in body fluids on the temperature sensitivity and drug delivering efficacy of the nanocarriers. Also, the role of amide and ester linkage in the thermal responsiveness of the amphiphilic scaffold was analysed.

The efficiency of temperature induced shape transformable nanocarriers with respect to loading and delivery of anti-cancer drugs was investigated. For this purpose, a new amphiphilic molecule consisting of hydrogen bonded amide linkage flanked between hydrophobic renewable resource 3-pendadecylphenol and hydrophilic oligoethylene glycols was custom designed. The amide-linkage acted as a self-organization director with respect to temperature induced phase-separation phenomena exhibited by amphiphilic scaffold. The amphiphilic scaffold self-assembled to form three dimensional core-shell nanoparticles at ambient temperature which transforms into one-dimensional rod-like nanoparticles at temperature close to cancer tissue temperature. The temperature induced *in-situ* transformation was confirmed by light scattering studies, electron microscopy, atomic force microscopy, variable temperature NMR and single crystal structure studies. The thermo-responsive core-shell nanoparticles efficiently encapsulated anticancer drugs, doxorubicin (DOX) and camptothecin (CPT) in their inner core. The shape transformation ability of the amphiphilic scaffold was retained after drug encapsulation, which was confirmed by electron microscopy and atomic force microscopy studies. The in-vitro drug release profile of DOX carried out at

temperature close to cancer tissue temperature revealed that DOX loaded scaffold was found to follow non-Fickian diffusion process. The non-toxic nature of the nascent scaffold was revealed by the cytotoxicity tests of the thermo-responsive nanocarrier on cervical cancer cells (HeLa) via MTT assay.

To translate the information gained on the thermo-responsive behavior from the studies carried out on small amphiphilic molecule based nanocarrier, a series of new amphiphilic copolymers consisting of hydrophobic monomer based on 3-pentadecylphenol (PDP) (renewable resource) and hydrophilic monomer of oligoethylene glycol chains were synthesised. In order to increase the efficacy of the newly designed amphiphilic scaffold, enzyme-responsive unit was incorporated in the copolymer structure. The composition of hydrophobic and hydrophilic unit in the copolymer structure was varied and the thermal-response of the copolymers with respect to copolymer composition was investigated. The copolymer with with 6 % of hydrophobic content (**P-6**) exhibited maximum phase-separation phenomena with LCST temperature close to cancer tissue temperature. In aqueous medium the **P-6** copolymer self-assembled to form core-shell nanoparticles of 230 ± 36 nm. The core-shell nanoparticle had tendency to undergo cluster formation at temperature above LCST, which was validated by light scattering techniques, electron microscopes and atomic force microscopy and variable temperature ^{1}H-NMR studies. These core-shell nanoparticles were employed for encapsulating DOX in their inner core. At temperature close to cancer tissue temperature burst release of DOX was observed while in the presence of esterase enzyme the controlled release of the drug over a period of 12 h occurred. The mode of release was found to be anomalous transport mechanism for thermo-response and enzymatic degradation followed non-Fickian diffusion mechanism. Cytotoxicity studies carried out on breast cancer (MCF-7) and cervical (HeLa) cancer cells revealed the non-toxic nature of the nascent scaffold.Confocal microscopic analysis confirmed the cellular uptake of the DOX and perinuclear accumulation of drugs by nano-particles in MCF-7cells.

The influence of anions present in body fluids on the thermal properties of the nanocarriers was investigated by synthesising an amphiphilic molecule with appropriate hydrophilic polyethylene glycol (PEG 750) unit and renewable resource 3-pentadecylphenol hydrophobic part to produce the super LCST amphiphile for more than 90 °C in water. The formation of micellar nanoparticle by the amphiphilic scaffold was authenticated by dynamic light scattering techniques and electron and atomic force microscopy studies. The effect of anions on the temperature sensitivity of the scaffold followed Hofmeister series. However, preferential binding of amphiphilic scaffold towards ATP over its precursors ADP, AMP and Pi was observed. The higher affinity of ATP was validated by estimating the binding constants via isothermal calorimetric experiments. Binding of Pi to scaffold was found to be exothermic, while formation of ATP + scaffold complex was endothermic process which facilitated the selective binding of ATP at cancer tissue temperature (42-43°C). MTT assay further proved the non toxic nature of the scaffold.

The role of ester and amide linkage in imparting the thermal property to an amphiphilic molecule was studied by development of new classes of amphiphilic AB diblock based on renewable resource hydrophobic rigid unit and different hydrophilic PEG content. The length of the hydrophilic PEG chain in the diblock played a crucial role in inducing the formation of strong inter-chain packing in the diblock membrane, thereby forming multi vesicular bodies (MVBs) and small unilamellar vesicles (SUVs) either by inward invagination or outward budding of diblock membrane. Theoretical models were adopted to determine the structural parameters such as relative volume (ν_e) and reduced area difference (Δa_o) and very good correlation between the theory and experimental results were obtained. The mechanistic pathways of formation of MVBs and SUVs were studied using pyrene as a probe. The drug loading and delivering capabilities of both MVBs and SUVs were determined by using DOX. The drug release kinetics of the DOX revealed that SUVs were notefficient to hold the drug under physiological conditions. On the other hand on MVBs drug molecules were trapped uniformly throughout the

hydrophobic layer of both outer and inner vesicular structures thereby showing two step DOX release.

Future Directions

In short, this thesis work brought together the concept of renewable resource based thermo-responsive small and polymeric nanocarriers. It was observed that these nanocarriers were capable of loading anticancer hydrophobic drug molecules at normal body temperature, while at temperatuter close to cancer tissues these nanocarriers collapsed to release the drug molecules. Since these nanocarriers were able to respond to small variation in temperature of their surrounding environment, they have the ability to treat cancer tissues (whose temperature is bit higher as comparec to normal body temperature). Although these nanocarriers loaded and delivered drug at cancer site efficiently, they were able to encapsulate only hydrophobic molecules in their inner core. Therefore, the efficacy of these nanocarriers can be increased by encapsulating dual drug or by incorporating dual stimulus responsive moieties.

(a) Biodegradable Dual-responsive Scaffolds

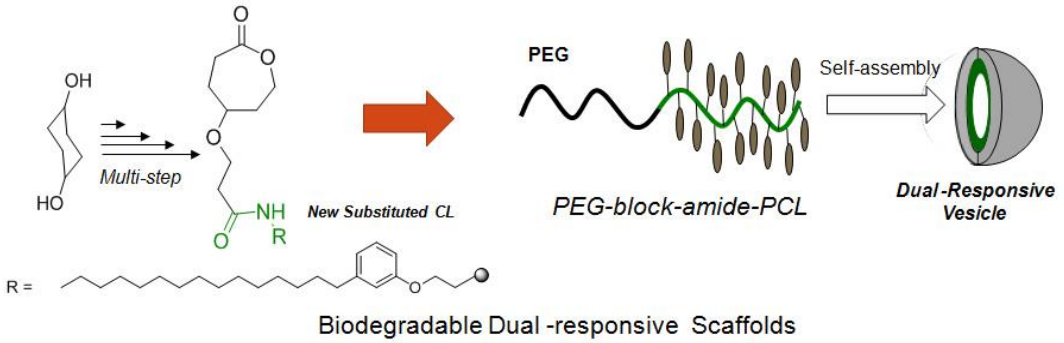

Future direction of thesis work: development of biodegradable dual-responsive polymeric scaffold as an efficient drug carrier.

The dual drug loading along with retention of dual stimuli characteristics can be achieved by design and development of new polymeric vesicular structures as shown below.Therefore ongoing projects concentrated on developing carboxyl group

functionalized polycaprolactone with PDP molecule consisting of amide-linkage as a pendant group.

(b) Multi/Dual-responsive Scaffolds

The efficacy of the nanocarriers can be enhanced by incorporating more than one stimulus in the same system. In other words, design and development of multi-responsivee scaffolds will lead to targeted drug delivery with highy specificity and efficiency (as shown below). For fabrication of such dual/multi-responsive scaffolds efforts are being made to synthesize acrylate based polymers consisting of amide-linkgae and carboxyl group in the pendant chain, which in turn will result in formation of pH and thermal-dual responsive drug delivery.

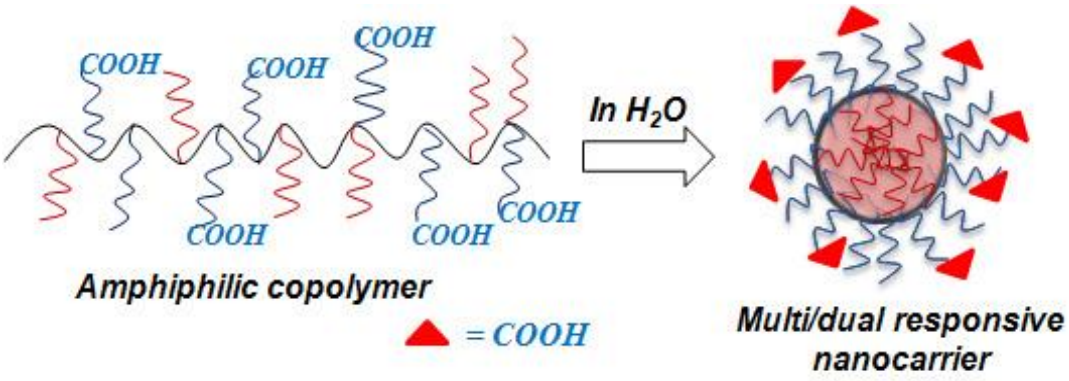

Future direction of thesis work: development of biodegradable multi/dual-responsive polymeric scaffoldfor drug delivery.

Thus, the next generation polymeric carriers should combine key features such as biodegradability, biocompatibility, stimuli (pH, temperature, reduction, enzyme etc.) responsiveness along with dual drug loading abilities. Therefore future research work focuses on merging the aspects of loading of both hydrophobic and hydrophilic drug molecules simultaneously by maintaining its stimuli sensitivity.

List of Publications

Publications in International Journals:

List of Publications:

1. Kashyap, S.; Jayakannan, M. Super LCST thermo-responsive nanoparticle assembly for ATP binding through the Hofmeistereffect.***J. Mater. Chem. B,*** **2015**, 3, 1957-1967.

2. Kashyap, S.; Jayakannan, M. Thermo-responsive and shape transformable amphiphilic scaffolds for loading and deliveringanticancer drugs ***J. Mater. Chem. B,*** **2014**,2, 4142-4152.

3. Kashyap,S.; Jayakannan, M. Amphiphilic Amphiphiles Sorting into Multivesicular Bodies and TheirFluorophore Encapsulation Capabilities.***J. Phys. Chem. B,*****2012**, 116, 9820−9831.

4. Kashyap, S.; Jayakannan, M. Enzyme and Thermal Dual Responsive Amphiphilic Polymers Core-shell Nanoparticles for Doxorubicin Delivery to Cancer Cells ***Biomacromolecules*** **2016**, 17, 384-398.

5. Kashyap, S.; Jayakannan, M. Hydrophilic and Hydrophobic Pyrene Fluorophores for unlocking the mechanistic aspects of thermo-responsive molecular self-assembly (*Manuscript under preparation)*

Publications in International Conference Proceedings:

1. Kashyap. S.; Jayakannan, M. Self-organized Hydrophobic-Hydrophilic AB-Diblock Amphiphiles for Drug Delivery" *CRSI symposium*, NCL-Pune, India, May 14-16, **2011**.

2. Kashyap. S.; Jayakannan, M. Self-organized Hydrophobic-Hydrophilic AB-Diblock Amphiphiles for Drug Delivery" *INTER IISER CHEMISTRY MEET,* Trivandrum, India, Dec. 10-12, **2011**.

3. Kashyap. S.; Jayakannan, M. Design and Development of AB- Diblock Thermo-responsive Assemblies and Polymeric Vesicle, *FAPS-MACRO2013*, Bangalore, India, May 15-17, **2013**.

4. Kashyap. S.; Jayakannan, M. Design and Development of AB- Diblock Thermo-responsive Assemblies and Polymeric Vesicle, *IMCB2013*, Pune, India, December, **2013**.